JOURNAL OF APPLIED PHYSICS

UNIVERSITY OF MICHIGAN
DEC 28 1953
CHEMISTRY LIBRARY

JOURNAL OF APPLIED PHYSICS

Vol. 24, No. 12 DECEMBER, 1953

In This Issue

		Page
Thermal Contraction of a Split Hollow Cylinder	W. Karush and A. V. Martin	1427
Exact Interpolation of Band-Limited Functions	Arthur Kohlenberg	1432
Attenuation of Gamma Rays. II. Transmission Values for Various Materials and Geometries	Glenn H. Peebles	1437
Microwave Diffraction Measurements in a Parallel-Plate Region	Ronald V. Row	1448
Theory of the Formation of Bubbles	Shunsuke Takagi	1453
Variational Methods for Problems in Resistance	J. F. Carlson and T. J. Hendrickson	1462
Approximate Solutions of the Space-Charge Problem for Some Unusual Electrode Geometries	Henry F. Ivey	1466
Response of Two-Material Laminated Cylinder to Simple Harmonic Environment Temperature Change	Herman H. Lowell	1473
Shapes of Floating Liquid Zones between Solid Rods	P. H. Keck, M. Green, and M. L. Polk	1479
Preparation of $p-n$ Junctions by Surface Melting	Kurt Lehovec and Emanuel Belmont	1482
Generation of Wind Waves on a Water Surface	Carl Eckart	1485
Electron Microscopy of Photographic Grains. Specimen Preparation Techniques and Applications	F. A. Hamm and J. J. Comer	1495
Electron Microscopical Studies of the Latent Image Obtained by Exposures to Alpha Particles, X-Rays, and Light	H. Hoerlin and F. A. Hamm	1514
Letters to the Editor:		
Modification of R-PAC for Interpretation of Patterson Maps in X-Ray Crystal Analysis	Ray Pepinsky	1520
Resistivity of Thin Silver Films	Uri Oppenheim and Joseph H. Jaffe	1521
Experiments in Hydrodynamic Lubrication Using Water as a Lubricant	Stanley Abramovitz	1521
Comment on "The Calibration of Photographic Emulsions for Electron Diffraction Investigations	I. L. Karle and J. Karle	1522
Reply to Comment on "The Calibration of Photographic Emulsions for Electron Diffraction Investigations	L. S. Bartell and L. O. Brockway	1523
Note on the Stress Dependence of the Activation Energy of the Rupture Process	Edward W. LaRocca	1523
Effect of Cross-Section Area and Compression upon the Relaxation in Permeability for Toroidal Samples of Ferrites	R. E. Alley, Jr., and F. J. Schnettler	1524
Internal Friction of Molybdenum during Tensile Deformation	R. E. Maringer	1525
Absorption of Microwaves in Gases	Krishnaji and Prem Swarup	1525
Discussion on Paper Entitled "Synthesis of Transfer Functions with Poles Restricted to the Negative Real Axis"	A. D. Fialkow and Irving Gerst	1525
Further Discussion on "Synthesis of Transfer Functions with Poles Restricted to the Negative Real Axis"	Louis Weinberg	1526
Electron-Shadowgraphs and Afterglow Pictures of Gas Jets at Low Densities	A. E. Grün, E. Schopper, and B. Schumacher	1527
Radiation from a Line Source Adjacent to a Conducting Half-Plane	James R. Wait	1528
Erratum: A Nonreciprocal Microwave Component	M. L. Kales, H. N. Chait, and N. G. Sakiotis	1529
Errata: Epicentral Displacement Caused by Elastic Waves in an Infinite Slab	Alan G. Mencher	1529
Author Index to Volume 24		1530
Subject Index to Volume 24		1537
Index to Advertisers		xxvi

ELMER HUTCHISSON, *Editor*

EARLE C. GREGG, *Assistant Editor*

Board of Editors

RAY E. BOLZ
LYLE D. BORST
WALLACE J. ECKERT
ROBERT D. HEIDENREICH
LEONARD B. LOEB
W. JAMES LYONS
LOUIS A. PIPES
ROMAN SMOLUCHOWSKI
W. R. SMYTHE

Publication of the American Institute of Physics

OFFICERS

GEORGE R. HARRISON, *Chairman*
GEORGE B. PEGRAM, *Treasurer*

GOVERNING BOARD

J. W. BUCHTA
KARL K. DARROW
G. J. DIENES
S. A. GOUDSMIT
GEORGE R. HARRISON
FREDERICK V. HUNT
DEANE B. JUDD
HUGH S. KNOWLES
C. C. LAURITSEN
WILLIAM F. MEGGERS
PHILIP M. MORSE
BRIAN O'BRIEN
GEORGE B. PEGRAM
I. I. RABI
DUANE ROLLER
FREDERICK SEITZ
WILLIAM SHOCKLEY
RICHARD M. SUTTON
J. H. VAN VLECK
MARK W. ZEMANSKY

Consultant on Printing
MELVIN LOOS

ADMINISTRATIVE STAFF

HENRY A. BARTON, *Director*
WALLACE WATERFALL, *Executive Secretary*
THEODORE VORBURGER, *Advertising Manager*
RUTH F. BRYANS, *Publication Manager*
EDITH I. NEFTEL *Circulation Manager*
KATHRYN SETZE *Assistant Treasurer*

The JOURNAL OF APPLIED PHYSICS, published monthly at Prince and Lemon Sts., Lancaster, Pa., is devoted to physics in its role as the science basic to other natural sciences and to the arts and industries. Previous to 1937 this publication was known as PHYSICS. The JOURNAL OF APPLIED PHYSICS publishes editorials and reviews, as well as technical papers of applied physics. Articles appearing in it are indexed regularly, according to their field, by Physics Abstracts, Chemical Abstracts, Engineering Index, Inc., Industrial Arts Index, etc.

Manuscripts should be submitted to Elmer Hutchisson, Editor, Case Institute of Technology, Cleveland 6, Ohio. Unless otherwise stated, submission of a manuscript is a representation that it has been neither copyrighted, published, nor submitted for publication elsewhere. The authors' institutions are requested to pay a **publication charge** of $8 per page which, if honored, entitles them to 100 reprints without further charge. Instructions will be sent with galley proofs.

Subscriptions, renewals, and orders for back numbers should be addressed to the American Institute of Physics, 57 East 55 Street, New York 22, New York.

Subscription Price	U.S. and Canada	Elsewhere
To members of the American Institute of Physics and Affiliated Societies	$10.00	$11.00
To all others	12.00	13.00

Back Number Prices

Yearly back number rate when complete year is available: $14.00. Single copies: $1.25 each.

Changes of address should be sent to the American Institute of Physics; **corrected proofs** should be sent to the Publication Manager, American Institute of Physics. **Advertising rates** supplied on request. Orders, advertising copy, and cuts should be sent to the American Institute of Physics.

Entered as second class matter January 22, 1937, at the Post Office at Lancaster, Pennsylvania, under the Act of March 3, 1879. Accepted for mailing at the special rate of postage provided for in paragraph (d-2), section 34.40, P. L. & R. of 1948, authorized May 2, 1932.

Copyright 1953, by the American Institute of Physics

Journal
of
Applied Physics

Volume 24, Number 12 December, 1953

Thermal Contraction of a Split Hollow Cylinder*

W. KARUSH, *The University of Chicago, Chicago, Illinois*

AND

A. V. MARTIN, *The University of California, Berkeley, California*

(Received January 5, 1953)

Consider a long hollow cylinder which is radially split along its entire length. When such a cylinder is heated, its inner radius undergoes a change δa. The cylinder is called stable if $\delta a \leq 0$. An approximate solution for δa is derived and is used to determine conditions for stability. The pressure against the inner surface required to prevent the contraction δa is also derived.

1. INTRODUCTION

CONSIDER a long hollow cylinder at initial temperature 0 of inner radius a, outer radius b, and length L (in cylindrical coordinates: $a \leq r \leq b$, $-\pi \leq \theta \leq \pi$, $0 \leq z \leq L$). Suppose that the cylinder is heated to a temperature $T(r)$ independent of θ and z. Then the inner radius a will change by an amount δa which, as shown below, is given by

$$\delta a = \alpha a \bar{T},$$

where α = coefficient of linear expansion and $\bar{T}$ = average of T. In particular if $\bar{T}$ is positive, the inner radius will expand.

If the hollow cylinder initially fitted snugly around a non-expanding rigid interior in the form of a solid or hollow core, then a positive value of δa denotes *instability* in the sense that the cylinder will free itself from the fixed interior. On the other hand, we can understand by *stability* that the change δa is negative or zero. A possible method of achieving stability for $\bar{T} > 0$ is to split the hollow cylinder radially along its length ($a \leq r \leq b$, $-\pi + \epsilon \leq \theta \leq \pi - \epsilon$, $0 \leq z \leq L$), for in this case the tendency of the split cylinder to close upon heating will compete with the expanding effect described above. The first part of this paper is concerned with the calculation of δa for such a split cylinder for a temperature field $T(r)$. The question of stability is decided by examining the sign of δa. The results depend upon the thermal boundary conditions and the ratio a/b. For example, if $T(r)$ is caused by a uniform heat production in the cylinder and satisfies the boundary conditions $\partial T/\partial r = 0$ at $r = b$ and $T = 0$ at $r = a$, then $\delta a < 0$ for $a/b > 0.05$ and the condition of stability holds in this range (for this result Poisson's ratio is taken as 0.35). If in place of the boundary condition $T = 0$ at $r = a$ we suppose a condition $hT = K(\partial T/\partial r)$ with heat transfer coefficient h (K = thermal conductivity), then a minimum value of h for stability may be calculated. Other similar results may be obtained.

The second part of the paper deals with the pressure p which a stable contracting split hollow cylinder exerts on the rigid interior preventing the decrease of inner radius. The problem is first considered independently of that of thermal stability, and the change δa which is produced by the action of a uniform pressure p on the inner surface of a split hollow cylinder is calculated. If we combine this result with that of the thermal problem, the pressure produced by a given temperature field is obtained.

The solutions presented here are approximate. One source of approximation is the application of the St. Venant principle in taking into account only the statical equivalents of stresses on the ends $z = 0$ and $z = L$, and on the boundaries $\theta = \pi - \epsilon$ and $\theta = -\pi + \epsilon$ of the radial split. In addition, ϵ is essentially taken as 0, the influence of the radial split being introduced by requiring unstressed boundaries in effect at $\theta = \pi$ and $\theta = -\pi$. Also, it is assumed that the temperature $T(r)$ of the unsplit cylinder undergoes a negligible change when the split

*This paper is based on work done at the Metallurgical Laboratory, University of Chicago, under the auspices of the Manhattan District. The project report numbers are CP-1900 and CP-2098.

is introduced, at least insofar as the calculation of δa is concerned.

2. CHANGE OF INNER RADIUS DUE TO TEMPERATURE FIELD

Consider first a hollow cylinder without a split. Suppose that the cylinder is raised from initial temperature 0 to a temperature $T(r)$. Suppose further that the extension in the z direction is uniform. We have the following relations between the extensional strains e and the normal stresses S:

$$\left.\begin{aligned} e_r&=\frac{1}{E}\{S_r-\sigma(S_\theta+S_z)\}+\alpha T,\\ e_\theta&=\frac{1}{E}\{S_\theta-\sigma(S_z+S_r)\}+\alpha T,\\ e_z&=\frac{1}{E}\{S_z-\sigma(S_r+S_\theta)\}+\alpha T. \end{aligned}\right\} \tag{1}$$

Here the subscripts r, θ, z refer to the directions normal to the surfaces $r=$ const, $\theta=$ const, $z=$ const respectively, $E=$ Young's modulus, $\sigma=$ Poisson's ratio, $\alpha=$ coefficient of linear expansion. The equilibrium condition for the stresses is

$$d/dr(rS_r)-S_\theta=0. \tag{2}$$

We wish to solve this equation subject to the conditions that $S_r(a)=S_r(b)=0$. Methods of solution are standard —we reproduce here a particularly simple derivation given by Murray and Young.[1]

Let $u_r(r)$ denote the radial displacement of a point. Then

$$e_r=du_r/dr, \quad e_\theta=u_r/r, \quad e_z=c,$$

with c constant. From these equations and Eqs. (1) we obtain

$$\left.\begin{aligned} du_r/dr&=1/E[S_r-\sigma(S_\theta+S_z)]+\alpha T\\ u_r/r&=1/E[S_\theta-\sigma(S_z+S_r)]+\alpha T\\ c&=1/E[S_z-\sigma(S_r+S_\theta)]+\alpha T. \end{aligned}\right\} \tag{3}$$

Multiply the second equation through by r and differentiate with respect to r. Eliminate the radial displacement in the resulting equation by use of the first equation in (3). Next, eliminate S_z by means of the third equation of (3). The result is

$$S_r-S_\theta+\sigma r\frac{dS_r}{dr}-(1-\sigma)r\frac{dS_\theta}{dr}-E\alpha r\frac{dT}{dr}=0.$$

Making use of Eq. (2), this equation becomes

$$d/dr(S_r+S_\theta)=-k(dT)/(dr),$$

where

$$k=E\alpha/(1-\sigma).$$

Thus

$$S_r+S_\theta=k(A-T),$$

where A is an integration constant. From this equation and (2),

$$r^2S_r=k\int_a^r r(A-T)dr+B,$$

where B is also an integration constant.

To determine A and B we impose the boundary conditions that the surfaces $r=a$ and $r=b$ are free of normal stress, i.e.,

$$S_r(a)=S_r(b)=0.$$

These conditions yield $B=0$ and $A=\bar{T}$, where

$$\bar{T}=2\pi/\pi(b^2-a^2)\int_a^b rTdr$$

is the average value of T. Thus, we have the solutions

$$\left.\begin{aligned} S_r+S_\theta&=k(\bar{T}-T)\\ r^2S_r&=k\int_a^r r(\bar{T}-T)dr. \end{aligned}\right\} \tag{4}$$

The end stress S_z should be considered. From the third equation of (3) we obtain

$$S_z=E(c-\alpha T)+\sigma k(\bar{T}-T).$$

This is the end loading required for uniform extension e_z. An exact solution of our problem requires that S_z vanish identically, and this condition is strictly incompatible with the above condition. However, if we settle for the approximation that the end stress shall be statically equivalent to zero, namely, that the total thrust and total moment shall vanish over the end, then the conditions become compatible. The vanishing of the total thrust yields $c=\alpha\bar{T}$, thus,

$$S_z=k(\bar{T}-T). \tag{5}$$

The vanishing of the total moment follows from the symmetry of S_z. Thus, we shall take (4) and (5) as the solution of the thermo-elastic equations for a hollow cylinder with boundary conditions that the stresses vanish at the surfaces $r=a$, $r=b$, $z=0$, $z=L$. In this solution the shear stresses vanish everywhere.

The radial displacement may be obtained from the second equation of (3). In particular, at $r=a$,

$$u_r(a)=\alpha a\bar{T}. \tag{6}$$

The inner radius thereby expands as though the entire cylinder were heated to a uniform temperature $\bar{T}$.

We now introduce the split cylinder $-\pi+\epsilon\leq\theta\leq\pi-\epsilon$. What is required in this situation is a solution in which the stress vanishes not only on the surfaces $r=a$, $r=b$, $z=0$, $z=L$, but also on the surfaces $\theta=-\pi+\epsilon$ and $\theta=\pi-\epsilon$. By symmetry it is only necessary to consider

[1] "On thermal stresses, strains, and warping," AECD-2960 (May, 1944) Clinton Laboratories, pp. 2-3.

$\theta=\pi-\epsilon$. We begin by imposing the solution (4) on the split cylinder. This solution is not correct because there are stresses on the surface $\theta=\pi-\epsilon$. Let F be the total thrust and N be the counter-clockwise moment about the origin on this surface. Integration by parts yields

$$F=\int_a^b S_\theta dr=0$$

$$N=\int_a^b rS_\theta dr=k\int_a^b r\log r(\bar{T}-T)dr.$$

To annihilate the moment N we may superimpose a well-known plane strain solution[2] of the equations of elasticity corresponding to the circular ring under pure bending. This is given by

$$\left.\begin{aligned} S_r&=D/r^2+H(1+2\log r)+2J\\ S_\theta&=-D/r^2+H(3+2\log r)+2J\\ S_z&=\sigma(S_r+S_\theta)\end{aligned}\right\} \tag{7}$$

in which the shear stresses vanish, and

$$\left.\begin{aligned} D&=\frac{4M}{Q}a^2b^2\log\frac{b}{a},\quad H=\frac{2M}{Q}(b^2-a^2)\\ J&=-(M/Q)\{b^2-a^2+2(b^2\log b-a^2\log a)\}\\ q&=(b^2-a^2)^2-4a^2b^2\log^2\frac{b}{a}.\end{aligned}\right\} \tag{8}$$

In this solution the lateral surfaces $r=a$ and $r=b$ are free of stress, the total thrust on $\theta=\pi-\epsilon$ is zero, and

$$M=\int_a^b rS_\theta dr.$$

Hence if we superimpose the solution (7) on (4) and (5) with

$$M=-N=-k\int_a^b r\log r(\bar{T}-T)dr, \tag{9}$$

we shall have a solution for the split cylinder in which the thrust and moment on $\theta=\pi-\epsilon$ vanish. To the degree of approximation permitted this superposition yields a solution in which the surfaces $r=a$, $r=b$, $\theta=\pi-\epsilon$, $\theta=-\pi+\epsilon$ are free of stress, as desired.

It remains to consider the end stress S_z of (7). A direct integration yields the fact that the total end thrust vanishes. Furthermore, since S_z depends only on r, the moment about the line $\theta=0$ vanishes while the moment about the line $\theta=\pi/2$ is proportional to the cut-out area. If we neglect this area we see that S_z is statically equivalent to a zero stress. Thus, the superposition of the two solutions will be taken as the final solution for which stresses on all free surfaces vanish.

The radial displacement for the solution (7) is given by

$$u_r=\frac{1+\sigma}{E}\left\{-\left(\frac{D}{r}+Hr\right)+2(1-2\sigma)r(H\log r+J)\right\}. \tag{10}$$

The total change δa of the inner radius taking into account both solutions is the sum of the displacements $u_r(a)$ in (6) and (10). The result may be simplified by observing that

$$H\log a+J=-\frac{1}{2}\left(\frac{D}{a^2}+H\right),$$

which is the condition that $S_r(a)$ of (7) vanish. We find that

$$\frac{\delta a}{a}=\alpha\bar{T}-\frac{2(1-\sigma^2)}{E}\left(\frac{D}{a^2}+H\right). \tag{11}$$

Equation (11) is the fundamental formula. For a given temperature field $T(r)$ we evaluate M by (9), and then determine D and H from (8). Notice that since D and H are proportional to k, that the right side of Eq. (11) is independent of E and proportional to α.

3. TEMPERATURE FIELDS

We shall be concerned with temperature fields depending only on r and corresponding to constant heat production P per unit volume. Thus,

$$\frac{d^2T}{dr^2}+\frac{1}{r}\frac{dT}{dr}+\frac{P}{K}=0.$$

Here, $K=$ thermal conductivity. The general solution of this equation is

$$T(r)=A+B\log\frac{r}{a}-\frac{Pr^2}{4K}, \tag{12}$$

where A and B are arbitrary constants to be determined by the thermal boundary conditions at $r=a$ and $r=b$. If we evaluate (11) with $T(r)$ as in (12) we get the following result:

$$\delta a/a\alpha=A+Bf(\gamma)-(Pa^2/4K)g(\gamma), \tag{13}$$

where

$$\gamma=a/b$$

[2] *Cf.* E. G. Coker and L. N. G. Filon, *Photo-elasticity* (Cambridge University Press, Cambridge, 1931), pp. 319–320. The formulas for the displacements appear on pp. 298–299. Notice that the meanings of a and b are reversed in this reference. The solution on pp. 319–320 is given for plane stress but the solution applies equally well to plane strain if the σ, in the notation of the reference, is taken as Poisson's ratio (which is η in that notation). The last remark is valid for carrying over other plane stress solutions in this reference to plane strain solutions.

and

$$f(\gamma)=-\frac{\sigma}{2(1-\gamma^2)}\left(1-\gamma^2+2\log\frac{1}{\gamma}\right)-1$$

$$g(\gamma)=\frac{1+\gamma^2}{2\gamma^2}-\frac{1+\sigma}{4\gamma^2}\,\frac{\left(\frac{1-\gamma^4}{\gamma^2}-4\log\frac{1}{\gamma}\right)\left(1-\gamma^2+2\log\frac{1}{\gamma}\right)}{\left(\frac{(1-\gamma^2)^2}{\gamma^2}-4\log^2\frac{1}{\gamma}\right)}.$$

Graphs of f and g may be constructed for ready reference; we shall not reproduce the results here. It may be remarked that $-f(\gamma)$ approaches ∞ at $\gamma=0$ and $1+\sigma$ at $\gamma=1$, while $-g(\gamma)$ approaches ∞ at $\gamma=0$ and $1+2\sigma$ at $\gamma=1$. For the value $\sigma=0.35$, $-f(\gamma)$ decreases monotonically from 1.98 to 1.35 in the range $0.1\leq\gamma\leq1$, while $-g(\gamma)$ decreases monotonically from 172.5 to 1.70 in this range.[3]

Several special temperature fields are of interest. Suppose that the cylinder is cooled internally, i.e., $(\partial T)/(\partial r)=0$ at $r=b$. In this case

$$T(r)=T(a)+\frac{Pa^2}{4K}\left(1+\frac{2}{\gamma^2}\log\frac{r}{a}-\frac{r^2}{a^2}\right).$$

Eq. (13) becomes

$$\delta a/a\alpha=T(a)-(Pa^2/2K)U(\gamma), \tag{14}$$

where

$$U(\gamma)=\tfrac{1}{2}g(\gamma)-(1/\gamma^2)f(\gamma)-\tfrac{1}{2}.$$

If we assume for the moment that $T(a)=0$, we see that the sign of U determines whether or not the cylinder is stable. It turns out that when $\sigma=0.35$ the function U is positive for $\gamma>0.05$; hence the cylinder is stable in this range. The function changes sign somewhere between 0 and 0.05.

If the above internal cooling occurs with a heat transfer coefficient h across the inner surface, the equation $hT(a)=K(\partial T)/(\partial r)$ holds at $r=a$. (Here zero temperature is that of the internal coolant.) Then

$$T(a)=\frac{Pa}{2h}\left(\frac{1-\gamma^2}{\gamma^2}\right),$$

so that

$$\frac{\delta a}{a\alpha}=\frac{Pa}{2h}\left(\frac{1-\gamma^2}{\gamma^2}\right)-\frac{Pa^2}{2K}U(\gamma).$$

To find the minimum h for stability we set the right side of the equation equal to zero. The result is

$$bh/K=(1-\gamma^2)/[\gamma^3U(\gamma)].$$

The right side of this equation decreases monotonically from 16.4 to 1.48 in the range $0.05\leq\gamma\leq1$ ($\sigma=0.35$).

Consider next the case of zero production, $P=0$, but a uniform flux G flowing into the cylinder normal to the outer surface $r=b$. Then

$$T(r)=T(a)+(Gb/K)\log r/a,$$
$$\delta a/a\alpha=T(a)+(Gb/K)f(\gamma).$$

For $T(a)=0$, the cylinder is always stable. If instead of $T(a)=0$, a heat transfer coefficient h is assumed at $r=a$, then $T(a)=(Gb)/(ah)$. The minimum h for stability is given by

$$ah/K=-1/[f(\gamma)].$$

Finally consider the special temperature field for which $T(a)=T(b)=t$. Then

$$T(r)=t+\frac{pa^2}{4K}\left\{1+\frac{1-\gamma^2}{\gamma^2\log\frac{1}{\gamma}}\log\frac{r}{a}-\frac{r^2}{a^2}\right\},$$

$$\frac{\delta a}{a\alpha}=t+\frac{pa^2}{4K}\left\{1+\frac{1-\gamma^2}{\gamma^2\log\frac{1}{\gamma}}f(\gamma)-g(\gamma)\right\}.$$

4. CHANGE OF INNER RADIUS DUE TO INTERNAL PRESSURE

Let us now turn from the thermo-elastic problem to the problem of determining the change δa of inner radius of a split hollow cylinder due to a uniform pressure p applied to the inner surface $r=a$. All other free surfaces are unstressed. The solution will be constructed in three steps. In the first step the unsplit cylinder is treated. In the next two steps the first solution is modified so as to take into account the effect of the split.

Step (1)

Consider an unsplit hollow cylinder with uniform pressure p applied to the inner surface. The plane strain solution for this problem is well known (Coker and Filon, pp. 299–301).

$$S_r=\frac{a^2p}{b^2-a^2}\left(1-\frac{b^2}{r^2}\right),$$

$$S_\theta=\frac{a^2p}{b^2-a^2}\left(1+\frac{b^2}{r^2}\right),$$

$$S_z=\sigma(S_r+S_\theta).$$

In this solution the shear stresses vanish and the surface $r=b$ is free of stress. The longitudinal stress S_z is a constant and if an equal and opposite stress is applied at the ends $z=0$ and $z=L$ the condition of stress-free ends is met. If we take into account the required end condition, the change of inner radius for this solution is given by

$$\frac{\delta a^{(1)}}{a}=\frac{p}{E}\left(\sigma+\frac{1+\gamma^2}{1-\gamma^2}\right). \tag{15}$$

[3] The numerical computations in this paper were carried out by Mrs. A. T. Monk.

Step (2)

The effect of the split is introduced by requiring that the stress S_θ on the surface $\theta=\pi-\epsilon$ have zero thrust and zero moment about the z axis. (This condition on $\theta=-\pi+\epsilon$ will be met by symmetry.) The above solution must therefore be modified so as to annihilate the total thrust F_1 and moment M_1 where

$$F_1=\int_a^b S_\theta dr=ap,$$

$$M_1=\int_a^b rS_\theta dr=\frac{a^2p}{2}\left(1-\frac{\log\gamma}{1-\gamma^2}\right).$$

In this step we shall annihilate the moment. This may be done by using the earlier solution (7) with $M=-M_1$. As was noted there, this solution preserves the stress-free boundary condition on $r=a$, $r=b$ and on the ends of the cylinder to the degree of approximation allowed, and has total thrust zero on $\theta=\pi-\epsilon$. If we use (10) we obtain with the present value of M,

$$\frac{\delta a^{(2)}}{a}=\frac{2p}{E}\cdot\frac{\gamma^2(1-\gamma^2-2\log\gamma)^2(1-\sigma^2)}{(1-\gamma^2)[(1-\gamma^2)^2-4\gamma^2\log^2\gamma]}. \tag{16}$$

Step (3)

To annihilate the thrust F_1, we employ the following well-known plane strain solution for a split ring (Coker and Filon, pp. 370–374):

$$S_r=\frac{C\cos\theta(b^2-r^2)(r^2-a^2)}{(a^2+b^2)r^3},$$

$$S_\theta=\frac{C\cos\theta[a^2b^2+r^2(a^2+b^2)-3r^4]}{(a^2+b^2)r^3},$$

$$S_{r\theta}=\frac{C\sin\theta(b^2-r^2)(r^2-a^2)}{(a^2+b^2)r^3},$$

where the last equation gives the shear stress and C is a constant to be determined. In this solution the normal and shear stresses vanish on $r=a$ and $r=b$. For the end loading we have $S_z=\sigma(S_r+S_\theta)$, which has total thrust zero and moment zero about $\theta=0$. The moment about $\theta=\pi/2$ does not vanish but we shall neglect this effect in the calculation of the radial displacement.

At any section $\theta=$ const we have

$$F_3=\int_a^b S_\theta dr=-C\cos\theta\left(\log\gamma+\frac{1-\gamma^2}{1+\gamma^2}\right),$$

$$M_3=\int_a^b rS_\theta dr=0.$$

Thus we may achieve thrust and moment zero on the split surface (taken as $\theta=\pi$) by setting

$$F_3=-F_1=-ap.$$

In this way the constant C is determined as

$$C=\frac{ap(1+\gamma^2)}{\gamma^2-1-(1+\gamma^2)\log\gamma}.$$

There is a radial force of amount

$$\int_a^b S_{r\theta}dr=-C\sin\theta\left(\log\gamma+\frac{1-\gamma^2}{1+\gamma^2}\right),$$

which vanishes on the split surface $\theta=\pi$.

The radial displacement at $r=a$ is given by

$$u_r(a)=\frac{2(1-\sigma^2)C}{E}\theta\sin\theta+e\cos\theta,$$

where e is a certain constant. The second term represents a rigid translation of amount e in the direction $\theta=0$ and may therefore be ignored. Thus the change of inner radius is

$$\frac{2(1-\sigma^2)C}{E}\theta\sin\theta.$$

We choose as $\delta a^{(3)}$ the average value of this expression over $-\pi\leq\theta\leq\pi$. Thus

$$\frac{\delta a^{(3)}}{a}=\frac{2p}{E}\cdot\frac{(1-\sigma^2)(1+\gamma^2)}{\gamma^2-1-(1+\gamma^2)\log\gamma}. \tag{17}$$

The final result is obtained by adding the displacements (15), (16), and (17). Thus,

$$(\delta a/a)=(2p/E)q(\gamma),$$

where $q(\gamma)$ is a certain explicit function of γ (containing the parameter σ).

Let us now return to the thermo-elastic solution (13) for a temperature field (12). The internal pressure p required to restrain a change of inner radius when the split cylinder is raised to the temperature $T(r)$ is given by the equation

$$(2p/\alpha E)q(\gamma)=-A-Bf(\gamma)+(Pa^2/4K)g(\gamma).$$

The constants A and B are determined by the thermal boundary conditions in the manner illustrated in the preceding section.

Exact Interpolation of Band-Limited Functions*

ARTHUR KOHLENBERG†
Lincoln Laboratory, Massachusetts Institute of Technology, Cambridge 39, Massachusetts
(Received March 9, 1953)

A general formula is derived for the spectrum of a multiply-periodic, amplitude modulated sequence of pulses. The result is used to show that a function which lies in a frequency band (W_0, W_0+W) is completely determined by its values at a properly chosen set of points of density $2W$. This verifies a supposition commonly accepted in communication theory.

The well-known, exact interpolation formula for a function $f(t)$ in a band (O, W) is

$$f(t)=\Sigma_n f(n/2W)\frac{\sin\pi(2Wt-n)}{\pi(2Wt-n)}.$$

The function is thus determined by its values at a set of evenly spaced points $\frac{1}{2}W$ apart.

For a function $f(t)$ in a band (W_0, W_0+W) it is shown that an exact interpolation formula is

$$f(t)=\Sigma_n[f(n/W)s(t-n/W)+f(n/W+k)s(n/W+k-t)]$$

in which k is subject to weak restrictions and

$$s(t)=\frac{\cos[2\pi(W_0+W)t-(r+1)\pi Wk]-\cos[2\pi(rW-W_0)t-(r+1)\pi WK]}{2\pi Wt\sin(r+1)\pi WK}$$
$$+\frac{\cos[2\pi(rW-W_0)t-r\pi Wk]-\cos[2\pi W_0t-r\pi Wk]}{2\pi Wt\sin r\pi Wk}.$$

Thus, the function is determined by its values at a set of points of density $2W$, but the points consist of two similar groups with spacing $1/W$, shifted with respect to each other.

INTRODUCTION

THE use of pulse techniques in communications has led to the study[1–3] of the spectra of amplitude modulated sequences of pulses of the form[4]

$$g(t)=\sum_n f(an)s(t-an), \tag{1}$$

in which $s(t)$ gives the shape of the basic pulse, and $f(t)$ represents the modulating amplitude.

There has also been considerable interest in the problem of the exact interpolation of band-limited functions because of its implications about the information content of periodically-sampled signals.

Many authors[5–11] have shown that a function $f(t)$, which is band-limited to the frequency range (O, W), is completely determined by its values at a set of points spaced $\frac{1}{2}W$ apart. In fact,

$$f(t)=\sum_n f(n/2W)\frac{\sin\pi(2Wt-n)}{\pi(2Wt-n)}. \tag{2}$$

The similarity between this interpolation formula, giving $f(t)$ in terms of its sampled values, and Eq. (1) for the form of an amplitude modulated sequence of pulses, suggests that a study of the spectra of such pulse sequences will lead to further interpolation formulas.

In the following a general formula for the spectrum of a multiply-periodic, amplitude modulated series of pulses is derived, and it is applied to show that $2W$ points per second are necessary and sufficient to determine a function lying in an arbitrary frequency band, (W_0, W_0+W), of width W. This fact has been intuitively accepted in communication theory for some time.

(It should be noted that no physical signal is ever infinite in duration, or exactly band-limited. However, if a section of duration T is excised from a theoretical, infinitely long, band-limited signal and this section is smoothed to zero at its ends, it will differ from a band-limited signal of finite duration by an error of order $1/T$, which can be made as small as desired by choosing T sufficiently large. It is with such signals that one deals in practice.)

SAMPLING

The Sampling Theorem

Let us call a function $g(t)$, as given in Eq. (1), a first-order sampling of $f(t)$. More generally, let us define a

* The research reported in this document was supported jointly by the Army, Navy, and Air Force under contract with the Massachusetts Institute of Technology.
† Now at Melpar, Inc., Cambridge, Massachusetts.
[1] S. C. Kleene, Proc. Inst. Radio Engrs. **35**, 1049 (1947).
[2] W. R. Bennett, Bell System Tech. J. **27**, 446 (1948).
[3] D. Middleton, J. Appl. Phys. **22**, 1153 (1951).
[4] All summations run from $-\infty$ to $+\infty$ unless otherwise indicated.
[5] H. Nyquist, Trans. Am. Inst. Elec. Engrs. **2**, 617 (1928).
[6] D. Gabor, J. Inst. Elec. Engrs. (London) **93**, (3), 429 (1946).
[7] C. E. Shannon, Proc. Inst. Radio Engrs. **37**, 10 (1949).
[8] J. Oswald, Compt. rend. **229**, 21 (1949).
[9] J. Ville, Câbles et Trans. **4**, 9 (1950).
General discussions from a purely mathematical viewpoint may be found in:
[10] J. M. Whittaker, *Interpolatory Function Theory* (Cambridge Tracts in Mathematics and Mathematical Physics, No. 33, Cambridge University Press, 1935).
[11] N. Levinson, *Gap and Density Theorems* (American Mathematical Society Colloquium Publications, New York, 1940, Vol. 26).

pth-order sampling as a function

$$g(t)=\sum_{i=1}^{p} g_i(t)=\sum_{i=1}^{p}\left[\sum_n f(a_in+k_i)s_i(t-a_in-k_i)\right], \quad (3)$$

in which the ith sampling $g_i(t)$ has "step size" a_i, "phase" k_i, and "sampling function" $s_i(t)$.

The sampling theorem which follows gives the Fourier transform of $g(t)$[12] in terms of the sampled function $f(t)$ and the sampling parameters.

Theorem: If the functions $f(t)$ and $s_i(t)$ possess Fourier transforms then

$$G(\omega)=\sum_{i=1}^{p} a_i^{-1}S_i(\omega) \times\left[\sum_n F(\omega+2\pi n/a_i)\exp(-i2\pi nk_i/a_i)\right]. \quad (4)$$

The proof is straightforward.[13] Consider

$$g_i(t)=\sum_n f(a_in+k_i)s_i(t-a_in-k_i). \quad (5)$$

If we use the Dirac δ function, we can write this as

$$g_i(t)=\sum_n \int_{-\infty}^{+\infty} f(x)s_i(t-x)\delta(x-a_in-k_i)dx, \quad (6)$$

and interchanging the order of summation and integration, we have

$$g_i(t)=\int_{-\infty}^{+\infty} f(x)s_i(t-x)\left[\sum_n \delta(x-a_in-k_i)\right]dx. \quad (7)$$

The summation in brackets represents a periodic function with period a_i and we can write it, using its Fourier-series expansion, as

$$\sum_n \delta(x-a_in-k_i)=\sum_n a_i^{-1}\exp[i2\pi n(x-k_i)/a_i]. \quad (8)$$

Thus we have

$$g_i(t)=\int_{-\infty}^{+\infty} f(x)s_i(t-x)a_i^{-1} \times\left\{\sum_n \exp[i2\pi n(x-k_i)/a_i]\right\}dx, \quad (9)$$

and, again interchanging the order of summation and integration, we get

$$g_i(t)=a_i^{-1}\sum_n\left\{\int_{-\infty}^{+\infty} s_i(t-x)f(x) \times\exp[i2\pi nx/a_i]dx\exp[-i2\pi nk_i/a_i]\right\}. \quad (10)$$

We can now take the Fourier transform of both sides of this equation. If we use the convolution theorem and the fact that

$$\mathfrak{F}[f(x)\exp(i2n\pi x/a_i)]=F(\omega+2\pi n/a_i), \quad (11)$$

we get

$$G_i(\omega)=a_i^{-1}\sum_n \exp(-i2\pi nk_i/a_i) \times S_i(\omega)F(\omega+2\pi n/a_i). \quad (12)$$

The sampling theorem (4) follows directly by summing over i.

For brevity we introduce sampling operators, z and z_i, and sometimes write (3) as

$$g(t)=\sum_{i=1}^{p} z_if(t)=zf(t). \quad (13)$$

z is thus an operator depending upon the sampling parameters.

INTERPOLATION

The interpolation problem is that of finding a sampling operator which, for a given class of functions, is equivalent to the identity operator. We shall first consider band-limited functions in the frequency range (O, W) and use the approach of our sampling theorem. While more complex than the usual derivation,[7] this will lead to the general case (W_0, W_0+W).

First-Order Sampling in (O, W)

Consider the functions $f(t)$ such that $F(\omega)=0$ for $|\omega|>2\pi W$. We seek a sampling operator z such that $f(t)=zf(t)$ for all such $f(t)$. Using first-order sampling with $k=0$, which is sufficient, (4) requires

$$F(\omega)=a^{-1}S(\omega)\sum_n F(\omega+2\pi n/a). \quad (14)$$

In Fig. 1 we show the behavior of the term $\sum_n F(\omega+2\pi n/a)$ (referred to simply as $\sum$ in labelling the figures) for various choices of a. It is clear from the figure that if (14) is to be satisfied for all possible $F(\omega)$ by one choice of $S(\omega)$ and a, we must take $a\leqslant \frac{1}{2}W$. In the case of $a>\frac{1}{2}W$, no single $S(\omega)$ could allow for the overlapping spectra for all $F(\omega)$.

The *smallest* acceptable number of sampling points will be achieved by taking $a=\frac{1}{2}W$, in which case (14) and Fig. 1 clearly require that

$$S(\omega)=\begin{cases} a & \text{for } |\omega|\leqslant 2\pi W \\ 0 & \text{for } |\omega|>2\pi W, \end{cases} \quad (15)$$

$$s(t)=\sin 2\pi Wt/2\pi Wt.$$

[12] We shall denote functions of time by lower-case letters, e.g., $f(t)$ and their Fourier transforms either by the corresponding capital letter, e.g., $F(\omega)$ (ω=angular frequency), or by $\mathfrak{F}[f(t)]$. Thus,

$$\mathfrak{F}[f(t)]=F(\omega)=\int_{-\infty}^{+\infty} f(t)e^{i\omega t}dt,$$

$$f(t)=(2\pi)^{-1}\int_{-\infty}^{+\infty} F(\omega)e^{-i\omega t}d\omega.$$

[13] The proof given here, while lacking in some fine points of mathematical generality, is relatively simple, and sufficient for most purposes. A more general proof can be given by applying the Euler-McLaurin summation formula to the function $[f(x)s_i(t-x)]$ and examining the behavior of the remainder term.

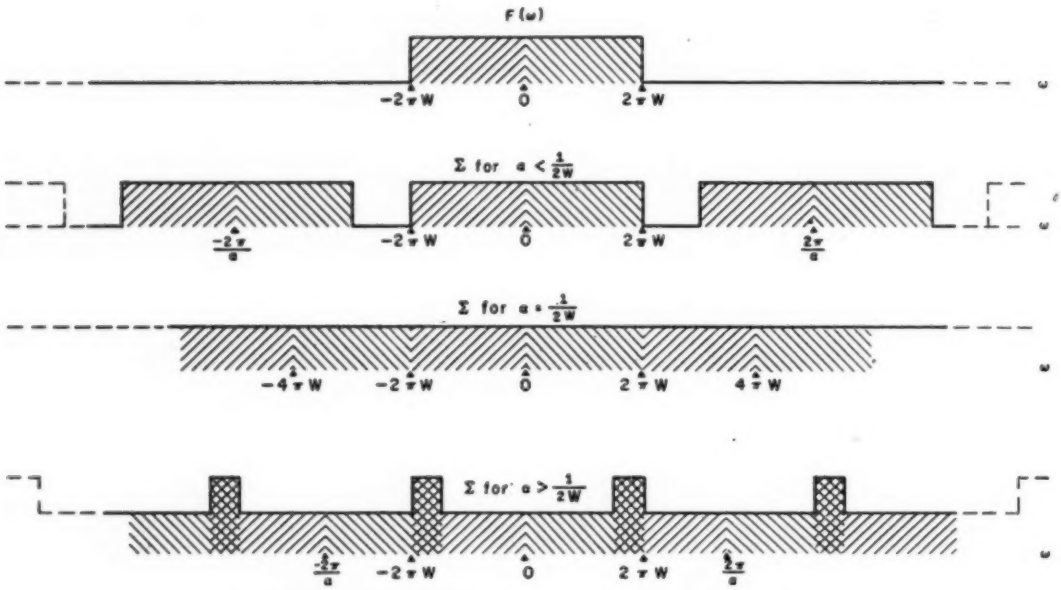

FIG. 1. $F(\omega)$ and $\Sigma_n F(\omega+2\pi n/a)$ for various cases; $f(t)$ in (O, W).

The interpolation formula thus becomes

$$f(t)=\sum_n f(n/2W)\frac{\sin\pi(2Wt-n)}{\pi(2Wt-n)}, \qquad (16)$$

which is the interpolation theorem as normally stated.[5–11]

It is easy to see that $s(0)=1$, $s(n/2W)=0$ for $n=\pm1, \pm2, \cdots$. This means that the sampled values are independent,[14] i.e., any set of numbers b_n, $n=0, \pm1, \pm2, \cdots$, will define a unique function

$$f(t)=\sum_n b_n\frac{\sin\pi(2Wt-n)}{\pi(2Wt-n)}, \qquad (17)$$

which lies in the frequency band (O, W) and for which $f(n/2W)=b_n$. Thus we have, in fact, the minimum number of sampling points, $2W$ per second.

If we choose $a<\frac{1}{2}W$, we see from (14) and Fig. 1 that we must have $S(\omega)=a$ for $|\omega|\leqslant 2\pi W$ and $S(\omega)=0$ for $-2\pi W+2\pi n/a\leqslant|\omega|\leqslant 2\pi W+2\pi n/a$, $n=\pm1, \pm2, \cdots$. In the remaining regions however, where $\sum_n F(\omega+2\pi n/a)=0$, $S(\omega)$ is arbitrary. Thus, we have great freedom in our choice of $s(t)$.

We can still choose the simplest acceptable $s(t)$, that given in (15), and write

$$f(t)=\sum_n f(an)\frac{\sin2\pi W(t-an)}{2\pi W(t-an)}, \qquad (18)$$

but $s(an)\neq0$ for $n\neq0$. This indicates that the points $f(an)$ are not independent, i.e., a set of numbers b_n will define a function,

$$f(t)=\sum_n b_n\frac{\sin2\pi W(t-an)}{2\pi W(t-an)}, \qquad (19)$$

lying in the proper frequency band, but we will not, in general, have $f(an)=b_n$, nor will a different set of b_n necessarily give a different $f(t)$. This is characteristic of sampling with points which are not algebraically independent.

First-Order Sampling in (W_0, W_0+W)

We might expect to be able to create a similar interpolation formula for a function in an arbitrary band (W_0, W_0+W), but with first-order sampling only some special cases can be treated completely. As before, it depends on the function $\sum_n F(\omega+2\pi n/a)$. Figure 2 shows the various possible types of behavior.

Only those a which do not cause overlapping in the range $2\pi W_0\leqslant|\omega|\leqslant 2\pi(W_0+W)$ can be used, and in these cases we must take

$$S(\omega)=\begin{cases} a & \text{for } F(\omega)\neq0 \\ 0 & \text{for } \sum_{n\neq0} F(\omega+2\pi n/a)\neq0 \\ \text{arbitrary otherwise.} \end{cases} \qquad (20)$$

[14] Note that these sampling points are independent in the sense of being *algebraically* independent when used in the interpolation formula. A band-limited random function will also have sets of points which are *statistically* independent, but only in special cases will the two meanings of independence lead to the same set of points.

A very important case in which the sampling points are both algebraically and statistically independent, is that of *white*, Gaussian noise in the frequency band $[cW, (c+1)W]$, $c=0, 1, 2, \cdots$. For signals in such a frequency band it will be seen below that $S(\omega)=a$ within the band and is zero outside. It is thus proportional to the power spectrum of white noise limited to the same band. The zeroes of $s(t)$, the sampling points, are thus the same as the zeros of the noise correlation function. For Gaussian noise, however, the zeroes of the correlation function are the statistically independent points.

If we take the simplest choice

$$S(\omega)=\begin{cases} a & \text{for } 2\pi W_0 \leqslant |\omega| \leqslant 2\pi(W_0+W) \\ 0 & \text{otherwise,} \end{cases} \tag{21}$$

we get

$$\begin{aligned} s(t)&=(a/\pi t)[\sin 2\pi(W_0+W)t-\sin 2\pi W_0 t], \\ f(t)&=\sum_n f(an)(a/\pi t) \\ &\quad\times[\sin 2\pi(W_0+W)(t-an)-\sin 2\pi W_0(t-an)]. \end{aligned} \tag{22}$$

It is not difficult to determine the permissible values of a. One finds that if $W_0 \neq 0$, a can be any number satisfying

$$m/2W_0 \leqslant a \leqslant (m+1)/2(W_0+W) \tag{23}$$

for m a non-negative integer. There will be a largest m, call it M, for which (23) has solutions. We will have M the largest integer $\leqslant W_0/W$, and the largest possible a will then be

$$a=(M+1)/2(W_0+W) \leqslant \tfrac{1}{2}W. \tag{24}$$

In general, the $s(t)$ in (22) will not satisfy $s(an)=0$ so that the largest a will still not give independent sampling. However, as $W_0/W \to \infty$, $a \to \frac{1}{2}W$ and the sampling points approach independence. If $W_0=cW$, $c=0, 1, 2, \cdots$, then $M=c$, the largest $a=\frac{1}{2}W$, and we will have independent sampling. Figure 2 shows that in this case the terms in $\sum_n F(\omega+2\pi n/a)$ do not overlap, and there is no arbitrariness in the choice of $s(t)$.

Thus, first-order sampling permits the exact reconstruction of $f(t)$ from its values at $2W$ points per second only if $W_0=cW$, $c=0, 1, 2, \cdots$. Otherwise, more points per second are needed and the sampled values are not independent.

We shall next see that second-order sampling permits us to use $2W$ independent points per second for any W_0 and W.

Second-Order Sampling in (W_0, W_0+W)

To use second-order sampling for interpolation, we can take $a_1=a_2=1/W$, $k_1=0$, $k_2 \neq 0$. We must satisfy the basic formulas [see (3) and (4)]

$$\begin{aligned} f(t)&=\sum_n [f(n/W)s_1(t-n/W) \\ &\qquad +f(n/W+k)s_2(t-n/W-k)], \end{aligned} \tag{25}$$

$$\begin{aligned} F(\omega)&=WS_1(\omega)\sum_n F(\omega+2\pi nW) \\ &\quad +WS_2(\omega)\sum_n e^{-ik2\pi nW}F(\omega+2\pi nW). \end{aligned} \tag{26}$$

If we plot $\sum_n F(\omega+2\pi nW)$, we see that there is overlapping in the regions $2\pi W_0 \leqslant |\omega| \leqslant 2\pi(W_0+W)$. Let the terms which overlap $F(\omega)$ in these regions be $F(\omega \pm 2\pi rW)$ and $F[\omega \pm 2\pi(r+1)W]$, as shown in Fig. 3. We must choose $S_1(\omega)$, $S_2(\omega)$ and k so that the overlapping terms are eliminated and (26) holds for any $F(\omega)$ in (W_0, W_0+W). There is no freedom in this choice.

For $|\omega|<2\pi W_0$ or $|\omega|>2\pi(W_0+W)$, we choose $S_1(\omega)=S_2(\omega)=0$.

For $2\pi W_0 \leqslant \omega \leqslant 2\pi(-W_0+rW)$ we are in the region where $F(\omega-2\pi rW)$ overlaps $F(\omega)$.

We set

$$WS_1(\omega)=1-b_{-r}, \quad WS_2(\omega)=b_{-r} \tag{27}$$

with

$$b_{-r}=(1-e^{i2\pi Wkr})^{-1}.$$

This gives us

$$\begin{aligned} &[S_1(\omega)+e^{-ik2\pi rW}S_2(\omega)]=0, \\ &W[S_1(\omega)+S_2(\omega)]F(\omega) \\ &+W[S_1(\omega)+e^{-ik2\pi rW}S_2(\omega)]F(\omega-2\pi rW)=F(\omega). \end{aligned} \tag{28}$$

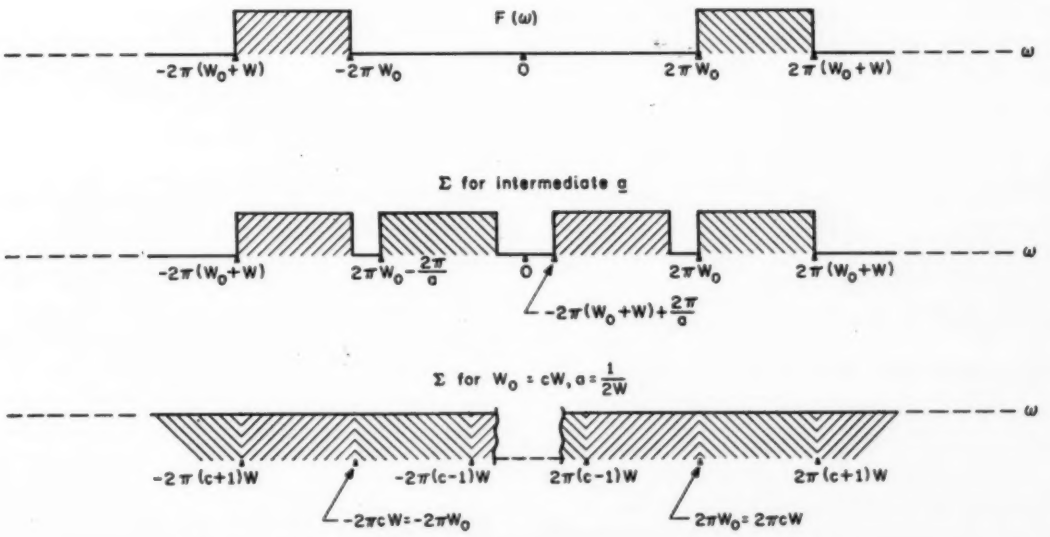

FIG. 2. $F(\omega)$ and $\Sigma_n F(\omega+2\pi n/a)$ for various cases; $f(t)$ in (W_0, W_0+W).

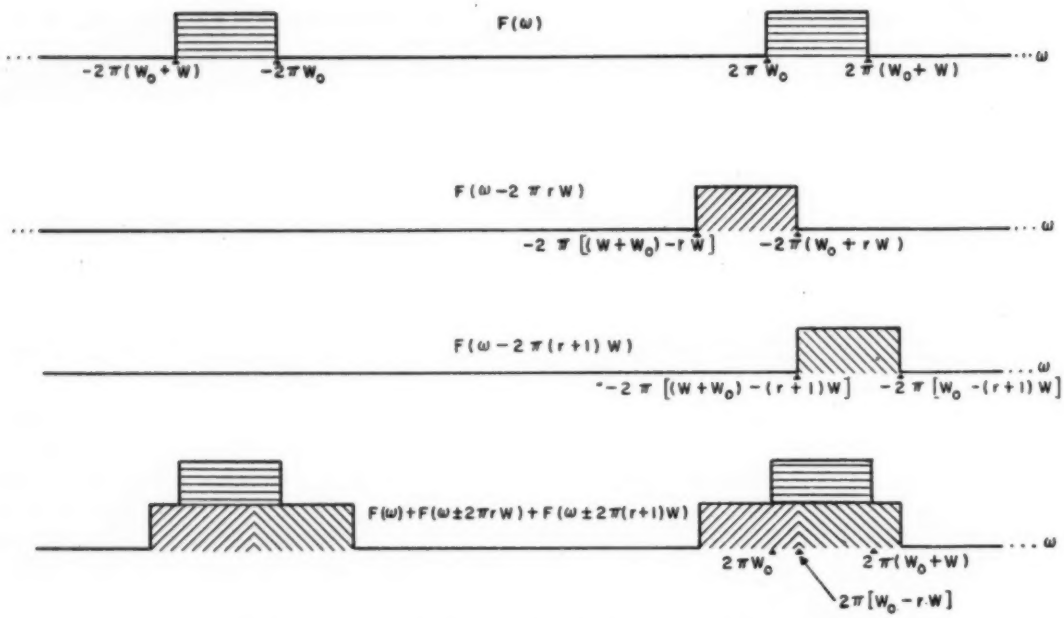

FIG. 3. $F(\omega)$ and terms in $\Sigma_n F(\omega+2\pi n/a)$ which overlap in $2\pi W \leqslant \omega \leqslant 2\pi(W_0+W)$ for $a=1/W$; $f(t)$ in (W_0, W_0+W).

For $2\pi(-W_0+rW)\leqslant\omega\leqslant 2\pi(W_0+W)$ we are in the region where $F[\omega-2\pi(r+1)W]$ overlaps $F(\omega)$ and we choose

$$WS_1(\omega)=1-b_{-(r+1)},\quad WS_2(\omega)=b_{-(r+1)},$$
$$b_{-(r+1)}=(1-e^{i2\pi Wk(r+1)})^{-1}. \tag{29}$$

For $-2\pi(W_0+W)\leqslant\omega\leqslant -2\pi W_0$ we make the corresponding choices with $-r, -(r+1)$ replaced by $r, (r+1)$. This gives us a solution of (26).

[Note that k, which gives the phase between the two sets of sampling points, n/W and $(n/W+k)$, is quite arbitrary. We must require only that $k\neq n/Wr$, $k\neq n/W(r+1)$, $n=0, 1, 2, \cdots$ because these values of k would make $b_{\pm r}$ or $b_{\pm(r+1)}$ infinite.]

It is easy to see that $S_1(\omega)=S_2(-\omega)$, $s_1(t)=s_2(-t)$. If we let $s(t)=s_1(t)$, we thus have the interpolation formula

$$f(t)=\sum_n [f(n/W)s(t-n/W) + f(n/W+k)s(n/W+k-t)] \tag{30}$$

in which, we find, by taking the Fourier transform of the $S(\omega)$ defined above,

$$s(t)=\frac{\cos[2\pi(W_0+W)t-(r+1)\pi WK]-\cos[2\pi(rW-W_0)t-(r+1)\pi Wk]}{2\pi Wt\sin(r+1)\pi WK} + \frac{\cos[2\pi(rW-W_0)t-r\pi Wk]-\cos[2\pi W_0 t-r\pi Wk]}{2\pi Wt\sin r\pi Wk}. \tag{31}$$

It follows that

$$s(0)=1,$$
$$s(n/W)=0 \quad \text{for} \quad n\neq 0,$$
$$s(n/W\pm k)=0 \quad \text{for} \quad n=0, \pm1, \pm2, \cdots,$$

which means that (30) gives a general interpolation formula in terms of the minimum, algebraically independent, $2W$ points per second.

ACKNOWLEDGMENTS

The author wishes to express his thanks to Dr. E. Lerner and Professor D. Middleton for many helpful comments on this work.

JOURNAL OF APPLIED PHYSICS VOLUME 24, NUMBER 12 DECEMBER, 1953

Attenuation of Gamma Rays. II. Transmission Values for Various Materials and Geometries*

GLENN H. PEEBLES
The Rand Corporation, Santa Monica, California
(Received March 27, 1953)

A discussion of the effect of variation of the total absorption coefficient on gamma-ray transmission probabilities is given, which leads to estimates of the build-up factors for a material of arbitrary atomic number Z.

Estimates are made of the photon and energy densities arising from a plane of sources, a line of sources, and a point source in an infinite homogeneous medium, where the material of the medium is (1) iron and (2) lead.

1. INTRODUCTION

THE attenuation of gamma rays is so difficult to calculate that it is highly desirable to extract as much information as possible from existing data. Even if the attenuation could be calculated fairly easily, the contributions of idealized problems to the solutions of most practical problems are so qualitative in character as to encourage the extension of old results, rather than the calculation of new. The purpose of this second part is to extend, where possible and profitable, the results which were presented in the first part for plane slabs of lead, of iron, and of the Compton scatterer.

The first extension is to other materials. A change of material becomes, in terms of gamma-ray attenuation, merely a variation of the total absorption coefficient. It is not difficult to see qualitatively how the various possible variations of the absorption coefficient affect the transmission. An understanding of these effects, together with the experience provided by the results presented in the first part, make possible the estimation of the transmission through slabs of almost any material. The build-up factors for photons normally incident on slabs of the elemental materials are estimated, in accordance with the notions developed, and the estimates are presented in the form of curves plotted against atomic number Z.

The second extension makes use of the principle of superposition of sources to transform results for the slab into results for other geometries.

2. TRANSMISSION THROUGH SLABS OF AN ARBITRARY MATERIAL

In Part I,† number and energy build-up factors for monoenergetic, monoangular beams of photons normally incident on slabs of lead and of iron were given. The number build-up factors were obtained by calculating for $k=0$, 1, 2, 3, and by estimating for $k=4$, 5, etc., the probability N_k that a photon will be transmitted with exactly k collisions. The energy build-up factors were obtained in a similar way from E_k, the expected energy corresponding to N_k. The intention, here, is to study the dependence of gamma-ray transmission on the total absorption coefficient and thus obtain, from the results for lead and iron, fair estimates for other materials. Some success with other materials is certain, since many materials have absorption coefficients not markedly different from those for lead or for iron.

Preliminary Discussion and Formulas

The study can best begin with a brief consideration of the total absorption coefficient. For the purposes of this section, the total absorption coefficient for an elemental material is conveniently written in the form

$$\mu=\nu(\sigma_{kn}+\sigma_{pp}/Z+\sigma_{pe}/Z),$$

where ν is the electron density, Z is the atomic number, σ_{kn} is the cross section per electron for Compton (or Klein-Nishina) scattering, and σ_{pp} and σ_{pe} are, respectively, the cross sections per atom for pair production and the photoelectric effect. The cross section σ_{kn} does not depend on the material, but σ_{pp} and σ_{pe} do, σ_{pp} being approximately proportional to Z^2 and σ_{pe} being roughly proportional to Z^5. Variation in the total absorption coefficient, therefore, comes from the variation in the electron density ν and the quantity $(\sigma_{pp}/Z+\sigma_{pe}/Z)$. The discussion below will attempt to determine, qualitatively, how changes in ν and $(\sigma_{pp}/Z+\sigma_{pe}/Z)$ affect transmission.

First, however, it is necessary to develop suitable forms for expressing N_k and E_k. The formula derived in Sec. 2 of Part I for the method of successive collisions becomes, for $k=1$,

$$dN_1=\exp(-\mu_0 s)\cdot\mu_0 ds\cdot\nu d\sigma/\mu_0\cdot N_0,$$

with

$$N_0=\exp[-(a-\gamma_0 s)\mu_1/\gamma_1].$$

Here a is the thickness of the slab in centimeters; γ_0 is the direction cosine of the incident photon; s is the slant distance of penetration before the first collision; and μ_1 and γ_1 are, respectively, the values after the first collision for the absorption coefficient and the direction cosine. The integration with respect to s on the interval

* This paper describes work done for the U. S. Air Force and U. S. Atomic Energy Commission.
† G. H. Peebles, J. Appl. Phys. 24, 1272 (1953).

$(0, a/\gamma_0)$ yields

$$dN_1=\nu\exp(-\mu_1 a/\gamma_1)\times\frac{\gamma_1\{\exp[-(\mu_0-\mu_1\gamma_0/\gamma_1)a/\gamma_0]-1\}}{\mu_1\gamma_0-\mu_0\gamma_1}d\sigma.$$

Of the several forms possible for this result, the most useful was found to be

$$N_1=KXe^{-X}\frac{\exp[(1-1/\gamma_0)X]}{\gamma_0}\times\int_{\sigma_1}\frac{\gamma_0[1-\exp(-\zeta X/\gamma_0)]}{\zeta X}\frac{d\sigma}{r^2}$$

$$=KXe^{-X}F_1(X,\alpha_0,\gamma_0),$$

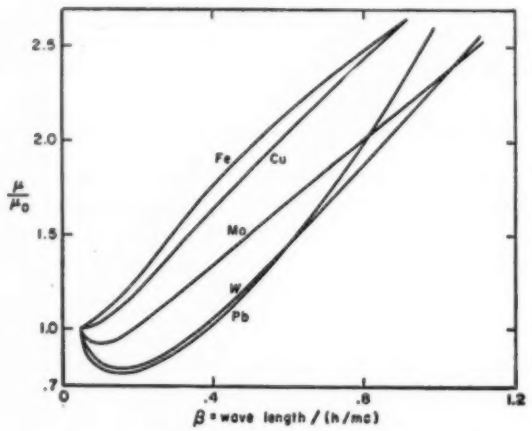

FIG. 1. μ/μ_0 *vs* β for several materials, $\alpha_0=20$.

where

$$X=\mu_0 a,$$

r = radius of the classical electron,

$$K=\nu r^2/\mu_0=r^2\Big/\left[\sigma_{kn}+\frac{\sigma_{pp}}{Z}+\frac{\sigma_{pe}}{Z}\right]_0,$$

$$\zeta=(\mu_1\gamma_0)/(\mu_0\gamma_1)-1,$$

and where details of the two-dimensional integration implicit in the differential $d\sigma$ are of no interest for present purposes. This form for N_1, although of somewhat artificial appearance, evolved more or less naturally as the answer to certain needs, and it serves here to introduce into the discussion the parameters X and K and the functional F_1.

The parameter K is seen from its definition to be directly associated with absorption by pair production and the photoelectric effect. An increase in the quantity $(\sigma_{pp}/Z+\sigma_{pe}/Z)$ causes a decrease in K. Since photons do not survive absorption by pair production or the photoelectric effect, K is an index of photon destruction in the first collision. This, however, is incidental; a better index is the probability of surviving the first collision, $[\sigma_{kn}]_0/[\sigma_{kn}+\sigma_{pp}/Z+\sigma_{pe}/Z]_0$.

The quantity F_1 also is associated with absorption by pair production and the photoelectric effect, although not so directly as K. The formula for F_1 shows that a change from one material to another affects F_1 only through the function μ/μ_0. But μ/μ_0 is independent of electron density and, therefore, is identical for two Compton scatterers. Hence, F_1 varies from one material to another only because larger or smaller components of pair production and the photoelectric effect appear in the total absorption coefficient.

To study further the dependence of F_1 on μ_1/μ_0, it is better to consider μ not as a function of the energy α in units of mc^2, but as a function of β, the reciprocal of α. In fact, throughout all the calculations of Part I, β in most cases was a more suitable variable than α. Since the energy of a photon never increases with a collision, the function μ/μ_0 is needed only for values of $\beta>\beta_0=1/\alpha_0$. Typical curves for μ/μ_0 are shown in Fig. 1; all the curves must have the value unity at $\beta=\beta_0$ and all must sooner or later rise as β increases. The function $[1-\exp(-\zeta X/\gamma_0)]/[\zeta X/\gamma_0]$ governing F_1 shows that the more rapidly μ/μ_0 increases with β, the smaller the value of F_1. It can be seen from Fig. 1 that F_1 for molybdenum ($\alpha_0=20$) must lie between F_1's values for lead and for iron, that F_1 for copper is slightly larger than F_1 for iron, and so on. Clearly, an estimate of F_1 for other materials can be obtained by making comparisons of the functions μ/μ_0.

Most of the development and discussion for F_1 can be duplicated for a general function, F_k, defined by the relation

$$N_k=\frac{(KX)^k}{k!}e^{-X}F_k,$$

where F_k can readily be reduced to a multiple integral of a function of $2k$ variables.[1] This function of $2k$ variables is well represented in form and behavior by the case of $k=1$ above. Like F_1, F_k for $k>1$ decreases as the average slope of μ/μ_0 (expressed as a function of β) increases, and like F_1, fair estimates of F_2 and F_3 can be obtained by comparing the function μ/μ_0 for the material under consideration with the same function for lead and for iron.

One is now in a position to see how ν and $(\sigma_{pp}/Z+\sigma_{pe}/Z)$ affect the build-up factor, which in terms of the F_k's becomes

$$\sum_{k=0}^{\infty}\frac{(KX)^k}{k!}F_k.$$

The question of the effect of electron density on transmission is disposed of by remarking that ν appears only in the dimensionless parameter X. The build-up factor, for example, is not affected by a change in ν, provided that the build-up factor is expressed as a function of X.

[1] Glenn H. Peebles and Milton S. Plesset, Phys. Rev. **81**, 433 (1951).

Absorption by pair production and the photoelectric effect is not handled so easily. There are two cases to consider: one is associated with pair production in the high-energy range where the photoelectric effect is negligible; the other is associated with the photoelectric effect in the low-energy range where pair production vanishes.

The cross section for pair production falls monotonically as β increases, and vanishes at $\beta=0.5$, the reciprocal of the threshold energy for pair production. Therefore, pair production decreases the slope of μ/μ_0 and increases F_k. In fact, for heavy materials such as lead, σ_{pp}/Z is so large that in the range $\beta<0.5$ its negative slope overcomes the positive slope of σ_{kn}. In such cases μ/μ_0 for $\alpha_0=10$, 20, falls and stays below unity on a fairly large range of β before beginning to rise monotonically. This behavior leads to large F_k's (see the formula in the case of F_1), which tend to slow the convergence of the series for total transmission. But the large value of $[\sigma_{pp}/Z]_0$ associated with large F_k gives K a small value which tends to hasten the convergence. To see whether K^k or F_k is the more powerful, one can turn to results for lead and iron shown in Table I. For $X=1$, the table shows N_1/e^{-X}, N_2/e^{-X}, and N_3/e^{-X} to be smaller for lead than for iron; for $X=8$, only N_3/e^{-X} is smaller; and for $X=20$, the order is reversed for all three quantities. Since lead has a much greater proportion of pair production in its total absorption coefficient than iron, this case indicates that K^k is the more powerful for thin slabs and F_k is the more powerful for thick slabs. However, the series for the total transmission must converge for all thicknesses. Hence, even for thick slabs, F_k dominates N_k/e^{-X} only for the first few values of k. Thus, one is led to the conclusion that, although an increase in pair production undoubtedly hastens the convergence of N_k to zero, the first effect, when the slab is sufficiently thick, is a more rapid rise of N_k to a greater maximum.

In the case of the photoelectric effect, K^k and F_k do not act one against the other. Since σ_{pe} is a monotonic increasing function of β, σ_{pe}/Z added to σ_{kn} increases the slope of μ/μ_0, and therefore decreases F_k as well as K. The result of increased photoelectric effect is always an increase, beginning immediately with N_1, in the rate of convergence of N_k to zero.

If one writes

$$\frac{E_k}{\alpha_0}=\frac{(KX)^k}{k!}e^{-X}G_k,$$

essentially all that has been done and said with regard to N_k and F_k applies almost unchanged to E_k/α_0 and G_k.

Estimates of the Build-up Factor for an Arbitrary Material

All the above discussion is in accordance with one's intuitive understanding. Since photons do not survive absorption by pair production and the photoelectric effect, one expects that an increase in the $(\sigma_{pp}/Z+\sigma_{pe}/Z)$ component will cause an increase in the rate of convergence of N_k. In the case of pair production, one may not foresee the delay with respect to k in the onset of the increased rate of convergence for thick slabs, although even this may be anticipated by an intuitive consideration of mean-free-path lengths. The purpose of the discussion of K^k and F_k, however, is not to establish the intuitively obvious, but to prepare the ground for estimates of the transmission through slabs of materials other than iron or lead.

TABLE I. Comparison of values of N_k/e^{-X} for photons of 20 mc[a] normally incident on slabs of lead and of iron.[a]

X	Material	N_1/e^{-X}	N_2/e^{-X}	N_3/e^{-X}
1	lead	0.152	0.024	0.0035
	iron	0.278	0.079	0.018
8	lead	1.58	1.35	0.767
	iron	1.34	1.16	0.833
20	lead	10.8	25.3	31.3
	iron	2.53	3.29	3.02

[a] N_k is the probability that a photon will be transmitted with exactly k scatterings; X is the thickness of the slab in mfp.

Provided with the preceding qualitative information and the quantitative information from the calculations of Part I for lead and for iron, one can make estimates of F_1, F_2, and F_3 for other materials. The values of N_1/e^{-X}, N_2/e^{-X}, N_3/e^{-X} can then be computed and rough estimates of N_4/e^{-X}, N_5/e^{-X}, $\cdots$ can be made by some means, say, by a simple and reasonable extrapolation such as is illustrated in Fig. 2, Part I. If the estimates of F_1, F_2, and F_3 are reasonably accurate, the resultant estimates of the build-up factor $\sum_{k=0}^{\infty} N_k/e^{-X}$ will also be reasonably accurate.

Figure 2 gives the number build-up factor *versus* the atomic number Z for the elemental materials;[2] the thickness X and the incident energy α_0 are parameters. The data leading to the curves shown were obtained not by the process just outlined but by one which may be described in the following way.

Suppose that photons of the same energy and direction are incident upon two slabs of the same thickness in mean free paths but of different materials. If the series for the two build-up factors converge to different values, as they presumably will, the cause must lie in the fact that absorption by pair production and the photoelectric effect appears in different proportions in the two total absorption coefficients. Realizing this, one may think to attempt to correlate the remainder of the series with the amount of absorption by pair production and the photoelectric effect. The difficulty with this thought lies in defining a variable which suitably measures "destructive" absorption and is also easily evaluated for each material.

[2] Estimates of the build-up factors for slabs of carbon, aluminum, molybdenum, cadmium, tantalum, and uranium were used to obtain Fig. 2. The total absorption coefficients for these materials were taken from Richard Latter and Herman Kahn, "Gamma-Ray Absorption Coefficients," (The Rand Corporation, R-170), 1949.

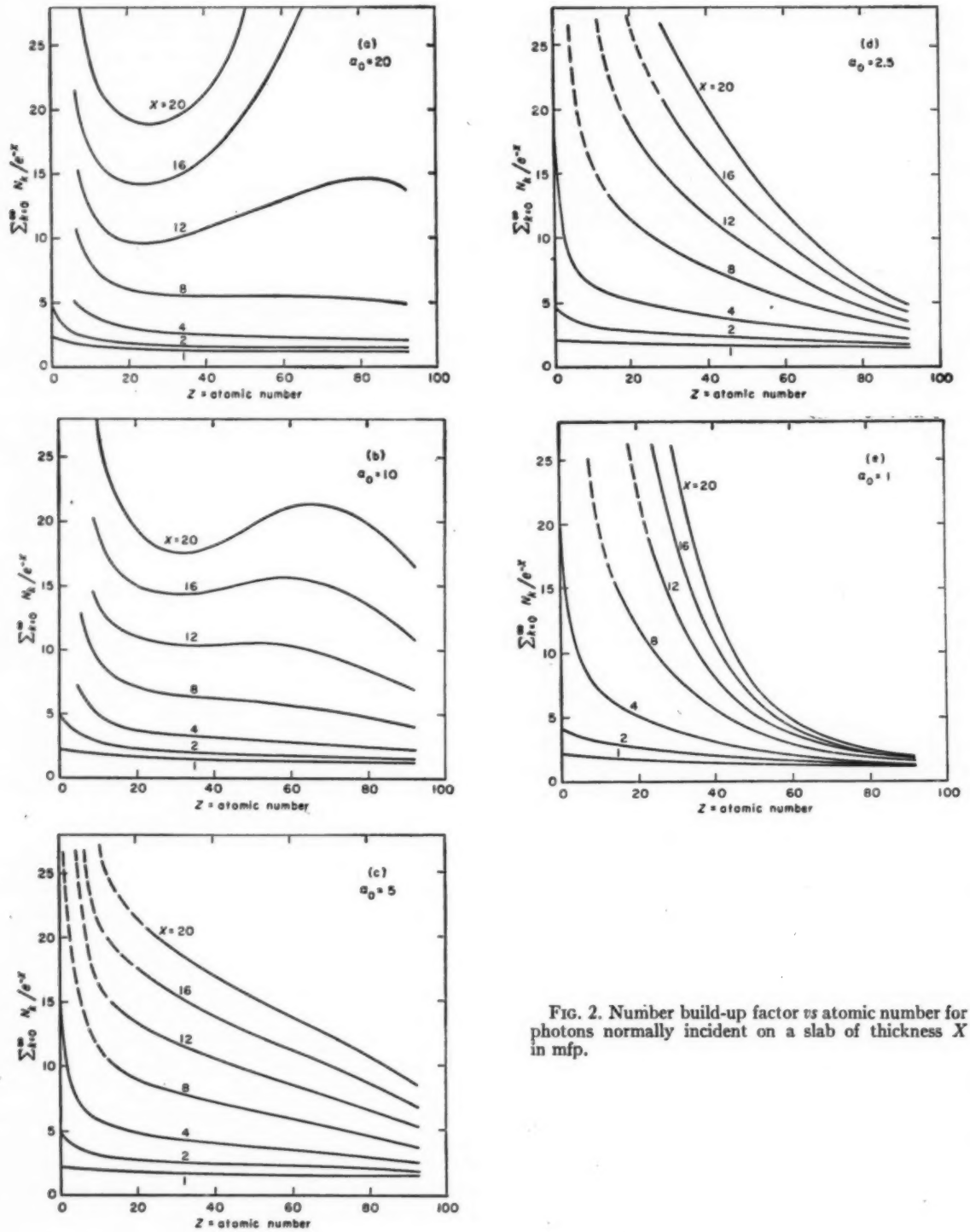

FIG. 2. Number build-up factor *vs* atomic number for photons normally incident on a slab of thickness X in mfp.

However, for the rough correlation contemplated, there is no need to be too exacting. A quantity such as

$$\frac{1}{b}\int_{\beta_0}^{\beta_0+b}\frac{\sigma_{pp}+\sigma_{pe}}{Z\sigma_{kn}+\sigma_{pp}+\sigma_{pe}}d\beta,$$

is undoubtedly adequate since, if b is properly chosen, it measures destructive absorption in a region of significance. It, therefore, might be used for the correlation, but when examined, it turns out to be so nearly a linear function of Z that Z itself, by virtue of its greater convenience, becomes the better choice.

When an attempt was made to fix the preceding concept in a working scheme, it was found, as is usually the case, that a modification of the original idea served better. It turned out to be more convenient and almost

as accurate to let the remainder begin with N_2/e^{-X} rather than with N_4/e^{-X}, and to correlate with Z for constant N_1/e^{-X} rather than for constant X. Since N_1/e^{-X} and the build-up factor tend to rise and fall together, the correlation for constant N_1/e^{-X} is as accurate as, if not more accurate than, that for constant X. Some loss of accuracy results from including N_2/e^{-X} and N_3/e^{-X} in the remainder, but investigation showed that the accuracy gained by estimating N_2/e^{-X} and N_3/e^{-X} separately hardly warranted the extra work.

An example of the correlation of $\sum_{k=2}^{\infty} N_k/e^{-X}$ with Z for constant N_1/e^{-X} is given in Fig. 3. The curves are determined by only two points, $Z=26$ and $Z=82$, except when N_1/e^{-X} is small. Since $\sigma_{pp}/Z+\sigma_{pe}/Z$ vanishes with Z, $Z=0$ corresponds here to the pure Compton scatterer. For small values of N_1/e^{-X}, the estimates of the build-up factor for the Compton scatterer provide a point at $Z=0$. Two and three points certainly constitute the minimum number for any degree of accuracy, but it must be remembered that the remainder is a monotonic decreasing function of Z with a presumably monotonic derivative. Such being the case, inaccuracies in the curves due to an insufficient number of determining points can hardly be large according to the standards of shielding calculations.

The task of computing N_1/e^{-X} for a given total absorption coefficient μ is not great for normal incidence, so that curves such as those of Fig. 3 make the estimation of build-up factors very rapid. However, most of the values of N_1/e^{-X} were not obtained by a direct computation but by use of some curves which are shown in small scale in Fig. 4. This figure gives F_1 in terms of the convenient parameter $(1+\lambda)X$, where λ is the slope of μ/μ_0 when μ/μ_0, expressed as a function of the wavelength in Compton units, is a straight line. Although no material has a total absorption coefficient which is a linear function of wavelength, the elemental materials have coefficients which are very roughly linear above a wavelength of about 0.15 in Compton units. By determining straight-line equivalents to μ/μ_0 for lead and for iron such that the value of F_1 is the same whether calculated from the true μ/μ_0 or its straight-line equivalents, one is soon able to gain enough experience to make satisfactory estimates of F_1.

As a matter of fact, average slopes were obtained not only on the basis of F_1, but also on the basis of G_1, F_2, and G_2. This operation disclosed that the straight-line equivalent of μ/μ_0 has a definite and easily understood pattern of behavior. The component of the transmission in high-energy photons is larger for large X than small, larger for the first scattering than the second, and especially for high incident energies, larger for energy than number. Consequently, the straight-line equivalent is governed by the portion of μ/μ_0 near β_0, more for large X than small, more for the first scattering than the second, and more for energy than number. Any departure from this pattern is an indication of error. A careful examination of the patterns for lead and iron

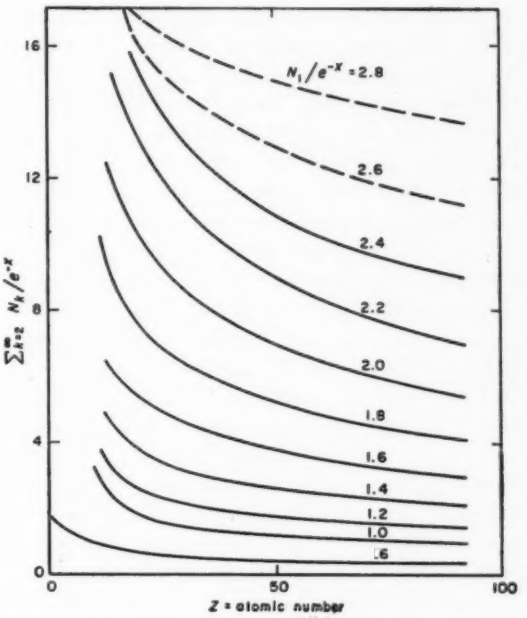

FIG. 3. The remainder $\Sigma_2^{\infty} N_k/e^{-X}$ *vs* Z with N_1/e^{-X} as a constant parameter. N_k is the probability that a photon will be transmitted with k collisions through a slab of thickness X in mfp.

slabs was used as a "spot check" for the values of N_k and $E_k(k=1, 2)$, which were calculated (but not tabulated) in connection with the build-up factors of Sec. 2, Part I.

Reliability of Estimates

When one comes to considering the accuracy of the build-up factors given in Fig. 2, one must first remember that the estimates can be no better than the build-up factors for lead and for iron. The question is, is the

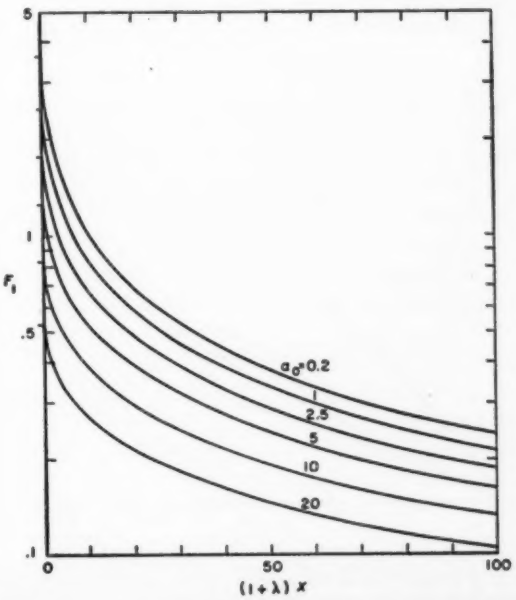

FIG. 4. Curves for estimating once-scattered transmission.

process of estimation such as to increase this inherent error? The sources of additional error lie in the choice of the average slope of μ/μ_0 and in the manner in which the curves illustrated by Fig. 3 are drawn. Errors due to the latter source are seen to be enormous when Z is small, but negligible compared with the inherent error when Z is large, say, greater than 26. As long as the monotonic character of the curves is retained, only relatively small changes in the readings for $Z>26$ can result. Much more important is the error due to an incorrect average slope. If μ/μ_0 departs far from linearity, as it does for large Z and large α_0, the average slope is not easy to determine. For $\alpha_0=10$, 20, the values of N_1/ϵ^{-X} were determined by direct calculation; for all other incident energies, a straight-line equivalent was used. Errors of as much as 5 percent appeared in N_1/ϵ^{-X} from an incorrect estimate of the average slope. Errors of this magnitude in N_1/ϵ^{-X} seemed to translate into errors in the build-up factor of about one-half the inherent error. In other words, it is necessary to suppose that, for $Z>26$, the errors in the build-up factors of Fig. 2 are about half again those stated in Sec. 2, Part I for the build-up factors for lead and iron slabs. This would mean an error approximately proportional to X and reaching about 30 percent at $X=20$.

Whatever the accuracy of the build-up factors of Fig. 2 may be, the behavior, in the large, is certainly correct as shown. For $\alpha_0=1$, 2.5, the build-up factor for large X is a rapidly decreasing monotonic function of Z. For $\alpha_0=5$, the build-up factor is still a monotonic decreasing function, but it is not so rapidly decreasing, particularly in the middle range of Z. A slight sinuosity, noticeable in the case of 5 mc², develops into a pronounced minimum and maximum by the time α_0 has reached 10 and becomes so large at $\alpha_0=20$ that the maxima for $X=16$ and $X=20$ are off the scale of the figure. The explanation for this whole pattern of behavior is implicit in the previous discussion of the effect of absorption by pair production and the photoelectric effect. For the low energies of 1 mc² and 2.5 mc², photoelectric absorption controls the magnitude of the build-up factor. As Z increases, the photoelectric absorption increases and the build-up factor decreases rapidly. The inflections noticed in the case of 5 mc² mark the appearance of the effect of absorption by pair production. The very large values of N_k/ϵ^{-X} for the first values of k in the cases of 10 mc² and 20 mc² cause the build-up factors to be so large that a minimum appears in the middle range of Z. However, as Z increases past the middle range, the diminishing effect of destructive absorption again takes control and a maximum is formed.

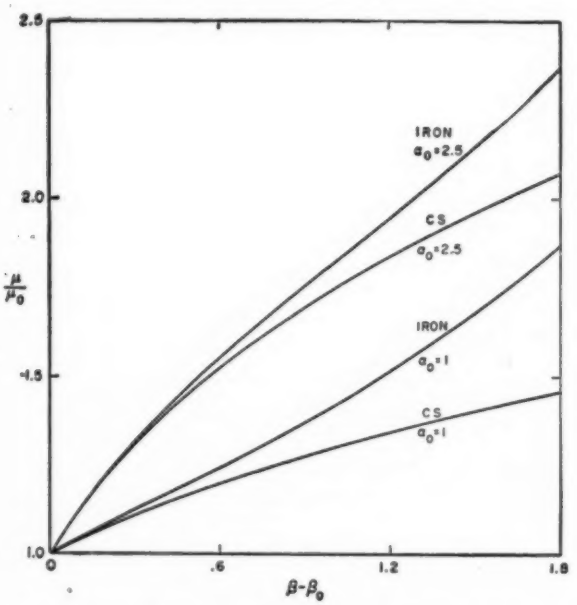

FIG. 5. A comparison of the magnitude of the photoelectric effect in iron when $\alpha_0=2.5$ with the magnitude when $\alpha_0=1$. β is the wavelength in Compton units.

On examining the curves in the neighborhood of $Z=0$, one notices the steepness at zero, particularly as the incident energy increases. One may well feel that more steepness near $Z=10$ or $Z=20$ and less near $Z=0$ would be correct. Since the region of greatest error is that of small Z, this feeling may be justified. However, a small amount of absorption acting through a decreased K can diminish greatly the sum of a slowly converging series. In any case, the data seemed not to permit a less precipitous descent from the value at zero.

Another phenomenon in the small Z range, which may catch the eye as a possible irregularity, is the existence, when X is large and Z is near zero, of values of the build-up factor which are larger for 1 mc² than for 2.5 mc². If one has noticed that the build-up factors for the Compton scatterer for small X, given in Fig. 17, Part I, increase with α_0, one may again suspect the existence of an error.

Since the remainder for large X and small Z depends entirely on the build-up factors for iron, the source of the error, if the error exists, must be found in the factors for iron. Figure 4, Part I, shows that the iron build-up factor for 1 mc² is slightly less than that for 2.5 mc² when X is small, but larger when X is large, reaching, at $X=20$, a value some 15 percent above the value for 2.5 mc². The appearance of the total absorption coefficient for iron does not seem to support this behavior of the build-up factors relative to each other. Figure 7, Part I, shows that the total absorption coefficient for iron is almost entirely Klein-Nishina scattering between 2.5 mc² and 1 mc²; at about 1 mc² the total absorption coefficient begins, as α decreases, to rise very rapidly above its Klein-Nishina component. Since a photon of energy 1 mc² is at the beginning of the region of large photoelectric absorption, one might well think that photoelectric absorption would surely reduce the build-up factor for 1 mc² at $X=20$ far below that for 2.5 mc² and that, consequently, a very large error, much larger than 20 percent, must exist in one or the other of the build-up factors.

TABLE II. Comparison of values of N_k/e^{-X} for 2.5- and 1-mc² photons normally incident on iron slabs.[a]

X	α_0	N_1/e^{-X}	N_2/e^{-X}	N_3/e^{-X}
1	2.5	0.485	0.181	0.060
	1.0	0.455	0.169	0.045
8	2.5	1.77	1.87	1.68
	1.0	1.71	1.90	1.68
20	2.5	2.67	4.41	5.01
	1.0	2.58	4.44	5.43

[a] N_k is the probability that a photon will be transmitted with exactly k scatterings; X is the thickness of the slab in mfp.

The total absorption coefficient, when plotted against α, as in Fig. 7, Part I, is somewhat misleading with regard to the effect of photoelectric absorption on the build-up factors. Figure 5, which shows μ/μ_0 *versus* $\beta-\beta_0$, gives a more accurate concept of the effect of photoelectric absorption because the abscissa $\beta-\beta_0$ provides a better scale than does α for comparison of the energy degradation at different energies. This figure shows that when β is in the range near β_0, the divergence of the function μ/μ_0 for iron from that for the Compton scatterer is not much greater for 1 mc² than it is for 2.5 mc². This means that photoelectric absorption will act to reduce N_k/e^{-X} for the first values of k with but little more strength in the case of 1 mc² than in the case of 2.5 mc². Support of this last statement is found in Table II, where approximately identical values of the three quantities N_1/e^{-X}, N_2/e^{-X}, and N_3/e^{-X} appear for the two energies at the same values of X. If the calculated values of N_k/e^{-X} are nearly equal, then the build-up factor for 1 mc² cannot be much smaller than that for 2.5 mc², and there is no reason to suppose an error in the build-up factors at $X=20$ larger than the 20 percent stated in Sec. 2, Part I.

As a matter of fact, at $X=20$, the value of N_3/e^{-X} for 1 mc² is some 8 percent larger than the value for 2.5 mc². This undoubtedly accounts for the fact that the build-up factor at $X=20$ for 1 mc² is 15 percent larger than the build-up factor for 2.5 mc², but it is difficult to believe that on the third scattering the transmission for 1 mc² should exceed that for 2.5 mc² by so much. It is easier to believe that the difference in N_3/e^{-X} for the two energies is the consequence of error and that the observed behavior of the build-up factors for large X, although not proof of error larger than stated in Sec. 2, Part I, is nevertheless evidence of error.

This conclusion, however, must be accepted with reservation. In Table III, which gives values of N_1/e^{-X} and N_2/e^{-X} for the pure Compton scatterer, one finds that N_1/e^{-X} at $X=20$ has nearly the same value for both 1 mc² and 2.5 mc², but that the value of N_2/e^{-X} for 1 mc² exceeds the value for 2.5 mc² by about 30 percent. If a similar inequality holds for N_3/e^{-X}, as seems likely, then the 8 percent inequality observed in the case of iron may not be an error at all. If the 8 percent inequality in N_3/e^{-X} is not an error, then the 15 percent inequality in the build-up factor, in all probability, is not an error.

The preceding comparison of the transmission for 1 mc² and 2.5 mc² in the case of iron raises the question of how transmission depends on α_0 in general. The answer can be formulated best in terms of the pure Compton scatterer, since this fictitious material, considered on the basis of total absorption coefficient, is the most general, or at any rate the most fundamental, material.

Suppose that two beams, monoenergetic but of different energies, are normally incident, first one and then the other, on a slab of the pure Compton scatterer; then α_0 is the only variable that differs in the two cases. This difference appears in the calculations in two ways: (1) as a difference in the distribution of the angular deflection, and (2) as a difference in the function μ/μ_0.

Since large angles of deflection become more probable as the incident energy diminishes, one expects N_f, the probability of transmission with one collision, to decrease and expects N_b, the probability of reflection with one collision, to increase as α_0 decreases. This will certainly be true, unless the decrease in average slope of μ/μ_0 produces a sufficiently powerful countereffect. The slope of μ/μ_0 can act only through F_1 in the case of transmission and through a function very like F_1 in the case of reflection. The formula for F_1 shows that as X decreases to zero, the effect of the average slope of μ/μ_0 disappears. It follows that the expected decrease in N_f and the expected increase in N_b surely occur for thin slabs. This can be observed in the data of Table II, Part I, although it will be noticed that even a slab of thickness 0.5 mfp is not thin enough to cause N_f to decrease with α_0 when α_0 is large. It also follows that the build-up factor for very thin slabs will decrease as α_0 decreases. This can be seen in the build-up factors of Fig. 17, Part I.

As slab thickness increases, the average slope of μ/μ_0 begins to act powerfully, so that in suitable data one should be able to see evidence of its effect. The rise and

TABLE III. N_k/e^{-X} for photons of 0.2 mc² to 10 mc² normally incident on slabs of the pure Compton scatterer.[a]

X	α_0	N_1/e^{-X}	N_2/e^{-X}
1	10	0.445	0.178
	5	0.473	0.183
	2.5	0.489	0.179
	1.0	0.468	0.175
	0.2	0.390	0.144
8	10	1.42	1.19
	5	1.63	1.62
	2.5	1.77	1.86
	1.0	1.67	1.98
	0.2	1.30	1.60
20	10	2.22	2.53
	5	2.40	3.21
	2.5	2.88	4.16
	1.0	2.59	5.50
	0.2	1.88	4.81

[a] N_k is the probability that a photon will be transmitted with exactly k collisions; X is the thickness of the slab in mfp.

fall of N_f and N_{ff} in Table II, Part I, and of N_1/e^{-X} and N_2/e^{-X} ($N_1=N_f$, $N_2=N_{ff}$) in Table III as α_0 ranges between 10 and 0.2 is evidence of more than one cause of variation. In fact, if $\alpha_0=0.2$ had not been included in Table III, N_1/e^{-X} and N_2/e^{-X} for 20 mfp would have appeared to be monotonic decreasing functions of α_0 and, therefore, would have seemed to be governed almost entirely by the average slope. Hence, to the extent that transmission is controlled by photons which have experienced only forward scatterings, the effect of the average slope is to reverse, when X is sufficiently large, the relative positions of the curves for the build-up factors of Fig. 17, Part I.

However, photons, which have experienced one or

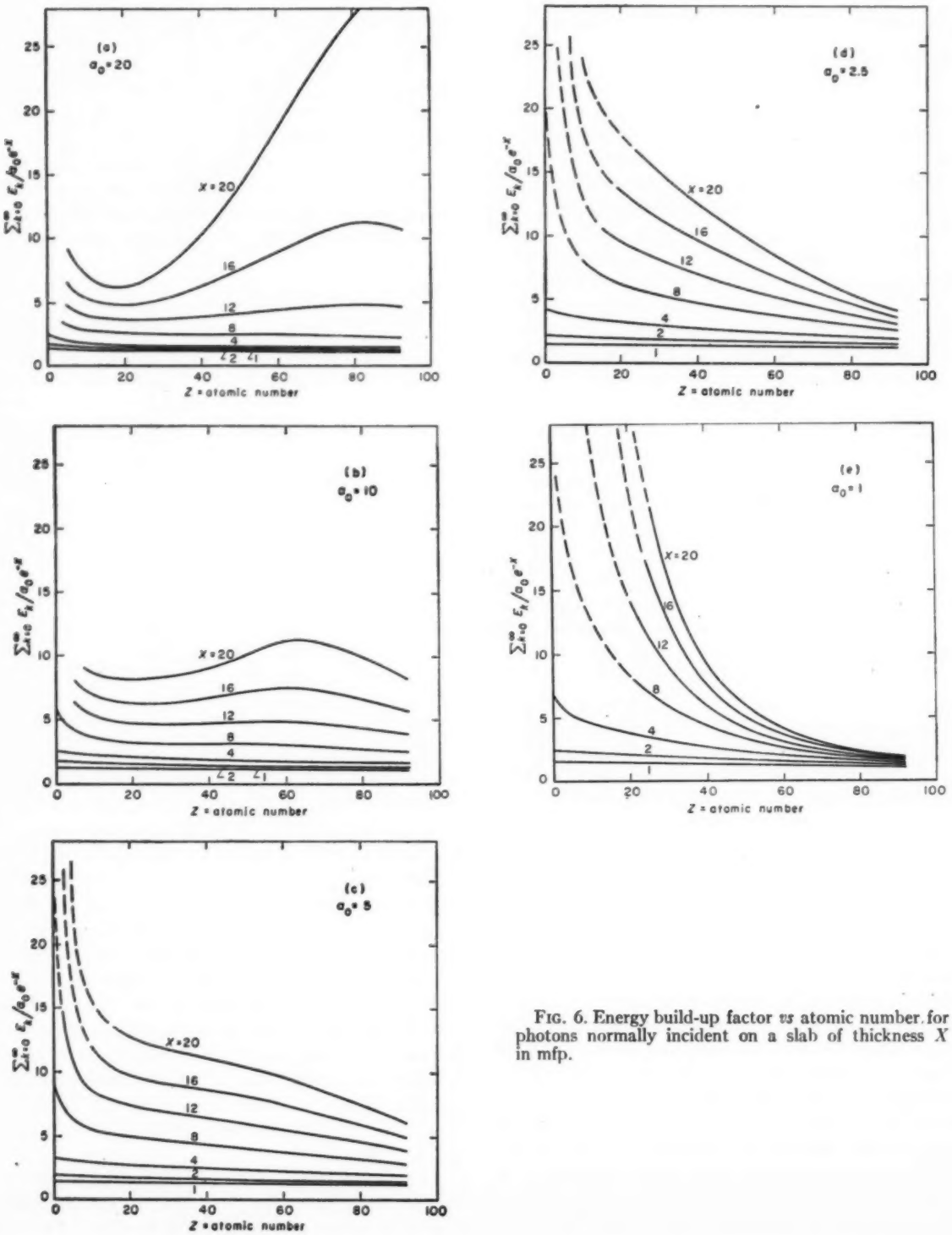

FIG. 6. Energy build-up factor *vs* atomic number for photons normally incident on a slab of thickness X in mfp.

more backward scatterings, are a large component of the transmission through even moderately thick slabs of the pure Compton scatterer. Therefore, the curves of Fig. 17, Part I, if determined for large values of X, will presumably not cross one over the other as X increases but, since photons in a long passage of many collisions tend to lose all "memory" of their incident energy, will approach each other asymptotically.

The discussion of the number build-up factor for an arbitrary material can be duplicated for energy with a few appropriate and obvious changes. Figure 6 gives the estimated energy build-up factors for slabs of an elemental material.

3. OTHER GEOMETRIES

If one knows the density of photons due to an isotropic point source in an infinite homogeneous medium, then by superposition one obtains the density arising from any configuration of point sources. In particular, if $p(r)$ is the density at the distance r from a point source of unit strength, the density $pl(x)$ at a distance x from a source plane of unit strength per unit area is readily found to be

$$pl(x)=\int_x^\infty 2\pi r p(r)dr.$$

Or again, if $l(y)$ is the density at a distance y from a line source of unit strength per unit length, then

$$l(y)=\int_y^\infty \frac{2rp(r)dr}{(r^2-y^2)^{\frac{1}{2}}}.$$

It is the intention here to apply these relations to the photon and energy densities arising from the four calculations by the thin-slab method of Sec. 3, Part I.

It will be recognized at once that the relation between $pl(x)$ and $p(r)$ does not hold for the densities calculated in Sec. 3, Part I, since the densities there come from slabs of finite thickness and planes of nonisotropic sources. Nevertheless, it may be possible to bring the integral relations to bear, if certain allowances are made.

The incident distributions of Sec. 3, Part I, correspond to a sheet of isotropic sources from which only those gamma rays in a cone of half-angle $\cos^{-1}$ 0.8 are accepted. The densities, therefore, are smaller than would be found had the full isotropic source been used. However, for large slab thickness, the density contribution of those photons whose angle of incidence exceeds $\cos^{-1}$ 0.8 is certainly small, so that beyond some thickness the density for the plane of isotropic sources can be considered as equal to the density calculated for the plane of nonisotropic sources. To get some indication of where the two densities might be expected to become nearly equal, one can refer to Fig. 8, Part I, which gives the distribution of the transmitted photons for three slab thicknesses. One finds in this figure that the discontinuities, which appear in the distributions of the transmitted photons because the full isotropic source was not used, may be expected to become negligible at a thickness of about 12 mfp. It seems reasonable, therefore, to assume that the two densities will have become approximately equal at about this thickness.

For thin slabs, the density corresponding to a plane of isotropic sources can be determined with fair accuracy from a calculation of the density of photons unscattered and once scattered. Suppose a calculation of this density, which is not a large task, is made for a thickness of 1 mfp. Then one has available for determining the density at the rear face of a slab of thickness X, when a sheet of isotropic sources lies in the front face, a value for $X=1$ and the approximate values (given in Sec. 3, Part I) for $X>12$. By drawing a curve passing through the point at $X=1$ and gradually approaching coincidence with the density curve calculated for the plane of nonisotropic sources, one should obtain a reasonably accurate curve of the density corresponding to a plane of isotropic sources.

This estimate, which is for a slab of finite thickness, must be converted to a like result for the infinite homogeneous medium. Clearly the density at a distance X from the source plane in an infinite homogeneous medium is greater than the density at the rear face of a slab of thickness X. But the difference is composed entirely of photons which have experienced at least one backward scattering. One would expect, therefore, in the case of the heavier materials such as iron and lead, that the absorption by the photoelectric effect would make the difference small. The difference in the density at $X=1$ was found to be about 10 percent. The important cause of the difference is those photons which pass through the slab without a collision but which are reflected back with one collision by the infinite medium. It seems likely that the difference would decrease percentagewise as X increases. For with increasing values of X, the difference must be composed more and more of reflected photons which have experienced several collisions at low energies. The probability of a photon's surviving several collisions in the low energy range is small.

The uppermost curve of the three curves displayed in each part of Fig. 7 gives the photon density (normalized by the factor c/e^{-X}, where c is the velocity of light) at a distance X from a plane of isotropic sources in an infinite medium. The materials are lead and iron, and the energies of the emitted photons are 20 mc^2 and 10 mc^2. In each of these four cases, the plane of isotropic sources is assumed to be emitting one photon per square centimeter per unit time. The photon densities are estimated in accordance with the preceding remarks. That is to say, the curve given is determined from an estimate of the densities at $X=1$ and $X>12$. At $X=1$, the 10 percent increase in the density for the infinite medium over the finite slab is taken, but as X increases to about 12 or 16, the difference between the two densities is allowed to dwindle to zero. This is equivalent

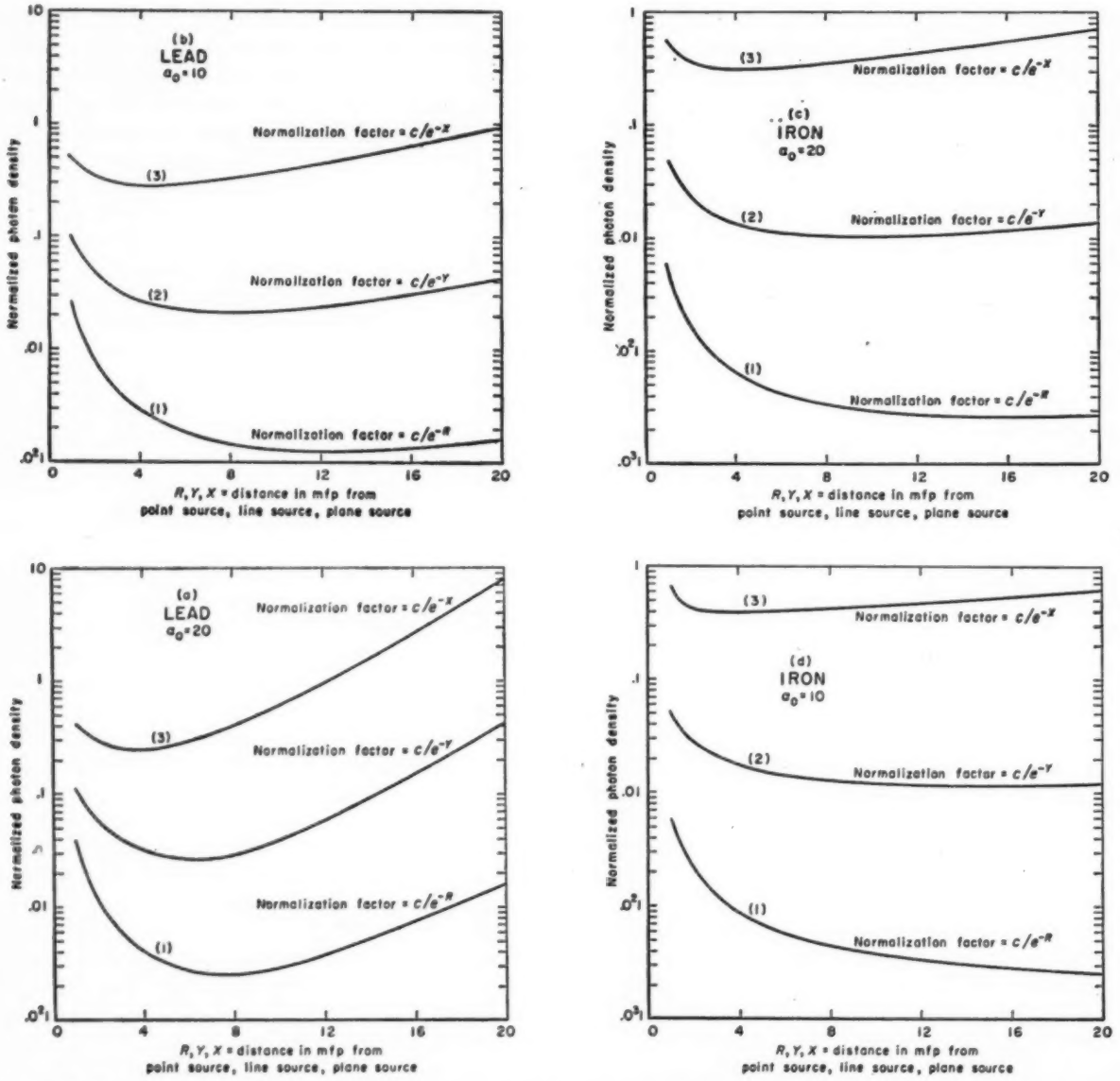

FIG. 7. Comparison of photon densities for three source configurations in an infinite homogeneous medium. The three source configurations are (1) point source of unit strength, (2) line source of unit strength per centimeter, and (3) plane source of unit strength per square centimeter (a source of unit strength is defined here as a source emitting one photon per unit time).

to assuming that beyond $X=12$ the density for the plane of isotropic sources in the infinite medium becomes identical with the density for the nonisotropic plane of sources and the slab of finite thickness.

The lowermost curve of the three curves presented in each part of Fig. 7 is obtained from the corresponding uppermost curve by means of the integral relation between $pl(x)$ and $p(r)$, given at the beginning of this section. Specifically, the lowest curve gives the photon density (normalized by the factor c/e^{-R}) at the distance R (in mean free paths) from a point source which emits in an infinite homogeneous medium one photon per unit time.

The middle curve is the photon density (normalized by the factor c/e^{-Y}) at a distance Y (in mean free paths) from a line source which emits in an infinite homogeneous medium one photon per centimeter per unit time. This curve is derived from the lowest curve by means of the integral relation between $l(y)$ and $p(r)$.

Figure 8 is identical with Fig. 7 except that the quantity under consideration is the energy density and the normalization factor contains $1/\alpha_0$.

The three curves forming a set are consistent.[3] So if it is assumed that the density for the plane source is accurate, then the densities for the line source and the

[3] Not only are the three curves of a set consistent with respect to the two integral relations stated, but also $pl(x)$ and $l(y)$ satisfy the relation

$$pl(x)=\int_x^\infty \frac{2yl(y)dy}{(y^2-x^2)^{\frac{1}{2}}}.$$

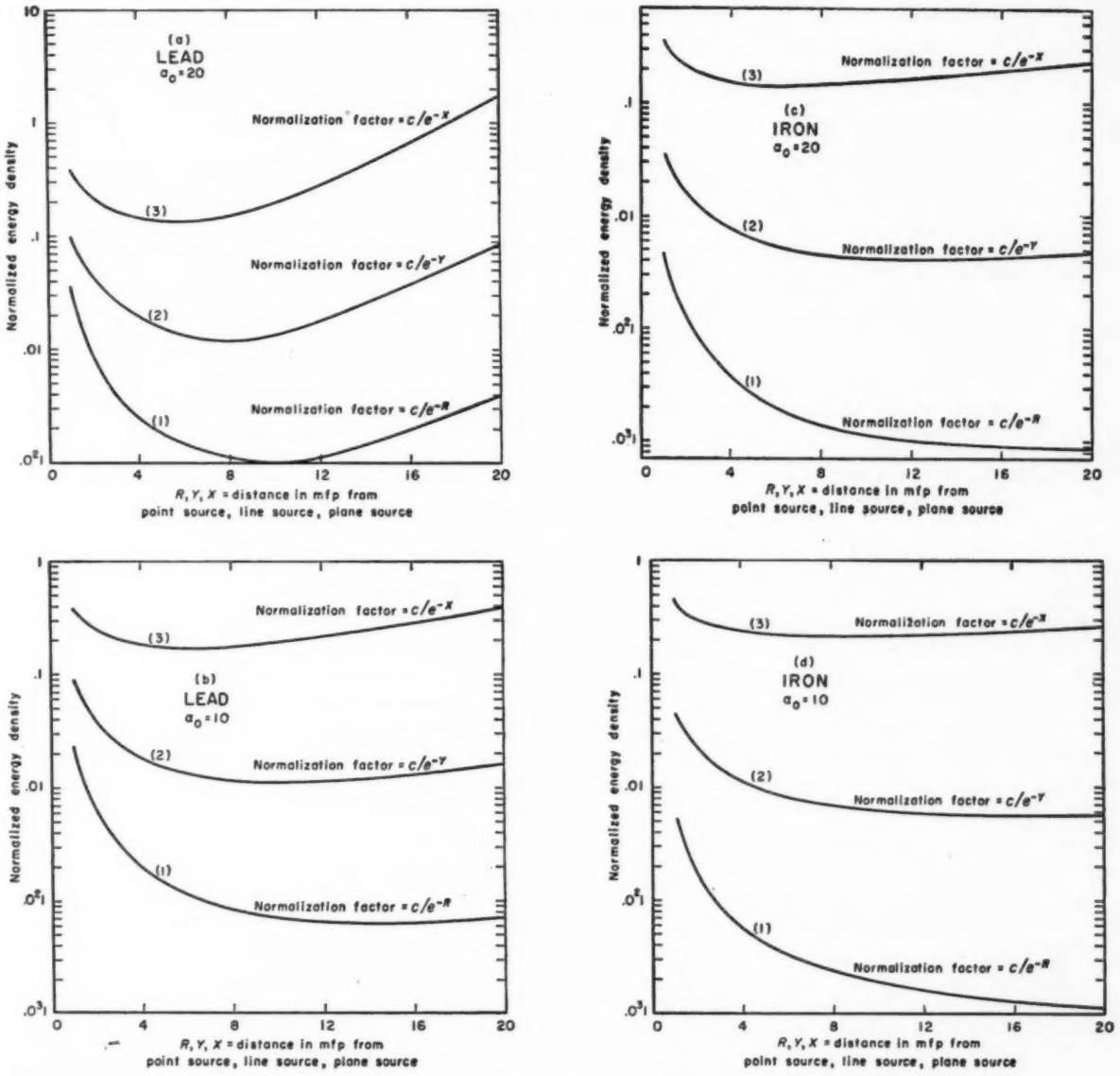

FIG. 8. Comparison of energy densities for three source configurations in an infinite homogeneous medium. The three source configurations are (1) point source of unit strength, (2) line source of unit strength per centimeter, and (3) plane source of unit strength per square centimeter (a source of unit strength is defined here as a source emitting one photon per unit time).

point source are also accurate. Whether or not the density for the plane source is reasonably accurate is difficult to say. It would seem that the errors, though possibly large, should be small enough to allow the set of three densities given to retain some interest. To be sure, the density corresponding to the point source is obtained by a numerical evaluation of a derivative, so that the error associated with the plane source is likely to be aggravated in the passage from plane source to point source, but if the assumptions under which the key density is obtained are not altogether erroneous, the error in the derived densities should not be serious in terms of practical attenuation calculations. In any case, the relative position of one curve to another has interest as an indication of the effect of geometry, even if the absolute position is judged to be too much in error to have value.

4. ACKNOWLEDGMENT

During the course of this work, the author has consulted Professor Milton S. Plesset a great many times. The author wishes to thank Professor Plesset for the considerable assistance given during these consultations and also for reading the manuscript.

Microwave Diffraction Measurements in a Parallel-Plate Region*

RONALD V. ROW
Cruft Laboratory, Harvard University, Cambridge, Massachusetts
(Received April 20, 1953)

Many infinite two-dimensional electromagnetic-scattering problems are strictly equivalent to the configuration obtained from the image principle by placing a finite-scattering obstacle between two parallel, infinite, and perfectly conducting planes and illuminating it with a plane or cylindrical incident wave confined to the parallel-plate region.

An experimental approximation to this arrangement is described for use in the 3-centimeter wavelength region. Finite rectangular parallel metal plates support a transverse incident electromagnetic wave with the electric field oriented perpendicular to the plates. Absorbing wedges at the boundary of the region reduce reflections from this discontinuity. The electromagnetic field scattered from any particular obstacle may be investigated by means of a dipole probe introduced into the region through a moveable section of one of the plates.

The success of this technique is demonstrated by comparing measurements of the total field scattered by infinite conducting wedges of included angle 0, 45, and 90 degrees with the known theoretical expressions, for perpendicular incidence. Agreement with theory is good.

The effect of finite thickness of the diffracting screen (case of 0° wedge) in increasing the amplitude of the scattered wave is noted and compared to theoretical results derived for scattering from a thin conducting half-plane with a cylinder superimposed on the edge.

I. INTRODUCTION

SEVERAL two-dimensional electromagnetic scattering problems involving a plane wave incident on an infinite obstacle with essentially cylindrical symmetry have been investigated theoretically through the use of scalar wave fields, and a complete list of the theoretical contributors to these problems would take too much space here. Using modern microwave techniques many of these problems have been investigated experimentally[1–6] for obstacles as large as several wavelengths in cross-sectional dimension. The experimental arrangements used necessarily involve several approximations to the idealized theoretical model. Kodis[3] has pointed out the advantages of using a single-image plane to isolate the experimenter and measuring equipment from the field being measured. In the same paper, Kodis points out that the non-uniform illumination of a large rectangular screen (approximating a half-plane) occasioned by the use of a point source does not give measurements in good agreement with the well-known theory for this case. This lack of agreement between theory and experiment has led to the development of a parallel-plate region in which both the obstacle and source are, essentially, infinite in extent by virtue of the electromagnetic-image principle.

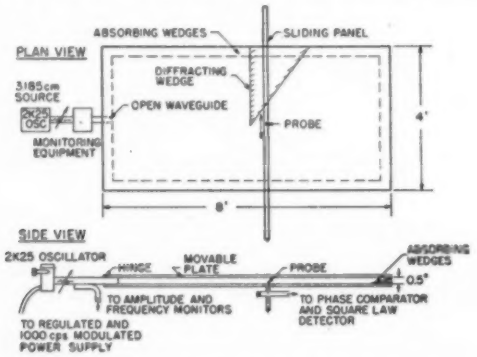

FIG. 1. Schematic layout of parallel-plate region and microwave components.

II. DESCRIPTION OF APPARATUS

The infinite parallel-plate region is approximated experimentally as shown in Fig. 1 by two-plane, parallel 4-ft by 8-ft rectangular duralumin sheets (38 by 76 wavelengths at an operating wavelength of 3.185 cm) spaced ½-in. apart with absorbing wedges inserted along the edges. A line source is approximated by the imaging of the open end of a standard 1-in. by ½-in. *X*-band wave guide in the parallel plates, and fed from a 1000 cycles/sec square-wave modulated 2K25 reflex-klystron. The spacing of the plates is 0.40 wavelength and is less than half a free-space wavelength, even allowing for spacing variations of 0.020 in., so that the incident wave will be pure transverse electromagnetic in the region occupied by the obstacle and measuring probe. The probe is a dipole antenna less than ¼-wavelength long formed by the continuation of the center conductor of a low-impedance coaxial line, and responds to the electric field perpendicular to the plates. It is inserted into the region through a 0.034-in. hole in a sliding panel section of the lower plate and may be moved a distance of 19

* This research was made possible through support extended Cruft Laboratory, Harvard University, jointly by the Navy Department (U. S. Office of Naval Research), the Signal Corps of the U. S. Army, and the U. S. Air Force, under U. S. Office of Naval Research Contract N5ori-76, T.O. 1.

[1] C. W. Horton and R. B. Watson, J. Appl. Phys. **21**, 16–21 (1950).
[2] B. N. Harden, Proc. Inst. Elec. Engrs., Pt. III, **99**, 229–235 (1952).
[3] R. D. Kodis, J. Appl. Phys. **23**, 249–255 (1952).
[4] M. J. Ehrlich, University of California Antenna Laboratory Report (June, 1951).
[5] Esau, Ahrens, and Kebbel, Hochfrequenz. und Electroakustik **53**, 113–115 (1939).
[6] W. E. Groves, University of California Antenna Laboratory Report 179, series 7 (1952).

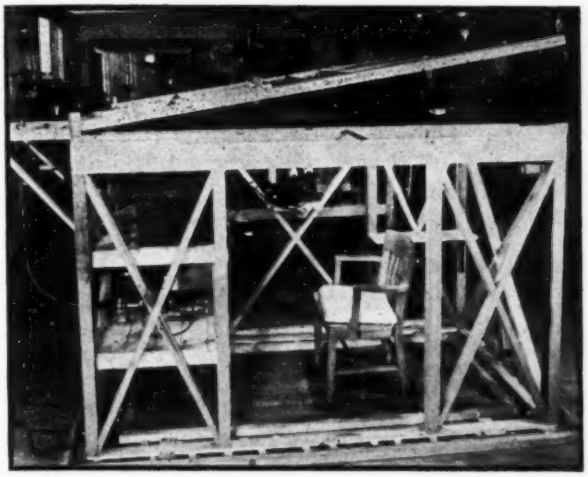

FIG. 2. General view of equipment with parallel plates open.

wavelengths along a straight line; its position being measured within 0.01 cm by means of a scale and vernier. The coaxial line from the probe drives one arm of a wave-guide magic-T phase comparator.[7] For amplitude measurements, the phase-reference signal is disconnected and the detected signal from one side arm of the magic-T amplified. This equipment allows phase and amplitude measurements accurate, at best, to within three degrees and 0.2 db, respectively, over an amplitude range of approximately 40 db. The measuring equipment is located underneath the parallel plate region as shown in Fig. 2.

The absorbing wedges located at the edge of the parallel plate region are made of maple wood coated with colloidal carbon, and reduce the voltage standing-wave ratio in the region traversed by the probe to about 1.05. Measurements of the amplitude and phase distribution from the source, show it to be closely approximated by a line source with its phase center placed approximately in the center of a short side of the region at a point 39.7 wavelengths from the line of probe travel, and this spacing was used in subsequent measurements.

The element of a conducting wedge inserted between the parallel plates is made by forming 0.003-in. silver foil over the edge of a $\frac{1}{2}$-in. thick polyfoam wedge. This resilient structure helps to insure good electrical contact between the wedge and parallel plates, and as an additional precaution, the contacting surfaces of the wedge were coated with a slow-drying silver paint.

III. COMPARISON OF THEORY AND MEASUREMENTS

As an example of its application, the apparatus just described has been used to measure the relative amplitude of the total electric field along a line parallel to and 4 wavelengths behind the illuminated face of conducting wedges of included angles 0, 45, and 90 degrees.

[7] T. Morita and L. S. Sheingold, "A Coaxial Magic-T," Cruft Laboratory Report No. 162, Harvard University (October, 1952).

The theoretical solution to this problem is well known.[8,9] Using the time dependence $e^{-i\omega t}$, the electric field $E_z(x, y)$ satisfies the two-dimensional wave equation,

$$(\nabla_{x,y}^2+k^2)E_z(x, y)=0, \quad k=2\pi/\lambda, \tag{1}$$

subject to the boundary condition that E_z vanish on the surfaces of the wedge, and that the scattered field satisfy the radiation condition at infinity. For a plane wave incident normally on a wedge as shown in Fig. 3, Macdonald[8] gives a solution in terms of the Bessel functions of the first kind,

$$E_z(r, \theta)=\frac{4\pi}{\theta_0}\sum_{n=1}^{\infty}\sin\frac{n\pi^2}{2\theta_0} \times\left(\exp-i\frac{n\pi^2}{2\theta_0}\right)J_{n\pi/\theta_0}(kr)\sin\frac{n\pi}{\theta_0}\theta. \tag{2}$$

Using Sommerfeld's contour integral representation for the Bessel function $J_{n\pi/\theta_0}(kr)$ and interchanging the order of summation and integration, Macdonald's integral formula is obtained. For large kr, the method of steepest descents applied to this integral yields the following approximate formula for the field,

$$E_z(r, \theta)=\frac{\exp(-i\frac{1}{4}\pi+ikr)}{2\theta_0}\left(\frac{2\pi}{kr}\right)^{\frac{1}{2}}\sin\frac{\pi^2}{\theta_0} \times\left(\frac{1}{\cos\pi^2/\theta_0-\cos\pi/\theta_0(\theta-\pi/2)} -\frac{1}{\cos\pi^2/\theta_0-\cos\pi/\theta_0(\theta+\pi/2)}\right). \tag{3}$$

This formula is not valid for angles near $\theta=3\pi/2$, i.e., along the light-shadow boundary, but away from this

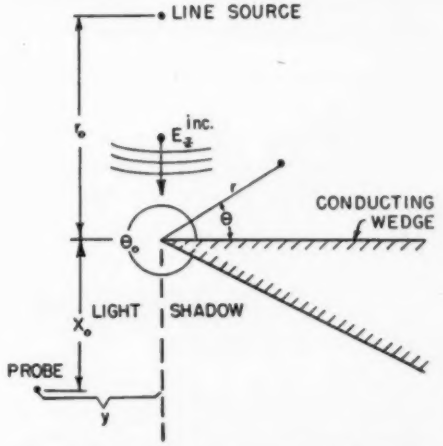

FIG. 3. Coordinate system for scattering from a wedge.

[8] H. M. Macdonald, *Electric Waves* (Cambridge University Press, Cambridge, 1902), p. 186.
[9] A. Sommerfeld, Math. Ann. 45, 263 (1894).

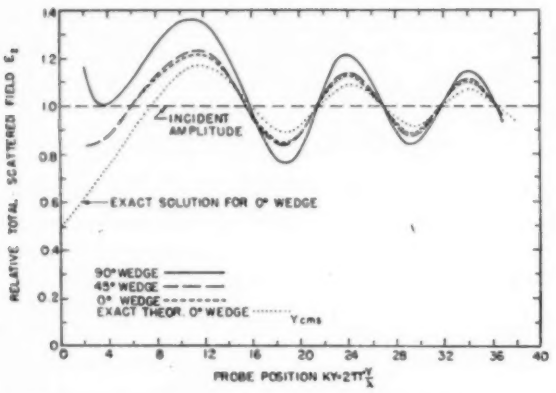

FIG. 4. Theoretical scattered field from wedges of various angles, computed from the saddle-point formula. (Phase corrected for a line source.)

boundary it shows the correct trend in the field as the angle θ_0 of the wedge is varied (see Fig. 4).

With a wedge of angle $\theta_0=2\pi$, the problem reduces to the well-known half-plane problem for which we have Sommerfeld's[9] solution,

$$E_z(r,\theta)=\exp(-ikr\sin\theta)+\frac{\exp(-i\frac{1}{4}\pi)}{\sqrt{\pi}}\exp(-ikr\sin\theta)\times\int_0^{(2kr)^{\frac{1}{2}}\cos\frac{1}{2}(\theta-\pi/2)}(\exp i\zeta^2)d\zeta, \quad (4)$$

valid in the region $\pi/2<\theta\leq 3\pi/2$.

In this last formula, the first term, $\exp -ikr\sin\theta=\exp -ikx$, represents the incident plane wave, and the second term represents the wave scattered by the half-plane.

Carslaw[10] has solved the same boundary value problem for a line-source of primary excitation. His results show for a large source to screen separation and for points not too far from the edge of the screen, that the scattered field is the same as the scattered field for plane-wave incidence multiplied by the factor $1/\sqrt{r_0}$, where r_0 is the separation between the line source and the edge. In making measurements the field at the point $x=x_0=4\lambda$, $y=0$ was used as a reference, hence the field at the edge is greater than this reference field by the factor $(r_0+x_0/r_0)^{\frac{1}{2}}$. Thus, in plotting the theoretical results for comparison with the relative measured field in Figs. 5 and 6 the formula

$$|E_z(r,\theta)|=\left|e^{i\phi(y)}+\left(\frac{r_0+x_0}{r_0}\right)^{\frac{1}{2}}\frac{\exp -i\frac{1}{4}\pi}{\sqrt{\pi}}\times\int_0^{(2kr)^{\frac{1}{2}}\cos\frac{1}{2}(\theta-\frac{1}{2}\pi)}(\exp i\zeta^2)d\zeta\right|, \quad (5)$$

was used. Where $\phi(y)$ is the phase corresponding to a line source located 35.7 wavelengths from the diffracting edge along a line perpendicular to the screen and passing through the edge. The integral in Eq. (5) is readily computed using tables of the Fresnel Integrals.

For the half-plane case there is excellent agreement between theory and measurements, certainly within the limits of reproducibility of the data. For the 45 and 90 degree wedges the theory is only approximate, and the experimental results confirm the trend predicted by theory.

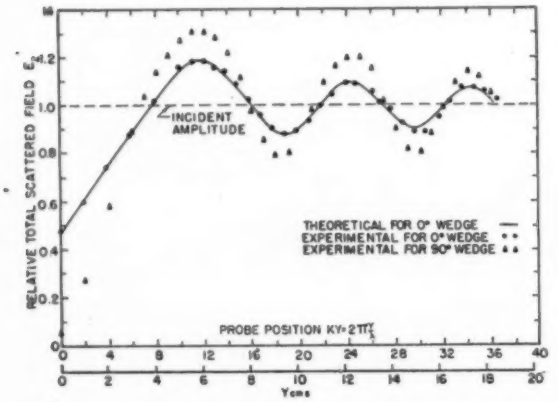

FIG. 5. Measured diffraction patterns from 0° and 90° wedges (line source).

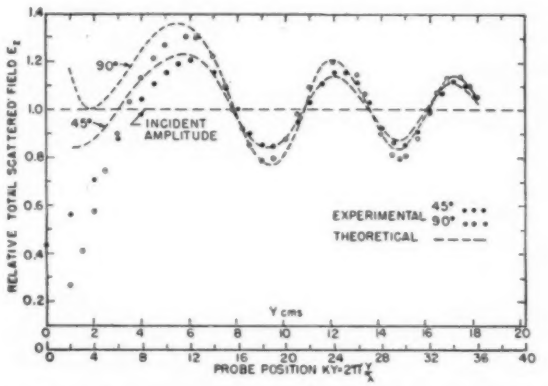

FIG. 6. Approximate theoretical and measured diffraction patterns from 45 and 90 wedges (line source).

IV. EFFECT OF EDGE THICKNESS

The exact theory for diffraction by a half-plane considers only the case where the plane is of zero thickness. However, the screen used in any experiment has some thickness, and it is important to know just what effect this thickness will have on the measurements. From simple physical considerations it is to be expected that regardless of its precise shape, a small increase in the thickness of the edge of a very thin screen will result in a corresponding linear increase in the amplitude of the scattered wave. Figure 7 shows results measured with rectangular edges of thickness 0.0024 wavelength, 0.125 wavelength, and 0.250 wavelength. In addition the exact theoretical result for the ideal half-plane is shown

[10] H. S. Carslaw, Proc. London Math. Soc. (1) **30**, 121 (1899).

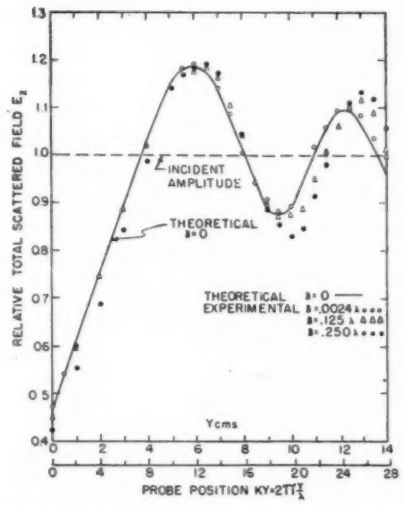

FIG. 7. Measured diffraction from a rectangular edge for different thicknesses (line source).

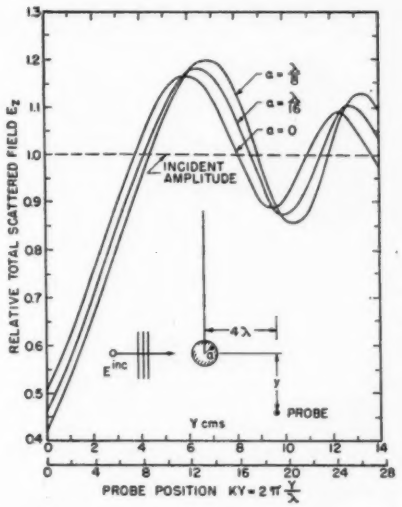

FIG. 9. Theoretical diffraction pattern from a half plane with a cylindrical edge (phase corrected for a line source).

for comparison. These indeed show an increase in the scattered wave, and a slight shift in the location of maxima and minima as the thickness increases above 0.125 wavelength. The successful theoretical analysis of diffraction by a rectangular edge remains as an unsolved problem.† However, Karp[11] has obtained the following solution to the problem of diffraction by a half-plane with a cylinder superimposed on the edge as shown in Fig. 8.

For a plane wave incident normally on a half plane the series solution (2) reduces to

$$E_z(r,\theta)=2\sum_{n=1}^{\infty}\sin\frac{n\pi}{4}e^{-in\frac{1}{4}\pi}J_{n/2}(kr)\sin\frac{n\theta}{2}.$$

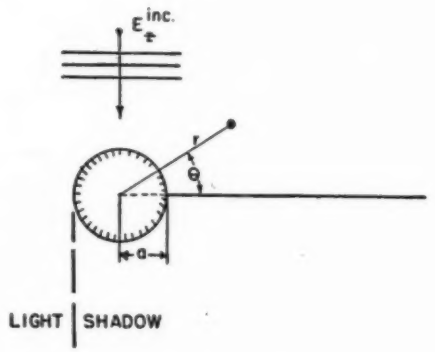

FIG. 8. Coordinate system for scattering from a half plane with a cylindrical edge (line source).

If from this result the series,

$$E_c(r,\theta)=2\sum_{n=1}^{\infty}\sin\frac{n\pi}{4}e^{-in\frac{1}{4}\pi}\times\frac{J_{n/2}(ka)}{H_{n/2}^{(1)}(ka)}H_{n/2}^{(1)}(kr)\sin\frac{n\theta}{2}, \quad (6)$$

is subtracted, the resultant field

$$E_z^{tot}(r,\theta)=E_z(r,\theta)-E_c(r,\theta), \quad (7)$$

satisfies the wave equation and vanishes on the conducting boundary surfaces.

Figure 9 shows a plot of Eq. (7) for cylinder radius $a=0$, $\lambda/16$ and $\lambda/8$, as the point of observation moves along a straight line parallel to and 4 wavelengths

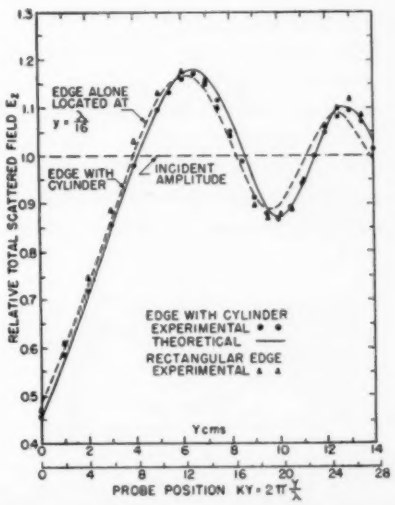

FIG. 10. Theoretical and measured diffraction from a half plane with a circular-cylindrical edge of radius=λ/16 and a rectangular edge of thickness=λ/8 (line source).

† In a recent paper D. S. Jones [Proc. Roy. Soc. (London) A217, 153 (1953)] gives the solution to this problem. However, no results were given in a form allowing comparison with the measurements made here.

[11] S. N. Karp, Progress Reports Nos. 8, 9 and 10, Washington Square College of Arts and Sciences, New York University.

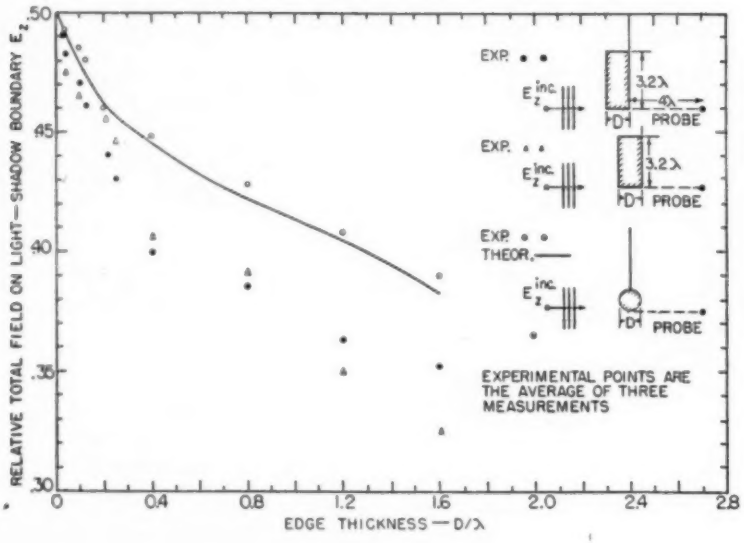

FIG. 11. Measured and theoretical field on the light-shadow boundary for a half plane with a cylindrical edge and measured field for a half plane with a rectangular edge (phase corrected for a line source).

behind the illuminated side of the screen. Figure 10 shows a comparison between theory and measurements for diffraction by a half plane with a cylindrical a swell as a rectangular edge of $\frac{1}{8}$-wavelength diameter.

For $ka<0.1$ the first term of the series (6) provides an accurate correction (within about 1 percent) to the field from the half-plane alone. For the field on the light-shadow boundary four wavelengths behind the screen this correction gives,

$$|E_z^{\text{tot}}| \simeq \tfrac{1}{2} - \frac{ka}{2\pi} + \left(\frac{ka}{2\pi}\right)^2 + \cdots. \tag{8}$$

This formula should also give a good indication of the behavior of the field on the light-shadow boundary in the case of diffraction by a thin screen with a rectangular edge of thickness $2a$. Figure 11 presents theoretical and experimental results for the relative total field on the light-shadow boundary for the circular edge, and in addition experimental results for the rectangular edge. As expected, for ka small ($ka<0.03$) there is agreement, within the reproducibility of the measurements, between the measured field on the light-shadow boundary with both the rectangular and circular edge, and the theory for the circular edge. The agreement between theory and experiment for the circular edge is good over the entire range of cylinder diameters measured.

V. CONCLUSIONS

The use of a parallel plate region provides an excellent approximation to an ideal two-dimensional space for the experimental study of a number of electromagnetic scattering problems. Measurements are, of course, limited to cases where (1) the incident electric field is oriented perpendicular to the parallel plates and (2) the obstacle is periodic in at least one direction. The problem of obtaining a closer approximation to plane-wave excitation than that afforded by the present line source still remains unsolved. However, even within this limitation, the apparatus remains a useful companion tool with theory in further investigations of scattering problems in the region between the quasistatic and optical limits. Investigations of the scattering by closely coupled circular cylinders and a pair of parallel slits in two parallel screens are now active.

ACKNOWLEDGMENT

The writer wishes to express his appreciation to Miss L. Gerould and Mrs. E. McGarvey for computations made from the theory and to Dr. S. N. Karp of New York University for communicating his solution to the cylindrically-tipped half-plane problem. Professor R. W. P. King and Dr. R. D. Kodis helped frequently with criticisms and suggestions.

JOURNAL OF APPLIED PHYSICS VOLUME 24, NUMBER 12 DECEMBER, 1953

Theory of the Formation of Bubbles

SHUNSUKE TAKAGI
Tokyo University of Agriculture and Technology, Fuchu-machi, Tokyo, Japan
(Received April 22, 1953)

We have not yet obtained a perfect theory of bubble formation. In this paper the perfect theory of the formation of bubbles in the case where the bubbles of vapor are nucleated spontaneously in pure liquid is presented. This is done by the systematization of the classical theory of M. Volmer (*Kinetik der Phasenbildung*, 1939) and the theory of D. Turnbull and J. C. Fisher [J. Chem. Phys. **17**, 71 (1949)] and it coincides satisfactorily with the experiment of K. L. Wismer [J. Phys. Chem. **26**, 301 (1922)].

Theory must be advanced further so as to afford a perfect explanation of the processes of boiling, cavitation and the critical phenomena of the movement of soil moisture [S. Takagi, *Monographs on Theoretical Soil Physics; Theoretical Considerations on the Thermodynamical and Kinematic Properties of Soil Moisture* (not yet published)]. To effect this object, the author has calculated the rate of formation of bubbles at a surface. The theoretical value, however, of the negative pressure at which the liquid fractures does not coincide by any means with the atmospheric pressure in the process of boiling. This is true also in the process of cavitation and in the process of critical phenomena of the movement of soil moisture. Some other factors must be introduced in order to bring the theory to a state of practical value.

PREPARATORY CONSIDERATIONS

THE condition for the stability of a bubble is written, denoting with $\bar{G}_b$ and $\bar{G}_l$ the chemical potentials per molecule in the bubble and liquid state respectively, as

$$(\bar{G}_b-\bar{G}_l)dn+(P-p)dV_b+\sigma dA_b=0, \tag{1}$$

where V_b means the volume, A_b the surface area of the bubble, n the number of gas molecules in the bubble, P the pressure of liquid, p the vapor pressure in the bubble, and σ the surface tension. If we may assume the bubble as spherical and n and V_b as independent, the conditions for the stability of the bubble are gotten as

$$\bar{G}_b=\bar{G}_l \tag{2}$$

and

$$p=P+2\sigma/r, \tag{3}$$

where r is the radius of the bubble assumed as spherical. The bubble, which satisfies both Eqs. (2) and (3), may be called here the *equilibrium nucleus*.

$\bar{G}_b$ and $\bar{G}_l$ is usually defined as

$$\bar{G}_b=G_\infty+kT\ln(p/p_\infty), \tag{4}$$

and

$$\bar{G}_l=G_\infty+(P-b)\bar{V}_w, \tag{5}$$

respectively, where G_∞ means the chemical potential per molecule of liquid water and water vapor, which are in thermal equilibrium with each other at vapor pressure p_∞ and temperature T°K, k the Boltzmann's constant, M the molecular weight, b the pressure of the liquid at the datum state and $\bar{V}_w$ the volume of liquid per molecule. The formula (4), however, is valid, as shown clearly in its derivation,[1] only for the *mechanically stable bubble*, of which the vapor pressure is defined by Eq. (3). The forms of the bubbles other than the mechanically stable ones are neither constant nor spherical.[2] The mass transfer always takes place between the bubble and the liquid, except for the bubbles which satisfy Eq. (2). In the present paper, however, we will treat only mechanically stable bubbles, and consider their gradual growth, as in the case of all the existing theories. Whether this assumption is warranted or not is not clear *a priori*. But we may think this permissible, when there is no agitation from outside sources and when bubbles are permitted to grow quietly.

Let us calculate the work W_n necessary to form a mechanically stable bubble. From the definition of chemical potential, we get

$$W_n=\int_0^n(\bar{G}_\nu-G_\infty)d\nu,$$

$$=kT\int_0^n\ln\frac{p_\nu}{p_k}\cdot d\nu, \tag{6}$$

where p_k stands for the vapor pressure of the equilibrium nucleus, $\bar{G}_\nu$ and p_ν the chemical potential and vapor pressure of the bubble composed of ν molecules. Assuming the vapor in the bubble as ideal, Eq. (6) is integrated to

$$W_n=\left[\nu kT\cdot\ln\frac{p_\nu}{p_k}\right]_0^n-\int_0^{r_n}\frac{\nu kT}{p_\nu}\frac{dp_\nu}{dr_\nu}\cdot dr_\nu,$$

$$=nkT\cdot\ln\frac{p_n}{p_k}+\frac{\sigma A_n}{3}, \tag{7}$$

where p_n means the vapor pressure, r_n the radius, and

[1] The chemical potential of a bubble which is not necessarily mechanically stable is

$$\bar{G}_b=G_\infty+kT\ln(p/p_\infty)+(P-p+2\sigma/r)v,$$

where v is the volume assigned to one molecule of vapor at pressure p. This equation, however, may not hold true accurately, because exact thermodynamical treatment will not be allowed to these bubbles.

[2] Compare M. Kornfeld and L. Suvorot, J. Appl. Phys. **15**, 495 (1944).

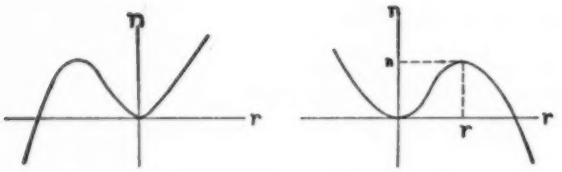

(a) $P>0$ (b) $P<0$

FIG. 1. To explain the rupture nucleus.

A_n the surface area of the bubble of n molecules.[3] Here the radius of the zero-molecule bubble is put equal to zero by Eq. (9) below. Equation (8) may be obtained in another way. The work necessary to form a vacant hole of V_n in liquid is $PV_n+\sigma A_n$, where V_n is the volume of the bubble of n molecules. Next, n molecules of the vapor under pressure p_k must be turned to the vapor of pressure p_n, and the work necessary for this change is $nkT\ln(p_n/p_k)$. When this vapor is introduced in the vacant hole of volume V_n, we need the work $-p_nV_n$. We obtain, therefore,

$$W_n=nkT\ln(p_n/p_k)+\sigma A_n+(P-p_n)V_n. \tag{8}$$

This is the same as (7).

The equation of state of the bubble is gotten as

$$n=(4\pi/3kT)r^2(Pr+2\sigma), \tag{9}$$

by the assumption of the ideality of the vapor. The graph of this equation is shown in Fig. 1. When $P>0$, n increases monotonously with r in the region of physical significance, i.e., in the region $r>0$ and $n>0$; but when $P<0$, n reaches the maximum

$$n_*=128\pi\sigma^3/81kTP^2 \tag{10}$$

at

$$r_*=4\sigma/3(-P). \tag{11}$$

But in the region $r>r_*$, n decreases monotonously with r. This means that the bubble enlarges itself spontaneously with no feeding of liquid molecules from without. Therefore, this may be taken as the rupture of liquid. The bubble of radius r_* and the number of vapor molecules n_* may be designated as the *rupture nucleus* in the present paper.

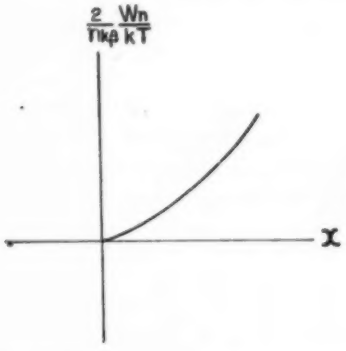

FIG. 2. Graph of $(2/n_k\beta)\times(W_n/kT)$ as function of x. Case I (when $P>p_k$, $\beta<0$).

To make systematical treatment, we put

$$x=r/r_k, \tag{12}$$

$$\beta=(p_k-P)/p_k=2\sigma/r_kp_k, \tag{13}$$

$$\bar{x}=\beta/(\beta-1), \tag{14}$$

and

$$x_*=r_*/r_k=(2/3)\bar{x}, \tag{15}$$

where r_k means the radius of the equilibrium nucleus. Using these notations W_n and its derivatives are expressed as

$$\frac{2}{n_k\beta}\frac{W_n}{kT}=2x^3\left(\frac{1}{x}-\frac{1}{\bar{x}}\right)\ln\beta\left(\frac{1}{x}-\frac{1}{\bar{x}}\right)+x^2 \tag{16}$$

and

$$\frac{2}{n_k\beta}\frac{d}{dx}\frac{W_n}{kT}=4x^2\left(\frac{1}{x}-\frac{1}{x_*}\right)\ln\beta\left(\frac{1}{x}-\frac{1}{\bar{x}}\right), \tag{17}$$

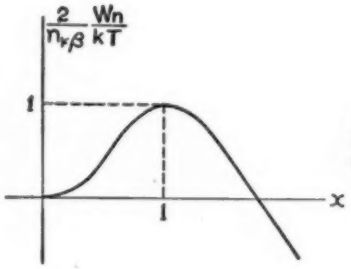

FIG. 3. Graph of $(2/n_k\beta)\times(W_n/kT)$ as function of x. Case II (when $0\leqq P<p_k$, $0<\beta\leqq 1$).

where n_k is the number of molecules of equilibrium nucleus, expressed by the formula

$$\frac{W_k}{kT}=\frac{\sigma A_k}{3kT}=\frac{n_k\beta}{2}, \tag{18}$$

W_k and A_k being the respective quantities of the equilibrium nucleus. The work to form the rupture nucleus is expressed as

$$W_*/kT=(n_k\beta/2)\cdot\gamma, \tag{19}$$

where

$$\gamma=x_*^2(1-(2/3)\ln\bar{x}). \tag{20}$$

The extreme values of W_n occur at $x=1$, i.e., at the equilibrium nucleus, and at $x=x^*$, i.e., at the rupture nucleus.

The dependence of W_n on x is visualized in the following.

Case I. When $P>p_k$, i.e., $\beta\leqq 0$, W_n increases monotonously with x (compare Fig. 2). In this case $\bar{x}$ is the lower limit of x, while in the following cases the relation $\beta>0$ holds true, and $\bar{x}$ becomes the upper limit of x, so long as $\bar{x}>0$.

[3] Fisher (reference 4) and Fürth (reference 5) use erroneous formulas for W_n. Volmer-Döring's formula (references 6 and 7) coincides with Eq. (7).

[4] J. C. Fisher, J. Appl. Phys. **19**, 1062 (1948).

[5] R. Fürth, Proc. Cambridge Phil. Soc. **37**, 276 (1941).

[6] M. Volmer, *Kinetik der Phasenbildung* (Theodor Steinkopf, Dresden and Leipzig, 1939).

[7] W. Döring, Z. Physik. Chem. **B36**, 371 (1937); **B38**, 292 (1938).

Case II. When $0<\beta\leqq 1$, i.e., $0\leqq P<p_k$, the curve has only one maximum, and continues to $x=+\infty$ (compare Fig. 3).

Case III. When $1<\beta\leqq 3$, i.e., $-2p_k<P<0$, the curve reaches the maximum at the equilibrium nucleus, and the minimum at the rupture nucleus (Fig. 4).

Case IV. When $\beta=3$, i.e., $P=-2p_k$, the equilibrium and the rupture nucleus coincide and form a point of inflexion (Fig. 5).

Case V. When $\beta>3$, i.e., $P<-2p_k$, the curve reaches the maximum at rupture nucleus and the minimum at the equilibrium nucleus (Fig. 6).

THE FRACTURE OF LIQUID BY NUCLEATION WITHIN LIQUID

Theory

Following the theory of Turnbull and Fisher,[8] we get the differential equation,

$$\frac{dZ_n}{dn}+Z_n\cdot\frac{1}{kT}\frac{dW_n}{dn}=-jr_n^{-2}, \tag{21}$$

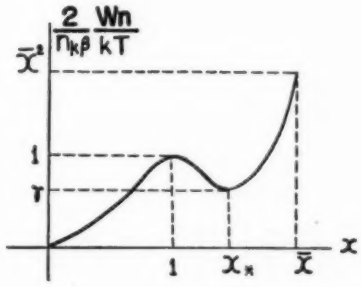

FIG. 4. Graph of $(2/n_k\beta)(W_n/kT)$ as function of x. Case III (when $-2p_k<P<0$, $1<\beta<3$).

where

$$j=J\Big/\left(\frac{akT}{h}\cdot 4\pi\cdot\exp(-\Delta f/kT)\right). \tag{22}$$

The meaning of the notations is as follows; J is the rate of the formation of equilibrium or rupture nuclei ($1/\text{cm}^3$ sec); a, the transmission coefficient used in the theory of rate processes; Δf the mean activation energy; Z_n, the concentration of the bubbles composed of n molecules; and h, Planck's constant. This equation can be solved, whatever expression W_n may take, as

$$Z_n=\exp(-W_n/kT)\left[N-j\cdot\frac{4\pi}{kT}\right.$$
$$\left.\times\int_{r_0}^{r_n}\left(1+\frac{4\sigma}{3r_\nu}\right)\exp(W_\nu/kT)dr_\nu\right], \tag{23}$$

where r_0 is the radius of the minimum bubble. The integration constant of this equation is determined as N, the number of liquid molecules per unit volume, because the relation $Z_0=N\exp(-W_0/kT)$ holds fairly constant

[8] D. Turnbull and J. C. Fisher, J. Chem. Phys. **17**, 71 (1949).

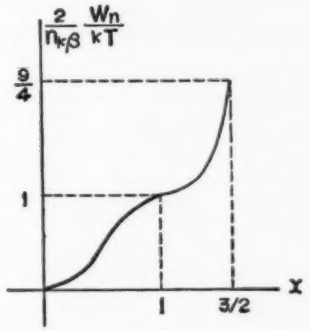

FIG. 5. Graph of $(2/n_k\beta)\times(W_n/kT)$ as function of x. Case IV (when $P=-2p_k$, $\beta=3$).

when Z_0 and W_0 mean the respective quantities of the bubble of the minimum number of molecules.

The physical meaning of J is explained according to Volmer[6] as follows. The liquid will explode in a moment, and the state of tension ($P<0$) will be brought to end, as soon as a single rupture nucleus does appear in the liquid. Therefore, in order to effect the thermodynamical consideration, we must put the rupture nuclei out of the system, as soon as they appear in the system. Thus, there arises a steady state of current of molecules in the system. This is the flux J itself.

In the cases I and II, there appear no rupture nuclei, and the assumption of Turnbull and Fisher,[8] that $Z_n\to 0$ when $n\to\infty$, may be admitted. In Figs. 2—6, the range that can be realized is shown by bold lines. j, therefore, is determined as

$$j=\frac{kT}{4\pi}N\Big/\int_{r_0}^{\infty}\left(P+\frac{4\sigma}{3r_\nu}\right)\exp(W_\nu/kT)dr_\nu. \tag{24}$$

In case I, however, this integral is divergent; we get therefore $j=0$ and $J=0$. Namely, no stationary flow of nucleation can exist in the system, and the density of bubbles is expressed as $Z_n=N\exp(-W_n/kT)$. This is the case assumed by Frenkel,[9] and Fürth,[10] when they explained the properties of liquid by the existence of bubbles in the liquid. In case II, by introducing x and β, Eq. (24) is changed to

$$J=B_2\cdot NA_k\frac{akT}{h}\exp[-(W_k+\Delta f)/kT], \tag{25}$$

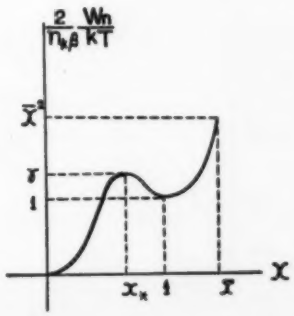

FIG. 6. Graph of $(2/n_k\beta)\times(W_n/kT)$. Case V ($P<-2p_k$, $\beta>3$).

[9] J. Frenkel, J. Chem. Phys. **7**, 538 (1939).
[10] R. Fürth, Proc. Cambridge Phil. Soc. **37**, 252 (1941).

TABLE I. Physical meaning of J.

Number of evolving nuclei	J 1/cm³·sec
100 in 1 sec	10^{2}
10 in 1 sec	10
1 in 1 sec	1
1 in 1 min	$10^{-1.778}$
1 in 1 hr	$10^{-3.556}$
1 in 1 day	$10^{-4.936}$
1 in 1 year	$10^{-6.449}$

where

$$\frac{1}{B_2}=2n_k\beta\int_{\epsilon}^{\infty}\left(\frac{1}{x}-\frac{1}{x_*}\right)\exp[(W_n-W_k)/kT]dx. \quad (26)$$

In this formula ϵ is put to correspond to r_0, but its value does little matter to the value of B_2, because the integrand becomes abnormally large in the very vicinity of zero. Strictly speaking, the value of ϵ cannot be smaller than the value at the minimum point of the integrand. This property of ϵ holds true in all the following cases. In case III the condition $Z_n\to 0$ for $n\to n_*$ must be adopted, and J is expressed by the same formula as Eq. (25), but B_2 must be replaced by B_3:

$$\frac{1}{B_3}=2n_k\beta\int_{\epsilon}^{x_*}\left(\frac{1}{x}-\frac{1}{x_*}\right)\exp[(W_n-W_k)/kT]dx. \quad (27)$$

In case IV, B_2 in Eq. (25) must be replaced by B_4:

$$\frac{1}{B_4}=6n_k\int_{\epsilon}^{1}\left(\frac{1}{x}-1\right)\exp[(W_n-W_k)/kT]dx. \quad (28)$$

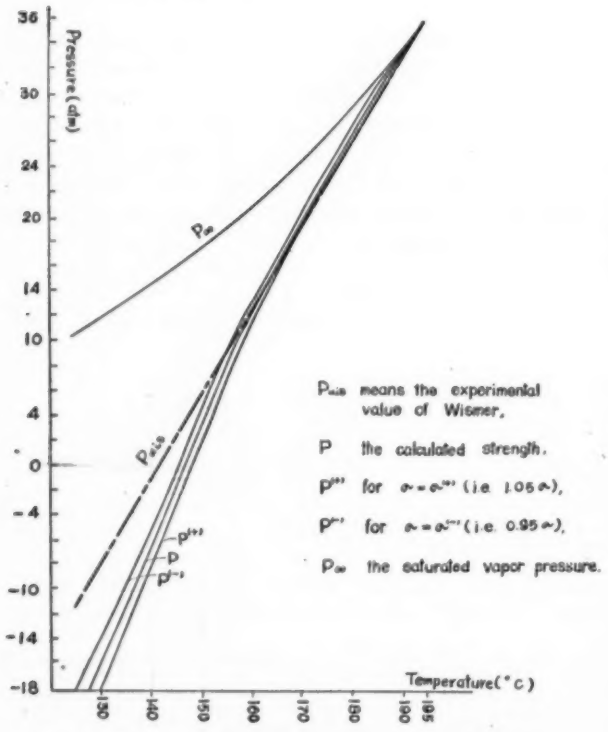

FIG. 7. The breaking strength of superheated ether.

In case V, the maximum takes place at rupture nucleus, and we get

$$J=B_5\cdot NA_k\cdot\frac{akT}{h}\exp[-(W_*+\Delta f)/kT], \quad (29)$$

where

$$\frac{1}{B_5}=2n_k\beta\int_{\epsilon}^{x_*}\left(\frac{1}{x}-\frac{1}{x_*}\right)\exp[(W_n-W_*)/kT]dx. \quad (30)$$

The results obtained are put together, as

$$\left.\begin{aligned} J&=C\exp[-(W_k+\Delta f)/kT], \quad \text{when} \quad 0<\beta\leqq 3\\ &=C\exp[-(W_*+\Delta f)/kT], \quad \text{when} \quad 3\leqq\beta<\infty \end{aligned}\right\} \quad (31)$$

where

$$C=BNA_k\cdot akT/h, \quad (32)$$

and

$$\begin{aligned} \frac{1}{B}&=2n_k\beta\int_{\epsilon}^{\infty}\left(\frac{1}{x}-\frac{1}{x_*}\right)\\ &\quad\times\exp[(W_n-W_k)/kT]dx, \quad \text{when} \quad 0<\beta\leqq 1,\\ &=2n_k\beta\int_{\epsilon}^{x_*}\left(\frac{1}{x}-\frac{1}{x_*}\right)\\ &\quad\times\exp[(W_n-W_k)/kT]dx, \quad \text{when} \quad 1\leqq\beta\leqq 3,\\ &=2n_k\beta\int_{\epsilon}^{x_*}\left(\frac{1}{x}-\frac{1}{x_*}\right)\\ &\quad\times\exp[(W_n-W_*)/kT]dx, \quad \text{when} \quad 3\leqq\beta<\infty. \end{aligned} \quad (33)$$

The exponential functions in the integrands of Eq. (33) attain their maxima at $x=1$ for the first two, and at $x=x_*$ for the last of them. Therefore the method of steepest descent may be applied, when $0<\beta\ll 3$, i.e., for B_2 and B_3. And the approximation of B in this case is gotten as

$$1/B\doteqdot(2\pi n_k(3-\beta)/\beta)^{\frac{1}{2}}. \quad (34)$$

The coefficient C [Eq. (32)], as determined by Eq. (34), is the same as that of Volmer,[11] except the terms which are introduced through the theory of rate processes. Volmer[6] and Döring[7] obtained an approximation formula for the range of $\beta\gg 3$ by applying the method of steepest descent, as

$$B_5'=\ln[(\beta-1)/2], \quad (35)$$

but this is not a good approximation as seen in Fig. 8 because $[(1/x)-(1/x_*)]$ becomes zero at the maximum point. Here exact values are obtained only by the numerical integration. When $\beta=3$, the approximation of

[11] See reference 6, p. 165, Eq. (53).

TABLE II. Values of characteristic functions of superheated ether.

t°C	p_∞	P_{vis}	$P^{(-)}$	P	$P^{(+)}$	β	p_k/kT	W_k/kT	$\log_{10}C$
130	12.05	−7.6	−13.75	−15.75	−17.75	2.460	0.8945	50.6	21.97
140	14.58	−1.0	−5.20	−6.24	−8.03	1.466	0.9187	49.7	21.57
150	17.48	6.0	4.44	3.41	2.36	0.7933	0.9436	49.0	21.33
160	20.80	11.5	12.54	11.94	11.27	0.4040	0.9633	48.7	21.15
170	24.57	19.8	20.22	19.88	19.53	0.1743	0.9796	48.2	20.95
180	28.81	26.0	27.17	27.13	26.92	0.05337	0.9918	47.6	20.69
190	33.57	32.3	33.43	33.41	33.39	0.00406	0.99921	46.6	20.26
193.8	35.52	35.52	35.52	35.52	35.52	0	1	0	

B_4 is obtained as

$$\frac{1}{B_4'}=6n_k\int_0^1\frac{y}{1-y}\exp(-6n_ky^2)dy$$

$$=\sum_{n=1}^{\infty}(6n_k)^{(2-n)/3}\int_0^{\infty}t^n\exp(-t^3)dt$$

$$=0.45068(6n_k)^{\frac{1}{3}}+0.33333$$
$$+0.29764(6n_k)^{-\frac{1}{3}}+0.300(6n_k)^{-\frac{2}{3}}+\cdots. \quad (36)$$

This formula also fails to give a good approximation as seen in Fig. 8.

The value of J at which the rupture is assumed to begin must be settled before entering into the numerical

TABLE III. Degree of ideality of superheated ether.

130	140	150	160	170	180	190	193.8
0.7321	0.7103	0.6722	0.6274	0.5736	0.5060	0.4042	0.2618

calculation. The numerical values of J are given in Table I. In this paper, the value of J is assumed as unity after Döring.[7] The process of calculation is as follows. From Eqs. (2), (4), and (5), we get the relation

$$P=b+(RT/Mv_l)\ln(p_k/p_\infty), \quad (37)$$

where R means the universal gas constant, M the molecular weight, and v_l the specific volume of liquid at T°K. The value of p_k/p_∞ is assumed to be given at the outset, and the values of P and β are computed by Eqs. (37) and (13), respectively. The values of W_k/kT and n_k are determined by

$$\frac{W_k}{kT}=\frac{n_k\beta}{2}=\frac{16\pi\sigma^3}{3kT}\cdot\frac{1}{(\beta p_k)^2}. \quad (38)$$

Substituting into (32) the relation

$$A_k=4\pi r_k^2=16\pi\sigma^2\cdot 1/(\beta p_k)^2, \quad (39)$$

we get

$$C/B=16\pi\sigma^2N(akT/h)\cdot 1/(\beta p_k)^2. \quad (40)$$

Equation (40) may be replaced by Eq. (41) below in the range $0<\beta\ll 3$, which is obtained by substituting Eq. (31) into Eq. (40).

$$C=(2(3)^{\frac{1}{2}}aN(kT)^{\frac{1}{2}}/h)\cdot[1/p_k(3-\beta)^{\frac{1}{2}}]. \quad (41)$$

In Eqs. (38)–(41), the first factors on the right side member are determined by temperature alone, while the second factors depend both on p_k and the temperature. A slight change in the values of σ brings a great change in the value of the exponential function, and the author has performed the computation by giving a variation of ±5 percent to the value of σ. The notations $J^{(+)}$, $P^{(+)}$, $\beta^{(+)}$ and others with (+) on the shoulders correspond to $\sigma^{(+)}$, i.e., 1.05σ, while $J^{(-)}$, $P^{(-)}$, $\beta^{(-)}$ and others with (−) on the shoulder correspond to $\sigma^{(-)}$, i.e., 0.95σ. As the value of a is not far from 1, we have put it equal to 1 throughout the calculation. In fact, the coefficient of the exponential factor is of the order of $10^{10}\sim10^{20}$, therefore, the factor of order of 1 has little effect. For the range of β outside $0<\beta\ll 3$, the accurate value of B must be determined by numerical calculation. Here, the values of $B^{(+)}$ and $B^{(-)}$ are not discriminated from that of B for convenience.

In the range of $p_k/p_\infty\doteqdot 1$, we had better to give β at the outset. Eliminating P between Eq. (13) and the transformation of Eq. (37) where the logarithmic function is expanded in accordance with the approximation introduced above, the approximation of p_k is obtained as

$$p_k=\left(p_\infty-\frac{v_l}{v_g}b\right)\Big/\left(1+\frac{v_l}{v_g}(\beta-1)\right)$$
$$=p_\infty-\frac{v_l}{v_g}(b+p_\infty(\beta-1)), \quad (42)$$

where v_g is the specific volume of vapor. Combining Eq. (42) with the transformation of Eq. (37) deduced above, the approximation of P is obtained as

$$P=-p_\infty(\beta-1). \quad (43)$$

TABLE IV. Dependence of J on P (ether at 130°C).

P (atmos.)	−19	−18	−17	−16	−15	−14	−13	−12
$J^{(-)}$	10^7/1 sec	8×10^5/1 sec	5×10^4/1 sec	2.5×10^3/1 sec	100/1 sec	3/1 sec	1/25 sec	1/1 hr
J	4×10^6/1 sec	2×10^3/1 sec	80/1 sec	25/1 sec	1/16 sec	1/1.5 min	1/2 hr	1/6.3 years
$J^{(+)}$	60/1 sec	8/1 sec	1/5 sec	1/20 min	1/1 day	1/3.1 years	$1/10^3$ years	$1/6\times10^5$ years

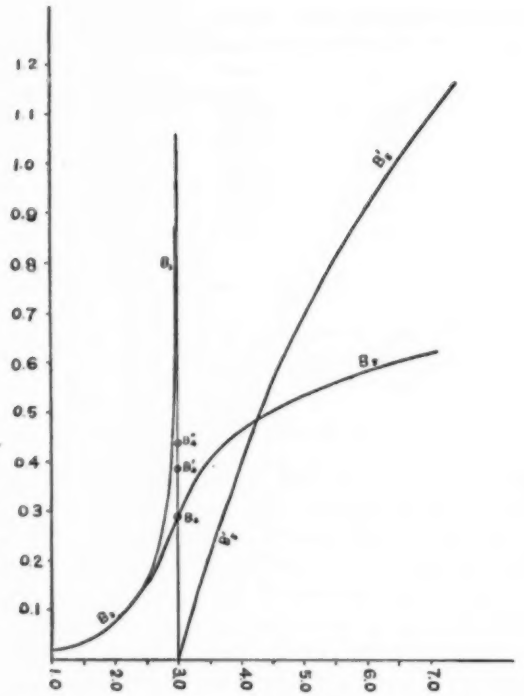

FIG. 8. Graph of value of B of ether at 130°C as functions of β. (B_4, B_5: numerical integration. B_2: graph of Eq. (34). B_4': graph of Eq. (36). B_4'': graph of the first term of Eq. (36). B_5': graph of Eq. (35).

Employing the foregoing formulas, we can determine the appropriate value of P, which makes the value of J equal to 1 under given conditions.

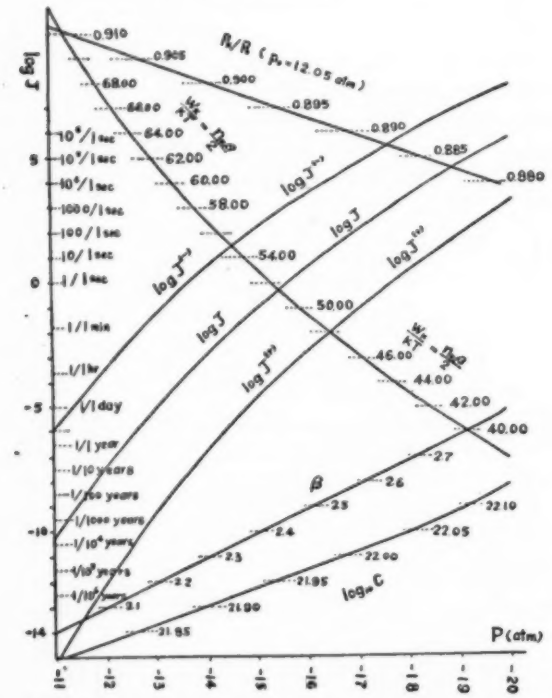

FIG. 9. Curves of several characteristic functions of ether at 130°C against pressure.

TABLE V. Dependence of J on Δf (ether at $P=-15.75$ atmos).

Δf kcal/mole	J
0	1/1 sec
1	1/3.6 sec
2	1/40 sec
4	1/2.7 min
6	1/35 min
8	1/7.4 hr
9	1/1.1 day
10	1/4 day
11	1/14 day

Superheated Ether at 130°C

Döring[7] compared his result with the experiment of Wismer,[12] and got almost perfect conformity. Since the ambiguous concept of the number of vacant holes in unit volume of the liquid is introduced in his paper, his factor in front of the exponential function cannot take definite value. But in the author's theory, precise value can be given to the factor, so long as the assumptions adopted are satisfied, and we will check the result of this theory with the experiment of Wismer.[12] The data of superheated ether necessary for this calculation are obtained from the *International Critical Tables*.

The result of the calculation is shown in Table II and Fig. 7. The experimental values do not enter into the range of calculated values, even though a variation of ± 5 percent is admitted to σ; whereas the theoretical values of Döring coincide perfectly with the experimental values of Wismer. The fact that the observed values do not reach the calculated ones under 165°C, as shown in Fig. 7, may suggest that some other secondary causes, which make bubbles evolve before the negative pressure corresponding to the spontaneous evolution of bubbles within liquid is attained, may exist in spite of the fact that Wismer's experiments were carried out with the utmost care. But seeing that the observed is a little lower than the calculated one, we must admit that this suggestion is not positive. And we can conclude with more probability that the discrepancy is caused by the deviation from the ideal gas, which is shown numerically in Table III. In spite of these defects, this result may well be said to be satisfactory, since it agrees with the experiment to this extent though no arbitrary constant is introduced in the formulas. According to Volmer, Döring calculated his value of J by assuming $C=25\times10^{28}$ at every temperature, but this assumption cannot be true as seen in Table II.

The numerical value of B of ether at 130°C is shown in Fig. 8 as a function of β. The curve of the exact value calculated by numerical integration is shown by the bold line. The curve of Eq. (34) coincides with the exact curve very well in the range $0<\beta<2.7$, but it diverges very much from the exact curve outside the range, becoming ∞ when $\beta\to3$. B_4' of Eq. (36) exceeds the exact

[12] K. L. Wismer, J. Phys. Chem. 26, 301 (1932).

1922

value a little, since the terms of higher order than x^4 are neglected on the shoulder of e. B_4'' in the figure is the value determined by the first term of Eq. (36). B_5' of Eq. (35) cannot give any good approximation, but it is only from three to five times the exact value in the range of practical use. And it may be used for the rough evaluation of B.

Values of several characteristic functions of ether at 130°C are computed by using the values of B in Fig. 8. As shown in Fig. 9 and Table IV, J changes enormously with P. The breaking strength of the liquid, therefore, may be taken as $-15\sim-16$ atmos in this case. The effect of surface tension is very remarkable, as seen by comparison of $J^{(+)}$ and $J^{(-)}$. Wismer used capillary tubes of volume 0.1 cc in his experiment. If the rupture is assumed to start when rupture nuclei form at the rate of one per second, ten nuclei are formed in this case in 1 cc every second. Volmer uses this value in his calculation. But it matters little which value of J is taken as the basis of calculation, when the value of J is chosen in the range of the uncertainty of experiment.

To evaluate the influence of activation energy of ether at 130°C, J is evaluated for some values of Δf in

TABLE VI. Dependence of Δf on P while maintaining $\log J=0$ (ether at 130°C).

p_k/p_∞	P (atmos)	$\log e$	$\log_{10}C$	Δf kcal/mole
0.93	−6.023	52.053	21.164	−56.0
0.92	−8.716	39.410	21.765	−32.5
0.89	−16.972	20.145	22.005	3.43
0.88	−19.786	16.732	22.134	9.96

Table V, on the condition that the other parameters are kept constant as to make $J=1$ when $\Delta f=0$, i.e., $P=-15.75$ atmos, $p_k/p_\infty=0.8945$ and $\beta=2.460$. And in Table VI the activation energy for some values of p_k/p_∞ is evaluated. In this table, however, the negative values of Δf cannot be adopted, because it is incompatible with the basic assumption in the theory of rate processes. But they are inserted, in order to see how much W_k must be diminished to realize $P_{\mathrm{Wis}}=-7.6$ atmos, where P_{Wis} means the experimental value of Wismer.

TABLE VII. Breaking strength of water at 100°C, by evolution of bubbles within liquid.

	Values obtained from $\sigma^{(-)}$	σ	$\sigma^{(+)}$
P(atmos.)	−1861.7	−1871.9	−1881.9
P_k/P_∞	0.31872	0.31675	0.31481
P	6006.48	6039.32	6071.1
W^*/kT	51.983	51.988	51.995
$\log_{10}C$	22.576	22.578	22.581
γ	2.8260	2.8276	2.8292
B		3.1004	

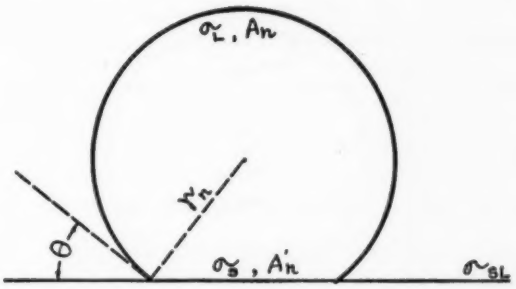

FIG. 10. A bubble on boundary surface.

Water at 100°C

The highest temperature at which the experimental value of the surface tension of water is available is 140°C,[13] and the author has given up to calculate the breaking strength of superheated water at each temperature. Only the breaking strength at 100°C is calculated (Table VII). What factor can really reduce this enormously high tension to as low a value as the barometric pressure, is a problem left for future research.

Water at 20°C

Similarly to the water at 100°C, the fracture strength at 20°C is calculated (Table VIII). The factor which can diminish this enormous tension to the aqueous vapor pressure at 20°C is to be sought in the future.

THE FRACTURE OF LIQUID BY NUCLEATION ON THE SURFACE OF ITS CONTAINER

Theory

The work necessary for nucleation on the surface is obtained in the similar way as Eq. (8).

$$W_n=nkT\ln(p_n/p_k)+\sigma_L A_L +(\sigma_S-\sigma_{SL})A_n'+(P-p_n)V_n, \quad (44)$$

where σ_{SL} means the surface tension between the liquid and the wall; σ_L and A_n, the surface tension and the area of the border surface between the liquid and the bubble; σ_S and A_n', those between the wall and the bubble (see Fig. 10). If, however, θ is taken for the

TABLE VIII. Breaking strength of water at 20°C, by evolution of bubbles within liquid.

	Values obtained from $\sigma^{(-)}$	σ	$\sigma^{(+)}$
P(atmos.)	−3737.0	−3741.0	−3745.1
P_k/P_∞	0.06058	0.06039	0.06019
B	2 681 700	2 691 800	2 701 890
W^*/kT	51.354	51.357	51.357
$\log_{10}C$	22.303	22.304	22.304
γ	4.6245	4.6257	4.6269
B		5.3328	

[13] The greatest values of contact angle ever obtained are summarized by Fisher (reference 4).

TABLE IX. Dependence of some characteristic functions on θ (water at 20°C).

θ	$P^{(-)}$(atmos)	P(atmos)	$P^{(+)}$(atmos)	β	p_k/p_∞	$n_k\beta/2$	γ	B
0°	−4756.2	−4771.0	−4776.9	7 429 680	0.02787	6.7045	5.0322	5.549
90°	−3171.5	−3175.0	−3178.8	1 495 800	0.092388	8.2236	4.4513	4.964
150°	−402.35	−402.50	−402.97	23 646	0.73881	12.463	3.2233	3.533
179°	−0.1974	−0.1976	−0.1979	9.583	0.99910	54.507	1.0950	1.569

contact angle including liquid, the following relations are obtained:

$$\sigma_L \cos\theta+\sigma_{SL}=\sigma_S, \tag{45}$$

$$V_n=(4\pi/3)r_n^3\cdot\mu, \tag{46}$$

$$A_n'=\pi r_n^2\cdot\sin^2\theta, \tag{47}$$

$$A_n=4\pi r_n^2\cdot\lambda, \tag{48}$$

$$\lambda=(1+\cos\theta)/2, \tag{49}$$

and

$$\mu=\lambda^2(2-\cos\theta). \tag{50}$$

By these equations, Eq. (44) is changed to

$$W_n=nkT\ln(p_n/p_k)+\mu\cdot\sigma(4\pi/3)r_n^2. \tag{51}$$

The equation of state of the bubble may be taken as

$$(P+2\sigma/r_n)\cdot(4\pi/3)r_n^3\cdot\mu=nkT. \tag{52}$$

Equation (52) determines the characteristic constants of the rupture nuclei; i.e., r_* is expressed also by Eq. (11) and n_*, by

$$n_*=\mu\cdot 128\pi\sigma^3/81kTP^2. \tag{53}$$

Introducing x, β, $\bar{x}$, and x_* by Eqs. (12), (13), (14) and (15), Eq. (51) is transformed to the same expression as Eq. (16), which means that all the effects of θ are brought into n_k. The value of n_k is determined by

$$\frac{W_k}{kT}=\frac{n_k\beta}{2}=\frac{16\pi\sigma^3}{3kT}\cdot\mu\cdot\frac{1}{(\beta p_k)^2}. \tag{54}$$

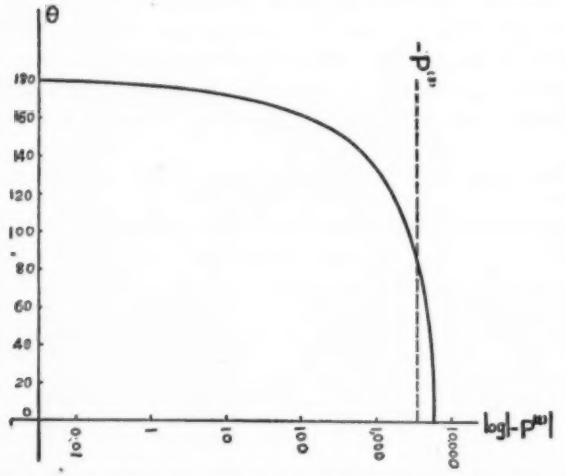

FIG. 11. Relation between θ and $P^{(2)}$. $P^{(2)}$ means the breaking strength for the nucleation on surface and $P^{(3)}$, for the nucleation within liquid.

The theories in the preceding chapter hold true intact in this case, with only one exception that N must express the number of liquid molecules on the area of the border surface, because Z_n means here the number of molecules on the unit area of the wall of the container. N in this case is expressed, therefore, as $N^{(2)}$. And by similar procedure used in Eq. (23), we obtain

$$Z_n=\exp(-W_n/kT)\left[N^{(2)}-j\frac{4\pi\mu}{kT}\times\int_{r_0}^{r_n}\left(P+\frac{4\sigma}{3r_\nu}\right)\exp(W_\nu/kT)dr_\nu\right]. \tag{55}$$

This equation brings us to the same formula as Eqs. (31) and (33), but Eq. (32) alone is subject to modification, as

$$C=(\lambda/\mu)\cdot BNA_k\cdot akT/h. \tag{56}$$

The approximate formulas of B are the same as before. In Eq. (56), $C\to\infty$ when $\theta\to 180°$, which means that a spot where a bit of substance with the contact angle 180° happens to adhere can be a center of evolution of bubbles. But the indifference to temperature is a remarkable characteristic of this phenomenon.

Water at 20°C

Values of some important characteristic functions for various values of θ calculated by putting $b=1$ atmos in Eq. (37) are shown in Table IX. Among them the relation of P and θ is plotted in Fig. 11, which shows that the variation of P is great against that of θ in the region $\theta>150°$. But the breaking strength P does not yet reach the saturated vapor pressure p_∞, even at $\theta=179°$. The greatest contact angle ever known,[13] however, does not exceed 155°. But this fact cannot yet deny the effect of contaminations, because the contact angle used in this paper may be defined in very narrow range, whereas the contact angle in usual sense must necessarily be a mean averaged in a fairly wide range.

$N^{(2)}$ is calculated by the relation $N^{(2)}=(N^{(3)})^{\frac{1}{3}}$, where $N^{(3)}$ means the number of molecules in 1 cc of liquid. Therefore, the breaking strength on surface $P^{(2)}$ at $\theta=0°$, is more negative than the breaking strength within liquid $P^{(3)}$, and it is at $\theta\div 90°$ that it becomes equal to $P^{(3)}$. We may conclude by this fact that the existence of walls or contaminations, of which $\theta<90°$, can have no influence on the evolution of bubbles, i.e., that the spontaneous formation of bubbles within liquid

is realized in this vessel. It must be noticed, however, that the contact angle θ, here used, is of microscopic character, and not of macroscopic character such as measured commonly. The old thought of Tomlinson[14] seems to support the idea of microscopic contact angle. According to his opinion, matter can be divided into two kinds. In the first category belong glass and the denser metals with a smooth non-porous surface. To all these bodies, when chemically clean, there is no separation of gas at their surfaces. And in the second category belong oils, fatty bodies, wax, resin and some other bodies. Their surfaces, although chemically clean, become covered with bubbles.

EVOLUTION OF BUBBLES IN PULVERULENT MATERIALS

It is well known among soil-physicists that, when the moisture content in soil reaches a specified moisture content to the soil, the so-called field capacity,[15] soil moisture cannot move as liquid and must go through only the vapor phase beyond this content. This phenomenon has been explained by the present author,[17] that from the theoretical point of view it occurs when the pressure of moisture reaches absolute zero, i.e., -1 atmos when the datum of pressure is taken as atmospheric pressure. The author thinks that this phenomenon may be of the same physical nature as cavitation, and will be explained by the theory of evolution of bubbles, although it is not yet well understood.

We will see, however, to what extent the enormously broad surface area of pulverulent material can amend the unsatisfactory result obtained in the previous articles. Let us express the flux of molecules for the nucleation on the surface by $J^{(2)}$. What is now sought is the rate of evolution of bubbles in unit volume of the material. Let us denote this quantity by J. Then the relation

$$J=SJ^{(2)} \tag{57}$$

hold true, where S means the specific area of pulverulent material, i.e., the surface area in its unit volume. The fundamental formulas are the same as Eqs. (31)–(33), but C in Eq. (32), which shall be expressed as $C^{(2)}$ here,

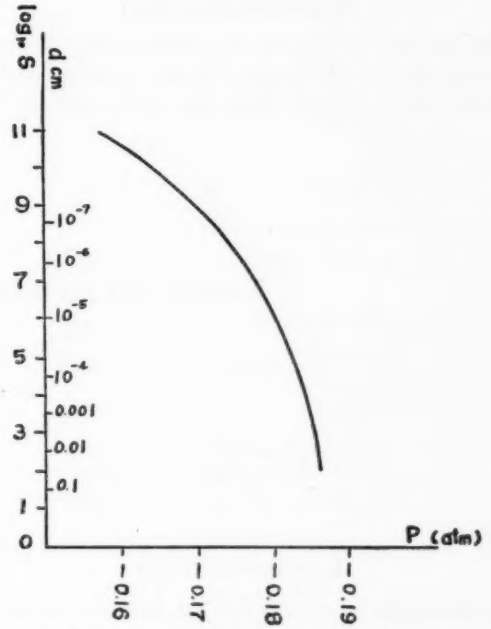

FIG. 12. Relation between S, the specific surface of pulverulent material and P, the breaking strength of water at 20°C, when θ is fixed at 179°. By d is meant the diameter (cm) of a particle.

must be replaced by

$$C=SC^{(2)}. \tag{58}$$

Numerical calculation is carried out on water at 20°C and $\theta=179°$. Pulverulent material is assumed to be spherical, of the same radius of curvature, and arranged in simple cubic lattice. The result of the calculation is shown in Fig. 12. But it cannot yet attain p_∞. Even if d, the diameter, may take as small a value as 10^{-7} cm, P is determined as high as -0.17 atmos. Namely the effect of the broad specific area is of little use. This conclusion holds true for all values of θ.

CONCLUSIONS

This theory cannot yet explain the physical meaning of boiling, cavitation and the critical phenomena of the movement of soil moisture. There are, however, many other points to be considered. At first, there may be holes on the boundary surfaces, which may collect some amount of gas in them and facilitate much nucleation Moreover, effects of coexisting substance[18] and impulse[19] must necessarily be taken into consideration. But there seems some greatly significant point left unheeded. In the nucleation theory of solids, the discrepancies between the theoretical and experimental values have forced us to consider the varieties of local atomic structure. This might also be true in the case of the nucleation of bubbles in liquid.

[14] C. Tomlinson, Phil. Mag. (4) **45**, 277 (1873). The experiments of Tomlinson are concerned with supersaturated solution, not with one-component liquid as with this theory. But they may be supposed of the same physical nature. Namely, the high tension of one-component liquid may be assumed to be brought down by supersaturation to barometric pressure, accessible to our daily experience.

[15] See reference 16, p. 233; C. F. Shaw, Soil Sci. **23**, 303 (1927); and F. J. Veihmeyer and A. H. Hendrickson, Soil. Sci. **32**, 181 (1931).

[16] L. D. Baver, *Soil Physics* (John Wiley and Sons, Inc., New York, 1948).

[17] S. Takagi, Monographs on theoretical soil physics, theoretical considerations on thermodynamical and kinematic properties of soil moisture (to be published); J. Appl. Phys. (Japan) **17**, 241 (1948); Rep. Inst. Sci. Tech. Univ. Tokyo **6**, 37 (1952) (in Japanese, with abstract only in English).

[18] A series of experiments on this subject have been conducted by C. Tomlinson (reference 20), and Phil. Mag. (4) **34**, 136, 229 (1867).

[19] For experiments on this subject see R. B. Dean, J. Appl. Phys. **15**, 446 (1944).

ACKNOWLEDGMENT

The author is pleased to acknowledge his sincere gratitude to Dr. M. Sugita, Dr. O. Nomoto and other members of Kobayashi Institute of Physical Research, Tokyo, Japan, for suggestion and encouragement during this research, and to Dr. D. Turnbull and Dr. J. C. Fisher, General Electric Research Laboratory, for reviewing the manuscript.

JOURNAL OF APPLIED PHYSICS VOLUME 24, NUMBER 12 DECEMBER, 1953

Variational Methods for Problems in Resistance*

J. F. CARLSON AND T. J. HENDRICKSON
Institute for Atomic Research and Department of Physics, Iowa State College, Ames, Iowa
(Received April 20, 1953)

Schwinger's variational methods are applied to a resistance problem with mixed boundary conditions. By the use of two formulations, both upper and lower bounds to the resistance are obtained. Results are given for a cylinder subject to given boundary conditions for a number of values of the relevant parameters.

I. INTRODUCTION

PROBLEMS in steady-state flow can be formulated as integral equations with a symmetric kernel and mixed boundary conditions. In most cases it is not possible to solve the integral equation directly but, as has been shown by Schwinger,[1] it is possible to set up a variation principle such that some quantity of physical interest is stationary to variations of the unknown function in the integral equation about its true value. Furthermore, as shown by Schwinger,[1] the calculated quantity is always greater than, or at least equal to, the true value. In some problems by using two independent formulations it is possible to obtain in one case a value greater than the true value and in the other case a value less than the true value of the quantity desired.

In this paper a simple problem of this type is considered in which the resistance is the quantity which is found to be stationary.

II. FORMULATION

Consider the problem of calculating the resistance of a circular cylinder of length l, radius b, and resistivity ρ, subject to the boundary conditions that one end of the cylinder is kept at a potential $\Phi=V_0$ while at the other end of the cylinder the annulus between $r=a$ and $r=b$ is kept at the potential $\Phi=0$ and there is no flow for $0<r<a$. Throughout the cylinder the potential will satisfy Laplace's equation

$$\left[\frac{1}{r}\frac{\partial}{\partial r}\left(r\frac{\partial}{\partial r}\right)+\frac{\partial^2}{\partial z^2}\right]\Phi(r,z)=0, \tag{1}$$

subject to the conditions:

$$\Phi(r,0)=V_0 \quad 0\leq r\leq b, \tag{2a}$$

$$\Phi(r,l)=0 \quad a<r<b, \tag{2b}$$

$$\frac{\partial\Phi(r,l)}{\partial z}=0 \quad 0<r<a, \tag{2c}$$

$$\frac{\partial\Phi(b,z)}{\partial r}=0 \quad 0\leq z\leq l. \tag{2d}$$

A Green's function appropriate to the problem satisfies the equation

$$\left[\frac{1}{r}\frac{\partial}{\partial r}\left(r\frac{\partial}{\partial r}\right)+\frac{\partial^2}{\partial z^2}\right]G_1(r,r',z,z')=\frac{-\delta(r-r')\delta(z-z')}{2\pi r}, \tag{3}$$

subject to the boundary conditions:

$$G_1(r,r',0,z')=0, \tag{4a}$$

$$\frac{\partial G_1(r,r',l,z')}{\partial z}=0, \tag{4b}$$

$$\frac{\partial G_1(b,r',z,z')}{\partial r}=0, \tag{4c}$$

$$G_1(r,r',z,z')=G_1(r',r,z',z). \tag{4d}$$

G_1 and Φ may be taken independent of ϕ by symmetry considerations.

The Green's function satisfying the above conditions is

$$G_1(r,r',z,z')=\frac{z_<}{\pi b^2}+\frac{1}{\pi b^2}\sum_{n=1}^{\infty}\left[\frac{\sinh(\lambda_n z_<)\cosh\lambda_n(l-z_>)}{\lambda_n\cosh\lambda_n l}\times\frac{J_0(\lambda_n r)J_0(\lambda_n r')}{J_0^2(\lambda_n b)}\right], \tag{5}$$

* Contribution No. 253 from the Institute for Atomic Research and Department of Physics, Iowa State College, Ames, Iowa. Work was performed in the Ames Laboratory of the Atomic Energy Commission.

[1] J. S. Schwinger (unpublished lecture notes, Massachusetts Institute of Technology).

where $J_0(\lambda_n r)$ is the Bessel function of zero order and the $\lambda_n b$ are the roots of $J_1(\lambda_n b)=0$. Furthermore, $(z_>, z_<)$ denotes (z, z') when $z>z'$ and (z', z) when $z<z'$.

By an application of Green's theorem the potential within the cylinder can be expressed as

$$\Phi(r, z)=V_0+\frac{2z}{b^2}\int_a^b \frac{\partial\Phi(r', l)}{\partial z'}r'dr' +\frac{2}{b^2}\int_a^b\left[\sum_{n=1}^{\infty}\frac{\tanh\lambda_n l}{\lambda_n J_0^2(\lambda_n b)}J_0(\lambda_n r)J_0(\lambda_n r')\right] \times\frac{\partial\Phi(r', l)}{\partial z'}r'dr'. \quad (6)$$

It is convenient to make the substitution

$$\frac{\partial\Phi(r, l)}{\partial z}=-\frac{V_0}{l}\chi(r), \quad (7)$$

after which application of boundary condition (2b) yields the relation

$$1-\frac{2}{b^2}\int_a^b \chi(r')r'dr'=\frac{2}{b^2}\sum_{n=1}^{\infty}\frac{\tanh\lambda_n l}{\lambda_n l J_0^2(\lambda_n b)} \times\int_a^b J_0(\lambda_n r)J_0(\lambda_n r')\chi(r')r'dr'. \quad (8)$$

The definition

$$1-\frac{2}{b^2}\int_a^b \chi(r')r'dr'=\frac{2}{b^2}\Gamma\int_a^b \chi(r')r'dr' \quad (9)$$

is now used to put Eq. (8) in the form

$$\Gamma\int_a^b \chi(r')r'dr'=\int_a^b K_1(r, r')\chi(r')r'dr'. \quad (10)$$

Equation (10) is formally an integral equation of the first kind with the symmetric kernel

$$K_1(r, r')=\sum_{n=1}^{\infty}\frac{\tanh(\lambda_n l)J_0(\lambda_n r)J_0(\lambda_n r')}{\lambda_n l J_0^2(\lambda_n b)}. \quad (11)$$

Multiplication of both sides of Eq. (10) by $r\chi(r)dr$ and integration from a to b produces the equation

$$\Gamma\left[\int_a^b \chi(r)rdr\right]^2 =\int_a^b\int_a^b r\chi(r)K_1(r, r')r'\chi(r')drdr'. \quad (12)$$

Γ can be shown to be stationary with respect to variations of $\chi(r)$ about its true value by taking the variation of Eq. (12),

$$\delta\Gamma\left[\int_a^b \chi(r)rdr\right]^2+2\Gamma\left[\int_a^b \chi(r)rdr\right]\int_a^b \delta\chi(r)rdr =\int_a^b\int_a^b[\chi(r)\delta\chi(r')+\chi(r')\delta\chi(r)]rK_1(r, r')r'drdr'. \quad (13)$$

From Eq. (10) and the symmetry of $K_1(r, r')$ we have $\delta\Gamma=0$.

We now use a theorem attributed to Schwinger[1] that the Γ obtained using a trial solution $\chi_t(r)$ for $\chi(r)$ is greater than, or at least equal to, the result obtained by using the true solution $\chi(r)$ for a kernel having the form of $K_1(r, r')$.

We can write the kernel in the form

$$K_1(r, r')=\sum_{n=1}^{\infty}u_n(r)u_n(r'), \quad (14)$$

with $u_n(r)=A_n J_0(\lambda_n r)/J_0(\lambda_n b)$ and $A_n=[\tanh(\lambda_n l)/\lambda_n l]^{\frac{1}{2}}$. Then

$$\Gamma=\sum_{n=1}^{\infty}\left[\int_a^b u_n(r)\chi(r)rdr\right]^2\Big/\left[\int_a^b \chi(r)rdr\right]^2. \quad (15)$$

Consider the expression

$$L=\sum_{n=1}^{\infty}\left\{\int_a^b u_n(r)\left[\chi(r)\Big/\int_a^b \chi(r')r'dr' -\chi_t(r)\Big/\int_a^b \chi_t(r')r'dr'\right]rdr\right\}^2\geq 0. \quad (16)$$

Therefore

$$L=\Gamma+\Gamma_t-2\sum_{n=1}^{\infty}\int_a^b u_n(r)\chi(r)rdr \times\int_a^b u_n(r')\chi_t(r')r'dr'\Big/\int_a^b \chi(r)rdr\int_a^b \chi_t(r')r'dr'. \quad (17)$$

Interchanging integration and summation in the last term we find

$$\int_a^b \chi_t(r')\left[\sum_{n=1}^{\infty}\int_a^b u_n(r)u_n(r')\chi(r)rdr\right]r'dr' =\Gamma\int_a^b \chi_t(r)rdr\int_a^b \chi(r)rdr, \quad (18)$$

and thus

$$L=\Gamma+\Gamma_t-2\Gamma=\Gamma_t-\Gamma\geq 0. \quad (19)$$

Therefore $\Gamma_t\geq\Gamma$.

The physical significance of Γ can be found by considering the current flow in the cylinder, given by

$$I=-\frac{2\pi}{\rho}\int_a^b \frac{\partial\Phi(r,l)}{\partial z}rdr=\frac{2\pi V_0}{\rho l}\int_a^b \chi(r)rdr. \quad (20)$$

From Eq. (9)

$$I=\pi b^2 V_0/\rho l(1+\Gamma), \quad (21)$$

and the resistance is consequently

$$R=V_0/I=\rho l(1+\Gamma)/\pi b^2. \quad (22)$$

Thus Γ is the fractional increase in the resistance due to the obstruction to the flow. If we write $R=R_0+R_x$, we have $R_0=\rho l/\pi b^2$ and $R_x=(\rho l/\pi b^2)\Gamma$, where R_0 is the resistance if the entire end at $z=l$ were at potential $\Phi=0$, and R_x is the extra resistance added by the obstruction. Since Γ_t is greater than or equal to Γ, $R_x^{(1)}$ calculated using Γ_t will be greater than or equal to the true R_x.

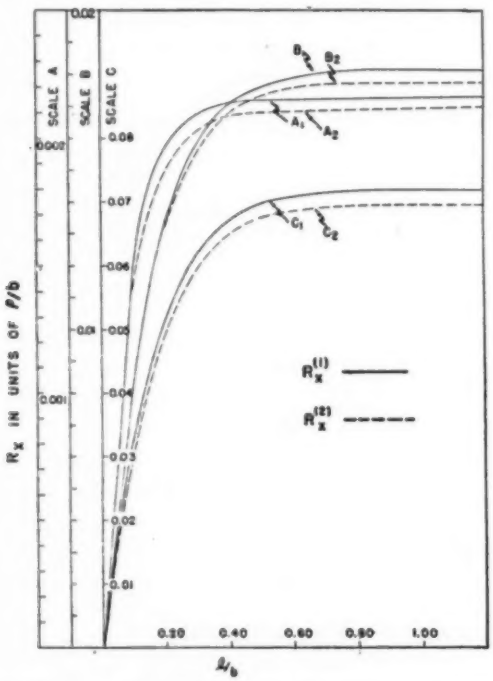

FIG. 1. $R_x^{(1)}$ and $R_x^{(2)}$ as functions of the ratio l/b. These curves are plotted from Tables III and IV. Note that the families of curves A, B, and C are plotted to different scales.

We now give another formulation of the same problem with different boundary conditions on the Green's function. Instead of the conditions given by Eqs. (4a, b) we now choose the Green's function to satisfy

$$G_2(r,r',0,z')=G_2(r,r',l,z')=0. \quad (23)$$

We then find the Green's function satisfying Eq. (23) and Eqs. (4c, d) is

$$G_2(r,r',z,z')=z_<(l-z_>)/\pi b^2 l+\frac{1}{\pi b^2}\times\sum_{n=1}^{\infty}\frac{\sinh(\lambda_n z_<)\sinh\lambda_n(l-z_>)J_0(\lambda_n r)J_0(\lambda_n r')}{\lambda_n\sinh(\lambda_n l)J_0^2(\lambda_n b)}. \quad (24)$$

Again applying Green's theorem, we find that

$$\Phi(r,z)=2\pi V_0\int_0^b \frac{\partial G_2(r,r',z,0)}{\partial z'}r'dr'-2\pi\int_0^a \Phi(r',l)\frac{\partial G_2(r,r',z,l)}{\partial z'}r'dr', \quad (25)$$

and

$$\frac{\partial\Phi(r,z)}{\partial z}=2\pi V_0\int_0^b \frac{d^2G_2(r,r',z,0)}{\partial z\partial z'}r'dr'-2\pi\int_0^a \Phi(r',l)\frac{\partial^2 G_2(r,r',z,l)}{\partial z\partial z'}r'dr'. \quad (26)$$

For $z=l$ and $0<r<a$ we have

$$0=\frac{\partial\Phi(r,l)}{\partial z}=2\pi V_0\int_0^b \frac{\partial^2 G_2(r,r',l,0)}{\partial z\partial z'}r'dr'-2\pi\int_0^a \Phi(r',l)\frac{\partial^2 G_2(r,r',l,l)}{\partial z\partial z'}r'dr'. \quad (27)$$

If we now put $\Phi(r',l)=V_0\psi(r')$ Eq. (27) becomes

$$1-\frac{2}{b^2}\int_0^a \psi(r')r'dr'=\frac{2}{b^2}\int_0^a \psi(r')\times\left[\sum_{n=1}^{\infty}\frac{\lambda_n l J_0(\lambda_n r)J_0(\lambda_n r')}{\tanh(\lambda_n l)J_0^2(\lambda_n b)}\right]r'dr'. \quad (28)$$

Letting

$$1-\frac{2}{b^2}\int_0^a \psi(r')r'dr'=\frac{2\Lambda}{b^2}\int_0^a \psi(r')r'dr' \quad (29)$$

TABLE I. $R_x^{(1)}$ for $l/b\gg1$, in units of ρ/b.

Trial field	$a/b=0.25$	$a/b=0.50$	$a/b=0.75$
1	0.00325	0.00223	0.0786
$r/(r^2-a^2)^{\frac{1}{2}}$	0.00274	...	...
$1/(r^2-a^2)^{\frac{1}{2}}$	0.00261	0.0304	0.0749
$A+1/(r^2-a^2)^{\frac{1}{2}}$	0.00216	0.0181	0.0720

TABLE II. $R_x^{(2)}$ for $l/b\gg1$, in units of ρ/b.

Trial field	$a/b=0.25$	$a/b=0.50$	$a/b=0.75$
$(a^2-r^2)^{\frac{1}{2}}$	0.00212	0.0177	0.0694
$(a^2-r^2)^{\frac{1}{2}}+B(a^2-r^2)^{\frac{1}{2}}$	0.00212	0.0177	0.0694

TABLE III. $R_x^{(1)}$ in units of ρ/b as a function of the ratio l/b. Calculated using the one-parameter trial field $A+1/(r^2-a^2)^{\frac{1}{2}}$.

l/b	$a/b=0.25$	$a/b=0.50$	$a/b=0.75$
0.10	0.00146	0.0083	0.0326
0.20	0.00196	0.0133	0.0515
0.30	0.00209	0.0158	0.0618
0.40	0.00214	0.0171	0.0671
0.50	0.00215	0.0176	0.0700
0.60	0.00215	0.0179	0.0709
0.80	0.00216	0.0181	0.0715
1.00	0.00216	0.0181	0.0719
∞	0.00216	0.0181	0.0720

and

$$K_2(r,r')=\sum_{n=1}^{\infty}\frac{\lambda_n l J_0(\lambda_n r)J_0(\lambda_n r')}{\tanh(\lambda_n l)J_0^2(\lambda_n b)}, \tag{30}$$

we have

$$\Lambda\int_0^a \psi(r')r'dr'=\int_0^a K_2(r,r')\psi(r')r'dr'. \tag{31}$$

If both sides are now multiplied by $\psi(r)rdr$ and integrated over r from 0 to a we find

$$\Lambda=\left[\int_0^a \psi(r)rdr\right]^{-2} \times\int_0^a\int_0^a r\psi(r)K_2(r,r')r'\psi(r')drdr'. \tag{32}$$

This expression can be shown to be stationary and to be greater than or at least equal to the true value of Λ. The current in this case is given by

$$I=-\frac{2\pi}{\rho}\int_0^b\frac{\partial\Phi(r,0)}{\partial z}rdr =\frac{\pi b^2V_0}{\rho l}-\frac{2\pi V_0}{\rho l}\int_0^a\psi(r)rdr. \tag{33}$$

Hence

$$I=(\pi b^2V_0/\rho l)(\Lambda/\Lambda+1), \tag{34}$$

and

$$R=V_0/I=(\rho l/\pi b^2)(1+1/\Lambda). \tag{35}$$

The extra resistance is thus

$$R_x=\rho l/\pi b^2\Lambda. \tag{36}$$

TABLE IV. $R_x^{(2)}$ in units of ρ/b as a function of the ratio l/b. Calculated using the one-parameter trial field $(a^2-r^2)^{\frac{1}{2}}+B(a^2-r^2)^{\frac{1}{2}}$.

l/b	$a/b=0.25$	$a/b=0.50$	$a/b=0.75$
0.10	0.00141	0.0083	0.0316
0.20	0.00190	0.0132	0.0498
0.30	0.00204	0.0156	0.0597
0.40	0.00209	0.0168	0.0647
0.50	0.00211	0.0173	0.0676
0.60	0.00211	0.0176	0.0684
0.80	0.00212	0.0177	0.0692
1.00	0.00212	0.0177	0.0694
∞	0.00212	0.0177	0.0694

Since Λ_t is always greater than or equal to Λ, the resistance $R_x^{(2)}$, calculated using Λ_t, will be less than the true resistance. Therefore the relation

$$R_x^{(1)}\geq R_x\geq R_x^{(2)} \tag{37}$$

holds, and upper and lower bounds can be placed on the magnitude of the resistance.

III. RESULTS

In order to show the effect of the choice of the trial field we give in Tables I and II numerical results for the extra resistance R_x with the ratio $l/b\gg1$. It should be noted that the normalization of the trial fields is irrelevant and that only their functional forms are important. The simplest form for $\chi(r)$, the gradient function, which gave good results was a one-parameter function. The value of the parameter was chosen to minimize the appropriate value of Γ_t.

In the second formulation where $\psi(r)$, the potential function, is used it must be chosen to satisfy the boundary condition $\psi(a)=0$. For this formulation the result was not significantly improved by using a one-parameter field; the simplest choice used gave an adequate result in this case. In Tables III and IV results are given for conductors of varying lengths using the appropriate one-parameter trial functions. Γ_t and Λ_t are minimized with respect to the parameter.

The calculations for $R_x^{(1)}$ are quite laborious since for reasonable trial functions the integral involved in each term of the series had to be evaluated numerically, except for $\chi(r)=1$. Graphs of R_x as a function of the ratios a/b and l/b are given in Fig. 1.

Approximate Solutions of the Space-Charge Problem for Some Unusual Electrode Geometries

HENRY F. IVEY
*Research Department, Westinghouse Electric Corp., Bloomfield, New Jersey**

(Received April 22, 1953)

An approximation technique for computing the space charge limited current between electrodes of unusual and complicated geometry that cannot be treated rigorously is discussed and applied to several electrode systems involving both cylindrical and sphreical emitters. This method was originally suggested by Matricon and Trouvé and by O'Neill. All that is required is a knowledge of the electrostatic capacitance of the system concerned. Many electrode systems of practical importance which were heretofore not susceptible of calculation are amenable to this technique.

THE solution of the problem of space-charge limited current flow for electrode geometries in which the particle trajectories coincide with the lines of electrostatic flux between the electrodes is fairly simple and has been known for some time. The electrode arrangements which satisfy this condition are parallel planes,[1,2] coaxial circular cylinders,[2,3] and concentric spheres.[4] In all these cases the trajectories are striaght lines, i.e., the flow is rectilinear. The more general case of curvilinear flow is much more complicated;[5,6] the only practical electrode arrangements for which rigorous solutions have been obtained are inclined parallel planes[6,7] and two coaxial right circular cones with coincident vertices.[6]

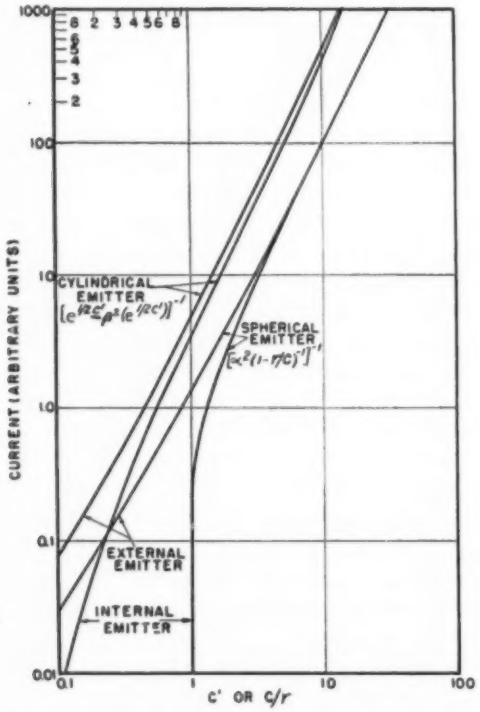

FIG. 1. Space-charge limited current for electrode systems with cylindrical emitters in terms of the capacitance (in esu) per unit length C', or for systems with spherical emitters in terms of the ratio of the capacitance (in esu) to the emitter radius C/r. The current values as plotted must be multiplied by the quantity $14.6\times10^{-6}V^{\frac{3}{2}}/r$ for cylindrical emitters to obtain the current in amperes per unit axial length of the system, and by $29.2\times10^{-6}V^{\frac{3}{2}}$ for spherical emitters to obtain the total current in amperes. (Note: 1 esu of capacitance = 1.11 $\mu\mu$f.)

Recently a technique has been suggested for obtaining approximate solutions for other electrode arrangements of practical interest.[8–10] According to this method the actual anode is replaced by a fictitious electrode of such geometry that it forms with the cathode a diode having the property of rectilinear flow, and of such dimensions that the fictitious diode has the same electrostatic capacitance as the real one. The perveance characteristics of the real diode are then assumed to be the same as those of the fictitious one, which can be calculated by the usual methods. Many techniques are available, of course, for calculating the capacitance between electrodes of unusual and complicated geometry. This description of the method of approximate solution makes it sound rather artificial, but Matricon and Trouvé[8] have shown that it is based on a very reasonable basic premise. The fundamental assumption is that the shape of the equipotential surfaces is the same in the presence and in the absence of space charge, and that only the value of the potential attached to each of these surfaces differs in the two cases.

This method of approximation has been submitted to experimental test for the case of eccentric cylindrical electrodes by Matricon and Trouvé,[8] and for the case of a cylindrical cathode and an anode of rectangular cross section by O'Neill.[9] Matricon and Trouvé, in four trials, report errors of 4.4, 6.6, 0.92, and 0.22 percent, while O'Neill states that "the experimental results were always within a few percent of predicted values." The

* Part of the work represented by this paper was performed while the writer was employed at the Skiatron Electronics and Television Corporation, New York City.

[1] C. D. Child, Phys. Rev. **32**, 494 (1911).
[2] I. Langmuir, Phys. Rev. **2**, 450 (1913).
[3] I. Langmuir and K. Blodgett, Phys. Rev. **22**, 347 (1923).
[4] I. Langmuir and K. Blodgett, Phys. Rev. **24**, 49 (1924).
[5] B. Meltzer, Proc. Phys. Soc. (London) **62B**, 431, 813 (1949).
[6] G. B. Walker, Proc. Phys. Soc. (London) **63B**, 1017 (1950).
[7] H. F. Ivey, J. Appl. Phys., **23**, 240 (1952).
[8] M. Matricon and S. Trouvé, Onde. Elec., **30**, 510 (1950).
[9] G. D. O'Neill, Sylvania Technologist, **22**, April (1950).
[10] W. G. Dow, *Fundamentals of Engineering Electronics* (John Wiley and Sons, Inc., New York, 1952), Second edition, pp. 156–165.

TABLE I. Geometries with internal cylindrical emitter of radius r.

NO.	ANODE	NOMENCLATURE	R'/r (R' = RADIUS OF EQUIVALENT FICTITIOUS CYLINDRICAL COLLECTOR COAXIAL WITH EMITTER)	REF.[a]
1	ECCENTRIC CYLINDER		$\exp\{\cosh^{-1}(\frac{R^2+r^2-d^2}{2dr})-\cosh^{-1}(\frac{R^2-r^2+d^2}{2dR})\}$ $=\exp\cosh^{-1}(\frac{R^2+r^2-d^2}{2Rr})\simeq\frac{R}{r}[1-(\frac{d}{R})^2]$ IF $r, d \ll R$	11-12 8 13
2	INFINITE PLANE	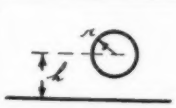	$\exp\cosh^{-1}(h/r)=\frac{h}{r}+[(\frac{h}{r})^2-1]^{1/2}$ $\simeq\frac{2h}{r}$ IF $r \ll h$	11-122 8 9
3	TWO EQUIDISTANT PARALLEL INFINITE PLANES	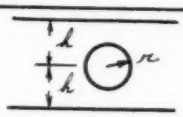	$\simeq(\frac{4h}{\pi r})=1.273\frac{h}{r}$ IF $r \ll h$	12-326 9 10
4	TWO INTERSECTING INFINITE PLANES, EMITTER ON BISECTRIX	$0<\theta<\pi$ 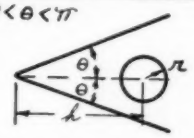	$\simeq 4\frac{\theta h}{\pi r}=1.273(\frac{\theta h}{r})$ IF $r \ll h$	11-237
5	SEMI-INFINITE PLANE	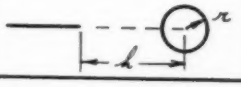	$\simeq\frac{4h}{\pi}$ IF $r \ll h$	
6	TWO INFINITE PLANES AT RIGHT ANGLES	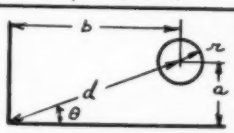	$\exp\{\cosh^{-1}(\frac{a}{r})+\cosh^{-1}(\frac{b}{r})-\cosh^{-1}(\frac{\sqrt{a^2+b^2}}{r})\}$ $\simeq\frac{2}{\pi}\frac{ab}{\sqrt{a^2+b^2}}=\frac{d}{r}\sin 2\theta$ IF $r \ll a, b$	
7	CYLINDER OF SQUARE CROSS-SECTION	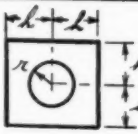	$(\frac{h}{r})\exp\{0.108-0.039\frac{1+0.905(r/h)^4}{1-0.905(r/h)^4}$ $-0.008\frac{1+0.163(r/h)^8}{1-0.163(r/h)^8}-0.002\frac{1+0.067(r/h)^{12}}{1-0.067(r/h)^{12}}\}$ $\simeq 1.061(h/r)$ IF $r \ll h$	12-327 14
8	TROUGH OF RECTANGULAR CROSS-SECTION AND INFINITE WALLS	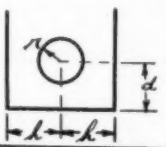	$\simeq(\frac{4h}{\pi r})\tanh(\frac{\pi d}{2h})=\frac{1.237h}{r}\tanh(\frac{1.571d}{h})$ IF $h, d \ll 3r$ $=1.168\,h/r$ IF $h=d$	12-327
9	EXTERNAL CYLINDER	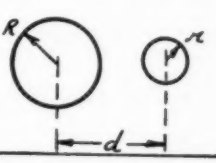	$\exp\{\cosh^{-1}(\frac{d^2+r^2-R^2}{2dr})+\cosh^{-1}(\frac{d^2-r^2+R^2}{2dr})\}$ $\simeq(\frac{d^2}{rR})\exp(-\frac{r^2+R^2}{d^2})\simeq\frac{d^2}{rR}$ IF $d>>r, R$ IF $R=r$, $\exp\{2\cosh^{-1}(\frac{d}{2r})\}\simeq(d/r)^2$ IF $d>>r, R$	11-120

[a] See references listed in text. Numbers after hyphen indicate page.

TABLE I.—*Continued.*

NO.	ANODE	NOMENCLATURE	(R' = RATIO OF EQUIVALENT FICTITIOUS CYLINDRICAL COLLECTOR COAXIAL WITH EMITTER) $R'=r_c/r$	REF.[a]
10	TWO EQUIDISTANT CYLINDERS	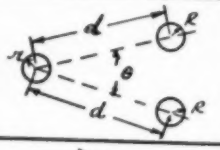	$\exp\{\cosh^{-1}\left(\frac{d^2+r^2-R^2}{2dr}\right),\cosh^{-1}\left(\frac{d^2-r^2+R^2}{2dR}\right) -\frac{1}{2}\cosh^{-1}\left[\frac{d\sin(\theta/2)}{R}\right]\} \simeq \left[\frac{d^3}{2r^2R\sin(\theta/2)}\right]^{1/2}$ IF $d>>r$ AND $d\sin\theta>>R$	
11	THREE EQUIDISTANT CYLINDERS AT APICES OF EQUILATERAL TRIANGLE	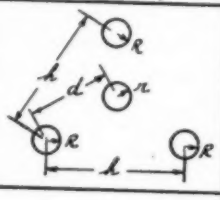	$\exp\{\cosh^{-1}\left(\frac{d^2+r^2-R^2}{2dr}\right),\cosh^{-1}\left(\frac{d^2-r^2+R^2}{2dR}\right) -\frac{2}{3}\cosh^{-1}\left(\frac{\sqrt{3}d}{2R}\right)\} \simeq \frac{d^{\frac{2}{3}}}{3^{\frac{1}{3}}rR^{\frac{1}{3}}} = \frac{h^{\frac{2}{3}}}{3rR^{\frac{1}{3}}}$ IF $d>>r, R$	
12	FOUR EQUIDISTANT CYLINDERS AT CORNERS OF SQUARE	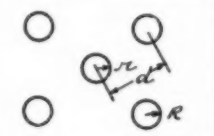	$\exp\{\cosh^{-1}\left(\frac{d^2+r^2-R^2}{2dr}\right)+\cosh^{-1}\left(\frac{d^2-r^2+R^2}{2dR}\right) -\frac{1}{2}\cosh^{-1}\left(\frac{d}{\sqrt{2}R}\right)-\frac{1}{4}\cosh^{-1}\left(\frac{d}{R}\right)\} \simeq \frac{d^{\frac{5}{4}}}{2^{\frac{1}{2}}rR^{\frac{1}{4}}}$ IF $d>>r, R$	
13	FOUR EQUIDISTANT CYLINDERS AT CORNERS OR RECTANGLE	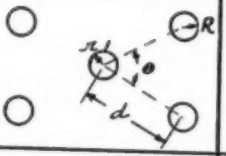	$\simeq \frac{d^{\frac{5}{2}}}{2^{\frac{1}{2}}rR^{\frac{1}{2}}\sin^{\frac{1}{2}}\theta}$ IF $d>>r$ AND $d\sin\theta>>R$	
14	n CYLINDERS EQUALLY SPACED ON CIRCLE	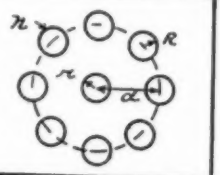	$\simeq \left(\frac{d}{r}\right)\left(\frac{d}{nR}\right)^{1/n}$ IF $d>>r, nR/\pi$	
15	CONCENTRIC SLOTTED CYLINDER	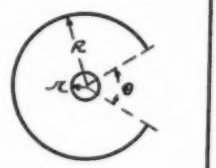	$\left[\left(\frac{R}{r}\right)\frac{\left\{\tan^2\left(\frac{\theta}{4}\right)+\left(\frac{R+r}{R-r}\right)^2\right\}^{1/2}+\sec\left(\frac{\theta}{4}\right)}{\left\{\tan^2\left(\frac{\theta}{4}\right)+\left(\frac{R+r}{R-r}\right)^2\right\}^{1/2}-\sec\left(\frac{\theta}{4}\right)}\right]$ $\simeq \left(\frac{R}{r}\right)\sec\left(\frac{\theta}{4}\right)$ IF $r<<R$	15
16	INFINITE PLANE WITH TWO EQUIDISTANT EMITTERS	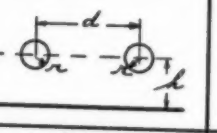	$\simeq \left(\frac{2h}{r}\right)\left[1+\left(\frac{2h}{d}\right)^2\right]^{1/2}$ IF $r<<d, h$ (TWO SEPARATE DIODES)	12-324
17	INFINITE PLANE AND ROW OF n EQUIDISTANT, EQUALLY SPACED EMITTERS	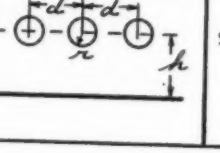	$\simeq \left(\frac{d}{2\pi r}\right)\exp\left(\frac{2\pi h}{d}\right)$ IF $\begin{cases} r<<d \\ h\geq d \end{cases}$ (n SEPARATE DIODES)	11-293 B

[a] See references listed in text. Numbers after hyphen indicate page.

TABLE I.—*Continued.*

NO.	ANODE	NOMENCLATURE	(R' = RADIUS OF EQUIVALENT FICTITIOUS CYLINDRICAL COLLECTOR COAXIAL WITH EMITTER.)	REF.[a]
18	TWO EQUIDISTANT PARALLEL INFINITE PLANES AND ROW OF EQUALLY SPACED EMITTERS	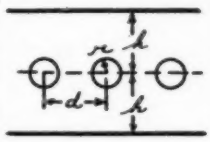	$\simeq \left(\frac{d}{2\pi r}\right) \exp\left(\frac{\pi h}{d}\right)$ IF $\begin{cases} r \ll d \\ h \geq d \end{cases}$ (n SEPARATE DIODES)	II-294
19	CYLINDER AND RING OF n EQUALLY SPACED EMITTERS		$\simeq \frac{d}{nr}\left(\frac{R}{d}\right)^n$ IF $\begin{cases} r \ll \pi d/n \\ d \ll R \end{cases}$ (n SEPARATE DIODES)	8
20	CYLINDER WITH TWO EMITTERS		$\simeq \frac{R^2 - d^2}{2rd}$ IF $r \ll d, R$ (TWO SEPARATE DIODES)	12-325
21	TWO CYLINDERS AND TWO EMITTERS	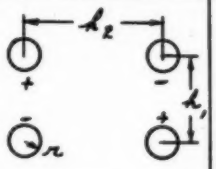	$\simeq \left[\frac{h_1 h_2}{r\sqrt{h_1^2 + h_2^2}}\right]^2$ IF $r \ll h_1, h_2$ (TWO SEPARATE DIODES)	12-329

[a] See references listed in text. Numbers after hyphen indicate page.

agreement is, in general, satisfactory for practical purposes. Since the capacitance of most electrode systems can be either calculated very easily or measured without the necessity for using evacuated envelopes, it would seem that the method has practical application as a convenient and time-saving device in electron tube design problems. The distribution of the emission over the emitter may also be determined by this technique.[8]

For the case of a cylindrical cathode of radius r and a coaxial cylindrical anode of radius R', the space-change limited electronic current per unit length of the electrode system is given by the well-known result

$$I/l = (2\pi)2.33\times10^{-6}V^{\frac{1}{2}}/R'\beta^2(R'/r), \qquad (1)$$

where V is the potential of the anode relative to the cathode and the quantity β^2, which is is a function of the radius ratio R'/r, has been tabulated.[2,3] The capacity per unit length of this electrode system is given by

$$C' = 1/2\ln(R'/r), \qquad (2)$$

where C' is in esu per cm (1 esu = 1.11 $\mu\mu f$). Since equation (2) may be used to determine the radius R' of the fictitious anode corresponding to an actual electrode system, substitution into equation (1) results in an expression for the current per unit length of an actual diode with cylindrical emitter of radius r in terms of its capacitance per unit length,

$$I/l = 14.6\times10^{-6}(V^{\frac{1}{2}}/r)\{[e^{1/2e'}\beta^2(e^{1/2e'})]^{-1}\}. \qquad (3)$$

In the case of a spherical cathode of radius r and a concentric spherical anode of radius R', the space-charge-limited current is given by

$$I = (4\pi)2.33\times10^{-6}V^{\frac{1}{2}}/\alpha^2(R'/r), \qquad (4)$$

where the function α^2 has also been tabulated.[4] Since the capacity (in esu) of this spherical diode is given by

$$C = R'r/(R'-r), \qquad (5)$$

the result may be expressed in terms of the capacitance of the actual diode as

$$I = 29.2\times10^{-6}V^{\frac{1}{2}}\{[\alpha^2(1-r/C)^{-1}]^{-1}\}. \qquad (6)$$

[11] E. Weber, *Electromagnetic Fields. Theory and Applications. Vol. I. Mapping of Fields* (John Wiley and Sons, Inc., New York, 1950).
[12] *Reference Data for Radio Engineers* (Federal Telephone and Radio Corporation, 1949), third edition.
[13] C. L. Dawes, Physics, **4**, 81 (1933).
[14] P. Parzen, J. Appl. Phys. **18**, 774 (1947).
[15] T. C. Fry, Am. Math. Monthly, **39**, 199 (1932).

TABLE II. Geometries with external cylindrical emitter of radius r.

NO.	ANODE	NOMENCLATURE	(R' = RADIUS OF EQUIVALENT FICTITIOUS CYLINDRICAL COLLECTOR COAXIAL WITH EMITTER) $R^{1/2\pi}$	REF.[a]
1	ECCENTRIC CYLINDER		$\exp\left[-\left(\cosh^{-1}\left(\frac{r^2-R^2-d^2}{2dR}\right)-\cosh^{-1}\left(\frac{r^2-R^2+d^2}{2dr}\right)\right)\right]$ $= \exp\left[-\cosh^{-1}\left(\frac{r^2+R^2-d^2}{2Rr}\right)\right] \simeq \frac{R/r}{1-(d/r)^2}$ IF $r \gg R$	11-121 13
2	TWO CYLINDERS		$\simeq \left[\frac{2Rd}{r^2-d^2}\right]^{\frac{1}{2}}$ IF $r \gg R, d$	12-325
3	n CYLINDERS EQUALLY SPACED ON CIRCLE		$\simeq \frac{d}{r}\left(\frac{2R}{d}\right)^{1/n}$ IF $R \ll 2\pi d$, $d \ll r$	
4	RIBBON		$\simeq h/2r$ IF $r \gg h$	11-320

[a] See references listed in text. Numbers after hyphen indicate page.

It may be noted that the consideration for both the cylindrical case and the spherical case apply to problems involving emitters external to the fictitious anode as well as to the more usual arrangement of an internal emitter, provided that the appropriate value of the function α^2 or β^2 is used, and if the sign of the capacitance C or C' is considered to be negative, so that $r > R'$. As is well known, for the case of an internal cylindrical emitter and $R'/r > 10$, β^2 may be approximated by unity. The functions in brackets in Eqs. (3) and (6) have been plotted in Fig. 1 for convenience.

The technique described above has been applied to many electrode arrangements, with the results shown in the attached tables. Table I refers to systems with

TABLE III. Geometries with internal spherical emitter of radius r.

NO.	ANODE	NOMENCLATURE	(R' = RADIUS OF EQUIVALENT FICTITIOUS SPHERICAL COLLECTOR CONCENTRIC WITH EMITTER.) $R^{1/2\pi}$	REF.[a]
1	INFINITE PLANE	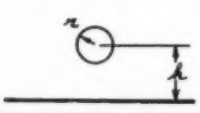	$\frac{1-\left(\frac{r}{2h}\right)^2}{\left(\frac{r}{2h}\right)\left[1-\left(\frac{r}{2h}\right)^2+\left(\frac{r}{2h}\right)^3\right]} \simeq \frac{2h}{r}$ IF $r \ll h$	11-104
2	TWO EQUIDISTANT PARALLEL INFINITE PLANES	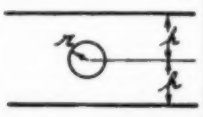	$\simeq \frac{h}{r \ln 2} = 1.443\,\frac{h}{r}$ IF $r \ll h$	11-217

[a] See references listed in text. Numbers after hyphen indicate page.

internal cylindrical emitters, Table II to systems with external cylindrical emitters, and Table III to systems with internal spherical emitters. For each system the ratio of the radius of the fictitious anode to that of the emitter is tabulated. In the case of systems involving more than one emitter, the equivalent simple geometry is a multiplicity of diodes, one for each emitter. Matricon and Trouvé[8] have considered the cases of a row of equally spaced cylindrical emitters parallel to a plane anode and of a ring of cylindrical emitters equally spaced on a cylindrical surface coaxial with a cylindrical emitter (items 17 and 20 of Table I) in more detail. They have shown that the current indicated by the results of the table should be multiplied by the factor $I_0(4\pi r/d)$, where I_0 is the modified Bessel function (complex argument) of the first kind and zeroth order, in the first case and by the factor

$$\frac{1}{\pi}\int_0^{\pi}[1+(r/d)^2+2(r/d)\cos\theta]^{n-1}d\theta \qquad (7)$$

in the second case. Both these functions are greater than unity but approach it as r/d becomes small.

It is of interest to compare the results of the method utilized here with those of some earlier attacks on this problem. The case of a row of cylindrical emitters midway between two parallel plane anodes (Table I, item 18) was discussed by Kusunose[16,10] and by Harris[17].

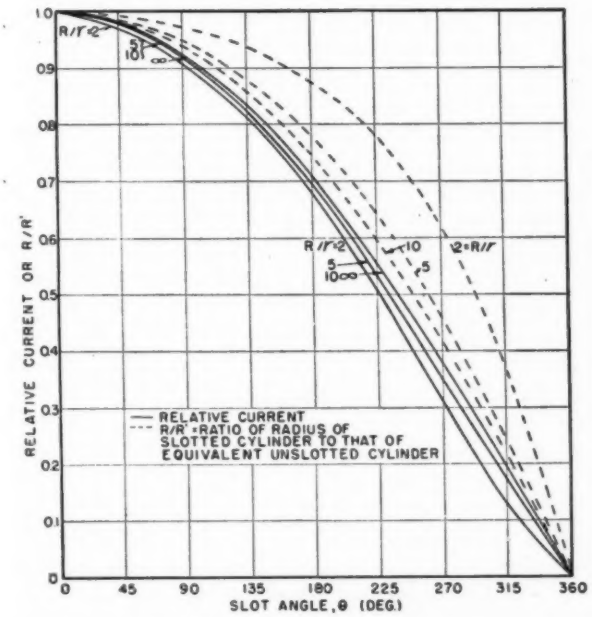

FIG. 2. Variation of space-charge-limited current and of equivalent unslotted collector radius for cylindrical emitter and coaxial slotted cylindrical collector as a function of the angular slot opening θ for various values of radius ratio R/r (current values normalized to unity for $\theta=0$).

[16] Y. Kusunose, Proc. Inst. Radio Engrs. 17, 1706 (1929).
[17] I. A. Harris, Wireless Engr., 18, 45, 153 (1941).

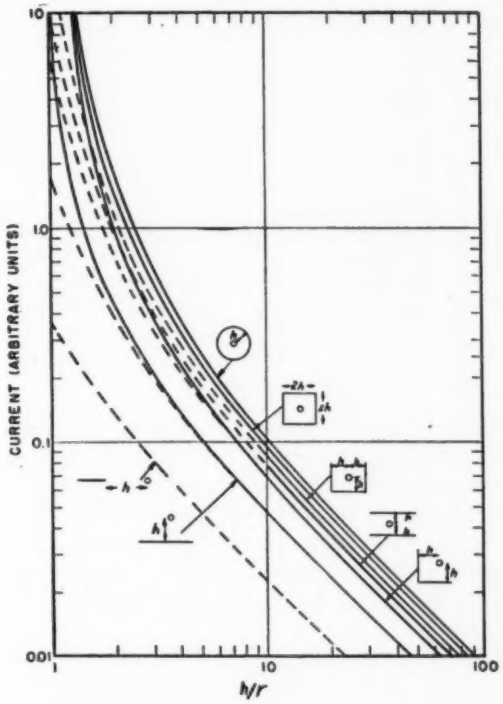

FIG. 3. Variation of space-charge-limited current between cylindrical emitter and collector system composed of a number of planes as a function of the ratio of electrode separation h to emitter radius r. The current values as plotted must be multiplied by the quantity $14.6\times10^{-6}V^{\frac{3}{2}}/r$ to obtain the current in amperes per unit axial length of the electrode system. (Dashed lines are approximations).

Harris' results may be put into the form

$$\frac{R'}{r}=\frac{\pi h/4r}{\int_0^{(d/h)}[(1+x^2)^{\frac{1}{2}}+x^{-1}\sinh^{-1}x]^{-2}dx}. \qquad (8)$$

Harris[17] has also considered the cases of a cylindrical anode with a coaxial ring of cylindrical emitters (Table I, item 20) and with a coaxial helical emitter. For the case of a single cylindrical emitter midway between two parallel plane anodes, Harris' method ($d=\infty$ in equation 8) indicates an equivalent cylindrical anode radius of $3\pi h/8=1.18h$, while the rather crude analysis of Kusunose[16,10] gives $\pi h/2=1.57h$. It may be noted that the present technique (Table I, item 3) indicates for this case, $R'=4h/\pi=1.27h$, intermediate to the earlier results.

It is of interest to note that not all problems involving spherical emitters may be solved by the technique discussed here. As an example may be mentioned the case of two spherical electrodes neither of which is inside the other. As the distance between the spheres is increased, the capacitance between them obviously approaches zero. This situation cannot be represented by two concentric spheres because as the radius of the outer of such spheres increases without limit, the

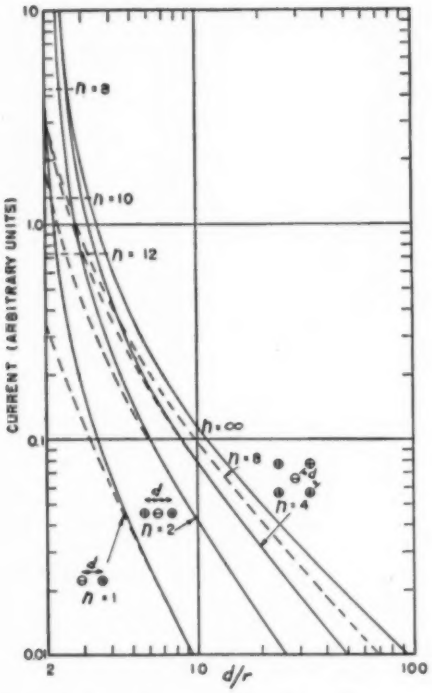

FIG. 4. Variation of space-charge-limited current between cylindrical emitter and collector system composed of n cylinders with radius r equal to that of the emitter, and equally spaced on a cylindrical surface of radius d coaxial with the emitter, as a function of the ratio d/r. The current values as plotted must be multiplied by the quantity $14.6\times10^{-6}V^{\frac{3}{2}}$ to obtain the current in amperes per unit axial length of the electrode system. (Dashed lines are approximations).

capacitance of the system (in esu) approaches the radius of the inner sphere, and not zero.

A system of practical interest is that of a cylindrical emitter with a coaxial slotted cylindrical anode (Table I, item 15). Figure 2 presents the results of calculations on this system. The dashed lines give the variation of R/R' (i.e., the ratio of the radius of the slotted cylinder to that of the equivalent unslotted cylinder) as a function of slot angle θ for several values of the ratio R/r (r=emitter radius), while the solid lines give the variation in space-charge-limited current relative to that for the unslotted anode ($\theta=0$). It is seen that because of the presence of the β^2 factor in equation (3), the variation of current with slot angle is not greatly dependent upon the relative sizes of the two cylinders, so that for even moderate values of R/r, the variation with angle may be expressed by the simple expression $\cos(\theta/4)$.

Result for several electrode systems involving a cylindrical emitter and a number of plane anodes are shown in Fig. 3. The dashed curves are approximations, while the solid curves correspond to the complete solutions as given in Table I.† Figure 4 gives similar results for a cylindrical emitter and a number of cylindrical anodes with radius equal to that of the emitter and equally spaced on a cylindrical surface coaxial with the emitter. The curve designated $n=\infty$ in Fig. 4 was obtained by employing the fact that the emission in such a system will obviously never be greater than that obtained if the cage of cylindrical anodes is replaced by the single inscribed cylinder which has a radius of $R'=(d/r-1)$. For $n>6$ a further maximum current limit is reached because as d/r is decreased, the anode cylinders will come in contact with each other before they can contact the central emitter. This will occur at $d/r=\csc(\pi/n)$ as shown by the horizontal dashed lines for $n=8$, 10, and 12.

† O'Neill[9] and Dow[10] give $R'/r=\coth(\pi r/4h)$ for the case of a cylindrical emitter midway between two parallel planes and consider the result given in Table I (item 3) as only an approximation to this better value. It will be noted, however, that this result remains finite as h/r approaches unity, instead of approaching infinity as it obviously should, and indeed always gives smaller current values than the result given in Table I. For this reason the latter expression seems preferable; for small values of h/r the actual current will be even greater and will be intermediate to that for a single plane anode and a square box anode as shown in Figure 3.

JOURNAL OF APPLIED PHYSICS VOLUME 24, NUMBER 12 DECEMBER, 1953

Response of Two-Material Laminated Cylinder to Simple Harmonic Environment Temperature Change

HERMAN H. LOWELL
Lewis Flight Propulsion Laboratory, National Advisory Committee for Aeronautics, Cleveland, Ohio
(Received May 7, 1953)

In current aeronautical research, rapidly-responding thermocouples and hot-wire anemometers are required. The use of oxide cylinders coated with more or less thin layers of metal effects substantial improvements in rates of instrument response. The theory and results of numerical calculations for six typical situations are given. It is shown that for ratios of metal thickness to over-all radius of 0.1, response amplitude gains of the order of 4 or 5 are to be expected as compared with typical gains of the order of 10 or more for infinitesimal shells (surface layers).

INTRODUCTION

ONE of the current goals of aeronautical research instrumentation development is improvement of responses of thermocouples and hot-wire anemometers to rapid changes of environment (fluid) temperature or mass-flow rate. "Improvement" means here, essentially, an increase in signal-to-noise ratio at high rates of signal amplitude change.

When such an increase of signal-to-noise ratio has been effected, greater gain can be used in either an "open" circuit or a closed loop (for example, a constant-temperature anemometer circuit) to achieve a more nearly flat response from very low to very high frequencies.

One possible technique whereby this desired increase in signal-to-noise ratio may be attained is that of substituting for the conventional homogeneous metallic wire a laminated structure consisting of a cylindrical core of electrically nonconducting and thermally poorly conducting material surrounded by a shell of electrically conductive material. The core may consist, for example, of an oxide such as fused silica or synthetic sapphire (monocrystalline alumina), while the shell will generally be metallic, but may be semimetallic (for the sake of a high-resistivity temperature coefficient product or resistance to oxidation or both).

Such a structure has certain obvious advantages and a few which are not obvious. First, as a result of concentration of the electrical active material near the surface, we have placed it in a region that is the first to sense, as it were, environmental changes. The result is that the amplitude becomes much greater under certain circumstances than that of a conventional wire of the same size; at the same time, the lag of the response behind the external change becomes smaller. Second, for the same cross section of material and same wire length, we reduce errors associated with heat conduction along the wire (to or from supports); this error is reduced because of the much smaller thermal conductivity of the core material. The higher electrical resistance of such a structure results in a more efficient transfer of electrical energy to high impedance devices such as amplifier input circuits, with certain additional advantageous consequences. Finally, because of the smaller length-to-diameter ratio made possible by the lower thermal conductance, the laminated structure should have higher strength than ordinary wires of certain materials. It might be added that while all of these improvements are possible, it will obviously be impossible to achieve substantial gains in all directions simultaneously. As usual, the unit will have to be designed for the application.

The basic idea was suggested at the Lewis Flight Propulsion Laboratory, Cleveland, Ohio, *ca* 1946, and some experimental work was done at that time in collaboration with H. W. Allen of that laboratory. In addition, it is understood that J. Strong of Johns Hopkins University has independently suggested (*ca* 1948) that, if an ordinary metallic wire is divided into two concentric regions by a thin subsurface shell of nonconducting material, the difference in the responses of the two regions may be used to automatize the task of achieving correct compensation in the case of a constant-current (open circuit) hot-wire anemometer.

The purpose of the present article is the presentation of both the analytical solution for the core-and-shell case, as arrived at recently at Lewis, and a few typical results. Additional analytical solutions for related situations are given in the articles listed in the appended Bibliography.

THEORY

Let us consider a cylindrical core of radius r_a the properties of which are the following: thermal conductivity k_1; specific heat $c_{p,1}$; density ρ_1; and thermal diffusivity $a_1{}^*$. Let the surrounding concentric shell have an outer radius r_b and properties denoted by the appropriate symbols and the subscript 2. In the following, t represents that portion of the temperature which is varying, while θ represents time. (All symbols in this paper are defined in a list following the text proper.)

The following are the equations governing the temperatures in the two regions:

$$\frac{\partial t_1}{\partial \theta} = a_1{}^* \left(\frac{\partial^2 t_1}{\partial r^2} + \frac{1}{r} \frac{\partial t_1}{\partial r} \right), \tag{1}$$

$$\frac{\partial t_2}{\partial \theta} = a_2{}^* \left(\frac{\partial^2 t_2}{\partial r^2} + \frac{1}{r} \frac{\partial t_2}{\partial r} \right). \tag{2}$$

If t_e represents the environment temperature and h^* the ratio of heat transfer coefficient to k_2, the following are the boundary conditions which must be fulfilled:

$$-(\partial t_2/\partial r)_b = h^*(t_{2,b} - t_e); \tag{3}$$

$$(\partial t_1/\partial r)_a = \gamma^*(\partial t_2/\partial r)_a, \tag{4}$$

where $\gamma^* = k_2/k_1$; and

$$(t_1)_a = (t_2)_a. \tag{5}$$

If t_e is now assumed to equal $t_{e,M}\cos\omega\theta$, t_1 and t_2 will be represented by the real parts of the solutions $t_1 = C_3\psi_1(r)\exp(i\alpha_1^2 a_1^*\theta)$, and $t_2 = C_4\psi_2(r)\exp(i\alpha_2^2 a_2^*\theta)$, where $\alpha_1^2 = \omega/a_1^*$, $\alpha_2^2 = \omega/a_2^*$ and ψ_1 and ψ_2 are the solutions of the modified Bessel's equations

$$\frac{d^2\psi_1}{dr^2} + \frac{1}{r}\frac{d\psi_1}{dr} - i\alpha_1^2\psi_1 = 0, \tag{6}$$

and

$$\frac{d^2\psi_2}{dr^2} + \frac{1}{r}\frac{d\psi_2}{dr} - i\alpha_2^2\psi_2 = 0, \tag{7}$$

for their respective regions.

It is finally found after a number of obvious elementary manipulations, that the required solutions are of the form

$$\text{(Real part of) } t_1 = [C_1 f_R(\alpha_1 r) + D_1 f_I(\alpha_1 r)]\cos\omega\theta + [D_1 f_R(\alpha_1 r) - C_1 f_I(\alpha_1 r)]\sin\omega\theta, \tag{8}$$

and

$$\text{(Real part of) } t_2 = [C_2 f_R(\alpha_2 r) + G_2 F_R(\alpha_2 r) + D_2 f_I(\alpha_2 r) + E_2 F_I(\alpha_2 r)]\cos\omega\theta + [D_2 f_R(\alpha_2 r) + E_2 F_R(\alpha_2 r) - C_2 f_I(\alpha_2 r) - G_2 F_I(\alpha_2 r)]\sin\omega\theta, \tag{9}$$

where $f_R(\alpha_1 r)$ is the real part of $J_0(\alpha_1 r i^{\frac{1}{2}})$, $f_I(\alpha_1 r)$ the imaginary part, $F_R(\alpha_1 r)$ the real part of any of the several different solutions of the second kind of the modified Bessel's equation, and so forth. Note that while we take $f_R = \mathrm{ber}_0$ and $f_I = \mathrm{bei}_0$, F_R may or may not be taken as ker_0, and so forth, depending upon the identity of the function of the second kind that is adopted for the purpose.

The constants $C_1, D_1, \cdots, G_2$ are then determined by using the relations (3), (4), (5), (8), and (9) to obtain a set of six simultaneous linear algebraic equations.

The manipulations are tedious. The final set is the following; certain additional nomenclature employed is explained below:

$$\begin{aligned}
&-f_I(\alpha_1 r_a)C_1^* + f_I(\alpha_2 r_a)C_2^* + f_R(\alpha_1 r_a)D_1^* - f_R(\alpha_2 r_a)D_2^* + F_I(\alpha_2 r_a)G_2^* - F_R(\alpha_2 r_a)E_2^* = 0;\\
&f_R(\alpha_1 r_a)C_1^* - f_R(\alpha_2 r_a)C_2^* + f_I(\alpha_1 r_a)D_1^* - f_I(\alpha_2 r_a)D_2^* - F_R(\alpha_2 r_a)G_2^* - F_I(\alpha_2 r_a)E_2^* = 0;\\
&f_I'(\alpha_1 r_a)C_1^* - \gamma f_I'(\alpha_2 r_a)C_2^* - f_R'(\alpha_1 r_a)D_1^* + \gamma f_R'(\alpha_2 r_a)D_2^* - \gamma F_I'(\alpha_2 r_a)G_2^* + \gamma F_R'(\alpha_2 r_a)E_2^* = 0;\\
&-f_R'(\alpha_1 r_a)C_1^* + \gamma f_R'(\alpha_2 r_a)C_2^* - f_I'(\alpha_1 r_a)D_1^* + \gamma f_I'(\alpha_2 r_a)D_2^* + \gamma F_R'(\alpha_2 r_a)G_2^* + \gamma F_I'(\alpha_2 r_a)E_2^* = 0;\\
&-[Ja_2 f_I(\alpha_2 r_b) + f_I'(\alpha_2 r_b)]C_2^* + [Ja_2 f_R(\alpha_2 r_b) + f_R'(\alpha_2 r_b)]D_2^*\\
&\qquad - [Ja_2 F_I(\alpha_2 r_b) + F_I'(\alpha_2 r_b)]G_2^* + [Ja_2 F_R(\alpha_2 r_b) + F_R'(\alpha_2 r_b)]E_2^* = 0;\\
&[Ja_2 f_R(\alpha_2 r_b) + f_R'(\alpha_2 r_b)]C_2^* + [Ja_2 f_I(\alpha_2 r_b) + f_I'(\alpha_2 r_b)]D_2^*\\
&\qquad + [Ja_2 F_R(\alpha_2 r_b) + F_R'(\alpha_2 r_b)]G_2^* + [Ja_2 F_I(\alpha_2 r_b) + F_I'(\alpha_2 r_b)]E_2^* = Ja_2.
\end{aligned} \tag{10}$$

In Eqs. (10), C_1^*, and so forth, are equal to $C_1/t_{e,M}$, etc., and are nondimensional; γ is defined as $(k_2/k_1)(a_1^*/a_2^*)^{\frac{1}{2}}$, Ja_2 as $h_f/(\omega k_2\rho_2 c_{p,2})^{\frac{1}{2}}$ and $f_I'(\alpha_1 r_a)$ as $[df_I/d(\alpha_1 r)]_{r=r_a}$, and so forth. (Note that Ja is an abbreviation of "Jakob.")

Formally, this set of equations represents the solution of the problem. In practice, the set was modified for computational purposes by elimination of G_2^*. From the fifth of Eqs. (10) we find that

$$\begin{aligned}
G_2^* = {}&[Ja_2 F_I(\alpha_2 r_b) + F_I'(\alpha_2 r_b)]^{-1}\\
&\times\{-[Ja_2 f_I(\alpha_2 r_b) + f_I'(\alpha_2 r_b)]C_2^*\\
&+[Ja_2 f_R(\alpha_2 r_b) + f_R'(\alpha_2 r_b)]D_2^*\\
&+[Ja_2 F_R(\alpha_2 r_b) + F_R'(\alpha_2 r_b)]E_2^*\}.
\end{aligned} \tag{11}$$

This relation was used to reduce the set of six equations to one of five. Again, the procedure is merely mechanical and the modified set is not given here. A few additional details of the computing procedure are, however, given in the appendix.

Since the constants $C_1^* \cdots G_2^*$ are now available, Eqs. (8) and (9), after modification by division by $t_{e,M}$, yield $\eta_1 = t_1/t_{e,M}$ and $\eta_2 = t_2/t_{e,M}$ directly, and these were the instantaneous local relative temperatures sought.

In practical work, however, the instantaneous mean shell temperature and relative phase are much more useful than a knowledge of the variation of local temperature. An averaging process was carried out as follows. $\eta_{2,C}$ and $\eta_{2,S}$ are defined by the relations [compare with Eq. (9)]:

$$\eta_{2,C} = C_2^* f_R(\alpha_2 r) + G_2^* F_R(\alpha_2 r) + D_2^* f_I(\alpha_2 r) + E_2^* F_I(\alpha_2 r),$$

and

$$\eta_{2,S} = D_2^* f_R(\alpha_2 r) + E_2^* F_R(\alpha_2 r) - C_2^* f_I(\alpha_2 r) - G_2^* F_I(\alpha_2 r). \tag{12}$$

Then,

$$\langle\eta_2\rangle_M = \frac{2}{\alpha_2^2(r_b^2 - r_a^2)} \times \int_{\alpha_2 r_a}^{\alpha_2 r_b} [\eta_{2,C}\cos\omega\theta + \eta_{2,S}\sin\omega\theta](\alpha_2 r)\,d(\alpha_2 r). \tag{13}$$

If we now designate the in-phase and out-of-phase components of instantaneous mean relative shell temperature $\langle\eta_2, c\rangle_M$ and $\langle\eta_2, s\rangle_M$, respectively, we now have

$$\langle\eta_2\rangle_M=(\langle\eta_2, c^2\rangle_M+\langle\eta_2, s^2\rangle_M)^{\frac{1}{2}}\cos\left[\omega\theta-\tan^{-1}\frac{\langle\eta_2, s\rangle_M}{\langle\eta_2, c\rangle_M}\right], \quad (14)$$

in which, defining $\beta=r_a/r_b$,

$$\begin{aligned}\langle\eta_2, c\rangle_M=&\frac{2}{\alpha_2 r_b(1-\beta^2)}\{C_2^*[f_I'(\alpha_2 r_b)-\beta f_I'(\alpha_2 r_a)]\\&+G_2^*[F_I'(\alpha_2 r_b)-\beta F_I'(\alpha_2 r_a)]\\&-D_2^*[f_R'(\alpha_2 r_b)-\beta f_R'(\alpha_2 r_a)]\\&-E_2^*[F_R'(\alpha_2 r_b)-\beta F_R'(\alpha_2 r_a)]\},\end{aligned}$$

and

$$\begin{aligned}\langle\eta_2, s\rangle_M=&\frac{2}{\alpha_2 r_b(1-\beta^2)}\{D_2^*[f_I'(\alpha_2 r_b)-\beta f_I'(\alpha_2 r_a)]\\&+E_2^*[F_I'(\alpha_2 r_b)-\beta F_I'(\alpha_2 r_a)]\\&+C_2^*[f_R'(\alpha_2 r_b)-\beta f_R'(\alpha_2 r_a)]\\&+G_2^*[F_R'(\alpha_2 r_b)-\beta F_R'(\alpha_2 r_a)]\}. \quad (15)\end{aligned}$$

Although of no physical significance in this problem, the mean temperature of the core is also given as a matter of completeness,

$$\begin{aligned}\langle\eta_1\rangle_M=&\frac{2}{\alpha_1 r_a}\{[C_1^* f_I'(\alpha_1 r_a)-D_1^* f_R'(\alpha_1 r_a)]^2\\&+[D_1^* f_I'(\alpha_1 r_a)+C_1^* f_R'(\alpha_1 r_a)]^2\}^{\frac{1}{2}}\\&\times\cos\left\{\omega\theta-\tan^{-1}\frac{[D_1^* f_I'(\alpha_1 r_a)+C_1^* f_R'(\alpha_1 r_a)]}{[C_1^* f_I'(\alpha_1 r_a)-D_1^* f_R'(\alpha_1 r_a)]}\right\}. \quad (16)\end{aligned}$$

RESULTS AND DISCUSSION

In the preceding equations, a number of nondimensional parameters occur, *viz.*, β, Ja_2, $\alpha_1 r_a$, $\alpha_2 r_b$, $\alpha_2 r_a$, and γ. In addition, the variables $\alpha_1 r$ and $\alpha_2 r$ occur. There are, in actuality, eight independent physical variables, *viz.*, r_a, r_b, h_f, k_1, k_2, a_1^*, a_2^*, and ω. It is a relatively straightforward matter to show, by means of the Buckingham II theorem or otherwise, that any physical situation describable in terms of those eight variables can be described in terms of only five properly chosen nondimensional parameters. Since six appear in the text and equations, one may be rejected, and we choose to reject $\alpha_2 r_a$. It is of interest to note that with the exceptions of β and γ, the remaining parameters are identifiable as Fourier numbers or combinations of a Fourier number and a Biot number. We have

$$Ja_2=Bi_2(Fo_2)^{\frac{1}{2}}=h^*/\alpha_2, \quad (17)$$

in which

$$Bi_2=h_f r_b/k_2,$$

and

$$Fo_2=(\alpha_2 r_b)^{-2}=a_2^*/\omega r_b^2=k_2/\omega\rho_2 c_{p,2} r_b^2.$$

Further,

$$\alpha_1 r_a=Fo_1^{-\frac{1}{2}}, \quad (18)$$

in which

$$Fo_1=a_1^*/\omega r_a^2=k_1/\omega\rho_1 c_{p,1} r_a^2.$$

The following is an alternative and more modern approach: We define two time constants—an "external" (τ_{ext}) and an "internal" (τ_{int}). τ_{ext} is the time required for the uniform temperature of a homogeneous cylinder of radius r_b—and made of material of infinite thermal conductivity but having the same volume specific heat $\rho_2 c_{p,2}$ as the shell—to change by $1-\epsilon^{-1}$ of the total change when the environment temperature is suddenly altered, the heat transfer coefficient being h_f. $\tau_{int,2}$ is the time required for the mean temperature of a homogeneous cylinder of radius r_b—and made of the same material as the shell—to change by $1-\epsilon^{-1}$ of the total change when the *surface* temperature is suddenly altered; the value of the heat transfer coefficient is not germane. Finally, $\tau_{int,1}$ is the time required for the mean temperature of a homogeneous cylinder of radius r_a—and made of the same material as the *core*—to change by $1-\epsilon^{-1}$ of the total change when the surface temperature (at radius r_a) is suddenly altered.

It is possible to show by elementary methods that these time constants are given by the following expressions:

$$\begin{aligned}\tau_{ext}&=r_b\rho_2 c_{p,2}/2h_f,\\ \tau_{int,2}&=\lambda r_b^2\rho_2 c_{p,2}/k_2,\\ \tau_{int,1}&=\lambda r_a^2\rho_1 c_{p,1}/k_1,\end{aligned} \quad (19)$$

in which λ is a nondimensional constant having the value 0.111+. For the purposes of these computations, the exact value 0.111 was adopted. This is equivalent to a redefinition of τ_{int} according to Eq. (19).

In terms of the products of $\omega(=2\pi\times\text{frequency})$ and the above time constants, three of the nondimensional parameters of interest may be expressed as follows:

$$\alpha_1 r_a=\lambda^{-\frac{1}{2}}(\omega\tau_{int,1})^{\frac{1}{2}},$$

or, in general,

$$\alpha_1 r=\lambda^{-\frac{1}{2}}(\omega\tau_{int,1})^{\frac{1}{2}}, \quad (20)$$

in which it is understood that r_a has been replaced by r;

$$\alpha_2 r_b=\lambda^{-\frac{1}{2}}(\omega\tau_{int,2})^{\frac{1}{2}}, \quad (21)$$

or, in general,

$$\alpha_2 r=\lambda^{-\frac{1}{2}}(\omega\tau_{int,2})^{\frac{1}{2}},$$

where the corresponding remark applies; and

$$Ja_2=(\omega\tau_{int,2})^{\frac{1}{2}}/2\lambda^{\frac{1}{2}}\omega\tau_{ext}. \quad (22)$$

In addition, γ and β remain as they were.

Since it is known that the product ρc_p is virtually the same (at room temperature and moderately high temperature, at any rate) for all nonporous solid materials, whether metallic or nonmetallic, the decision was made to simplify the systematic coverage of the ranges of the five parameters by restricting calculations to cases in which $\rho_1 c_{p,1}=\rho_2 c_{p,2}$; little generality is thereby lost.

The initial analytical-solution calculations were, further, made on the basis of a β value of 0.9, which is

TABLE Ia. Thermal responses of cylinders to sinusoidal environment temperature change. Parameter values for various combinations of cylinders and conditions.

Case	k_2/k_1	$\omega\tau_{ext}$	$\omega\tau_{int,2}$	Ja_2	$\alpha_1 r_a$	$\alpha_1 r_b$	$\alpha_2 r_a$	$\alpha_2 r_b$
A	40	10	0.1	0.047458	5.4027	6.0030	0.854244	0.94916
B	5	100	0.1	0.0047458	1.9101	2.1224	0.854244	0.94916
C	40	100	0.1	0.0047458	5.4027	6.0030	0.854244	0.94916
D	40	100	1.0	0.0150075	17.0848	18.9832	2.70135	3.0015
E	5	1000	1.0	0.00150075	6.0404	6.7116	2.70135	3.0015
F	40	1000	1.0	0.00150075	17.0848	18.9832	2.70135	3.0015

TABLE Ib. Thermal responses of cylinders to sinusoidal environment temperature change. Relative amplitude η (or mean relative amplitude $\bar{\eta}$) and relative phase lag φ (or mean relative phase lag $\bar{\varphi}$), radians.

								Metallic shell over oxide core			
				Homogeneous metallic cylinder: exact solution		Homogeneous metallic cylinder: "first-order" solution		Shell thickness 0.1 r_b ($\beta=0.9$)		Oxide surface value—equivalent to limiting case of zero shell thickness ($r_a=r_b$, $\beta=$unity)	
Case	k_2/k_1	$\omega\tau_{ext}$	$\omega\tau_{int,2}$	$\bar{\eta}$	$\bar{\varphi}$	η	φ	$\bar{\eta}$	$\bar{\varphi}$	η	φ
A	40	10	0.1	0.098405	1.4718	0.099504	1.4711	0.20317	0.95513	0.25804	0.65669
B	5	100	0.1	0.0099883	1.5608	0.0099995	1.5608	0.011381	1.2366	0.012147	1.1057
C	40	100	0.1	0.0099883	1.5608	0.0099995	1.5608	0.022457	1.1202	0.031153	0.82871
D	40	100	1.0	0.0099049	1.5577	0.0099995	1.5608	0.037680	1.2826	0.090430	0.73953
E	5	1000	1.0	0.00099905	1.5695	0.0010000	1.5698	0.0024910	1.1291	0.0035264	0.84163
F	40	1000	1.0	0.00099905	1.5695	0.0010000	1.5698	0.0038086	1.3156	0.0096051	0.79782

equivalent to a shell relative thickness of 0.1 of the over-all radius. It had been ascertained that the response is rather sensitive to shell thickness, but thicknesses less than 0.1 of the radius, particularly in the case of fine wires, are suspect in view of the possibilities of oxidation, evaporation and mechanical damage.

Table I presents an initial picture of the responses of a series of homogeneous metallic wires and of laminated "wires" having oxide cores and metallic shells of both 0.1 radius thickness and vanishingly small relative thickness. The results for the finite shell thickness cases have been quantitatively confirmed by another method of calculation (numerical integration). The so-called "first-order" response of the homogeneous metallic cylinder is that obtained when the assumption is made that the cylinder responds as a thermal unit; it will be noted that, in these cases (and this is usually true up to very high frequencies for metallic cylinders) the differences between the "first-order" results and the exact results are small. For these all-metal cases, $r_2=r_a=0$.

Single-material theory[1] was used in the case of the homogeneous cylinder (metallic and oxide) calculations, except that the expression in that article yielding local instantaneous temperature was integrated to provide a cylinder-mean temperature. The cylinder results of reference 1 and of the integration in question are, of course, also deducible as a simple special case from the results of the present treatment.

For convenience, the table has been printed in two parts; certain entries are therefore duplicated. In the first part, the values of the thermal conductivity ratio k_2/k_1, $\omega\tau_{ext}$, $\omega\tau_{int,2}$, Ja_2, $\alpha_1 r_a$, $\alpha_1 r_b$, $\alpha_2 r_a$, and $\alpha_2 r_b$ are given. Note that the latter four parameters apply, as a group, only in the laminated-cylinder situation and then only for $\beta=0.9$. In the homogeneous metallic cylinder situation, no second material is present, so that α_1 has no meaning and $r_a=0$; in that case, only $\alpha_2 r_b$ has significance. In the zero-thickness shell case, that is, the situation in which we are concerned with the surface temperature amplitude and phase lag when an oxide cylinder is used, the applicable parameter is $\alpha_1 r_b$. In any given row of the table, the following may be considered to be fixed: r_b, ω, h_f, and the ratio of metal thermal conductivity (if any) to oxide (if any). From row to row, r_b, ω and h_f are free to change in any manner as long as the resulting nondimensional parameters have the values listed. The ratio $\beta=r_a/r_b$ remains fixed at 0.9 for all of the finite shell thickness cases.

The numerical results are rather striking. In general, amplitude gains of the order of 2 to 4 are attained over

[1] Heinrich Gröber, Forsch. Gebiete Ingenieurw. No. 300, 1–13 (1928).

the parameter range considered here when a laminated cylinder for which $\beta=0.9$ is substituted for a metallic wire of the same over-all radius, the heat-transfer coefficient and frequency also being fixed. (Gains for other cases in which laminated cylinders are used have been as high as about 5 for a β of 0.9.)

If it were possible to reduce the shell thickness virtually to zero, the results indicate that gains of the order of 10 would be available even over the parameter range for which data are presented here. For other ranges, the gains are markedly higher.

It would appear that shell thicknesses such that $\beta\cong 0.95$ might be practicable in many instances, so that it is hoped gains intermediate between the zero-shell thickness situation and the $\beta=0.9$ situation will be realized in practice.

Such improvements in actual temperature response would be accompanied by the other advantages referred to previously, so that substantially improved thermocouples and hot-wire (or "cooled-tube") anemometers should result from the use of such structures; the expression "cooled-tube" anemometer refers to an anemometer (intended for application involving fluids at very high temperatures) which is cooled by a steady axial flow of cooling fluid and reheated to some temperature below that of the ambient fluid by a steady or controlled electric current.

SYMBOLS

a^*	Thermal diffusivity ($k/\rho c_p$).
Bi	Biot number, dimensionless.
$C_1, C_2, \cdots, G_2$	Undetermined coefficient defined by Eqs. (8) and (9), dimensions of temperature.
$C_1^*, C_2^*, \cdots, G_2^*$	$C_1/t_{e,M}, C_2/t_{e,M}$, etc., dimensionless.
C_3, C_4	Undetermined dimensional coefficient defined by textual equations.
c_p	Specific heat.
F_R, F_I	Real and imaginary parts of solutions of second kind of modified Bessel's equation (see also appendix).
f_R, f_I	Real and imaginary parts of solutions of first kind of modified Bessel's equation (ber_0 and bei_0, respectively).
Fo	Fourier number, dimensionless.
h_f	Heat transfer coefficient.
h^*	h_f/k_2.
i	$(-1)^{\frac{1}{2}}$.
Ja_2	Jakob number, dimensionless; $Ja_2=h_f/\omega k_2\rho_2 c_{p,2}$ [see also equation (22)].
k	Thermal conductivity.
r	Radial coordinate.
t	Temperature (generally, here, varying part of temperature).
α	$(\omega/a^*)^{\frac{1}{2}}$.
β	r_a/r_b, dimensionless.
γ	$(k_2/k_1)(a_1^*/a_2^*)^{\frac{1}{2}}$, dimensionless.
γ^*	k_2/k_1, dimensionless.
η	$t/t_{e,M}$, that is, ratio of instantaneous local temperature to maximum amplitude of environment effective temperature oscillation, dimensionless.
θ	Time.
λ	Theoretical dimensionless constant having approximate value 0.111; this value is adopted as an exact figure in computations.
ρ	Density.
τ	Time constant [see Eqs. (19)].
ψ	Function of radial coordinate in temperature solutions.
ω	$2\pi f$; angular frequency.

Subscripts

a	At interface.
b	At surface.
C	In-phase component.
ext	External.
e	Effective (having reference to aerodynamic situations in which the temperature as "seen" by an otherwise unheated object immersed in a fluid stream approaches the total, or stagnation, temperature and therefore considerably exceeds the true, or static, temperature).
f	Film value (characteristic of boundary layer surrounding cylinder).
int	Internal.
M	Maximum (half) amplitude.
S	Out-of-phase component.
1	Characteristic of core material.
2	Characteristic of shell material.

Superscripts

$'$	Differentiation (when used with variable).
a bar ($^-$)	Denotes (space$-$) mean value.

APPENDIX

As stated in the text, it is possible to define the functions F_R and F_I in various ways. In fact, it is possible to define f_R and f_I in various ways, although ber_0 and bei_0 have been well established as those functions.

For reasons not germane to the present treatment, ker_0 and kei_0 were in fact chosen as F_R and F_I, respectively. Various tables of the ber_0, bei_0, ker_0, and kei_0 functions are available. The most useful volumes insofar as the present computations were concerned, were found to be the NBS[2] and Tölke[3] tables. The nomenclature of

[2] (a) Mathematical Tables Project, National Bureau Standards, *Table of the Bessel Functions $J_0(z)$ and $J_1(z)$ for Complex Arguments* (Columbia University Press, New York, 1947), second edition. (b) Computation Laboratory, National Bureau Standards, *Table of the Bessel Functions $Y_0(z)$ and $Y_1(z)$ for Complex Arguments* (Columbia University Press, New York, 1950).

[3] F. Tölke, *Besselsche und Hankelsche Zylinderfunktionen* (Verlag von Konrad Wittwer, 1936).

those two references and of other sources in the field is, to say the least, inconsistent.

Values of $J_0(z)$ and $J_1(z)$ are given in the first volume of reference 2, while values of $Y_0(z)$ and $Y_1(z)$, where z is in general complex, are given in the second volume of reference 2. Values for the argument range 0(0.01)10 are given to ten decimal places. The notation in the formulae which follow is that of the *second* volume. In this connection, a word of caution is required: The notation of even these volumes is not entirely internally consistent. In particular, in the first volume, we find that

$$J_\nu(z)=J_\nu(\rho e^{i\varphi})=U_\nu(\rho,\varphi)+iV_\nu(\rho,\varphi),$$

whereas in the *second* volume, we find that

$$J_\nu(z)=J_\nu(\rho e^{i\varphi})=u_\nu(\rho,\varphi)+iv_\nu(\rho,\varphi),$$

and

$$Y_\nu(z)=Y_\nu(\rho e^{i\varphi})=U_\nu(\rho,\varphi)+iV_\nu(\rho,\varphi).$$

The denotation of Y_ν in these volumes should be noted, as given on page xxi of reference 2b, since definitions of the functions of the second kind vary greatly.

The following relations enable calculation of the various functions indicated:

$$\mathrm{ber}_0(x)=u_0(x,\pi/4);$$
$$\mathrm{bei}_0(x)=-v_0(x,\pi/4);$$
$$\mathrm{ber}_1(x)=-u_1(x,\pi/4);$$
$$\mathrm{bei}_1(x)=v_1(x,\pi/4);$$
$$\mathrm{ker}_0(x)=-(\pi/2)[U_0(x,\pi/4)+v_0(x,\pi/4)];$$
$$\mathrm{kei}_0(x)=(\pi/2)[V_0(x,\pi/4)-u_0(x,\pi/4)];$$
$$\mathrm{ker}_1(x)=(\pi/2)[U_1(x,\pi/4)+v_1(x,\pi/4)];$$
$$\mathrm{kei}_1(x)=(\pi/2)[-V_1(x,\pi/4)+u_1(x,\pi/4)];$$
$$\mathrm{ber}_0'(x)=(\sqrt{2}/2)[\mathrm{bei}_1(x)+\mathrm{bei}_1(x)]=(\sqrt{2}/2)[v_1(x,\pi/4)-u_1(x,\pi/4)];$$
$$\mathrm{bei}_0'(x)=(\sqrt{2}/2)[\mathrm{bei}_1(x)-\mathrm{ber}_1(x)]=(\sqrt{2}/2)[v_1(x,\pi/4)+u_1(x,\pi/4)];$$
$$\mathrm{ker}_0'(x)=(\sqrt{2}/2)[\mathrm{kei}_1(x)+\mathrm{ker}_1(x)]=(\pi\sqrt{2}/4)[U_1(x,\pi/4)-V_1(x,\pi/4)+u_1(x,\pi/4)+v_1(x,\pi/4)];$$
$$\mathrm{kei}_0'(x)=(\sqrt{2}/2)[\mathrm{kei}_1(x)-\mathrm{ker}_1(x)]=(\pi\sqrt{2}/4)[-U_1(x,\pi/4)-V_1(x,\pi/4)+u_1(x,\pi/4)-v_1(x,\pi/4)].$$

Unfortunately, in many cases of interest values of the arguments $\alpha_1 r_a$ and $\alpha_1 r_b$ exceed ten, and it is necessary either to use the well-known series expansions of the functions or the tabulated values of reference 3, in which four-figure values are given over the argument range 0(0.01)21. Reference 3 contains, in addition, a large number of very useful relations by means of which large-argument values may be calculated.

The functions of interest here may be obtained from the values of reference 3 as follows; the unfamiliar notation is that of reference 3:

$$\mathrm{ber}_0(x)=J_{0,1}(x);$$
$$\mathrm{bei}_0(x)=-J_{0,2}(x);$$
$$\mathrm{ker}_0(x)=G_{0,1}(x);$$
$$\mathrm{kei}_0(x)=-G_{0,2}(x);$$
$$\mathrm{ber}_0'(x)=-[J_{11}(x)-J_{12}(x)]/\sqrt{2};$$
$$\mathrm{bei}_0'(x)=[J_{11}(x)+J_{12}(x)]/\sqrt{2};$$
$$\mathrm{ker}_0'(x)=-[G_{11}(x)-G_{12}(x)]/\sqrt{2};$$
$$\mathrm{kei}_0'(x)=[G_{11}(x)+G_{12}(x)]/\sqrt{2}.$$

The coefficients C_1^*, C_2^*, and so forth, of the main text were calculated on the Card-Programmed Electronic Calculator of the Lewis Flight Propulsion Laboratory. The program deck used was one devised by N. Patton of the Laboratory staff; it makes use of the Crout reduction technique. The resulting solutions were found to be correct to better than seven significant figures on direct substitution.

BIBLIOGRAPHY

1. H. Bucholtz, "Besondere Probleme der Erwärmung elektrische Leiter" (Problems Involving and Insulated Wire), Z. angew. Math. u. Phys. **9**, 280–298 (1929).
2. G. B. Shanklin and F. H. Buller, "The Theory of Oil-Filled Cable," Gen. Elec. Rev. p. 253 (September, 1931).
3. K. W. Miller and F. O. Wollaston, "Transients and Oil Demands in Cables," Trans. Am. Inst. Elec. Engrs. **52**, 98 (1933).
4. J. H. Awbery, "The Periodic Flow of Heat in a Hollow Cylinder." Phil. Mag. **28**, 447–451 (1939).
5. J. C. Jaeger, "Heat Conduction in Composite Circular Cylinders," Phil. Mag. **32**, 324–335 (1941). (Sudden inner and outer surface temperature change, also consideration of instantaneous source distributions.)
6. Stewart Paterson, "The Conduction of Heat in a Medium Generating Heat," Phil. Mag. **32**, 384–392 (1941). (Generalized solution of heat-flow equation for situations involving time, location, and temperature dependence of heat generation, and surface heat loss.)
7. R. L. Perry and W. P. Berggren, "Transient Heat Conduction in Hollow Cylinders after Sudden Change of Inner-Surface Temperature," Univ. Calif. (Berkeley) Publs. Eng. **5**, 59–88 (1944). (Graphical and analytical solutions and experimental results.)
8. H. S. Carslaw and J. C. Jaeger, *Conduction of Heats in Solids* (Clarendon Press, Oxford, 1947). (Generalized treatment of solid cylinder by transform method.)
9. L. M. K. Boelter, *et al.*, *Heat Transfer Notes*, University of California Syllabus Series (University of California Press, California). (Reproduction by Edwards Brothers, Inc., Ann Arbor, Michigan, 1948), pp. VI–30–VI–37. (Section on Gröber's cylinder theory and results.)
10. W. Traupel, "Instationäre Wärmeleitungsvorgänge in Platten, Zylindern und Kuglen," Schweiz. Arch. angew. Wiss. u. Tech. **14**, 193–205 (1948).
11. A. H. Van Gorcum, "Theoretical Consideration of the Conduction of Fluctuating Heat Flow," Appl. Sci. Research **A2**, 272–280 (1950).
12. J. C. Jaeger, "Conduction of Heat in Composite Slabs," Quart. Appl. Math. **8**, 187–198 (1950).
13. V. Vodicka (H. H. Lowell, translation), "Wärmeleitung in geschichteten Kugel und Zylinderkörpern," Schweiz. Archv. angew. Wiss. u. Tech. **16**, 297–308 (1950). (Generalized treatment of multilayered spheres and circular cylinders in the case of a fixed heat transfer coefficient.)
14. V. R. Thiruvenkatachar and B. S. Ramakrishna, "A Case of Combined Radial and Axial Heat Flow in Composite Cylinders," Quart. Appl. Math. **10**, 255–262 (1952). (Theoretical solution and numerical results for adiathermanous surface case.)

Shapes of Floating Liquid Zones between Solid Rods

P. H. KECK, M. GREEN, AND M. L. POLK
Signal Corps Engineering Laboratories, Fort Monmouth, New Jersey
(Received May 27, 1953)

The present paper seeks to describe the shapes of liquid floating zones between solid rods of silicon and of germanium and to discuss stability conditions. The shapes were deduced from the equation given by Laplace,

$$p=\gamma(1/R_1+1/R_2),$$

where p indicates the pressure difference across the surface membrane of a liquid at any point, R_1 and R_2 are the principal radii of curvature at that point, and γ is the surface tension of the liquid.

The floating liquid zone is analyzed within a wide stability range. Its dimensions were theoretically determined and experimentally confirmed.

A NEW method was recently described[1] which permits crystallization of silicon from a melt without requiring a crucible. A zone of molten silicon is in this case held by surface tension between two vertically aligned solid rods of silicon. Figure 1 illustrates the geometrical arrangement of such a floating zone. The purpose of this paper is to determine the shapes which a floating zone assumes as a function of the parameters involved and to discuss the limits of stability.

EQUATIONS FOR THE FLOATING ZONES

The shapes of liquid surfaces have been mathematically developed by many authors[2,3] and elucidated by others.[4] These shapes are expressed by the familiar equation of Laplace,

$$p=\gamma(1/R_1+1/R_2), \tag{1}$$

where p indicates the pressure difference across the surface membrane of a liquid at any point, R_1 and R_2 are the principal radii of curvature at that point, and γ is the surface tension of the liquid. For surfaces of revolution such as hanging drops (1) takes the form*

$$\frac{y''}{[1+(y')^2]^{\frac{3}{2}}}+\frac{y'}{x[1+(y')^2]^{\frac{1}{2}}}=\frac{2(h-y)}{a^2}, \tag{2}$$

where R_1 and R_2 of Eq. (1) have been replaced by their differential equivalents, x and y are the coordinates of a point measured from the bottom of the drop as origin and the axis of symmetry as y axis, and h is equal to the height of liquid which corresponds to the pressure, $p=\rho gh$, at the vertex of the drop where ρ is the density of the liquid and g is the gravitational constant; a, the capillary constant, equals to $(2\gamma/\rho g)^{\frac{1}{2}}$ and has the dimensions of length.

Equation (2) can be modified to a dimensionless form

$$\frac{\bar{y}''}{[1+(\bar{y}')^2]^{\frac{3}{2}}}+\frac{\bar{y}'}{\bar{x}[1+(\bar{y}')^2]^{\frac{1}{2}}}=2(\bar{h}-\bar{y}), \tag{3}$$

where $x=a\bar{x}$, $y=a\bar{y}$, and $h=a\bar{h}$. The solution of Eq. (3) gives a family of curves parametric in $\bar{h}$. These curves are shown in Fig. 2 as taken from Freund and Harkins.[4] This family of curves is applicable to hanging drops; however, it also applies to floating zones between solid rods if, in this case, one considers only the section of the curves which correspond to the liquid zone. The hanging drop and the floating zone are both satisfied by the same differential equation, (2) or (3).

From Fig. 2 it can be seen that for $\bar{h}$ smaller than 2.0 the curves do not intersect; therefore, the shape of the liquid body in this range is uniquely determined by either the coordinates $\bar{x}$ and $\bar{y}$ of a point on the surface or by the slope $\bar{y}'$ for a given abscissa $\bar{x}$ or a given ordinate $\bar{y}$. For $\bar{h}$ larger than 2.0 the curves intersect, and an additional boundary condition, such as the coordinates of a point on the surface and by the slope at that point is required to determine which of the curves describes the shape of the liquid.

In the case of floating zones the following quantities

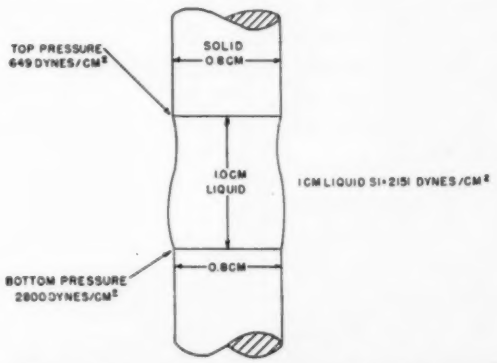

FIG. 1. Geometrical arrangement of floating zone.

[1] P. H. Keck and M. J. E. Golay, Phys. Rev. **89**, 1297 (1953).
[2] C. Runge, Math. Ann. **46**, 175 (1895).
[3] T. Lohnstein, Ann. Physik (4) **20**, 237, 606 (1906); **21**, 1032; **22**, 767 (1907).
[4] B. B. Freund and W. D. Harkins, J. Phys. Chem. **33**, 1217 (1929).

* Equation (2) is for a condition of constant temperature. In the floating zone technique this is not exactly the case, however, the temperature gradient is small enough to be neglected. If the gradient is to be considered, the appropriate differential equation for static equilibrium is

$$\frac{d}{dx}\left[\gamma x\frac{y'}{[1+(y')^2]^{\frac{1}{2}}}\right]=\rho g(h-y),$$

where γ and ρ are temperature dependent.

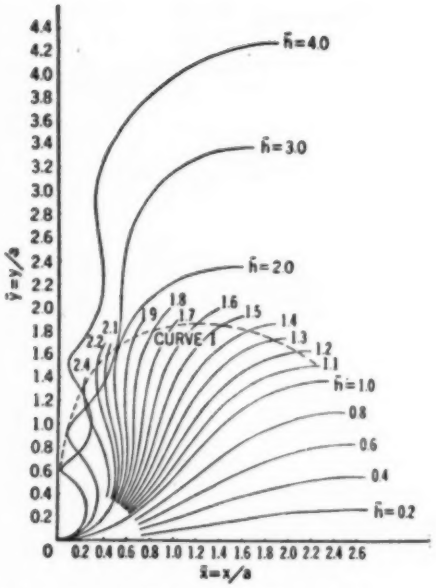

FIG. 2. Graphical solutions of Eq. (3), family of curves parametric in $\bar{h}$.

are controllable: (a) the radius $\bar{x}_1$ of the upper rod, (b) the radius $\bar{x}_2$ of the lower rod, (c) the length of the liquid zone and finally to a certain extent, (d) the amount of liquid or the hydrostatic pressure in the liquid zone.

If the values for $\bar{x}_1$ and $\bar{x}_2$ are given, which means that conditions (a) and (b) are fixed, all possible shapes of the floating zone are determined by the sections of the curves extending between the two straight lines $\bar{x}=\bar{x}_1$ and $\bar{x}=\bar{x}_2$. For $\bar{x}_1>\bar{x}_2$ there is a large variety of possible shapes. For $\bar{x}_1=\bar{x}_2$ solutions are only possible in the areas where the straight line $\bar{x}=\bar{x}_1$ has more than one intersection with one curve. These conditions are of particular interest. From Fig. 2 it can be seen that for $\bar{x}_1>0.65$ any straight line $\bar{x}=\bar{x}_1$ will intersect each curve in one and only one point. Therefore, stable floating zones cannot exist for rods of equal radii greater than

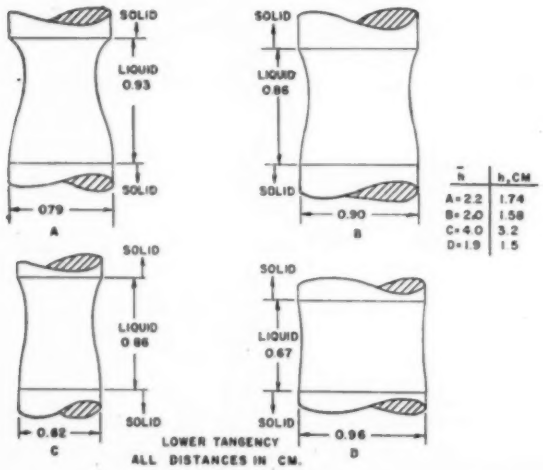

FIG. 3. Stable shapes of floating silicon zones with lower vertical tangency.

TABLE I.

Liquid	Temperature °C	Density ρ [grams/cc]	Surface tension γ [dynes/cm]	$a=(2\gamma/\rho g)^{\frac{1}{2}}$ [cm]
H_2O	20	1.0	72	0.38
Ge	958.5	5.4	600	0.48
Si	1420	2.3	720	0.79
Hg	15	13.6	487	0.27

$\bar{x}_1=0.65$. For $\bar{x}_1<\bar{x}_2$ there are stable shapes especially in the region of rods with small radii.

APPLICATION TO SILICON

In order to apply these curves to a specified material, the capillary constant $a=(2\gamma/\rho g)^{\frac{1}{2}}$ of this material has to be known. In Table I the values of a are listed for four liquids as determined from their densities and surface tensions.[5] The capillary constant of silicon, taken from Table I, is 0.79. For the curves of Fig. 2 we have then for silicon $x=0.79\bar{x}$, $y=0.79\bar{y}$, and $h=0.79\bar{h}$. Since the maximum radius for rods of equal radii, which support a stable floating zone, occurs for $\bar{x}=0.65$ we obtain for silicon $x_{\max}=0.52$ cm. The separation between the solid rods corresponding to the length of the liquid zone, is given by the distance between two out of three intersections of the straight line, $\bar{x}=$constant, and the curve for a fixed $\bar{h}$ value. If we use as an example $\bar{h}=2.0$ and $\bar{x}=0.5$, we obtain from Fig. 2 for silicon the three possible values for the height of the floating zone: 1.0, 0.6, and 0.4 cm. The curves between the points of intersection correspond to the shapes of the liquid floating zones. Figure 1 illustrates the case of a liquid zone of 1-cm height and radii of 0.4 cm which corresponds to $\bar{x}=0.5$. Other examples for stable shapes of the floating zone are shown in Fig. 3. The shapes in Fig. 3 are selected so that

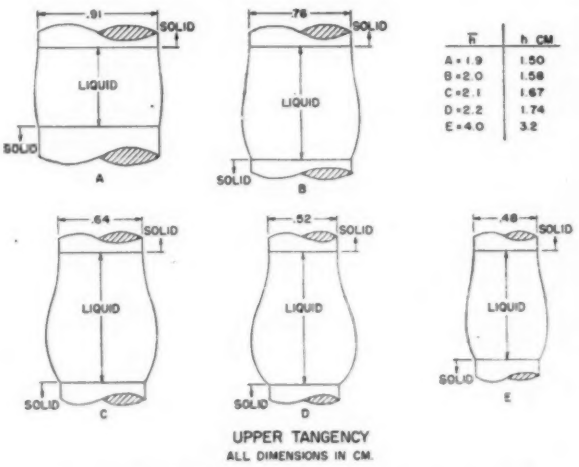

FIG. 4. Stable shapes of floating silicon zones with upper vertical tangency.

[5] The surface tension values of Si and Ge were taken from P. H. Keck and W. VanHorn, Phys. Rev. 91, 512 (1953). The remaining values are from *Handbook of Chemistry and Physics*, thirty-third edition. (1951–52).

the tangents at the lower boundary are vertical, whereas the conditions shown in Fig. 4 are such that the tangents at the upper boundaries are vertical.

For the purpose of purification and formation of single crystals the floating zone is caused to travel vertically along the rod. In this process the solid rod melts before the advancing zone and solidifies in its wake. It follows then that the shape which the recrystallized material assumes depends on the angle of the liquid at the liquid-solid boundary on the freezing side. This is explained in Fig. 5. In Fig. 5A the case is shown where the volume of liquid silicon is so small as to cause the circular cross section of the liquid to be smaller than that of the solid at the lower liquid-solid boundary. As the liquid zone moves upward, part of the top rod melts and silicon crystallizes on the lower rod. As a consequence, the circular cross section of the lower rod is decreasing which means that more silicon is melting from the top rod than is crystallizing on the bottom rod. This situation is indicated in Fig. 5B. As we continue the liquid is increasing in volume and bulges out. Therefore, the circular

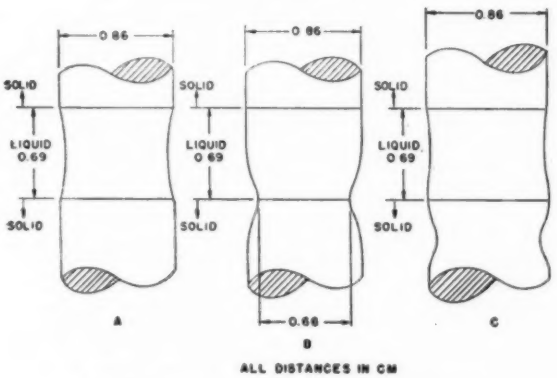

FIG. 5. Successive stages in the development of a stable floating zone.

cross section of the lower rod starts to grow after having passed through a minimum. Finally equilibrium is reached, as indicated in Fig. 5C, when the tangent at the lower liquid-solid boundary is vertical and both boundary cross sections are equal. This shows that the process tends to stabilize itself.

Movement of the liquid zone in the opposite direction, namely downward, is also possible. Here a situation occurs which is similar to the one described above, and after a period of self-adjustment, a vertical tangent forms at the upper liquid-solid boundary. However, experimental evidence indicates that the downward motion of the zone is not as stable as the upward motion.

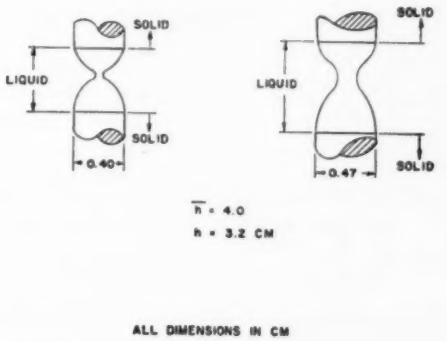

FIG. 6. Examples of nonstable floating zones.

The solutions of Eq. (3) represent a condition of static equilibrium, but they give no information about the degree of stability of zones which assume the shapes corresponding to these solutions.

Some qualitative conclusions on the degree of stability of various shapes can be deduced from elementary considerations. When the column of liquid between the supporting rods is very large or when the available amount of liquid between them is inadequate, narrow necks or constrictions form such as shown in Fig. 6. If the neck gets too small in diameter there is insufficient surface available to support the molten zone and it breaks apart. When on the other hand, there is a great deal of liquid in the column, a bulge forms near the base of the melt as shown for instance in Fig. 4D. If too much liquid collects in the bulge, the surface can no longer support it. In general it can be stated that, for an upper rod of given radius, the degree of stability of the liquid zone decreases with the length of the liquid column.

SUMMARY

From the foregoing it follows that given the equation of Laplace for surface tension, $p=\gamma(1/R_1+1/R_2)$ and sucffient boundary conditions then the shapes of the floating zones can be uniquely determined. If we use these conditions with the capillary constant of silicon 0.79, we arrive at the conclusion that silicon floating zones between rods of equal radii are stable up to approximately 1.0 cm diameter. Zone melting under the condition of constant rod diameter requires that a vertical tangent forms at the liquid-solid boundary on the solidifying side of the moving molten zone. This condition holds for the motion of the zone either upward or downward.

Preparation of $p-n$ Junctions by Surface Melting*

KURT LEHOVEC AND EMANUEL BELMONT
Sprague Electric Company, North Adams, Massachusetts
(Received June 3, 1953)

A new method is described for preparation of $p-n$ junctions in single-crystal semiconductors: the upper part of a slice cut from a single-crystal semiconductor is melted by radiation. Impurities of the opposite type than those present in the crystal are introduced into the melt. Upon slow solidification of the melt a single crystal is obtained with a $p-n$ junction at the original position of the solid-liquid interface. The method is capable of producing multiple junctions.

The influence of (a) heater temperature, (b) forced cooling, and (c) thickness of the slice on the position of the solid liquid interface is calculated for a one-dimensional model, assuming that the temperature difference between bottom and top of the semiconductor is small compared to the melting temperature of the semiconductor. The time constant characterizing the rate of reaching equilibrium conditions after a sudden small change in heater temperature is estimated.

INTRODUCTION

MANY semiconducting devices, e.g., transistors, rectifiers, and photocells, employ a junction between two regions of opposite type of conductivity. On one side of the junction the current is normally carried by electrons, whereas on the other side of the junction the current is normally carried by holes. The electrons and holes, respectively, are generated by thermal ionization of suitable impurities; e.g., in germanium, electrons are supplied by fifth-group elements (n-type impurities), substituted for the germanium, whereas holes are supplied by third-group elements (p-type impurities).

Present methods of preparing junctions are based on (a) pulling of a crystal from a melt, containing initially an excess of one type of impurity (e.g., p type), and doping of the melt during the crystal pulling[1] to contain an excess of the other type of impurity (n type); (b) pulling of a crystal from a melt, containing both types of impurities in a carefully chosen concentration range and varying the speed of the crystal pulling such that at one speed an excess of one type of impurity is incorporated into the crystal, and at another speed an excess of the other type of impurity is incorporated;[2] this method is based on the dependence of the ratio of distribution coefficients of impurities between solid and liquid phase on the speed of crystal pulling; (c) diffusion of the impurities in the crystal at elevated temperatures.[3] These methods have the following drawbacks: In method (a), it takes a certain time before the added impurities are distributed homogeneously through the melt. During this time a length of the crystal is pulled in which the impurity content changes rather gradually. It is difficult by method (a) to prepare junctions with the change in impurity content being restricted to a region less than 0.1 mil. In method (b) one is limited to a certain range of concentration of n-type and p-type impurities. Method (c) does not lead readily to junctions in the bulk of the crystal because of the small diffusion rate of the impurities.

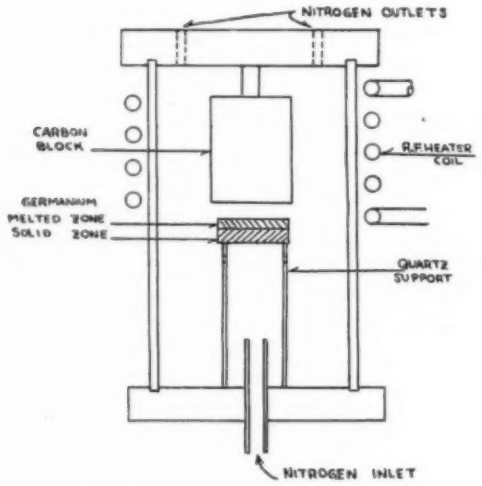

FIG. 1. Surface melting apparatus.

$p-n$ JUNCTIONS BY SURFACE MELTING

In what follows a method is described which permits preparation of $p-n$ junctions with abrupt change of concentration of impurities within the bulk of a single crystal. Junctions in single crystals of germanium were prepared by surface melting. The surface zone of a single crystal slice is melted by radiation while the bottom is cooled. The position of the solid-liquid interface can be shifted arbitrarily by changing the heating or cooling rates. When the interface has been adjusted to the proper position, appropriate doping material is introduced into the melted portion. If the cooling is conducted sufficiently slowly, the melt solidifies into a single crystal with the same orientation as the non-melted portion. $p-n$ junctions prepared in this manner had electrical properties comparable to those in pulled crystals; in addition, the concentration gradient at the junction can be easily varied over a large range in surface-melted crystals. The apparatus used is shown in

* A preliminary report of this work was presented at the 1953 Spring Meeting of the Am. Phys. Soc. in Washington, D. C.

[1] Teal, Sparks, and Buehler, Phys. Rev. 81, 637 (1951).

[2] R. N. Hall, Phys. Rev. 88, 139 (1952).

[3] C. S. Fuller, Phys. Rev. 86, 136 (1952); W. C. Dunlap, Jr., and D. E. Brown, Phys. Rev. 86, 417 (1952).

Fig. 1. The success of the method depends on the degree of control of the position of the solid liquid interface. The degree of control is indicated by the following calculations.

TEMPERATURE DISTRIBUTION IN THE SEMICONDUCTOR DURING SURFACE MELTING

In what follows, we shall examine the temperature distribution in the semiconductor assuming a simplified one-dimensional arrangement as shown in Fig. 2. A summary of the symbols to be used is given in Table I. In order to simplify calculations, and since values of radiation constant and the heat conductivity for semiconductors above the melting point are in general not known, we have used the same values for heat conductivity and the radiation constant, respectively, above and below the melting point. We shall make the further simplifying assumption that the temperature difference between top and bottom of the semiconductor is small compared to the melting temperature of the semiconductor. We shall show later, that this condition is well satisfied for surface melting of slices of germanium of ordinary thickness.

TABLE I. List of symbols used.

T_h	Temperature of heater.
T_m	Melting point of semiconductor.
K	Heat conductivity of semiconductor near T_m.
σ	Blackbody radiation constant.
σ_s	Semiconductor-radiation constant.
L	Thickness of semiconductor.
H	Heat removed from bottom of semiconductor by forced cooling.
δ_1	Temperature difference between top of semiconductor and solid-liquid interface.
δ_2	Temperature difference between bottom of semiconductor and solid-liquid interface.
l_1	Depth of melted zone.
l_2	Depth of solid zone.
ρ	Density of semiconductor.
Q	Heat of fusion of semiconductor.

(a) Stationary State

In a stationary state the heat balance at the upper surface and at the lower surface of the semiconductor, respectively, yields the two equations (since we use a carbon heater, we shall use the blackbody radiation constant for the heater in the calculations)

$$\sigma T_h^4=\sigma_s(T_m+\delta_1)^4+K(\delta_1+\delta_2)/L \tag{1}$$

and

$$K(\delta_1+\delta_2)/L=\sigma_s(T_m-\delta_2)^4+H. \tag{2}$$

If we expand the terms containing δ_1 and δ_2 and neglect all terms of higher than first order in δ_1, δ_2, assuming $\delta_1, \delta_2 \ll T_m$, we obtain two linear equations for δ_1, δ_2 with the solutions

$$\delta_1=\frac{H+\sigma_s T_m^4+(\sigma T_h^4-H-2\sigma_s T_m^4)\cdot[1+K/(4L\sigma_s T_m^3)]}{4\sigma_s T_m^3[1+K/(2L\sigma_s T_m^3)]} \tag{3}$$

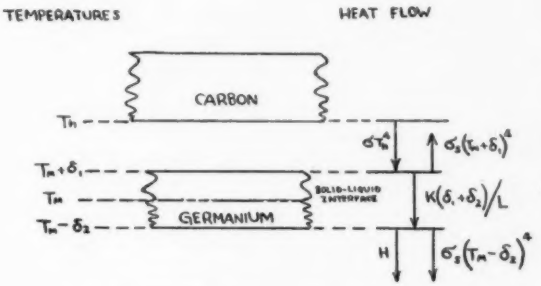

FIG. 2. Simplified one-dimensional geometry, used in the calculations.

and

$$\delta_2=\frac{H+\sigma_s T_m^4-(\sigma T_h^4-H-2\sigma_s T_m^4)\cdot K/(4L\sigma_s T_m^3)}{4\sigma_s T_m^3[1+K/(2L\sigma_s T_m^3)]}, \tag{4}$$

and, therefore,

$$\delta_1+\delta_2=\frac{H+\sigma T_h^4}{4\sigma_s T_m^3\cdot[1+K/(2L\sigma_s T_m^3)]}. \tag{5}$$

The distance of the solid liquid interface from the bottom of the crystal is

$$l_2=L\cdot\frac{\delta_2}{\delta_1+\delta_2}=L\cdot\frac{H+\sigma_s T_m^4-(\sigma T_h^4-H-2\sigma_s T_m^4)\cdot K/(4L\sigma_s T_m^3)}{H+\sigma T_h^4}. \tag{6}$$

We are interested especially in the change of the position of the interface with change in heater temperature,

$$-\frac{\partial l_2}{\partial T_h}=L\cdot\frac{(H+\sigma_s T_m^4)[1+K/(2L\sigma_s T_m^3)]}{(H+\sigma T_h^4)^2}\cdot 4\sigma T_h^3. \tag{7}$$

Equation (7) can be transformed by using the heat balance of the system,

$$\sigma T_h^4=\sigma_s(T_m+\delta_1)^4+\sigma_s(T_m-\delta_2)^4+H, \tag{8}$$

and neglecting terms of the order of δ_1, δ_2 or smaller,

$$\sigma T_h^4\sim 2\sigma_s T_m^4+H. \tag{9}$$

If we introduce this expression into Eq. (7), we obtain

$$-\frac{\partial l_2}{\partial T_h}=\frac{L}{T_h}[1+K/(2L\sigma_s T_m^3)]\cdot\frac{(H+2\sigma_s T_m^4)}{(H+\sigma_s T_m^4)}. \tag{10}$$

The change in heater temperature necessary to shift the solid-liquid interface from the bottom of the crystal to the top of the crystal is

$$(T_h)_{\delta_2=0}-(T_h)_{\delta_1=0}\approx-\frac{L}{\partial l_2/\partial T_h}=\frac{T_h}{1+K/(2L\sigma_s T_m^3)}\cdot\frac{(H+\sigma_s T_m^4)}{(H+2\sigma_s T_m^4)}. \tag{11}$$

TABLE II.

	$H=0$	$H\gg\sigma_s T_m^4$
Heat balance	$\sigma T_h^4 \sim 2\sigma_s T_m^4$	$\sigma T_h^4 \sim H$
$-\dfrac{\partial l_2}{\partial T_h}$	$\dfrac{2L}{(T_h)_{H=0}}[1+K/(2L\sigma_s T_m^3)]$	$\dfrac{L}{(T_h)_H}[1+K/(2L\sigma_s T_m^3)]$
$(T_h)_{\delta_2=0}-(T_h)_{\delta_1=0}$	$\dfrac{(T_h)_{H=0}}{2[1+K/(2L\sigma_s T_m^3)]}$	$\dfrac{(T_h)_H}{1+K/(2L\sigma_s T_m^3)}$

It is interesting to investigate the role of forced cooling. For this purpose let us consider the two extreme cases $H=0$ and $H\gg\sigma_s T_m^4$. Equations (9), (10), and (11) become then the expressions listed in Table II. Since $(T_h)_H$ depends only slowly on H [$T_h\sim(H)^{\frac{1}{4}}$ for large H], $\partial l_2/\partial T_h$ and $(T_h)_{\delta_2=0}-(T_h)_{\delta_1=0}$ vary only by about a factor 2 from zero forced cooling to extreme conditions.

(b) Time Constant of Surface Melting

Another important aspect of our method is the time required to restore equilibrium conditions when the heater temperature is changed. When the temperature of the heater is abruptly changed, the increase in the rate of heating is $4\sigma T_h^4\cdot\Delta T_h/T_h$. This increase in rate of heating leads eventually to the melting of a section

$$\Delta l=-(\partial l_2/\partial T_h)\Delta T_h \qquad (12)$$

of the semiconductor, where $\partial l_2/\partial T_h$ is given by Eq. (10). The heat necessary to melt a unit area of this section is $\rho Q\Delta l$. Hence the time constant of the change in position of the solid liquid interface is

$$\tau=\frac{\text{heat required}}{\text{rate of heating}}=\frac{\rho Q\Delta l}{4\sigma T_h^4\Delta T_h/T_h}=-\frac{\rho Q\partial l_2/\partial T_h}{4\sigma T_h^3}. \qquad (13)$$

Since $\partial l_2/\partial T_h$ depends only little on forced cooling (by about a factor 2), τ is also rather independent of forced cooling.

NUMERICAL VALUES FOR THE CASE OF GERMANIUM

The numerical values listed in Table III were calculated for the case $H=0$ by using values of the parameters estimated to apply for germanium. It is seen that the condition δ_1, $\delta_2\ll T_m$ is well satisfied. The factor $K/2\sigma_s T_m^3$ is of the order of 27 cm for germanium. Hence, for slices of less than 1-cm thickness, $[1+K/(2L\sigma_s T_m^3)]\approx K/(2L\sigma_s T_m^3)$. In this case the change of position of solid-liquid interface with heater temperature [Eq. (10)] becomes independent of the thickness of the slice.

PREPARATION OF MULTIPLE JUNCTIONS

Multiple junctions can be produced as follows: The top layer of a single crystal slice containing one type of impurity, e.g., p type, is melted. After a stationary state is established, sufficient n-type impurities are introduced into the melt to convert it to n type. The heater temperature is then decreased causing a thin layer of the melt to solidify. When a stationary state has again been established, the still melted region is redoped to contain an excess of p-type impurities. The melt is then slowly solidified.

If the heater temperature can be controlled within ± 0.1°C, one can control the position of the solid-liquid interface within ± 0.004 cm (1.7 mils). The temperature has to be maintained within these limits for at least a time of the order $\tau\approx 33$ minutes, to obtain establishment of a stationary state.

In this procedure, the long time necessary to obtain a stationary state is inconvenient. The slow rate of change of the solid-liquid interface, when changing from one stationary state to another one, enables convenient doping and redoping during the migration of the posi-

TABLE III.[a]

T_h	1340°K
$K/(\sigma_s T_m^3)$	54.2 cm
$\delta_1+\delta_2$	13.8°C
$-\partial l_2/\partial T_h$	0.0415 cm/°C
$(T_h)_{\delta_2=0}-(T_h)_{\delta_1=0}$	15.2°C
τ	1970 sec

[a] These values were calculated using:
$T_m=1210$°K; $K=0.1$ cal/cm² per degree/cm;
$\rho=5.4$ g/cm³; $Q=114$ cal/g;
$\sigma=1.39\times10^{-12}$ cal/cm² degree⁴;
$\sigma_s=0.75\sigma$; $L=0.63$ cm ($=\frac{1}{4}$ in.).

tion of the interface. This procedure is equivalent to the slow pulling of a single crystal from the melt, the mechanical motion being replaced by the slow advancement of a solid-liquid interface.

When doping the melt in stationary-state conditions, after subsequent recrystallization extremely steep transitions from p regions to n regions are obtained, which can be approximated by a step function. For such junctions, the field distribution in the junction can be calculated which enables comparison of experimental results with theory of electric properties of $p-n$ junctions.

ACKNOWLEDGMENT

It is a pleasure to acknowledge our gratitude to Dr. P. Robinson for his support of this program and to Mr. A. Fermanian and Mr. R. Koch for their help in constructing the equipment.

JOURNAL OF APPLIED PHYSICS VOLUME 24, NUMBER 12 DECEMBER, 1953

The Generation of Wind Waves on a Water Surface

CARL ECKART*
Institute for Advanced Study, Princeton, New Jersey
(Received June 15, 1953)

The statistical methods for treating continuous media developed elsewhere are applied to the generation of surface gravity waves. The wind stress is assumed to be everywhere normal to the disturbed surface of the water and caused by a known ensemble of "gusts." Each gust is considered to be a center of high or low pressure, which moves with the mean wind speed, and has a radius L, and duration T. The rms value of the variable wind pressure is assumed to vary systematically from point to point in a storm. The calculations are made for an idealized, long continuing storm; before applying the statistical equations, the effect of a single gust is calculated.

It is shown that the single gust produces a V-shaped wake, which, after the gust has blown itself out ($t>T$) can be considered as a packet of free gravity waves, which moves and spreads under the influence of divergence and dispersion.

The results of the statistical calculation are compared with known general facts, and with an actual storm. From the fact that the storm waves have a non-sinusoidal character, and arrive at any one point in groups of 5 to 10 crests, it is deduced that the duration of a gust is from 15 to 30 seconds. From the fact that the majority of the wave energy travels in directions that are within 30° of the wind, and with phase velocities that are nearly equal to the wind speed, the mean radius of the gusts is deduced to be about 40 meters in the case of a wind speed of 20 meters per second. The crest length of the waves is proportional to the distance r from the storm, and inversely to its diameter, D; when $r/D=10$, the dominant length of the crests is 2.2 wavelengths.

The rms displacement, H, of the sea-surface from its horizontal mean is a function of the parameters already mentioned and of P, the rms value of the variable component of the wind pressure at the center of the storm; for the idealized storm considered, and for $r/D\gg1$, this is approximated by

$$H^3=10P^2D^2/rL,$$

all quantities being in centimeters, including P, which is measured in centimeters on a water barometer. Comparison with data for an actual storm indicates that this theory requires a value of P that is possibly 10 times greater than its actual value.

While the theory explains many of the phenomena of storm waves, it is therefore incapable of accounting quantitatively for the wave height. The possible reasons for this inadequacy are discussed. The relation of the theory to Jeffreys' sheltering theory is also discussed, and it is shown that both postulate that the variable component of the wind stress is normal to the water surface. The sheltering theory also postulates that the wind pressure lags 90° behind the surface disturbance. A similar phase lag is a consequence of the assumptions of the present theory.

1. INTRODUCTION

THE mechanism by which a wind blowing over a water surface produces gravity waves is not well understood. During the past ten years, much new observational material has been accumulated and summarized in useful semi-empirical relations.[1,2] The starting point of this analysis has been the equations of free, sinusoidal, infinitesimal, and irrotational surface waves. That each of the four adjectives represents an oversimplification is clear, and the necessity for modifying the equations before they will conform to the observed phenomena is not to be interpreted as a failure of any of the basic equations of hydrodynamics.

The present paper develops a theory of forced, non-sinusoidal, but infinitesimal and irrotational surface waves. The term "infinitesimal," in this connection, refers to the neglect of nonlinear terms in the hydrodynamic equations; it seems certain that this must ultimately be remedied if all phenomena connected with the interaction of wind and water are to be treated theoretically. However, there are some that appear to be largely independent of the nonlinear terms, and it is therefore justified to retain this simplification for the time being. Much the same can be said about the simplifying assumption of irrotationality.

Since the wind exerts forces on the water, wind-waves are not free, by definition. This has been recognized in the past by dividing the problem into two: waves in the generating, or storm area, and waves in the relatively calm or decay area at a distance from the storm. In the decay area, the equations of free waves can certainly be justified: this will appear in Sec. 8 below. The primary problem in this region is not the transfer of energy from air to water, but rather the relation between the free waves and the forces that generated them at an earlier time.

In the generating area the waves may be many meters high, and thus represent a large surface density of energy. This energy cannot be supposed to have been obtained from the air instantaneously and locally. Much of it will have been obtained from the air earlier and at a considerable distance from the point of observation (though still in the storm area). It will have been transported by the water essentially according to the laws of free wave motion. This has long been recognized by the use of the concept of *fetch*, introduced more or less empirically into the theory. In Sec. 7 a definite integral will be encountered that corresponds fully with this concept and enables certain of its aspects to be clarified. It is in many ways analogous to the concept of *optical depth* in theories of scattering and visibility.

From what has been said, it is to be expected that the

* On leave from the Scripps Institution of Oceanography. This is SIO Contribution No. 648 (New Series).

[1] H. U. Sverdrup and W. H. Munk, *Wind, Sea, and Swell*: Theory of Relations for Forecasting, (U. S. Navy Hydrographic Office Publication No. 601, 1947).

[2] C. L. Bretschneider, Trans. Am. Geophys. Union 33, 381 (1952).

equations of free wave motion will be useful even in the storm area: in Sec. 7, it will be shown that this is a consequence of an approximation justified by preliminary considerations given in Sec. 5. It is not to be supposed, however, that the forces of the wind can be completely neglected and that the equations of free wave motion can be used from the beginning. For this reason, the rather lengthy development in the earlier sections is unavoidable.

In these sections the wind stress is treated as a function of space and time that is known, at least in a statistical sense. One limitation on this force is imposed by the decision to consider only irrotational motion: it must everywhere be normal to the air-water interface. Since this surface is inclined, the wind-stress may have a horizontal component (see Sec. 10) but any tangential component would generate vorticity, and must therefore be neglected in order to remain consistent with the previous decision.

This is perhaps unfortunate, for as a result of the empirical analysis of wind-sea phenomena, it is generally considered that the tangential stress is not negligible.[1] The possibility of introducing tangential stresses into the theory of wave generation has been considered by Jeffreys.[3] The solutions of his differential equations did not conform to the facts, and he therefore abandoned them in favor of a theory that considers only normal pressures. While following Jeffreys in this, the present calculation differs from his in another important respect.

Surface waves can be caused only by a variable pressure, since a constant atmospheric pressure merely adds to the hydrostatic pressure in the water without deforming the surface. Jeffreys supposes that the variable component of the wind pressure is caused by the waves already present (see above) and that there would be no variable wind pressure if the air-water interface were perfectly flat. Specifically, he supposes that the wind pressure is 90° out of phase with the sinusoidal waves, so that the pressure on the up-wind side of a crest is greater than on the down-wind side. The quantitative relation between this pressure and the wind speed and the slope and velocity of the crest is formulated in terms of the constant known as the sheltering coefficient.[4]

In the following, no such relation will be assumed. Instead, it will be supposed that the wind pressure (even on a flat horizontal surface) has a variable component. This is considered to be the result of moving centers of high (or low) pressure, as described in Sec. 3. These centers, or gusts, are assumed to move with the mean wind speed. It is shown, in Secs. 5 and 8, that this one assumption explains many of the facts used by Jeffreys in constructing his sheltering theory. Finally, in Sec. 10, it is shown that there is a phase difference between the wind pressure and the surface waves which it causes, which results in a horizontal component of the wind pressure the time average of which does not vanish. The present theory is therefore a kind of inverse of the sheltering theory—inverse with regard to cause and effect.

Crucial experiments are difficult to perform in an area where large storm waves are being generated, but there is some evidence for the existence of pressure fluctuations capable of producing waves on an undisturbed water surface.† Observations were made[5] on a small pool, in a location where the early morning is often a period of dead calm with a thermally stable atmosphere. As the ground is heated by the sun, small centers of convection are apparently produced in the air, and as these move across the previously mirror-flat surface of the pool, they cause ripples and waves having the typical V-shaped configuration of a wake. The theory of such wakes is similar to that of Lambs' "fish-line problem"[6] and it is readily seen that their most prominent components are short-period gravity waves (not surface tension ripples, although these are present also). When the wind reaches the "catspaw" stage, the observations suggest that the surface of the pool is simultaneously subjected to a multitude of pressure centers.

There is also evidence which suggests that the disturbance caused by higher winds on a somewhat larger body of water consists of such wakes. The observations were made on a nearly rectangular pond, 240 m by 60 m, and 2 m deep: ". . . at all winds, one had the impression that, in contrast to the conventional picture of . . . waves advancing before the wind, there were instead two sets of waves, to the right and left of the wind-direction. Moreover, the angle between the wind direction and wave travel appeared to depend on wind speed, being initially about 75° and decreasing to a minimum of about 15° at the highest winds observed."[7]

On still larger bodies of water, it is probable that the pressure centers or gusts of wind will "blow themselves out", leaving their wakes to dissipate as free gravity waves under the influence of divergence and dispersion. The theory of this phenomenon, for a single gust, is the subject of Secs. 2, 5, and 6.

Perhaps the most certain part of the following calculation, which is least likely to require modification when the simplifying assumptions are dropped, is the statistical treatment of the wind stress and the sea surface. This is accomplished by means of a general formula developed elsewhere,[8] and which will merely be summarized here. The basic statistical device is that of the time average, as commonly used in the theory of

[3] H. Jeffreys, Proc. Roy. Soc. (London), **A107**, 189 (1925).

[4] See reference 3. This theory is also discussed in H. Lamb *Hydrodynamics* (Cambridge University Press, Cambridge, 1932), sixth edition, p. 625, as well as in Reference 1.

† However, see the discussion of Eq. 52.1.

[5] By G. C. Ewing; the writer is indebted to him for permission to quote his unpublished observations.

[6] See Reference 4, p. 468; it should be noted that the essential feature of this problem is not the small diameter of the fish-line, but its low velocity relative to the water.

[7] W. G. Van Dorn, *Wind Stress over Water*, dissertation, Scripps Institution of Oceanography, (1952) Reference No. 52-60.

[8] C. Eckart, Phys. Rev. **91**, 784 (1953).

turbulence. Let $h(x, y, t)$ be the displacement of the sea-surface, then the symbol $\langle hh' | \tau \rangle$ is defined by

$$\langle hh' | \tau \rangle = \lim_{T \to \infty} \frac{1}{2T} \int_{-T}^{T} h(x, y, t) h(x', y', t-\tau) dt,$$

and is the correlation of h at the two points xy and $x'y'$, delayed by the interval τ. Similarly

$$\{hh' | \tau\} = \int_{-\infty}^{\infty} h(x, y, t) h(x', y', t-\tau) dt$$

is the delayed convolution of h at the two points. It can be seen that, if the correlation of h is finite, its convolution will diverge; and if the convolution is finite, the correlation will be zero. The solutions of Eqs. (1) to (5) below therefore fall into two classes: class A, for which the correlation is finite, and class I, for which the convolution is finite.

If the sea surface is idealized as a statistically steady phenomenon, the appropriate solution will be of class A. The difficulty is that the appropriate solution is then not easily obtained; those solutions of the equations that are furnished by the usual Fourier integral methods are all of Class I. This, however applies to the function h itself; it can be shown that its correlation $\langle hh' | \tau \rangle$ satisfies certain other equations, whose solutions are readily exhibited. Let $h_{\mathbf{q}}$ be a family (ensemble) of class I solutions of the Eqs. (1) to (5); in the present case, $h_{\mathbf{q}}$ will be the surface disturbance produced by a single gust centered at the point $\mathbf{q}$. Then it is at least very probable that the correlation of the disturbance h produced by a large number of such gusts distributed at random through space and time will be given by

$$\langle hh' | \tau \rangle = \int w(\mathbf{q}) \{h_{\mathbf{q}} h_{\mathbf{q}}' | \tau\} d\mathbf{q},$$

where $w(\mathbf{q})$ is a positive function of $\mathbf{q}$—the distribution function of the gusts in space. Their distribution in time is to be such that the correlation exists. A very similar equation will connect the wind pressure of a single gust to the correlation of the pressure due to the whole random ensemble of gusts which makes a storm.

2. THE BASIC EQUATIONS

It will be supposed that the water can be treated as a non-viscous incompressible fluid, and that the wind pressure, a, is given, at least in a statistical sense. It will be convenient to express all pressures in cm of water-barometer so that the wind pressure in dynes/cm^2 is $\rho g a$, ρ being the density of water, and g the acceleration of gravity. Similarly, let $g\phi$ be the velocity potential; then, if the positive z-axis is vertical and upwards,

$$\nabla^2 \phi = 0 \quad \text{when} \quad z < 0; \tag{1}$$

$$\nabla\phi, \phi \longrightarrow 0 \quad \text{as} \quad z \to -\infty; \tag{2}$$

$$\frac{\partial^2 \phi}{\partial t^2} + g \frac{\partial \phi}{\partial z} = \frac{\partial a}{\partial t} \quad \text{at} \quad z = 0. \tag{3}$$

Since no initial conditions are specified, these equations do not uniquely define ϕ, and the condition of outgoing waves must be added to complete the formulation of the problem.

The primary interest centers on the free surface: let its equation be

$$z = h(\mathbf{x}, t), \tag{4}$$

where here, as throughout the following, $\mathbf{x}$ is the two-dimensional horizontal vector whose components are x, y. Then h may be obtained from

$$h(\mathbf{x}, t) = (\partial\phi/\partial t)_{z=0} - a(\mathbf{x}, t). \tag{5}$$

3. THE WIND PRESSURE

It is supposed that the wind pressure can be represented by an ensemble of gusts, $a_{\mathbf{q}}(\mathbf{x}, t)$, so that its correlation is

$$\langle aa' | \tau \rangle = \int w(\mathbf{q}) \{a_{\mathbf{q}} a_{\mathbf{q}}' | \tau\} d\mathbf{q}, \tag{6}$$

w being the weight function of the ensemble. For simplicity, it is supposed that the gusts are all identical except for the location of their centers, and that these have the coordinates $\mathbf{q}$, so that

$$a_{\mathbf{q}}(\mathbf{x}, t) = a_0(\mathbf{x} - \mathbf{q}, t). \tag{7}$$

The function a_0 is to be real, and such that it can be represented by the Fourier integral

$$a_0(\mathbf{x}t) = \int\int A(\mathbf{k}\omega) \exp[i(\mathbf{k}\cdot\mathbf{x} - \omega t)] d\mathbf{k} d\omega, \tag{8}$$

the integration over ω and the two components of $\mathbf{k}$ running from $-\infty$ to ∞.

Then, by the Parseval theorem,

$$\{a_0 a_0' | \tau\} = 2\pi \int\int\int A(\mathbf{k}\omega) A^*(\mathbf{k}'\omega) \times \exp[i(\mathbf{k}\cdot\mathbf{x} - \mathbf{k}'\cdot\mathbf{x}' - \omega t)] d\mathbf{k} d\mathbf{k}' d\omega \tag{9}$$

and the evaluation of the integral in Eq. (6) can be simplified by introducing the function

$$W(\boldsymbol{\alpha}) = \int\int w(\mathbf{q}) \exp(-i\boldsymbol{\alpha}\cdot\mathbf{q}) d\mathbf{q}/(2\pi)^2, \tag{10}$$

so that

$$\langle aa' | t \rangle = (2\pi)^3 \int\int\int W(\mathbf{k} - \mathbf{k}') A(\mathbf{k}\omega) A^*(\mathbf{k}'\omega) \times \exp[i(\mathbf{k}\cdot\mathbf{x} - \mathbf{k}'\cdot\mathbf{x}' - \omega\tau)] d\mathbf{k} d\mathbf{k}' d\omega. \tag{11}$$

The change of variables

$$\begin{aligned} \mathbf{r} &= \tfrac{1}{2}(\mathbf{x} + \mathbf{x}'), \quad & \boldsymbol{\xi} &= \mathbf{x} - \mathbf{x}', \\ \mathbf{m} &= \tfrac{1}{2}(\mathbf{k} + \mathbf{k}'), \quad & \boldsymbol{\alpha} &= \mathbf{k} - \mathbf{k}', \end{aligned} \tag{12}$$

reduces this to

$$\langle aa' | t \rangle = (2\pi)^3 \int\int\int W(\boldsymbol{\alpha}) A(\mathbf{k}\omega) A^*(\mathbf{k}'\omega) \times \exp[i(\boldsymbol{\alpha}\cdot\mathbf{r} + \mathbf{m}\cdot\boldsymbol{\xi} - \omega\tau)] d\boldsymbol{\alpha} d\mathbf{m} d\omega. \tag{13}$$

It will appear below that W is appreciable only for very small values of the components of $\boldsymbol{\alpha}$, so that $\mathbf{k}$ and $\mathbf{k}'$ may both be replaced by $\mathbf{m}$ in the factors A and A^*. The integration over $\boldsymbol{\alpha}$ can then be carried out by the inverse of Eq. (10) and

$$\langle aa' | \tau \rangle = (2\pi)^3 w(\mathbf{r}) \int\int |A(\mathbf{m}\omega)|^2 \times \exp[i(\mathbf{m}\cdot\boldsymbol{\xi} - \omega\tau)] d\mathbf{m} d\omega. \quad (14)$$

Setting $\boldsymbol{\xi}=0$, $\tau=0$, one obtains the mean square wind pressure in the form

$$\langle a^2 \rangle = (2\pi)^3 w(\mathbf{r}) \int\int |A(\mathbf{m}\omega)|^2 d\mathbf{m} d\omega.$$

If a_0 is normalized so that

$$(2\pi)^3 \int\int |A|^2 d\mathbf{m} d\omega = 1, \quad (15)$$

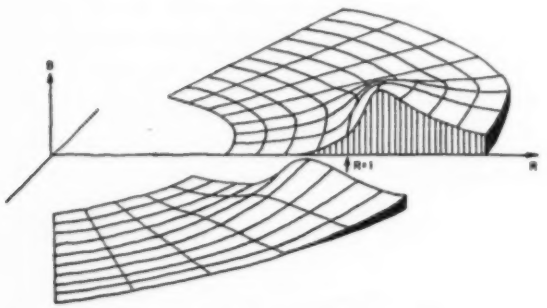

FIG. 1. The function B in its dependence on R and θ, for $\mathcal{T}=10$, $\mathcal{L}=3$. R is the distance from the center of the disturbance, $\mathcal{T}$ its duration, $\mathcal{L}$ its radius, all in non-dimensional form. The angle θ is the direction relative to the motion of the gust, and B is the amplitude of the disturbance.

this becomes

$$\langle a^2 \rangle = w(\mathbf{r}) \quad (16)$$

and furnishes a concise interpretation of the weight function w. Moreover, if the extent of the storm, i.e., of the region over which w is different from zero, is large compared to a single gust, and if w varies only slowly in this region, this justifies the approximation leading to Eq. (14).

The quantity

$$\Psi = (2\pi)^3 |A(\mathbf{m}\omega)|^2 \quad (15.1)$$

may be called the spatio-temporal spectrum of the wind pressure. It represents an analysis of this pressure into elementary waves of frequency ω, wave number $\mathbf{m}$, and phase velocity ω/m. These waves therefore do not all have the same phase velocity, but all velocities are represented. It may be remarked that the factorization of $\langle aa' | \tau \rangle$ into the product of w and the integral over Ψ is somewhat artificially introduced by the assumption that the gusts are all identical except for their centers. A more realistic assumption would have them differing in other respects as well, and the factorization would no longer be possible.

4. A SPECIAL EXAMPLE

Thus far, no special properties of the function a_0 have been specified. It will now be supposed that each gust consists of a pressure area (either high or low) that moves with the mean wind.[9] To an observer moving with this same velocity $\mathbf{U}$, the gust would have a fixed center, a radius L, and a duration T. In stationary coordinates, it might be represented by the function

$$a_0(\mathbf{x}, t) = \text{const.} \exp\{-\tfrac{1}{2}[(\mathbf{x}-\mathbf{U}t)^2/L^2 + t^2/T^2]\}. \quad (17)$$

Then A is found to be

$$A(\mathbf{k}\omega) = b \exp\{-\tfrac{1}{2}[k^2L^2 + (\omega - \mathbf{k}\cdot\mathbf{U})^2T^2]\}, \quad (18)$$

and in order to satisfy Eq. (15), it is seen that

$$(2\pi)^3 b^2 = L^2T/\pi^3. \quad (19)$$

The Eq. (14) then becomes

$$\langle aa' | \tau \rangle = w(\mathbf{r}) \exp\{-\tfrac{1}{4}[(\boldsymbol{\xi} - \mathbf{U}\tau)^2/L^2 + \tau^2/T^2]\}. \quad (20)$$

The function w will also be specialized:

$$w(\mathbf{r}) = P^2 \exp(-\tfrac{1}{2}r^2/D^2); \quad (21)$$

the constant P is the rms value of the wind pressure at the center of the storm, whose radius is D. It follows from Eq. (21) that

$$W(\boldsymbol{\alpha}) = (P^2D^2/2\pi) \exp(-\tfrac{1}{2}\alpha^2D^2). \quad (22)$$

5. THE SURFACE WAVES CAUSED BY A SINGLE GUST

It is next necessary to obtain the solution of Eqs. (1) to (5) inclusive, when a is replaced by a_0. Using the abbreviation

$$\kappa = \omega^2/g, \quad (23)$$

this is given by

$$g\phi_0 = \Re \int\int\int 2\omega A(\mathbf{k}\omega) \exp[-i\sigma(k-\kappa) + i(\mathbf{k}\cdot\mathbf{x} - \omega t) + kz] d\mathbf{k} d\omega d\sigma, \quad (24)$$

where the integrations with respect to ω and the auxiliary variable σ both run from 0 to $+\infty$ only. Care must be exercised in the order of integration, since the integral is conditionally convergent. This is of considerable physical significance, for it endows the integral with a protean ability to enter into the description of a very diverse set of phenomena. That Eq. (24) gives a solution of Eqs. (1) and (2) is clear; that ϕ_0 also satisfies Eq. (3) is most readily seen by substituting from Eq. (24) into the left of Eq. (3). The integration over σ can then be performed first, and the result is the time deriv-

[9] In light winds, the velocity of the gusts may be quite different from that of the mean wind. In well developed advection, there seems no good reason to suppose that the gusts move with a velocity appreciably different from that of the mean wind at, say 10 meters elevation.

ative of the right side of Eq. (8). That ϕ_0 satisfies the condition of outgoing waves, will become clear below (Eq. (26)).

It then follows from Eq. (5) that the surface displacement caused by the single gust is

$$h_0=\Re\int\int\int(-2ik)A(\mathbf{k}\omega)\exp[-i\sigma(k-\kappa)+i(\mathbf{k}\cdot\mathbf{x}-\omega t)]d\mathbf{k}d\omega d\sigma. \quad (25)$$

These integrals represent the solution for all values of $\mathbf{x}$ and t, including values near the origin, where the wave motion is not free, but forced by the wind pressure. For many purposes, it is convenient to have an approximate solution, valid only in regions of space and time where a_0 is negligible. Such an approximation can readily be obtained by the method of stationary phase, and is (using Eq. (18))

$$h_0=0 \quad \text{when} \quad t\ll T; \quad (26.a)$$

$$h_0=[2^{7/2}\pi^2 b/L^2 t]B\sin(\kappa_0 r-\omega_0 t) \quad (26.b)$$

when $t\gg T$ and $r\gg L$. In this equation,

$$B(\omega_0\theta)=\kappa_0^2L^2\exp[-\tfrac{1}{2}\kappa_0^2L^2-\tfrac{1}{2}(\omega_0-\kappa_0U\cos\theta)^2T^2], \quad (27)$$

where $r=|\mathbf{x}|$, and θ is the angle between $\mathbf{x}$ and $\mathbf{U}$, while ω_0 is to be determined from the group velocity equation

$$r=(g/2\omega_0)t=\tfrac{1}{2}c_0t. \quad (28)$$

Here c_0 is the phase velocity, and $\frac{1}{2}c_0$ the group velocity of gravity waves of frequency ω_0.

While B is, in the first instance, a function of ω_0 and θ, it becomes a function of r/t because of Eq. (28). For fixed t, its dependence on r and θ determines the instantaneous amplitude of the waves on the surface of the sea. It is convenient to express B in terms of the dimensionless variable

$$R=2r/Ut=g/\omega_0U=c_0/U, \quad (29)$$

which may be interpreted as the distance traveled by the waves, as their period, or as their phase velocity, all in dimensionless form. Also introducing the dimensionless parameters

$$\mathfrak{L}=gL/U^2, \quad \mathfrak{T}=gT/U, \quad (30)$$

Eq. (27) becomes

$$B(R,\theta)=(\mathfrak{L}^2/R^4)\times\exp\{-\tfrac{1}{2}[\mathfrak{L}^2+\mathfrak{T}^2(R-\cos\theta)^2]/R^4\}. \quad (31)$$

6. DISCUSSION OF THE AMPLITUDE FUNCTION

Figures 1 and 2 show B as a function of R and θ for two sets of values of $\mathfrak{L}$ and $\mathfrak{T}$. It will be found that this function dominates the remainder of the theory, and a somewhat detailed analysis of its characteristics is therefore justified. The most prominent characteristic visible on Figs. 1 and 2 is the maximum that occurs for a certain value of R, when θ, $\mathfrak{L}$, and $\mathfrak{T}$ are fixed. The

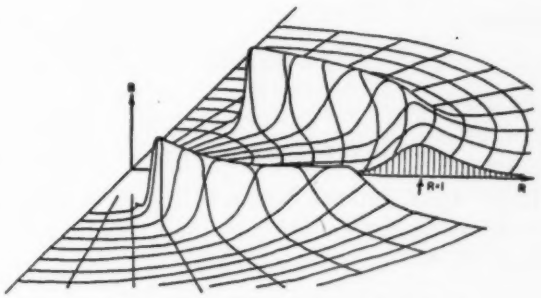

FIG. 2. Same as Fig. 1, but for $\mathfrak{T}=10$, $\mathfrak{L}=\frac{1}{4}$.

position of this maximum is determined by the roots of the equation

$$M+4N(u-1)(u-2)-2u^4=0, \quad (32)$$

in which

$$u=R/\cos\theta, \quad M=\mathfrak{L}^2/\cos^4\theta, \quad N=\mathfrak{T}^2/8\cos^2\theta. \quad (33)$$

Figure 3 is a Runge diagram[10] of Eq. (32). The coordinates of a general point P, in the diagram are M, N, and the roots of Eq. (32) are found by drawing tangents from P to the solid curve. The value of u is determined by the point of tangency, as marked on the curve. If $\mathfrak{L}$ and $\mathfrak{T}$ are kept fixed, and θ is allowed to increase from 0 to $\pi/2$, P will move away from the origin along a parabola, as shown by the dotted curve. The corresponding change in any of the roots of Eq. (32) is readily visualized. If the point P is chosen at random in the first quadrant, there is seen to be a high probability that a root of Eq. (32) will occur either very close to $u=1$ or very close to $u=2$. If $\theta=0$, $u=R$ and reference to the preceding section shows that $R=1$ corresponds to waves whose *phase* velocity is U, while $R=2$ corresponds to waves whose *group* velocity is U.

If the root lies near $u=1$, the following formula is

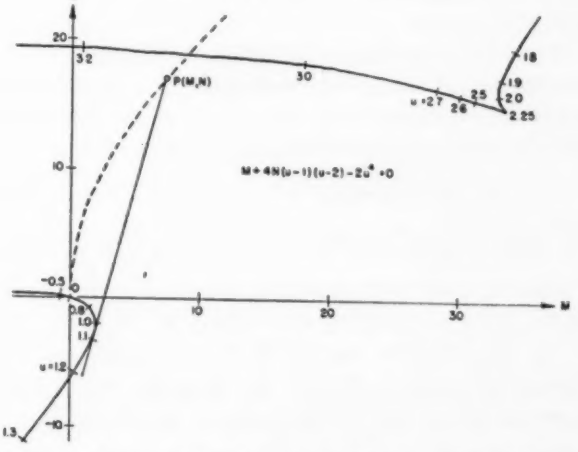

FIG. 3. A tangent from the point $P(M,N)$ to the solid curve determines one of the roots of the equation $M+4N(u-1)(u-2)-2u^4=0$, in accordance with the scale marked on the curve. The dotted parabola is the locus of $P(M,N)$ as the angle θ varies.

[10] F. Klein *Elementary Mathematics from an Advanced Standpoint* (Dover Publications, New York, 1939), pp. 90–94.

available:

$$u=1+[(M-2)/4(N+2)]+\cdots, \tag{34}$$

while if it is near $u=2$

$$u=2+[(M-32)/4(N-16)]-\cdots. \tag{35}$$

These considerations determine the location of the extrema of B; the variation of their magnitudes as θ changes is determined largely by the factor

$$B_m=(\mathfrak{L}^2/\mathfrak{R}^4)\exp(-\tfrac{1}{2}\mathfrak{L}^2/\mathfrak{R}^4).$$

Since u usually remains nearly constant as θ varies, B_m will diminish rapidly with decreasing $\cos\theta$ provided that $\mathfrak{L}$ is large, as in Fig. 1. If $\mathfrak{L}$ is small as in Fig. 2, B_m will at first increase, until $\cos\theta$ becomes less than a critical value, after which it rapidly approaches zero. This then manifests itself by the appearance of a prominent ridge, the projection of which on the R,θ plane nearly coincides with the circle of unit diameter and center at $R=\frac{1}{2}$, $\theta=0$.

Further insight into Figs. 1 and 2 can be obtained as follows, if only the case of roots near $u=1$ is discussed. These figures apply only to the disturbance at great distances (in time and space) from the wind gust that produces it. The first effect of the gust must be to produce a typical, V-shaped wake, as discussed in the Introduction. When the gust has "blown itself out," the further development of this wake will be that of free waves, and the combined effect of divergence and dispersion will be to resolve it into its spatio-temporal spectrum. Now it is characteristic of the elementary theory of wakes to suppose that $\mathfrak{T}=\infty$, $\mathfrak{L}=0$, and that their sinusoidal components are all described by $u=1$. According to this elementary theory, therefore, Figs. 1 and 2 should simply show cylinders of unit diameter, with axes at $R=\frac{1}{2}$, $\theta=0$. The departure from such knife-edge ridges is caused by the finite radius and duration of the gust.

While Eq. (31) is not elaborate, considered from the standpoint of numerical evaluation, it is difficult to integrate, even approximately. A somewhat more tractable expression, which corresponds to Eq. (34), is

$$B=M\exp\{-\tfrac{1}{2}[M+8(N+2)(u-1)^2]\}. \tag{36}$$

7. THE CORRELATION OF THE SURFACE WAVES

Since Eq. (25) is the rigorous expression for the waves caused by a single gust, the correlation of the storm waves may now be calculated in a manner entirely analogous to Sec. 3, though the integrals involved are more elaborate. The starting point is the ensemble

$$h_{\mathbf{q}}=h_0(\mathbf{x}-\mathbf{q},\,t) \tag{37}$$

and the ensemble integral

$$\langle hh'|\tau\rangle=\int w(\mathbf{q})\{h_{\mathbf{q}}h_{\mathbf{q}}'|\tau\}d\mathbf{q}. \tag{38}$$

Proceeding as in Eqs. (9) to (13):

$$\langle hh'|\tau\rangle=\Re\int\int\int\int\int 2m^2\Psi(\mathbf{m}\omega)W(\boldsymbol{\alpha})$$
$$\times\exp\{i[-\sigma(k-\kappa)+\sigma'(k'-\kappa)+\boldsymbol{\alpha}\cdot\mathbf{r}+\mathbf{m}\cdot\boldsymbol{\xi}-\omega\tau]\}$$
$$d\boldsymbol{\alpha}d\mathbf{m}d\omega d\sigma d\sigma'; \tag{39}$$

in order to carry out the integration over α, the further approximations

$$k,k'=m\pm\tfrac{1}{2}\boldsymbol{\alpha}\cdot\mathbf{m}_1,\quad \mathbf{m}_1=\mathbf{m}/m, \tag{40}$$

are permissible and, together with the change of variables

$$v=\sigma-\sigma',\quad s=\tfrac{1}{2}(\sigma+\sigma'), \tag{41}$$

leads to

$$\langle hh'|\tau\rangle=\Re\int\int\int\int 2m^2\Psi(\mathbf{m}\omega)w(\mathbf{r}-s\mathbf{m}_1)$$
$$\cdot\exp\{i[-v(m-\kappa)+\mathbf{m}\cdot\boldsymbol{\xi}-\omega\tau]\}d\mathbf{m}d\omega dvds, \tag{42}$$

the integration over v extending from $-2s$ to $+2s$, and that over s, from 0 to $+\infty$. The integration over v can be performed at once, and results in

$$\langle hh'|\tau\rangle=\int\int\int 4m^2\Psi(\mathbf{m}\omega)w(\mathbf{r}-s\mathbf{m}_1)$$
$$\cdot\{\sin[2s(m-\kappa)]/(m-\kappa)\}\cos(\mathbf{m}\cdot\boldsymbol{\xi}-\omega\tau)d\mathbf{m}d\omega ds.$$

When the point $\mathbf{r}$ is outside the storm area, the factor w will have appreciable values only for very large values of s; the factor immediately following w will correspondingly have appreciable values only when $m-\kappa$ is very small. Except in this factor, m may therefore be replaced by κ. When the point $\mathbf{r}$ is in the storm area, the first step of this argument fails; closer study shows that the conclusion remains valid, because the effect of the few nearby gusts (for which s is small) is negligible compared to the many distant gusts for which s is large. This is true, of course, only when the dimension, D, of the storm is much greater than that of the single gust, L.

The integration $d\mathbf{m}$ may be resolved into $mdmd\vartheta$, m being the magnitude of $\mathbf{m}$, and ϑ the angle between $\mathbf{m}$ and $\mathbf{U}$. After replacing m by κ everywhere except in the one factor, the integration over m can be performed leading to

$$\langle hh'|\tau\rangle=4\pi\int\int\kappa^2\Phi(\omega\vartheta)S(\mathbf{r}\vartheta)$$
$$\cdot\cos[\kappa(\xi\cos\vartheta+\eta\sin\vartheta)-\omega\tau]d\vartheta d\omega, \tag{43}$$

where

$$\Phi(\omega\vartheta)=\Psi(\kappa\mathbf{m}_1,\,\omega)$$

and

$$S(r\vartheta)=\int_0^\infty w(x-s\cos\vartheta,\,y-s\sin\vartheta)ds \tag{44}$$

while ξ,η are the components of $\boldsymbol{\xi}$, xy those of $\mathbf{r}$.

Comparing Eq. (43) with the analogous Eq. (14) for the wind pressure, several differences become apparent. In Eq. (43), the integration is only over ϑ, the direction of $\mathbf{m}$, while in Eq. (14) the integration is also over the magnitude of m. The wind pressure is composed of waves of all phase velocities, while those composing the surface disturbance all have the velocity $\omega/\kappa=g/\omega$ characteristic of free gravity waves of frequency ω.

Instead of the integration over m, the Eq. (43) contains the function S, which is an integral of the factor w that appears outside the integral of Eq. (14). The correlation of h at $\mathbf{r}$ depends, not on the local intensity of the wind disturbance at $\mathbf{r}$, but on the integral of this intensity over the "fetch"—i.e., over the path by which waves‡ traveling in the direction ϑ reach the point $\mathbf{r}$. The function S may be called the fetch intensity.

The expression for S can be obtained explicitly if w is given by Eq. (21); let $\bar{x}\bar{y}$ be the components of $\mathbf{r}$ parallel and perpendicular to the direction ϑ: then

$$S(r,\vartheta)=(\pi/2)^{\frac{1}{2}}P^2D\exp(-\tfrac{1}{2}\bar{y}^2/D^2)\operatorname{erfc}(+\bar{x}/2^{\frac{1}{2}}D). \quad (45)$$

If $\bar{y}=0$, the fetch passes through the center of the storm and S is given by the error-function alone; if $\bar{y}\neq 0$, the fetch passes to one side of the point of maximum wind-pressure, and S is correspondingly reduced by the exponential factor. If $\bar{x}\ll -D$, the error function will be practically zero: no waves are propagated backwards along the fetch. If $\bar{x}\gg D$ the point $\mathbf{r}$ is outside the storm-area, but in a down-wind direction, and the error-function will be practically equal to 2.

The disturbance at any point $\mathbf{r}$ will thus consist of free gravity waves of all frequencies and directions, each elementary wave having the intensity $4\pi\kappa^3\Phi S$ appropriate to its period and fetch. This product is the spatio-temporal spectrum of the waves, and should be compared with that of the wind, given by Eq. (15.1).

8. THE WAVES OUTSIDE THE STORM AREA

The further evaluation of the integral in Eq. (43) for points with large positive $\bar{x}$ can be accomplished by setting the error function in Eq. (45) equal to 2. If ψ is the angle between $\mathbf{r}$ and $\mathbf{U}$, $\bar{y}$ will be zero when $\vartheta=\psi$, and the exponential in Eq. (45) will diminish rapidly for increasing $|\vartheta-\psi|$. An estimate of $\langle hh'|\tau\rangle$ is thus obtained by setting $\vartheta=\psi$ in the factor Φ, and expanding the argument of the cosine only to first order in $\vartheta-\psi$. The integration over ϑ can then be performed with adequate precision, leading to

$$\langle hh'|\tau\rangle=(8\pi^2P^2D^2/r)\int\kappa^3\Phi(\omega,\psi)\cdot\exp(-\tfrac{1}{2}\kappa^2\eta_r^2D^2/r)\cos(\kappa\xi_r-\omega\tau)d\omega, \quad (46)$$

‡ As used here, the word "fetch" has a slightly different meaning than in the current literature on surface waves. It is usually defined as the path over which the wind travels in order to reach the point $\mathbf{r}$. Since the usual assumption is that the waves travel only in the direction of the wind, the ultimate intents of the two definitions are the same.

where

$$\xi_r=\xi\cos\psi+\eta\sin\psi,\qquad \eta_r=-\xi\sin\psi+\eta\cos\psi, \quad (47)$$

are the components of ξ parallel and perpendicular to $\mathbf{r}$.

Before attempting to perform the remaining integration, it is convenient to make the change of variable

$$R=g/\omega U;$$

then, after some reductions, Eq. (46) becomes

$$\langle hh'|\tau\rangle=8\pi^{\frac{1}{2}}(P^2D^2/rL)(\mathcal{T}/\mathcal{L})\cdot\int B^2\exp(-\tfrac{1}{2}\kappa^2\eta_r^2D^2/r^2)\cos(\kappa\xi_r-\omega\tau)dR, \quad (48)$$

where B is obtained from Eq. (27) by replacing θ by ψ, and κ_0 by κ. The integral of Eq. (48) remains intractable, however, unless the approximate Eq. (36) is used for B. Then since $4(N+2)>1$, it may be evaluated by the method of steepest descent, and the result is

$$\langle hh'|t\rangle=H^2\exp\{-[(2\kappa_1\xi_r-\omega_1\tau)^2/\mu^2+\kappa_1^2\eta_r^2/\nu^2]/4\pi^2\}\cdot\cos(\kappa_1\xi_r-\omega_1\tau), \quad (49)$$

in which the symbols have the meanings explained in the following paragraphs.

The factor $\cos(\kappa_1\xi_r-\omega_1\tau)$ indicates that the waves have the dominant wave number and frequency

$$\kappa_1=g/U^2\cos^2\psi,\quad \omega_1=g/U\cos\psi. \quad (50)$$

Since the surface disturbance has a random character, no unique value of wave number and frequency can be assigned to it; these dominant values correspond roughly to a maximum in the spectrum. The appearance of ξ_r in the cosine factor indicates that the dominant direction of wave travel is radially outward from the center of the storm. Equation (50) shows that the dominant waves depend on the angle ψ which this direction makes with the wind. In particular, the dominant phase velocity is $\omega_1/\kappa_1=U\cos\psi$, which corresponds to the discussion of Sec. 6, and to the observation that, when ψ is small, the phase velocity is nearly equal to the wind velocity. There is no empirical evidence bearing on the dependence of phase velocity on ψ.

In the exponential factor of Eq. (49), the quantities μ and ν are defined by

$$\pi^2\mu^2=64+(4\mathcal{T}^2/\cos^2\psi),\qquad \pi^2\nu^2=r^2/2D^2. \quad (51)$$

This factor determines the coherence properties of the wave field. It may conveniently be discussed first for the special case $\xi_r=\eta_r=0$, which corresponds to observations made at one point over the time interval τ. The factor diminishes from 1 to $1/e$ when $\omega_1\tau$ increases from 0 to $2\pi\mu$; μ is therefore the number of waves in a coherent train. Observationally, this ranges from 5 to 10, corresponding (with $\psi=0$) to $\mathcal{T}=7$ to 15. For $U=20$

meters per second, the corresponding range of T, the life of the gust, is 15 to 30 seconds.

The exponential factor may next be considered for $\eta_r=0$, $\tau=0$ which corresponds to simultaneous measurements (say on an aerial photograph) at two points separated a distance ξ_r in the radial direction. The factor then diminishes to $1/e$ when $2\kappa_1\xi_r=2\pi\mu$ or $\xi_r=\frac{1}{2}\mu$ wavelengths. The factor 2 is readily identified with the ratio of phase and group velocity; because of this, the dominant number of waves in a train, when observed in this manner, should be only 2 to 5. This is confirmed by the fact that aerial photographs generally appear to be even less periodic than are the height-time graphs produced by wave recorders. When $\xi_r=0$, $\tau=0$ the exponential factor determines the crest length of the waves to be ν wavelengths. If $r=10D$, $\nu=2.2$ in fair agreement with aerial photographs, although no quantitative data are available.

By setting $\xi_r=\eta_r=0$, $\tau=0$ in Eq. (49), it is seen that H is the rms value of h; this quantity is defined by

$$H^2=8\pi(P^2D^2/rL)G^2/[1+(16\cos^2\psi/\mathcal{T}^2)]^{\frac{1}{2}}, \quad (52)$$

and

$$G^2=(\mathcal{L}/\cos^2\psi)^3\exp[-(\mathcal{L}/\cos^2\psi)^2] \quad \text{if} \quad \cos\psi>0;$$
$$=0 \quad \text{if} \quad \cos\psi<0. \quad (53)$$

Because of the large value of $\mathcal{T}$, the radical in Eq. (52) may be considered as a correction factor whose value differs only little from unity; except for this factor, H is independent of $\mathcal{T}$, to the approximation here achieved. For constant ψ, H varies inversely as r, as is required for the conservation of energy. The function G^2 has a maximum value $G_m^2=0.640$ when $\mathcal{L}/\cos^2\psi=1.225$, and approaches zero for larger and smaller values of this argument. For $\mathcal{L}>1.225$, the value G_m is not attained, but G has its largest value ($<G_m$) when $\psi=0$, and diminishes fairly rapidly with increasing $|\psi|$. For $\mathcal{L}<1.225$, $\psi=0$ is a minimum, and G attains the value G_m for some angle ψ_m, dropping rapidly to zero when $|\psi|>\psi_m$. These properties of G reflect those of the function B, from which it is derived.

In any actual storm, there will undoubtedly be gusts that have any pre-assigned value of $\mathcal{L}$. From what has just been said it is clear that those for which $\mathcal{L}$ is large (>3) will be ineffective in producing waves of any kind. Those gusts for which $\mathcal{L}$ is small ($<\frac{1}{3}$) will cause waves that travel at a large angle to the wind, and have a correspondingly short period. One may therefore conclude that those gusts which cause waves traveling in the general direction of the wind§ have values of $\mathcal{L}$ in the range 0.3 to 3. A typical gust might therefore be characterized by $\mathcal{L}=1$, $U=20$ m/sec, and thus have an actual radius of $L=40$ meters.

By using wave-height data from an actual storm, Eq. (52) may be used to estimate the value of P, which is the rms wind pressure at the center of the idealized storm under consideration here. For this purpose, one may take $G=G_m$, and simplify Eq. (52) to the form

$$H^2=10P^2D^2/rL. \quad (54)$$

The weather maps for January 17 and 18, 1945 show a storm at about lat 45° N., long 165° W., with winds of at least 46 knots=24 m/sec for more than 14 hours. The waves due to this storm were recorded[11] at various points on the west coast of the United States, and the average height, reduced to deep water off Morro Bay, California, was $2H=2.8$ m, while the period was 16 sec. From the maps, $D=425$ km, $r=3800$ km. The value of L may be estimated at 58 m, a value obtained from $U=24$ m/sec and $\mathcal{L}=1$. Eq. (52.1) then yields $P=1.6$ cm. This value may be compared with $\frac{1}{2}\rho_a U^2=3.8$ cm, ρ_a being the density of air.

The writer is indebted to R. S. Arthur for additional data enabling the comparison of this theory with the equations used in forecasting storm waves. The predicted heights of storm waves, when used as above in Eq. (52.1), yielded a value of the ratio $P\div\frac{1}{2}\rho_a U^2$ that was nearly unity in the trial case examined.

The question arises, whether fluctuations of this magnitude in the pressure exerted by the wind on a horizontal surface are observed. No relevant measurements appear to have been reported in the literature, but G. C. Ewing and L. N. Liebermann have each kindly made preliminary measurements of the effect by exposing a water manometer to the action of the wind. In general, they agree in setting 0.1 cm as an upper limit to the observed pressure fluctuations, although the former noted values of 0.5 cm on one occasion. These results are not conclusive, but may be taken as an indication of the probable result of more adequately instrumented work.

9. THE WAVES INSIDE THE STORM AREA

The explicit calculation of the waves inside the storm area is rendered difficult because of the integration over ϑ in Eq. (43); outside the storm, this integration was made feasible by the special properties of the function $S(r\vartheta)$, and led to Eq. (46). At the storm center ($r=0$), this function becomes a constant, independent of ϑ, but this does not make the integration any easier. However, in any case the integration over ω can be performed as above, and the expression

$$\langle hh'|\tau\rangle=(4/L)\int_{-\pi/2}^{\pi/2}\{SG^2/[1+(16\cos^2\vartheta/\mathcal{T}^2)]^{\frac{1}{2}}\}$$
$$\cdot\exp[-(2\kappa_1\xi_\vartheta-\omega_1\tau)^2/4\pi^2\mu^2]\cos(\kappa_1\xi_\vartheta-\omega_1\tau)d\vartheta \quad (55)$$

is obtained for the correlation of h. In Eq. (55),

$$\xi_\vartheta=\xi\cos\vartheta+\eta\sin\vartheta,$$

§ Present observational practice does not ascribe waves to a distant storm unless their direction of travel is within 30° of the wind in the storm area. It is also known that short period waves are more subject to dissipation than are long period waves, and therefore less likely to travel to great distances.

[11] R. T. Hermanson and R. S. Stump, Tech. Rept. H. E. 116–124, University of California (Berkeley) (unpublished).

and the remaining symbols have the same significance as above, except that ϑ replaces ψ throughout.

While the quantitative evaluation of this integral is difficult, its physical interpretation is clear. It has been seen that outside the storm area, there is, at each point, a dominantly radial direction of wave-travel; inside the storm, the wave components have not yet separated, and there is no similarly dominant direction. Each point is traversed by waves traveling in many directions; at the center, the only limitation on the sector from which the waves come is the function G. If the parameter $\mathfrak{L}$ is large, the sector will be relatively narrow, as described above; if $\mathfrak{L}$ is small the sector will be wider and, moreover, the period and wavelength will depend strongly on the direction of arrival. At points other than the geometric center of the storm, the function $S(\mathbf{r}\vartheta)$ will also tend to limit the sector from which the waves come, and to cause it to be asymmetric with respect to the wind direction. But, not until the point is well outside the storm area does S narrow the sector into the radial direction as described in the first paragraph of the preceding section.

The Eq. (55) can be used to obtain an estimate of the wave height at the center of the storm; here, from Eq. (45),

$$S=(\pi/2)^{\frac{1}{2}}P^2D$$

and hence

$$H^2=\langle h^2\rangle=4(\pi/2)^{\frac{1}{2}}P^2D\int G^2d\vartheta,$$

provided the radical in Eq. (55) is ignored. The integral can be evaluated graphically; for $\mathfrak{L}=1$, its value is about 0.4, so that finally

$$H^2=2P^2D/L \quad \text{at} \quad r=0.$$

Using the data for the storm of January 17 and 18, 1945, we find that $2H=4.2$ m. The highest waves of the storm should be somewhat greater and occur down-wind from the center.

10. THE HORIZONTAL COMPONENT OF THE WIND STRESS ON THE SEA SURFACE

Since the sea surface is not everywhere horizontal, and since the wind pressure exerts a force perpendicular to the surface, there will be horizontal forces acting on the water. For simplicity, the mean value of these forces, per unit area of undisturbed surface, will be called the [mean] horizontal [component of the] wind stress—the bracketed words being omitted when no confusion can result. It will be shown that this quantity is not zero in the storm area; it is a horizontal vector, and will be shown to have the same direction as the wind. The unit inward normal to the sea surface has, to a sufficient approximation, the components

$$\partial h/\partial x, \quad \partial h/\partial y, \quad -1;$$

the horizontal wind pressure is therefore

$$\rho g\langle a\nabla h\rangle \text{ dynes/cm}^2. \tag{56}$$

To calculate this, the correlation $\langle ha'|0\rangle$ is first calculated:

$$\langle ha'|0\rangle=\int w(\mathbf{q})\{h_{\mathbf{q}}a_{\mathbf{q}}'|0\}d\mathbf{q}$$

$$=-2(2\pi)^3\Re\int\int\int\int ikA(\mathbf{k}\omega)A^*(\mathbf{k}'\omega)W(\mathbf{k}-\mathbf{k}')$$

$$\cdot\exp\{i[-\sigma(k-\kappa)+\mathbf{k}\cdot\mathbf{x}-\mathbf{k}'\cdot\mathbf{x}']\}d\mathbf{k}d\mathbf{k}'d\omega d\sigma.$$

Proceeding as before, this is seen to be approximately

$$\langle ha'|0\rangle=-2\Re\int\int\int im\Psi(\mathbf{m}\omega)w(\mathbf{r}-\tfrac{1}{2}\sigma\mathbf{m}_1)$$

$$\cdot\exp\{i[-\sigma(m-\kappa)+\mathbf{m}\cdot\xi]\}d\mathbf{m}d\omega d\sigma,$$

so that, neglecting terms in ∇w as small,

$$\langle a\nabla h\rangle=z\int\int\mathbf{m}m\Psi(\mathbf{m}\omega)K(\mathbf{r},\mathbf{m},\kappa)d\mathbf{m}d\omega \tag{57}$$

where

$$K(\mathbf{r},\mathbf{m},\kappa)=\int_0^\infty w(\mathbf{r}-\tfrac{1}{2}\sigma\mathbf{m}_1)\cos[\sigma(m-\kappa)]d\sigma. \tag{58}$$

Now, it follows from the properties of w that $K\to 0$ for $|m-\kappa|\to\infty$ and has a sharp peak at $m=\kappa$; therefore, as before, m may be replaced by κ everywhere except in K. The integration over m can then be performed, approximately, with the aid of the Fourier theorem, resulting in

$$\langle a\nabla h\rangle=2(2\pi)^4w(\mathbf{r})\int\int\mathbf{m}_1\kappa^3\Phi(\omega\vartheta)d\vartheta d\omega. \tag{59}$$

Thus, the horizontal wind stress is at every point proportional to $w(\mathbf{r})=\langle a^2\rangle$, the mean square total wind pressure. The integration over ω, in Eq. (59), can be performed as before, and the result is

$$\langle a(\partial h/\partial x)\rangle=[4w(r)/L]$$

$$\times\int_{-\pi/2}^{\pi/2}\{G^2\cos\vartheta/[1+(16\cos^2\vartheta/\mathfrak{T}^2]^{\frac{1}{2}}d\vartheta, \tag{60}$$

$$\langle a(\partial h/\partial y)\rangle=0.$$

The integral in Eq. (60) may be evaluated numerically; for $\mathfrak{L}=1$, it is about 0.3. Hence

$$\langle a(\partial h/\partial x)\rangle=1.3w(\mathbf{r})/L;$$

using the same data as before, we find that, at the center of the storm,

$$\rho g\langle a(\partial h/\partial x)\rangle=0.5 \text{ dynes/cm}^2.$$

This may be compared with

$$2.6\times 10^{-3}\rho_a U^2=20 \text{ dynes/cm}^2,$$

whlch is the accepted value[12] for the tangential stress. The two differ by more than an order of magnitude, so that the horizontal wind stress cannot be called upon to explain those empirical relationships that seem to require the postulate of a tangential stress. Even if one postulates that the actual wind contains many small centers of pressure, that do not contribute appreciably to the formation of long period waves, it is doubtful whether the horizontal wind stress would be increased by a factor of 40.

11. CONCLUSIONS

The theory here developed appears to account for a considerable fraction of the observed phenomena, but is unable to account quantitatively for the observed height of the waves. Before speculating about the reason for this, one other phenomenon, which the theory does not clearly explain, should be mentioned.

It is generally believed that there are changes in the spectrum of the waves with position. In the decay area, this is theoretically impossible, except as a result of selective attenuation of the energy in the different frequency regions. However, since, in the present theory the energy is concentrated in a relatively narrow frequency band, it seems very improbable that such an explanation is tenable. Should the existence of a change of wave period in the decay area be established beyond doubt, it would be extremely difficult to construct any theory to account for it.

Inside the storm area, the dependence of the fetch integral, $S(\mathbf{r}, \vartheta)$, on position implies a variation of the spectrum of the waves with position. There is thus a general similarity between theory and observation. It is difficult to believe that this is a quantitative identity, however. It is possible that selective attenuation (breaking of shorter waves) must be invoked, or even that the empirical analysis of the data is in error at this point.

Turning now to the basic question of the adequacy of the mechanism assumed for the purposes of this calculation, the value of P required for the generation of surface waves of the observed heights is possibly 10 times greater than the actual value of this quantity.

Moreover, in laboratory experiments,[13] wind waves have been generated under conditions that preclude the possibility of this mechanism. These laboratory waves were highly rotational, as is shown by the strong surface current and shear that were associated with them. Their major cause was undoubtedly a tangential wind-stress, rather than a normal pressure—not even a sheltering effect would account for the surface currents, although such an effect may have been contributory to the growth of the waves.

The interpretation of such experiments therefore requires the construction of a theory of forced, rotational waves, which will be considerably different than the one developed above. It is not certain that this is also necessary for the interpretation of ocean waves. The question is this: is the ratio (tangential stress: normal stress) independent of wavelength and the other parameters that are different in the laboratory than in the open? The answer is not obvious, nor are all the relevant parameters known.

It does appear certain that the normal wind pressure is not the only mechanism by which energy is transferred from the air to the water. Apart from the tangential stresses, one other mechanism suggests itself. This is the one that is responsible for the well-known Helmholtz instability.[14] While the relation of this effect to observed phenomena is in considerable doubt, and certainly is not simple, the effect itself is scarcely to be questioned. Apart from the question of the quantitative adequacy of Helmholtz's equations, they show that the kinetic energy of the wind can become available to the growing water wave even in the absence of tangential stresses. This source of energy has not been included in the present calculations, but may well be important.

ACKNOWLEDGMENT

This paper has had the benefit of discussion by a number of people. Several erroneous conclusions have consequently been eliminated, which would not otherwise have been detected; however, the author alone is responsible for any that remain. He is especially indebted to R. S. Arthur, G. C. Ewing, L. N. Liebermann, and W. H. Munk, for ideas and material that have been included in the text.

[12] See reference 1, p. 11.

[13] J. W. Johnson and E. K. Rice, Trans. Am. Geophys. Union 33, 845 (1952).

[14] See Reference 4, pp. 109, 373. A summary of later work is contained in the article by W. H. Munk, J. Marine Research (Sears Foundation) 6, 203 (1947).

JOURNAL OF APPLIED PHYSICS VOLUME 24, NUMBER 12 DECEMBER, 1953

The Electron Microscopy of Photographic Grains. Specimen Preparation Techniques and Applications*

F. A. HAMM AND J. J. COMER
General Aniline and Film Corporation, Central Research Laboratory, Easton, Pennsylvania

(Received June 26, 1953)

Several electron microscopical specimen preparation techniques are described, including two replica techniques. The most important specimens utilize the thin film of the silver-gelatin complex which exists as a tightly fitting skin around the photographic grains. This relatively inert and insoluble complex is referred to as the combined envelope; a study of this structure is given.

Latent image centers are enlarged in several ways so as to be readily resolvable in the electron microscope. After this partial development the matrix or intergrain gelatin is removed and the grains are fixed. The final specimen consists of developed centers retained by the combined envelope.

Applications of the replica technique to grain shape, size distribution, and growth nature of photolytic silver are given. Utilization of the combined envelope in conjunction with the special development techniques to provide information which substantiates independent sensitometric data is also demonstrated.

INTRODUCTION

NO one has yet reported the resolution of the latent image in a silver halide grain in a photographic emulsion. The electron microscope has however been used to study the effects of exposure and development on silver halide grains. Ardenne[1] was perhaps the first to demonstrate this approach. Since then others[2] have illustrated the effects of electron microscope exposure on the grain as well as the appearance of variously light exposed grains after specific types of development. However, direct, useful correlations between these observations and the mechanism of latent image formation are almost completely lacking. This is largely due to limitations inherent in the specimens.

It is the main purpose of this paper to describe several more useful electron microscope specimen preparations. The subsequent companion paper demonstrates the application of one particular technique to the study of latent image distribution with a dependence on the rate of energy dissipation during exposure and for different degrees of total exposure. Some attention is directed to present day theories on the mechanism of latent image formation.

Several types of photographic emulsions have been investigated. They are negative, high contrast, double coated, black and white emulsions, having a mean grain diameter (flat view) of about 0.75μ. They may be described more specifically as follows:

Type *A*—A fast, bromoiodide-ammonia emulsion of relatively high ratio of surface to internal sensitivity. The mean grain thickness is about 0.75μ.

Type *B*—Very similar to Type *A* except that it has a greater internal sensitivity.

Type *C*—A relatively slow bromoiodide-boiled emulsion whose grains are roughly one half as thick as those in Types *A* and *B*.

Type *D*—A pure bromide emulsion otherwise similar to Type *C*.

The grains are, of course, embedded in a matrix of gelatin comprising the emulsion which is supported by a cellulose ester film base.

An RCA Type EMU electron microscope was used. There has been no attempt to demonstrate high resolution. A 2-mil platinum limiting physical aperture or a combination of brass projector apertures was used to improve the gross contrast.

SPECIMEN PREPARATION AND EVALUATION OF ELECTRON MICROGRAPHS

Examination of Grains *Per Se*

The first requirement in the preparation of grains for direct examination in the electron microscope is the removal of the matrix or inter-grain gelatin. This is conveniently done by enzymatic hydrolysis. In practice the film strip, the ½-in.×2-in. standard sample, is immersed in a 0.2 percent Takamine[3] solution at room temperature for several hours or at 35°C for 20 minutes or less. The grains separate from the base and settle to the bottom of the centrifuge tube. The degraded gelatin is removed by centrifugation (2500 rpm), accompanied by washing. Five such treatments are adequate to remove all water soluble components.

An aqueous suspension of the grains is pipetted onto substrate coated specimen screens. After drying the specimen is ready for examination in the electron microscope. Figure 1 illustrates a specimen prepared from emulsion *B*. Extremely rapid photolysis occurs, and for grains normally used in black and white negative emulsions this complete photolysis imposes

* Presented in part at a meeting of the New York State Section of the American Physical Society, October 5, 1951, Rochester, New York, and at the Electron Microscope Society of America Meeting, November 6, 1952, Cleveland, Ohio.

[1] M. von Ardenne, Z. angew. Phot. Wiss. u. Tech. 2, 14 (1940).

[2] C. E. Hall, and A. L. Schoen, J. Opt. Soc. Am. 31, 281 (1941). R. Reed and A. Millard, Proc. Leeds Phil. Lit. Soc. Sci. Sect. 5, 81 (1948). H. Arens, Veröffentl. wiss. Photolab., AGFA 7, 253 (1951). A. Küster, Veröffentl. wiss. Photolab., AGFA 7, 268 (1951). G. Baroni and C. Castagnoli, Rend. ist. super sanita 13 (No. 4), 360–5 (1950).

[3] Takamine, a proteolytic enzyme, sold by the Takamine Laboratory, Inc., 195 Arlington Avenue, Clifton, New Jersey.

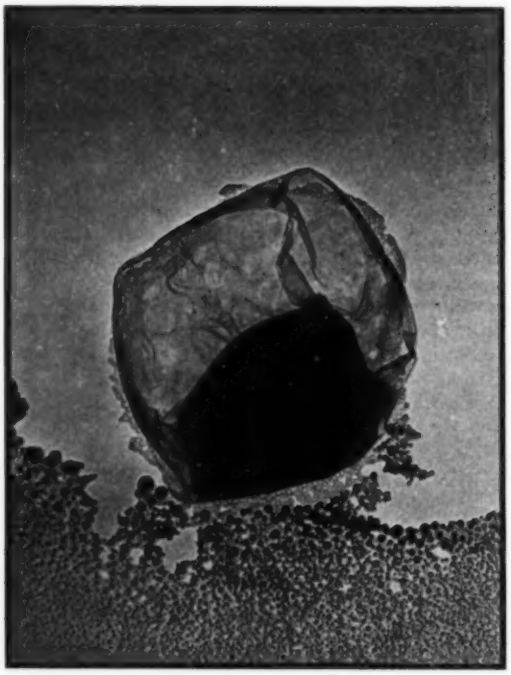

FIG. 1. 32 000×. A photographic grain completely photolyzed by direct illumination with the electron beam.

serious limitations on the benefits derivable from this type of specimen.

The energy of each illuminating electron is about 50 kev. The maximum intensity of illumination in the specimen plane is about 1 ampere per square centimeter for the standard instrument using a biased gun. Use of a photometer[4] permits a good estimation of the intensity of the illumination. A consideration of the energy involved in this photolysis is reserved for the Discussion Section.

The most significant structure illustrated in Fig. 1 is the transparent, partially overlapping, residual film retaining the large opaque mass of free silver remaining after the photolysis. The numerous small opaque specks probably consist entirely of free silver which condensed from the seething silver halide grain during the photolysis. The frothing is undoubtedly due to the rapid liberation of bromine gas which escapes in quantities too great to be absorbed by the thin silver gelatinate film surrounding the grain. This highly transparent film will henceforth be referred to as the "combined envelope." It appears in most of the subsequent electron micrographs, and it represents the framework upon which most of the electron microscopical results depend.

The evidence, to be described in detail in later sections of this paper, suggests that this combined envelope consists of gelatin chains coordinated with silver ions forming a rather insoluble and inert complex. Very brief mention of this structure had been made by some of the early workers;[2] in other publications the appearance of this combined envelope was illustrated by some of the micrographs but not referred to. Little or no importance had been attached to it. Based on the investigations carried out in this laboratory, it is conceivable that this combined envelope plays a fundamental role in the formation of the surface latent image.

The following details apply to all of the preparative techniques in this paper.

(1) Appreciable use of a darkroom safelight is required in only one operation, namely the pipetting of the grains onto the specimen screen or onto a support for subsequent replication. Total darkness may conveniently be used for the other manipulations. The brief exposure to the safelight at a distance of 15 inches has no significant actinic effect on the grains; this is important to the later discussions. Unless exposed deliberately to actinic illumination the specimens will be referred to as unexposed.

(2) Doubly distilled water is used at all times. This is necessary to eliminate specimen contamination that might be introduced by the finely divided solids normally found in tap water.

(3) All treatments such as enzyme hydrolysis, selective oxidation, grain development, washing, etc., are applied to ½-in. ×2-in. strips of film which are immersed in the particular solution in 13-cc capacity centrifuge tubes. Four samples are prepared during a preparation. Centrifugation is used to separate the grains from the aqueous medium. Variations in the enzyme treatment are possible. If the enzyme solution is several weeks old an hour at elevated temperatures may be required. Bacterial growth increases with the age of the solution; filtration through a glass sintered funnel is then required before use.

(4) Stainless steel (200-mesh) specimen screens are used because the copper or nickel grids normally used are corroded by the photographic fixer solutions.

The removal of the matrix gelatin by means of the enzyme treatment with five subsequent washings is basic to most of the specimen preparations described in this paper. The hydrolyzed gelatin consists of shorter chains which are readily soluble in water. Modifications of the enzyme treatment are necessary, depending upon the nature of the sample. In a few cases the matrix gelatin was removed with warm water. These preparations aid in demonstrating that the combined envelope does not inadvertently form as a result of using the enzyme.

One Step Silica Replicas

Because a replica prepared by evaporation usually involves the use of a luminescent hot wire filament, it is not possible to make such a replica without exposing the grains to strong actinic illumination. Primarily for this reason, this replica technique is not useful for studying latent image distribution resulting from controlled exposures of practical interest. Furthermore, only the surface of the grains may be studied with this technique. In general, replica specimens are most useful in determining size distribution and morphology of grains smaller than the useful limit of light microscopical resolution. Special sensitometric characteristics of interest in regard to their rapid print out effect (photolysis) may also be studied in this way. One of several techniques is briefly described as follows:

[4] F. A. Hamm, Rev. Sci. Instr. 22, 895–898 (1951).

The enzymatic degradation of the matrix gelatin is carried out as described earlier. After the last centrifugation to remove the gelatin degradation products the supernatant wash water is removed by means of a pipette, and the concentrate of photographic grains is spread over a glass microscope slide. After air-drying, the grains are scraped into a test tube containing low boiling petroleum ether; red safelight conditions may be used if the exposure is to be limited to the evaporation cycle only. Thorough agitation yields a temporary suspension of the grains which are then pipetted onto a polystyrene coated glass slide, producing a uniformly dispersed specimen. This specimen is then replicated with silicon dioxide or silicon monoxide using customary high vacuum techniques. Subsequent shadowing with metals adds contrast and permits the determination of grain thickness. For reasons not well understood the use of petroleum ether prevents undesirable clumping of the grains.

The combination of shadowed replica plus the grains is then floated off in benzene after scoring to give one-eighth inch squares, transferred to a mixture of benzene and ethylene dichloride to remove all traces of polystyrene, and finally picked up on electron microscope specimen screens. After air drying, the grains are dissolved away from the shadowed replica by immersion in a commercial photographic fixer (Ansco 201) for 15 minutes. Thorough washing is accomplished by passing the specimens through five changes of doubly distilled water. After drying, the specimen is ready for examination in the electron microscope. Figure 2 is a typical electron micrograph of this type of specimen prepared from emulsion type *D*; Fig. 3 illustrates a specimen prepared from emulsion *C*.

The opaque areas (see arrows) are photolytic silver formed during the evaporation of the silica. Because these areas do not cast shadows, this metallic silver must have grown inwardly through the silver halide grain. This internal growth of photolytic silver has also been demonstrated by two step replicas; the photolytic silver in this case had formed over a five hour period during exposure to diffuse room light. A similar growth is therefore probable for latent image silver during practical exposures. This aspect is of interest because it is commonly believed that surface latent image projects outwardly from the grain.

FIG. 2. 19 200×. One step silicon monoxide replica of photographic grains. Shadowed on air side with chromium at 20°. Emulsion *D*.

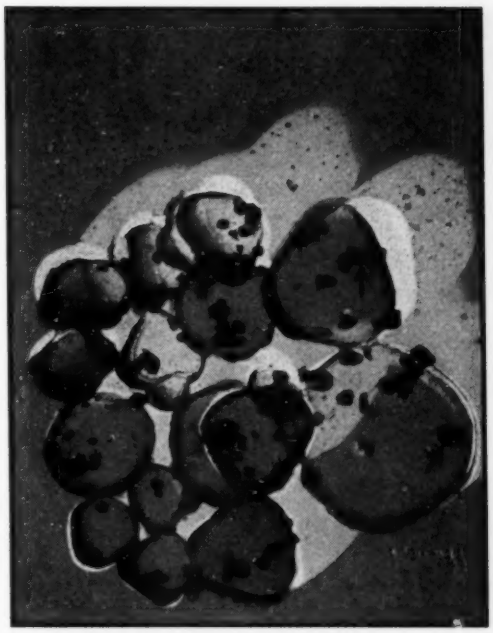

FIG. 3. 12 800×. Same as Fig. 2. Emulsion *C*.

Figures 2 and 3 should be compared in several respects. Emulsion *D* consists of well defined severely flattened octahedra supporting very tiny similarly shaped crystals. (These small crystals are rather poorly resolved at the low magnification in Fig. 2.) The small octahedra are very probably individual silver halide crystals and not lattice imperfections. Emulsion *C* on the other hand consists of well rounded octahedra containing virtually no tiny crystals. The significant difference in the preparation of these emulsions is their iodide content.

If carefully controlled specimen preparations are used, this replica technique is useful for illustrating differences in the tendency for grain clumping.

Two Step Replicas

The value of this technique lies in the avoidance of exposing the grains to actinic illumination, normally encountered during the preparation of the one step evaporated replicas. Thus, the nature of the grain surface, after a predetermined exposure, may be studied in this way. The technique is described as follows:

A rather thick aqueous slurry of the emulsion, removed from the film base by gently scraping in warm (50°C) water, is drawn out on a microscope slide as a thin coating. This is conveniently done by drawing a glass microscope slide over the surface of another slide on which the photographic emulsion had been deposited. The matrix gelatin is removed as before by placing the preparation in an enzyme solution. After drying the grains were

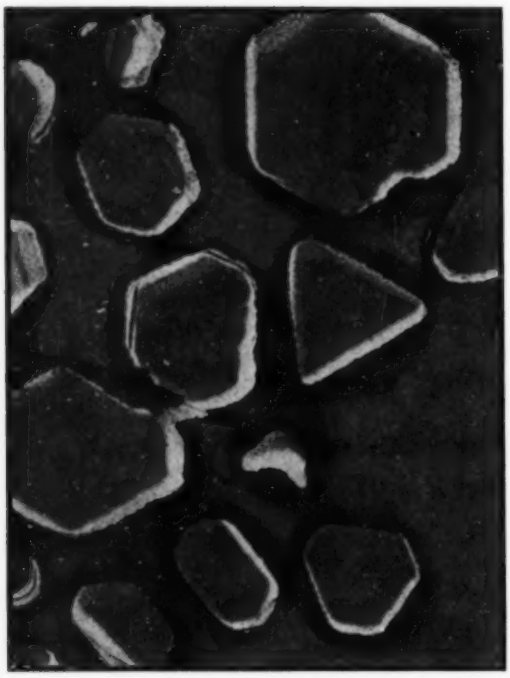

FIG. 4. 20 800×. Two step silica replica of photographic grains. Unshadowed. Note the combined envelope (see arrow).

coated with a 10 percent solution of polystyrene in benzene. This forms the first or negative replica, which is readily mechanically stripped from the glass slide, especially after refrigeration (*ca* 4°C) for a few hours (light tight box may be required). Most of the grains are retained by the negative replica. These grains are dissolved by the usual 15-minute fixation, followed by washing as before. Subsequent manipulation can, of course, be carried out in room light. The specimen at this point is a thin negative replica resin film; the manipulations are easily accomplished by means of forceps and a square of 100-mesh stainless steel screen of size commensurate with the specimen. The positive replica is prepared in the conventional way by evaporating silica or silicon monoxide at normal incidence to the contact side of the polystyrene replica. Shadowing with evaporated metals may also be desirable. Immersion of the preparation in benzene or other suitable solvents facilitates removal of the negative replica; these straightforward procedures will not be further described because they are now well known.

Figure 4 illustrates this two step replica specimen; the grains are from emulsion type *D*. Note the retention of the combined envelope; see arrows. The combined envelope exhibits a rather well defined octahedral shape around the outline in silica of the original grain. The larger outline of the combined gelatin stems from the fact that this film collapses and exists in essentially just two dimensions after dissolution of the grain. The light, highly transparent zone around the periphery of the grain outline is characteristic of this preparation technique. An unequivocal explanation is difficult although it is quite probably associated with the collapse of the combined envelope after the hypo treatment. The silica replica exhibits poor strength along the peripheral edges of the large top face, and often this portion of the replica moves in the electron beam. Photolytic silver on the surface of the grain is retained despite the several manipulations, and it appears on the final replica; the quantitativeness of this transfer is not known with certainty. The specimen illustrated in Fig. 4 had not been exposed to actinic light. Unlike the case for Figs. 2 and 3, no photolytic silver is to be expected in this case. Note that some of the combined envelopes are joined together. This is also illustrated in Figs. 4–8. This behavior is common.

Because the surface latent image during exposures of practical interest may in many cases grow inward through the grain, and because good quality replicas are possible only if the matrix gelatin is thoroughly removed, these replica techniques find only limited use. Perhaps the greatest deterrent to the value of any replica technique is the combined envelope which seems to interfere with the replication of fine surface detail.

The Silver Gelatinate Combined Envelope

Because of the limitations inherent in the examination of grains *per se*, or the replicas thereof, it soon became apparent that the best way to study any structure dispersed throughout the grain was to attempt to utilize the combined envelope, mentioned earlier and illustrated in Figs. 1 and 4. Subsequent investigations demonstrated that it was possible to put these combined envelopes to good advantage. In fact, the main theme of the companion paper and similar unpublished works is based on electron micrographs of these combined envelopes which are isolated after special "development" techniques.

In view of the preparations described earlier, the preparation of this type of specimen is given only briefly.

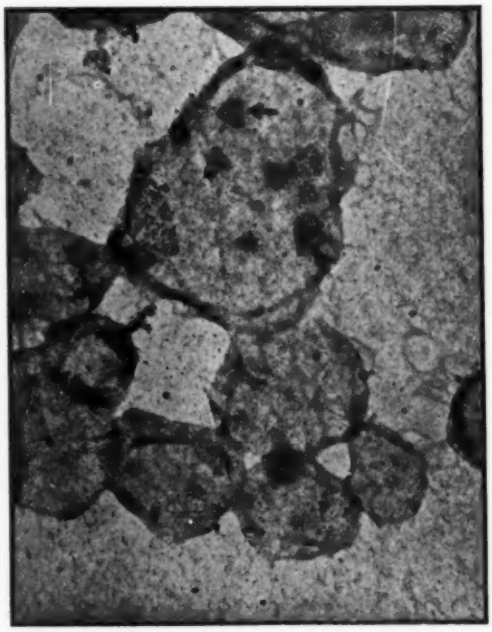

FIG. 5. 16 800×. Combined envelopes of emulsion *A*. Unexposed and undeveloped. Note the triangular regions.

The strip of film is immersed in a *freshly* prepared enzyme (0.2 percent Takamine) solution for about 15–20 minutes. After centrifugation, accompanied by washing, an aqueous suspension of the grains with their combined envelopes is pipetted onto substrate coated specimen screens. After fixation, washing, and drying, the specimen is ready for examination in the electron microscope. The rate of gelatin degradation may vary for different emulsions depending amongst other things on the type of gelatin. For this reason, as a matter of principle, it is desirable to stop the enzyme hydrolysis immediately after the emuslion separates from the base. Brief examination under the safelight serves as a guide for starting the washing.

Figure 5 illustrates a typical specimen of this type. The original emulsion exhibited a net fog density of 0.14 (four-minute development in Ansco Liquadol at 68°F). The small somewhat triangularly shaped areas

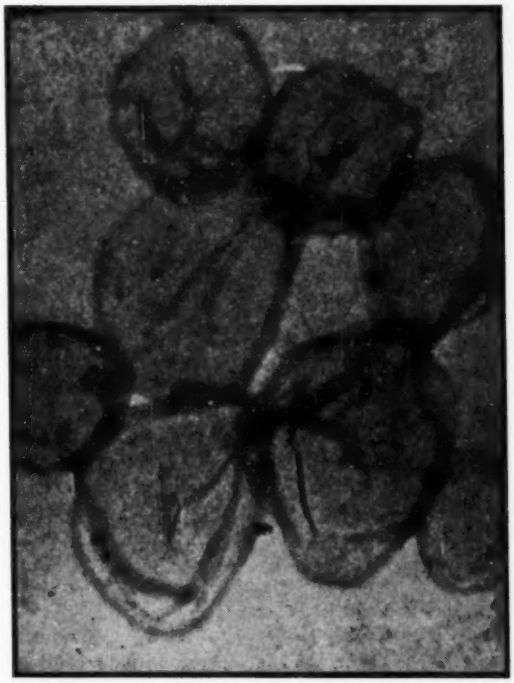

FIG. 6. 20 800×. Combined envelopes from emulsion type *A*. Matrix gelatin removed with warm water; grains fixed in 201. Unexposed and undeveloped.

within the combined envelopes very probably contain higher concentrations of silver, free and coordinated with the gelatin. Almost each of these areas contains one relatively large speck of silver. These specks are clearly visible on glossy prints at magnifications of about 50 000×. It will be later shown that latent image development often starts at these specks.

The existence of the combined envelope may be demonstrated in another way. The matrix gelatin may be removed by means of warm water rather than using the enzyme. In practice the film sample is immersed 1 hour in warm water that had been heated to 70°C outside of the darkroom. Warm water must be added occasionally to maintain the temperature. After this time the emulsion separates from the base. The subsequent manipulations including centrifugation, washing, pipetting the grains, etc., are as described before. Figure 6 illustrates such a specimen which had been fixed on the stainless steel grids in Ansco 201. The removal of the matrix gelatin is not as complete as

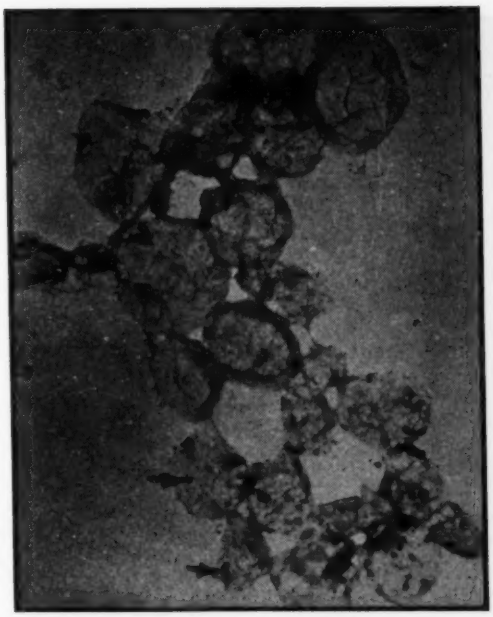

FIG. 7. 7200×. Mixed combined envelopes from grains type *A* exposed and type *B* unexposed. No development. Takamine digestion and fixation in 201. Note the photolytic silver retained by the combined envelopes.

FIG. 8. 19 200×. Combined envelopes from emulsion *C*, showing in a rather precise way the original grain morphology. Inadequate arrested organic development to produce a detectable amount of free silver.

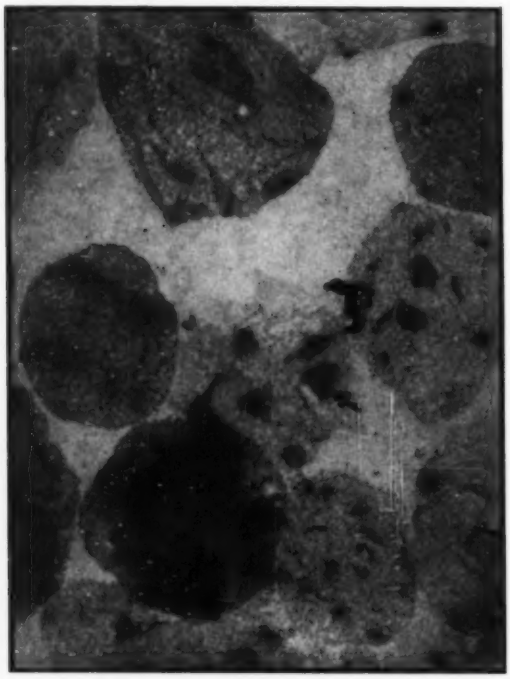

FIG. 9. 16 800×. Combined envelopes from emulsion type *A*. Matrix gelatin removed with warm water. Grains fixed in two solution alkaline fixer. Unexposed and undeveloped.

when the enzyme is used. The combined envelopes are sometimes difficult to see because of the undissolved gelatin.

The appearance of the combined envelopes under these conditions of specimen preparation shows that the enzymatic hydrolysis with Takamine is not responsible for the formation of the silver gelatinate combined envelope. The proteolytic enzymatic hydrolysis gives rise to peptones, proteoses, and amino acids all having greater silver ion combining capacity than the gelatin molecule. Thus, it is conceivable that these reactive gelatin derivatives might react with the surface silver ions in the grain lattice. Although this reaction is not precluded, the enzyme is *not* a prerequisite to the formation of the combined envelopes. Furthermore the use of warm water during this specimen preparation does not cause the formation of the silver gelatinate complex because any such thermal effects would have already been manifest during the emulsion manufacture.

Inasmuch as fixation of the grains represents an important phase of the electron microscope specimen preparation, cognizance of possible effects on the appearance of the combined envelope had to be taken. Also the effect of *p*H during fixation on the nature of the silver gelatinate was of some interest, especially in connection with the interpretation of the developed specimens to be described later.

In this regard Carroll and Hubbard[5] many years ago discussed the effects of sodium thiosulfate during fixation. They pointed out two important aspects: first, the solubility of latent image silver is lower on the alkaline side; second, soluble, slightly dissociated silver thiosulfates decompose to produce some insoluble silver sulfide. This second effect may be minimized by keeping the ratio of thiosulfate ion to silver ion very high; the temperature during fixation should be below room temperature.

The following two alkaline fixer solutions were used in these investigations:

(1) *p*H=7.85 This is a 30 percent $Na_2S_2O_3 \cdot 5H_2O$ solution containing 0.2 g Na_2SO_3 per 500 cc.

(2) This alkaline fixer is composed of two solutions:

A. *p*H=10.5 300 g $Na_2S_2O_3 \cdot 5H_2O$, 5 g Na_2SO_3, 1 g Na_2CO_3 per 1000 cc water.

B. *p*H=10.9 50 g $Na_2S_2O_3 \cdot 5H_2O$, 5 g Na_2SO_3, 1 g Na_2CO_3 per 1000 cc water.

(Immersion time is 10 minutes in each solution; the temperature of the solutions was never more than 20°C, and it was usually about 10°C.)

It should be noted that no hardening salts (i.e., potassium chrome alum) are present in these alkaline fixing solutions.

All combinations of matrix gelatin removal (enzyme *vs* warm water) and fixation (commercial Ansco 201 with hardeners *vs* alkaline) have been used for electron microscope specimen preparations. Combined envelopes are always observed. Some differences in the structure of the combined envelopes are exhibited, but it is not important in this paper to elaborate on this aspect. The salient results of this combined envelope study, applied in particular to unexposed and undeveloped emulsion type *A* may be summarized as follows:

(1) When alkaline fixation, *p*H=7.85 or *p*H=10.5 (two solution), is used, a combined envelope exhibiting a continuum of many small highly scattering specks is observed. Within these combined envelopes regions of greater opacity are found; these smaller areas are often triangularly shaped. Within these somewhat opaque areas are often found large (several hundred Angstroms) completely opaque specks.

These small rather opaque regions with the large specks are observed regardless of the method for fixation; see Figs. 6 and 9.

(2) When the Ansco 201 (*p*H=4.5) fixer is used, most of the combined envelopes do not appear highly speckled; they do not exhibit the large number of very small highly electron scattering specks. However, the small regions of greater opacity consisting of relatively large opaque specks are often present. These regions within the envelope are again often triangularly shaped; each region again contains a large completely opaque speck several hundred Angstroms in size.

(3) For reasons not understood, when the commercial acid fixer (201) is used, the removal of the matrix gelatin by means of enzyme is conducive to the formation of the relatively opaque (often triangular) regions. On the other hand, Fig. 6 represents the case when warm water is used. The small relatively opaque regions are scarce; this particular micrograph shows none.

(4) There is little danger of hydrolyzing the combined envelope too far when the matrix gelatin is removed with water at 60°C. On the other hand, the enzymatic degradation may shred this

[5] B. H. Carroll, and D. Hubbard, J. Research Natl. Bur. Standards 8, 711 (1932).

envelope if care is not taken to remove the film strip immediately after the emulsion begins to separate from the film base.

Comparison of Figs. 6 and 9 demonstrates the major differences in the structure of the combined envelope resulting from the type of fixation. Note that in the latter micrograph the envelope exhibits a speckled continuum of very finely divided scattering material unlike the structure illustrated in Fig. 6. The arrow in Fig. 9 designates the somewhat triangularly shaped regions of greater opacity.

Specific areas of high electron scattering power undoubtedly represent regions of high silver ion concentration. The functional groups in the gelatin molecule that contain nitrogen atoms probably are largely responsible for the coordination with the silver ion. These basic nitrogen atoms would be expected to exhibit greater silver ion binding capacity on the alkaline side of the isoelectric point (pH$\cong$5). The appearance of the combined envelope with respect to the pH of the fixation bath may, therefore, be qualitatively explained in this way.

The preparation of the combined envelope for electron microscopical examination may be carried out in still another way. In this technique the fixation *precedes* the enzyme treatment. The method is described as follows:

A ½-in.×2-in. strip of film is immersed in warm (60°C) water for about 1 hour. After removing the film base (with forceps), the emulsion is centrifuged and the supernatant discarded. A drop of an aqueous suspension is pipetted onto substrate coated specimen grids. After the grains have settled the supernatant is withdrawn with a micropipette (red safelight). Some of the matrix gelatin is still present at this point. The grids are then immersed in Ansco 201 for 15 minutes for removal of the silver halide grains. Washing is done by transferring the specimen through several changes of water (Petri dish). The room lights may be turned on at this point. The remaining matrix gelatin is now removed by immersing specimen grids in fresh 0.2 percent Takamine for 5 to 10 minutes, slightly warmed (30–35° C). After washing out the degraded gelatin and air drying, the specimen is ready for examination.

Figure 10 illustrates such a specimen prepared from emulsion *A*. The combined envelopes are somewhat similar to those illustrated in Fig. 9. The small strongly electron scattering regions (see arrow in Fig. 10) usually containing a single, large speck are very characteristic of this type of specimen. It is worth noting that this electron microscopical specimen preparation technique is, in a sense, the antithesis of the original preparation of the photographic emulsion. That is, the grains were initially precipitated in the presence of some gelatin, whereas in this specimen preparation the silver halide is dissolved with sodium thiosulfate in the presence of some of the matrix gelatin.

Although not imperative for retention of the partially developed latent image, it is highly desirable to use the standard fixer with hardener.[6] When the potassium chrome alum is removed from the Ansco 201 formula, poorly formed combined envelopes are produced.

Although this type of preparation (Fig. 10) served as a corollary check in the study of the combined envelope, this technique is not normally used. All the remaining micrographs and discussions pertaining thereto refer to specimen preparations in which the removal of matrix gelatin always precedes the fixation.

These several different silver gelatinate specimens are of interest because the existence of the combined envelopes in *immediate* contact with the grain is demonstrated in this way.

Several other points in regard to the combined envelope are worth noting. First, exposure to visible light or high-energy radiation (x-rays, α particles, β rays) makes the silver gelatinate in the combined envelope slightly less readily attacked by enzymes. Thus, a "tanning" action similar to the effects of oxidizing agents (potassium ferricyanide, chromic acid, bromine water) occurs. The enzymatic digestion for unexposed systems may require roughly 15 minutes at 35°C, whereas some exposed emulsions may require up to 30 minutes. Second, if selective oxidation[7] prior to development is used to study, for example, the chemical nature of the developed centers, correspondingly longer enzyme treatment is necessary to hydrolyze the matrix gelatin. The free combined envelopes are more opaque in this case, indicating the presence of more strongly

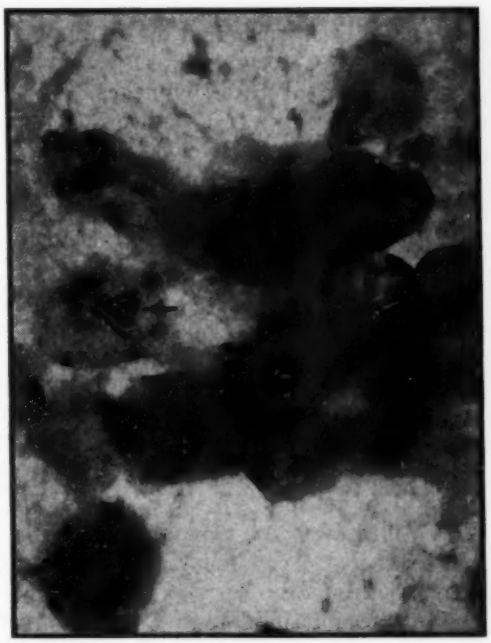

FIG. 10. 15 200×. Combined envelopes from emulsion type *A*. Grains first fixed in 201 then matrix gelatin was removed with enzyme. Unexposed and undeveloped.

[6] So-called hardening agents such as potassium chrome alum are usually used in commercial fixers or "hypos" so as to harden the gelatin in the emulsion prior to washing and drying; scratches and dust contamination are lessened.

[7] Lowe, Jones, and Roberts, "Some chemical factors in emulsion sensitivity," in *Fundamental Mechanisms of Photographic Sensitivity* (Butterworths Scientific Publications, 1951), p. 112; G. W. W. Stevens, "Destruction of internal image by reagents applied at the grain surface," *ibid.*, p. 227.

electron scattering elements such as iron or chromium which presumably have also coordinated with the gelatin molecules. If a 0.25-percent chromic-acid solution is used as a selective oxidant prior to development, about one hour at 35°C is required to permit washing out of the degraded matrix gelatin.

A third point important in insuring high-quality electron microscope specimens has to do with the activity of the enzyme solution. The previous discussion pertained to freshly prepared 0.2-percent Takamine solutions. Equally good specimens may be prepared by using a solution two or three weeks old.

Development of Grains

It is generally assumed[8] that the latent image exists as small specks of metallic silver. Webb[9] in his study of low intensity reciprocity law failure has shown that the stable subimage probably consists of 2 silver atoms, whereas a developable latent image speck may contain as few as 8 silver atoms. This latent image center therefore represents only two unit cells, which are roughly 4A on edge (face centered cubic). For the sake of argument it is assumed that a latent image center contains as many as 108 silver atoms, from the grouping of the 27 unit cells it is apparent that this structure is of the same order of magnitude as the limit of resolution of the electron microscope. For exposures to charged particles, x-rays, or instantaneous light exposures of practical interest, the latent image is probably more highly dispersed than suggested by the nucleus of 108 silver atoms. It is not surprising, therefore, that the resolution of the latent image by means of the electron microscope still presents a real challenge. In this regard, utilization of the combined envelope affords an excellent means for retaining the latent image, especially the surface image. As a matter of fact, this approach is probably the only present method that holds much promise; furthermore, the exposure conditions should be such that the *deepest* electron traps serve as loci for the formation of relatively large latent image nuclei. More will be said about this in the companion paper.

It is the main purpose of this section to describe how the latent image may be modified so that it is readily resolvable. The retention of this enlarged image by the combined envelope is of vital concern in this electron microscopical approach.

Figure 7 illustrates the retention of photolytic or print out silver by the combined envelopes. The type *A* emulsion had been exposed to a 15-watt fluorescent bulb at 15 inches for 10 minutes. The type *B* emulsion was not exposed. No development of any kind was used. The electron microscope specimens were prepared using Takamine digestion and fixation in 201. The grains had been mixed prior to fixation. The combined envelopes in the upper half of the micrograph (Fig. 7) represent the unexposed grains. The photolytic silver (see arrows) in the lower portion of the figure represents emulsion *A* which had been "tagged" by exposure. When only emulsion *B* is exposed, then only these combined envelopes exhibit photolytic silver.

Attention is now directed to the more important aspect of developing the latent image so that the electron microscopical approach becomes useful.

(1) *"Arrested Organic" Development*

Black and white photographic emulsions are normally developed with solutions that almost invariably contain an organic reducing agent such as metol or hydroquinone. All the silver ions in a grain rendered "developable" by exposure deposit as metallic silver to form an opaque mass. Electron micrographs illustrated by the early workers[1,2] in this field demonstrated this development phenomenon. An average grain 1μ in diameter would deposit roughly 10^{12} atoms of silver. It is immediately obvious that a grain completely developed appears as a large opaque mass in the electron microscope. However, keeping in mind theories on the mechanism of development,[10] it is logical to assume that an observation of the *very early* stages of development should demonstrate at least a part of the developable latent image. Thus, the exposed grains are developed in greatly diluted developers for short periods of time, or in normal strength developers for even shorter periods of time. The choice of the phase "arrested organic" development is therefore valid. By judicious choice of developments it has been possible to prepare a series of micrographs which illustrates in time sequence the development of a latent image center.

A variety of specific modifications in technique is not given here. Rather it is more important to discuss the salient features of this approach in general terms. First, an abbreviated development technique would be expected to enlarge only the largest developable centers, and more important, only those centers largely confined to the surface of the grain. Second, by judiciously removing the surface latent image with oxidizing agents, and incorporating silver halide "solvents" in the organic developer, a combination of controlled experiments can by used to distinguish between the surface and internal image. The use of sodium thiosulfate during fixation or as a "solvent" for silver bromide in developing the internal latent image introduces another aspect which must be considered in any study of finely divided silver on the scale of interest here. In this regard the solubility of finely divided atomic silver in sodium thiosulfate and the possible deposition of silver sulfide has already been mentioned.[5] It suffices to say that the electron microscopical observations of the structural details must be made with caution. Wherever possible the electron microscopical results should be correlated with independent sensito-

[8] See N. F. Mott, reference 7, "Introduction." This book is also known in the photographic field as the "Bristol Report."
[9] J. H. Webb, J. Opt. Soc. Am. 40, 3 (1950).
[10] C. E. K. Mees, *The Theory of the Photographic Process* (Macmillan Company, New York, 1945), Chap. VIII.

metric data. For example the distribution of the latent images observed in the electron microscope has, in this laboratory, been correlated with the measured densities (for a given exposure) for total, surface, and internal development.

The general procedure for preparing electron microscope specimens using the arrested organic development technique is briefly described as follows:

A ½-in.×2-in. strip of film is immersed in the developer for specific conditions of time, temperature, and concentration. The development is arrested by removing the sample (with forceps) and placing it in a short stop. After washing with five changes of water, the film strip is immersed in the enzyme solution. Again as soon as the emulsion separates from the film base the base is removed and the emulsion is washed; the grains are concentrated by centrifugation as before. Subsequent manipulation including pipetting the grains onto specimen grids and fixation are carried out as described earlier.

Figure 8 illustrates a specimen (emulsion type *C*) developed for 45 seconds, at 68°F, in a commercial developer diluted 1:20. The emulsion had been exposed to 65-kv x-rays so as to yield maximum density ($D=3.0$) when normally developed in Liquadol for 3 minutes. This illustration serves two purposes. First the arrested organic development conditions were such that no evidence of latent image development is observed even though on the basis of the exposure some development had been anticipated. Less severely arrested organic development conditions were required to demonstrate the early stages of development. The second feature of this micrograph is that it illustrates the continuity and morphology of the combined envelopes after the enzyme treatment. The flattened octahedral shape of the photographic grains has been retained by the combined envelope, and Miller indices can be readily assigned to the crystal faces illustrated. The grains are lying on the $\overline{111}$ face. The thickness and morphological aspects of these combined envelopes vary for different types of photographic emulsions as would be expected. The rather exact retention of the original grain shape by the combined envelope is characteristic of emulsion type *C*. The illustration does show that the combined envelope exists as a tightly fitting "skin" around the grains. Note again that the combined envelopes for several grains are joined together.

Figure 11, on the other hand, does demonstrate the effectiveness of this arrested organic development technique; it also illustrates a typical distribution of grain sensitivities. One minute development in a metol-hydroquinone developer, diluted one to twenty, of a red light exposure of emulsion type *B* produced partially developed grains of extreme differences in sensitivity. Five grains show many small developed latent image centers. One grain is almost completely developed, indicating greater sensitivity, whereas another grain appears to have been insensitive by comparison.

The sequence of micrographs in Figs. 12–14 illustrates an application of this arrested organic development technique. A comparison of emulsion types *A* and *B* during successive stages of development is shown. The micrographs illustrate different grains of varying sensitivity exposed and developed under a given set of conditions. Figure 12(a) should be compared with Fig. 13(a), and 12(b) with 13(b). They may be interpreted as illustrating a given grain for each emulsion at stages subsequent to the start of development.

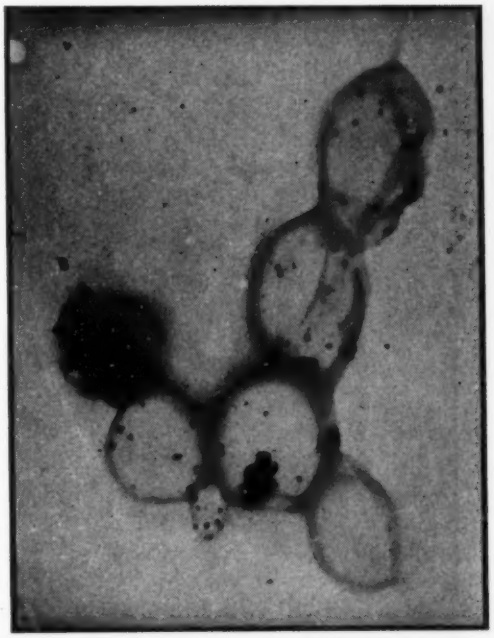

FIG. 11. 8800×. Combined envelopes from grains of emulsion *B* exhibiting different degrees of sensitivity. Arrested organic development of a tungsten exposure.

Figure 12 represents a two-minute exposure at fifteen inches to a 10-watt bulb through an Ansco A-4 red safelight filter. The development consisted of a 30-second immersion in the Ansco 30 formula diluted 1:80. Emulsion *A* was known to have a relatively high red sensitivity.

Figure 13 represents for emulsion *B* the same exposure and development except that the dilution factor was 1:20. This difference is inconsequential insofar as the comparison of these grains is concerned. The lesser dilution was necessitated by the lower red sensitivity.

Based on the distribution of the developed latent image centers the electron micrographs suggest that emulsion *A* has *fewer* but *deeper* electron traps than emulsion *B*. This is indeed substantiated by the reciprocity characteristics[11] of these two emulsions.

Figure 14(a) should be compared with Figs. 12(a) and (b). Similarly Fig. 14(b) represents a more or less final development stage subsequent to Figs. 13(a) and (b). The few deep traps in emulsion *A* produce shorter but thicker filaments of silver which eventually form a rather compact mass of silver. Emulsion *B* on the other

[11] The authors are indebted to the Ansco Laboratories for these and other sensitometric data.

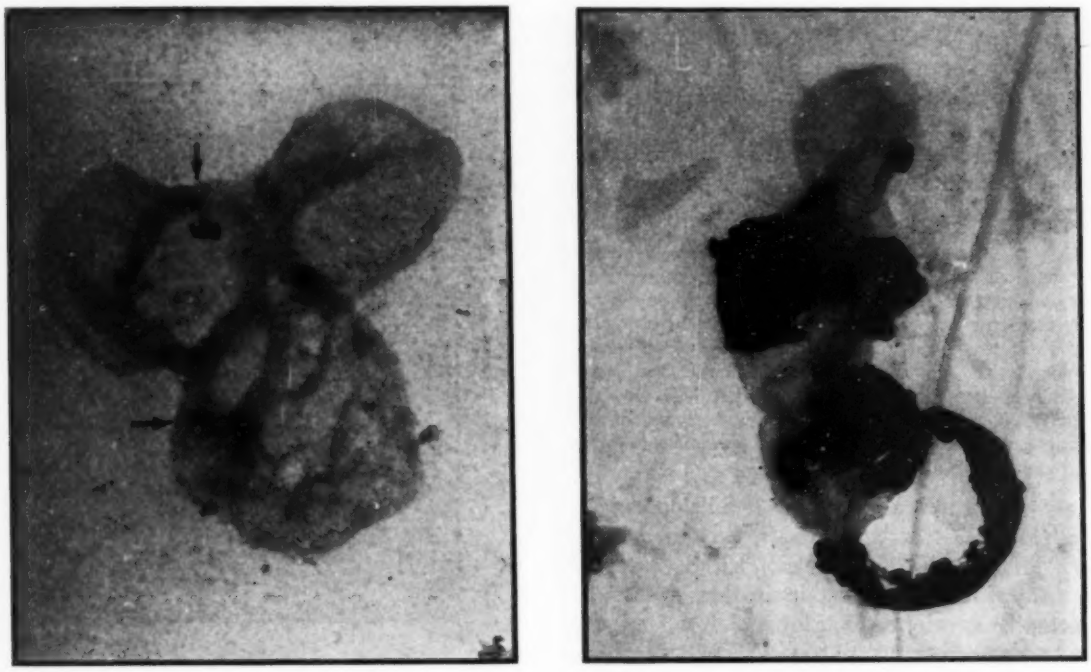

(a) 28 800× (b) 23 200×

FIG. 12. (Red light exposures—Emulsion *A*) (a) Very early stages of development. (b) A later stage.

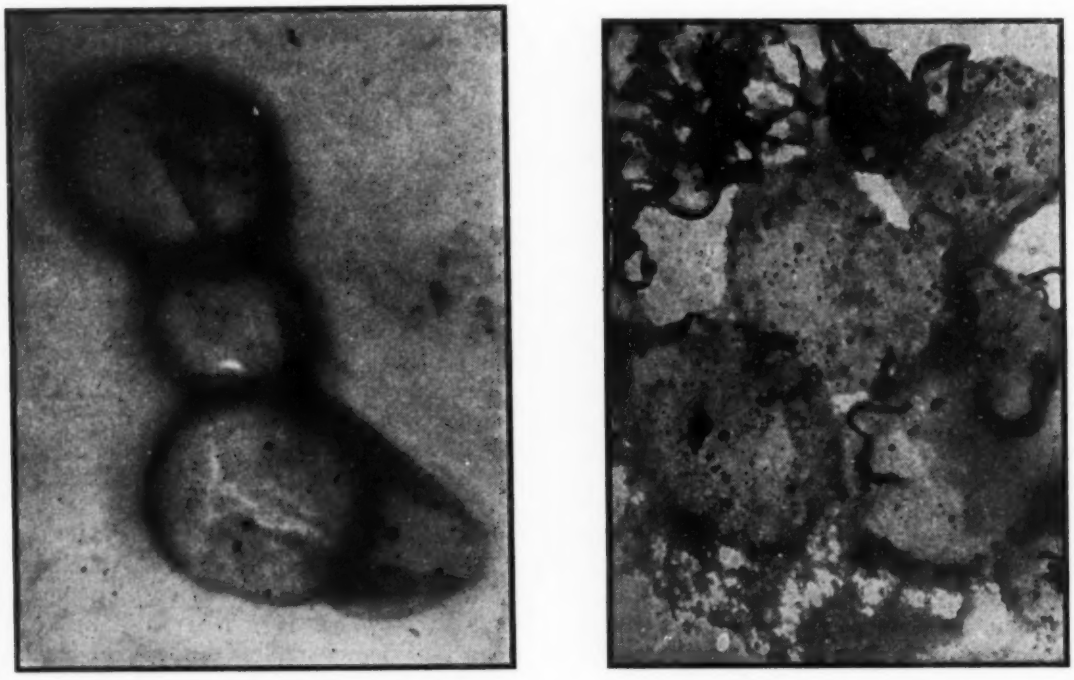

(a) 17 600× (b) 18 400×

FIG. 13. (Red light exposures—Emulsion *B*) (a) Very early stages of development. (b) A later stage.

hand gives rise to relatively long, thin threads of silver which finally produce a porous, spongy mass of silver. It is of course intended that these micrographs illustrate "average" fields in the specimen.

Sure comparisons of two or more photographic emulsions demand extremely careful specimen preparations. It is imperative that the arrested organic development of all specimens to be compared be carried out

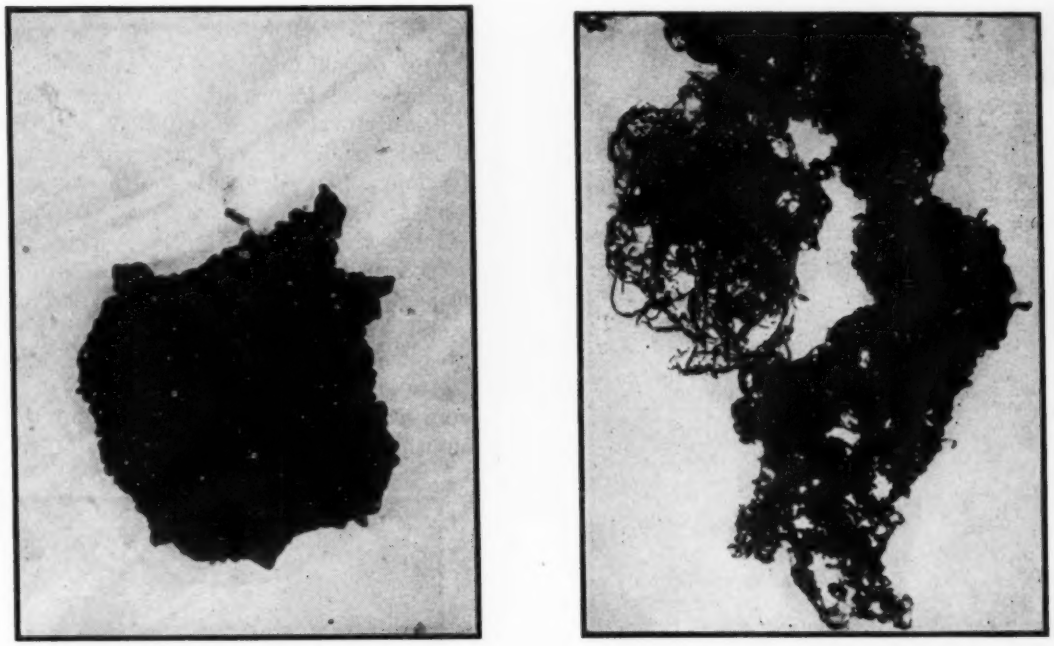

(a) 27 200× (b) 8800×

FIG. 14. (a) Emulsion *A*—development stage subsequent to that illustrated in Fig. 12b.
(b) Emulsion *B*—development stage subsequent to that illustrated in Fig. 13b.

simultaneously. Subtle differences in developer strength may exert significant differences in the development *stage.*

Mention of selective oxidation prior to development has already been made. The earlier publications[7] have been concerned with the chemical factors affecting photographic sensitivity, and with mechanisms for explaining the action of selective oxidants.

Of interest in these investigations was the application of the *selective oxidation* technique to serve as a convenient method for evaluating the amount of *internal latent image.* A typical group of electron micrographs is illustrated by Figs. 15–17. This study does not represent arrested development as previously defined; it is included here because it does represent different stages in development. Furthermore, the usefulness of the technique is demonstrated.

The specimen preparations consisted of a 10-minute treatment in 0.25 percent chromic acid, thorough washing, and then a 3 minute development in an internal developer. The sample is carefully washed (5 times) immediately after the oxidation treatment. The fourth washing gives a negative test for chromium; this test is sensitive for solutions of the order of 1×10^{-4} percent with respect to chromate ion. Similar tests are used when potassium ferricyanide is used as a selective oxidant. The subsequent enzyme treatment and general specimen manipulations are similar to those described earlier. The internal developer contains 8-grams hypo, 0.1-gram potassium iodide, and 4.0-grams sodium bromide (fog retarder) per liter of Ansco 125 commercial developer. The photographic emulsion used to prepare the specimen illustrated in Fig. 17 was type *B*; emulsion type *A* is illustrated in Figs. 15 and 16. Both emulsions had been simultaneously exposed to a red safelight under controlled conditions and the electron microscope specimens had been prepared simultaneously. The internally developed densities for emulsions *A* and *B* are 0.19 and 0.34, respectively; the relative amounts of developed silver illustrated by this group of micrographs is therefore not surprising.

Of greater interest is the fine detail illustrated in Figs. 15 and 16. The combined envelope in Fig. 15 illustrates only one slightly developed latent image center, indicated by the arrow. The general structure, especially the regions of high electron scattering, is very similar to that illustrated in Fig. 10. The photographic emulsions were of the same type, although as indicated in the captions the histories of the electron microscope specimens are distinctly different. Figure 16 illustrates a greater degree of development than does Fig. 15; the presence of a greater amount of internal image (note arrows) is indicated. Note the confinement of the developed silver within the somewhat triangularly shaped region. Figure 17 is at a significantly lower magnification than its two counterparts. This is the consequence of the growth of porous, spongy silver in emulsion *B.* Furthermore, the significantly larger amount of developed silver is the manifestation of the greater red light sensitivity; this average electron micrograph field corroborates the independent sensitometric data.

Although this arrested development technique is informative, it has several limitations. First, during the very earliest stages of development probably only the largest latent image centers are enlarged. Second, the enlargement of developable centers, especially those that are subsurface or internal, is undoubtedly dependent upon a diffusion process. The brief arrested organic

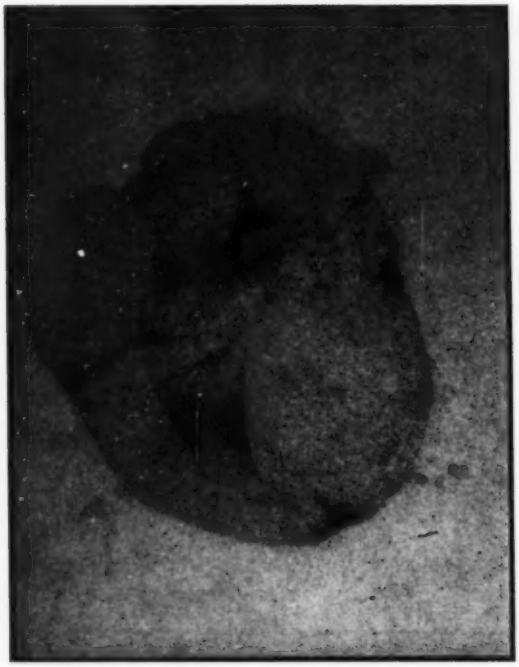

FIG. 15. 31 200×. Combined envelope (emulsion *A*). Grain had been surface oxidized then developed with internal developer. Compare with Fig. 10.

development procedure inherently leaves something to be desired in this connection. A slower, less rate dependent specimen preparation technique is described in the next section.

FIG. 16. 24 000×. Same specimen as shown in Fig. 15. Development had proceeded further presumably due to greater amount of latent image.

(2) *Gold Development*

The use of gold in photographic emulsions has taken on considerable importance in recent years. James[12] has critically evaluated the effect of gold treatment in the kinetics of development using hydroquinone types of developer. In general, his conclusions indicate that bathing an exposed emulsion in a solution of aurous ions increased the size of the latent image centers and, by a similar token, converted sublatent image into developable latent image centers. The end result is that this gold treatment presumably increases the rate of direct development, decreases the induction period, and certainly increases the emulsion speed.

From a somewhat different viewpoint the effect of aurous thiocyanates, incorporated in the silver halide

FIG. 17. 6400×. Combined envelopes (emulsion *B*) with a considerable amount of developed silver. Same specimen preparation as Figs. 15 and 16. Greater amount of silver is due to greater internal sensitivity.

emulsion *during* its preparation, on the photographic speed with a wavelength dependence has appeared in recent publications.[13,14,15]

Advantage of the prior art was taken in planning this electron microscopical preparation based on the

[12] T. H. James, J. Colloid Sci. 3, 447 (1948).
[13] F. W. H. Mueller, J. Opt. Soc. Am. 39, 494 (1949).
[14] H. Hoerlin, and F. W. H. Mueller, J. Opt. Soc. Am. 40, 246 (1950).
[15] N. Bjerrum and A. Kirschner, "Die Rhodanide des Goldes Und das Freie Rhodan mit einem Anhang uber das Goldchlorid," Kgl. Danske Videnskab. Selskab. Skrifter Naturwidenskab. Math. Afdel. 8, 1–76 (1918). This old but very exhaustive non-photographic study of a variety of thiocyanate complexes of gold may be of some interest to those readers concerned with photographic gold sensitization. It is not within the scope of this paper to interpret these electron microscopical results in the light of the information given in this reference.

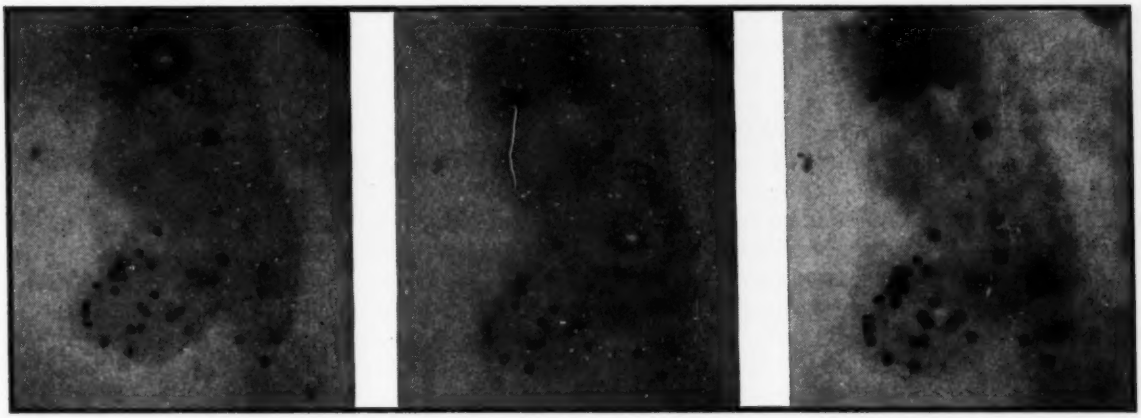

(a) (b) (c)

FIG. 18. 20 000X. (a) Reference field. (b) Same field after 10 minute treatment in 3 percent $K_3Fe(CN)_6$. (c) Same field after 10 minute treatment in 0.25 percent chromic acid.

enlargement of centers developed by the deposition of gold atoms. The gold developer solution used in this investigation is essentially the same as that described by James.[12]

In practice 4 ml of a 0.1 percent stock solution of a cp gold salt ($AuCl_3 \cdot HCl \cdot 3H_2O$) are diluted to 100 ml, to which are added 0.05 gram of potassium thiocyanate and 0.06 gram of potassium bromide. This developing solution is prepared just prior to use. Usually four different samples are developed during each series of preparations. The centrifuge accommodates four—13-cc capacity test tubes which are filled with the gold solution after the strips of film are inserted. The gold developer is about 1×10^{-4} molar with respect to total aurous ions. The subsequent manipulations have, for the most part, been described under the section entitled *The Silver Gelatinate Combined Envelope.* The ½-in.×2-in. strip of photographic film is immersed in this gold solution before the enzyme treatment. Total darkness is employed except where red safelight illumination makes pipetting the grains onto the specimen screens more convenient. Less than one minute exposure to weak red safelight is all that is required. It is highly probably that no manifestations of this exposure are observed in the final specimen.

The emulsion is essentially free of aurous ions during the enzyme treatment because a colorimetric test applied to the fifth wash after gold development is negative. This test detects 5 micrograms of gold per ml. The gelatin degradation products could conceivably react with the aurous ions, hence this test is important.

The aurous ion apparently does not react appreciably with the combined envelope during the development. The electron scattering of these silver gelatinate films is not noticeably altered.

The time of gold development is not critical. Development times of 36, 48, 66, and 72 hours have been investigated. From a study of various exposures of emulsion *A* the size of the gold developed center increases with time; the average number of developed centers per grain is not significantly affected. In applying this technique to a variety of problems, 48 hour gold development has been used as a standard practice. Also, gold development does occur after an oxidation treatment consisting of bathing the emulsion in a 0.25 percent chromic acid solution for 10 minutes. The depth within the grain for which latent image silver is removed by this oxidizing action is, of course, not precisely known. However, it should be noted that for low concentrations of aurous ion in the interior portions of the grain the tendency for deposition of gold atoms greatly decreases because of the smaller free energy loss.

An especially important aspect to consider if this gold development technique is to be used to demonstrate the latent image is the possibility of other emulsion components reducing the aurous ion to the metallic state. Although these emulsion components are present in small quantities some of them are reducing agents. This possibility was precluded by washing the film strips in continuously running cold water for 20 minutes or longer before immersing them in the gold developing solution. The gold speck patterns illustrated in the subsequent companion paper were observed with and without this washing treatment.

The sequence of pictures in Fig. 18 demonstrates that the developed centers are inert to oxidizing agents. Colloidal silver is soluble, because of oxidation, in potassium ferricyanide and chromic acid (dichromate ions). Silver sulfide in the colloidal size range is soluble in chromic acid. It follows, therefore, that the specks appearing after gold development consist of gold, at least on the surface. This confirms the report by James.[12] The slightly larger size of the gold specks in 18(c) is due to slight underfocusing of the image and possibly specimen contamination caused by the electron beam. The passivity of the gold developed centers to oxidizing agents is also observed on specimens not having been previously exposed to the illuminating beam. The solubility is therefore not due to a thin film of contaminant sometimes caused by the electron beam.

Speculations on the mechanism of this gold development will be described in the Discussion section. It suffices now to cite Koslowsky's[16] theory in which he

[16] R. Koslowsky and F. W. H. Mueller, Agfa Film Plant, Wolfen, Germany (1936). Bibliography of Scientific and Industrial

explains the formation of aurous ions from the solution of auric ions. The deposition of gold atoms thus requires only one electron transfer from the developable center.

Confidence in this type of specimen preparation has been gained because of the reproducibility of results, especially in the case of controlled exposures. The results of the application of this 48 hour gold development to alpha particle, 65-kv x-ray, and tungsten light exposures constitute the main theme of the companion paper. For purpose of demonstration a typical envelope of a gold developed grain (48 hrs.) exposed to light is shown in Fig. 19.

DISCUSSION

The Silver Gelatinate Combined Envelope

The reactions of gelatin with ions, and especially silver ions, have been studied by Northrop and Kunitz[17] and also by Carroll and Hubbard.[18] Gelatin is an amphoteric degraded protein whose combining power with ions is largely determined by the *p*H. This metallic ion combining ability increases as the *p*H increases above the isoelectric point; this is roughly *p*H=5 for these photographic gelatins. The nitrogen atoms in free amino groups (usually terminal) and possibly in some peptide linkage (−CONHC−) have unshared electron pairs which can coordinate the silver ion. The chemistry of these systems is not simple, but the following general equation serves to illustrate the formation of the silver-gelatin complex:

$$AgR \rightleftharpoons Ag^{+} + R^{-}, \qquad (1)$$

where R^{-} = gelatin molecule with the unshared electron pair.

Two amperometric titrations using a dropping mercury electrode or a rotating platinum electrode were used to study the change in silver ion concentration on adding increments of silver ions to a photographic gelatin solution of known concentration. However, a potentiometric method using a silver-silver ion electrode against a saturated calomel reference electrode is more satisfactory.[19] Measurement of the potential difference between the silver-silver ion electrode and the saturated calomel half cell as an expression of the silver ion concentration according to the equation

$$E_{\text{measured}} = 0.553 + 0.0591 \log[Ag^{+}] \text{ at } 25°C \qquad (2)$$

served as the basis for determining equilibrium constant values for the dissociation of the silver-gelatin complexes (Eq. 1). The end point is determined by the inflection of a plot of millivolts *versus* ml of silver nitrate solution.

No specific dissociation constant (K_D) can be assigned because a mixture of silver gelatinates is formed. Nevertheless, an average value of $K_D = 1\times10^{-13}$ may be assigned. Experimentally it has been shown that any excess silver ion added to such gelatin solutions can be titrated with chloride ions. Thus, the K_D for the silver gelatinates must be smaller than that for AgCl ($K_D = 1.56\times10^{-10}$). When a solution of potassium iodide is used, two end points are exhibited. The first corresponds to *excess* silver ion only and the second to the *total* silver. This indicates a K_D for silver gelatinate greater than that for silver iodide (1.5×10^{-16}). By a similar use of potassium bromide it has been demonstrated that some of the silver-gelatinates have dissociation constants greater than that for silver bromide (7.7×10^{-13}), while others have a smaller value. The effect of *p*H on the position of the dissociation equilibrium has also been determined. The titration results showed a mean deviation of about ±3 percent.

During the titration a white cloudiness develops. This changes to red-brown and finally after standing for 10 or 12 hours in darkness a grey color develops. This darkening takes place more rapidly in strong light, suggesting that the silver gelatinate is photosensitive.

One other very important point must be noted. That is, the results of these silver-gelatin titrations are not caused by halide impurities in the gelatin.

It is of some interest to treat these titrations on a molecular basis, especially in view of the appearance of the combined envelopes in the electron microscope

FIG. 19. 16 000×. A typical gold development (48 hours) of grains exposed to light.

Reports, U. S. Dept. of Commerce, Washington, Vol. 8, p. 873, PB 70053, fr. 381–50. R. Koslowsky, Zeit. wiss. Phot. **46**, 66 (1951).

[17] J. H. Northrop, and M. Kunitz, J. Gen. Physiol. **11**, 481 (1928).

[18] B. H. Carroll, and D. Hubbard, J. Research Natl. Bur. Standards **7**, 811 (1931); **8**, 481 (1932).

[19] The author is indebted to R. L. Edsberg of this laboratory for permission to use the results of his investigations of silver-gelatin titrations. His work has not been published.

image. Because the molecular weights and the distribution of molecular weights of the photographic gelatins are not accurately known, the following relationship can only be qualitative. From Edsberg's[19] study it is known that for a variety of gelatins about 2 mg of silver ion are associated with 1 gram of gelatin (average molecular weight assumed to be 1×10^5 on the basis of calculations using the Svedberg equation). Thus, roughly 2 silver ions are coordinated with each gelatin chain, or 500 amino acid constituents per silver ion, assuming an average of 100 for the molecular weight of the constituents. It appears, therefore, that under these conditions of titration the nitrogen atoms in the peptide linkage do not coordinate silver ions. The terminal amino group and one of the relatively scarce amino groups along the gelatin chain probably represent the reactive loci.

The conditions of photographic emulsion manufacture are however much more conducive to the formation of the silver-gelatin complex; thus, some of the nitrogen atoms in the peptide linkage may react. Knowing that the average dissociation constant of this complex and the $K_{S.P.}$ of the silver bromide are very similar, it may be presumed that the formation of these compounds is competitive during emulsion making. Furthermore, it is highly conceivable that this combined envelope consists of gelatin molecules coordinated with surface silver ions in the grain lattice, thereby existing as a tightly fitting skin around the grain.

The aspect of nonhalide silver is of interest in connection with the earlier discussion of the combined envelope. From the Carroll and Hubbard[5] data an average grain in emulsion *A* containing some 1×10^{10} AgBr molecules would have associated with it about 1×10^5 nonhalide silver atoms. Sheppard *et al.*[20] from colloidal studies of silver bromide-gelatin systems have postulated that the gelatin molecules are oriented parallel to the faces of the grain with from 2×10^3 to 8×10^3 A^2 of grain surface covered per molecule of gelatin. The latter figure depends, of course, on the molecular weight of gelatin. The gelatin molecules are presumably randomly coiled. Assuming an average molecular weight of 50×10^3 and a "coverage" of 4×10^3 A^2 per gelatin molecule, approximately 8×10^4 gelatin molecules are required to cover the entire grain surface with a monomolecular layer. (A cubic grain having a 0.75μ edge is assumed for this simple calculation.) From the potentiometric silver-gelatin titration[18] data presented earlier, two atoms of silver are coordinated with each gelatin molecule. Thus, about 1.6×10^5 atoms of silver are present in an average combined envelope. The agreement between this value and the value of 1×10^5 nonhalide silver atoms (based on Carroll and Hubbard's analyses) is surprisingly good. This agreement may be fortuitous.

[20] Sheppard, Lambert, and Swinehart, J. Chem. Phys. **13**, 372–377 (1945).

The qualitative relation between the rate of matrix gelatin degradation and the age of the enzyme solution was discussed earlier. By a similar token the residual silver-gelatinate combined envelopes may also be degraded with enzymes. This hydrolysis reaction rate is, not unexpectedly, considerably slower than for the matrix gelatin. Also, for any gelatin chain length if the silver ions are still coordinated, their presence would be expected to decrease the solubility of the complex. The degradation of the combined envelope by enzymes requires comparatively severe conditions; even then insoluble fragments of the combined envelope are readily visible in the electron microscope. For emulsion *A* about 5 hours at 35–40°C in fresh 0.2 percent Takamine are required to degrade completely the combined envelope into fragments thereof.

The matrix gelatin shows a high positive temperature solubility coefficient. This is not true for the combined envelopes. Also, the lack of quantitative assay notwithstanding, there is little danger of hydrolyzing the combined gelatin envelopes during the electron microscope specimen preparation by repeated washings carried out to dissolve the degraded gelatin or processing chemicals as described herein. As a matter of fact, some degraded matrix gelatin persists, and it can often be observed in the final specimen. Such fragments are illustrated as very weakly electron scattering material in many of the illustrations (i.e., Figs. 5, 6, 10, 13, etc.).

Gold Development Theory

In order to demonstrate the usefulness of gold development in the study of various problems, some thought must be given to certain aspects of photographic theory. For example, the mechanism of latent image formation, and the nature of the gold development must be considered in order to evaluate critically this electron microscopical approach. Although many publications on photographic theory have appeared in the literature, three rather comprehensive references are worth mentioning: the book by Mott and Gurney,[21] the so-called Bristol Report cited in reference 8, and a recent publication by Seitz.[22]

Although it is not possible to apply accurately thermodynamic principles to the gold development, certainly it is advisable to consider the feasibility of the reaction, $Au^+ + e^- = Au^0$, taking place on and within the photographic grain. The standard electrode potential for this reaction is 1.50 volts for *unit activity* of aurous ion. The statistical average free energy loss is 1.50 ev for each gold atom formed. It must be remembered however that the original gold developer solution is only about 1×10^{-4} molar with respect to total available aurous ion. The deposition of gold atoms in terms of electromotive force measurements

[21] N. F. Mott, and R. W. Gurney, *Electronic Processes in Ionic Crystals* (Oxford University Press, London, 1948).
[22] F. Seitz, Revs. Modern Phys. **23**, 328–352 (1951).

may be represented by the following equation:

$$E_{meas.} = E_0 - 0.0591 \log \frac{1}{[Au^+]} \qquad (3)$$

$$E_0 = 1.50 \text{ volts.}$$

Thus, for some value of aurous ion activity, or concentration for the sake of simplicity $E_{meas.}$ becomes zero, and the deposition of gold atoms no longer occurs. This value for aurous ion concentration is roughly 3×10^{-25} molar. In this regard the concentration of aurous ions is probably adequate, even within the photographic grain. From known data involving complex ions of silver it is possible to determine that on an equal molar basis the solvent action on silver bromide for sodium thiosulfate is about two orders of magnitude greater than that for the thiocyanate ion. The rather lengthy 48 hour development period should facilitate enough solvent action by the low concentration of thiocyanate ions to aid development of some of the internal image by the aurous ion. Furthermore the small ionic radius (1.37A) of the aurous ion permits diffusion of these ions through the silver bromide grain lattice ($a_0=5.75$A).

There is some temptation on first thought to assume that gold atoms merely replace silver atoms, which would be liberated as silver ions. This is suggested because of their relative positions in the electromotive force series for the elements. Such a simple replacement mechanism is not completely adequate because no significant gain in size of the metallic speck would be realized. Furthermore, as has been mentioned earlier, the size of the gold nuclei does increase with time of gold development. The replacement reaction cannot be ruled out completely and may, in fact, represent the very early stages of development of latent image in exposed grains. The codeposition of silver and gold atoms is however a possibility. Some solid solution could exist; the solubility of silver in oxidizing agents under these conditions is unknown.

From a consideration of the energies involved, the deposition of a gold atom at the expense of a silver atom assoicated with the silver halide lattice may require an energy transition as great as that accompanying the Herschel effect. In this connection radiation of wavelength ~8000A corresponds to quanta of 1.54 ev; this is the optical energy required for the reaction $Ag^0=Ag^+ + e$ (now in the conduction band). Assuming that the required thermal dissociation energy for the above reaction is only one-half, or 0.77 ev, this energy would have to be provided for the reaction, $Au^+ + Ag^0 = Au^0 + Ag^+$, to occur. The 0.77 ev would presumably be provided by the thermal vibrations of the grain lattice; the energy is released when the ions shift to new equilibrium positions. If the deposition of gold atoms from aurous ions does develop latent image centers, it is desirable that these image centers be negatively charged for the sake of electrostatic attraction. No matter what type of sensitivity center is postulated, the neutralization of the negatively charged photoelectron trap by the migrating silver ions may not be complete. This is especially true for exposures of high rate of energy dissipation where the number of conduction electrons formed far exceeds the number required for grain "developability."

The mechanism of "trap resetting" by Seitz[22] is particularly appealing in regard to the charge on the latent image center. Assuming that a bromide ion vacancy causes the formation of a Taylor dislocation jog, the latent image forms at the jog terminals which have an effective coulombic charge of $e/2$ prior to exposure. After exposure and capture of the electron from the conduction band, the charge becomes $-e/2$, with the subsequent capture of a silver ion. The charge is now $e/2$. The trap has thereby been "reset," and the cycle may repeat itself. It is reasonable to assume that the final condition of the jog dislocation is negative especially if the exposure is such as to produce a large number of conduction electrons. A cluster of F centers could, of course, also carry a negative electrostatic charge under similar conditions.

Any mechanism concerning the nature of the gold development must also include the amount of gold depositied in terms of the number of available aurous ions in the gold developer. The gold developing bath is approximately 1×10^{-4} M with respect to aurous ions. (This figure disregards the slight dissociation of the aurous thiocyanate complex, which would, however, continue to dissociate as the aurous ions are removed.) In the standard electron microscope preparation some 6×10^9 grains ($\frac{1}{2}$-in.$\times$2-in. sample) are immersed in 13 cc of gold developer. Thus, there are only roughly 1×10^{-2} as many aurous ions in the solution as there are silver ions in the total grains. For the sake of simplicity it is assumed that the gold developed centers are spherical. Thus for a typical gold development of a tungsten exposure there may be some 2×10^6 gold atoms/developed center. Assuming that the average grain exhibits two dozen gold centers, approximately 5×10^7 gold atoms are deposited per grain. Therefore only about 0.4 of the available gold ions, on a grain basis, are deposited. Much longer gold development times would be required to determine if the size of the gold specks attains the theoretical value based on the number of available aurous ions. This experiment has not been carried out.

In the final analysis the mechanism of this gold development is not well understood. This is admittedly not a desirable state of affairs. Nevertheless, the applications described in the subsequent companion paper and the results derived therefrom appear valid despite this incomplete explanation.

Inasmuch as the size of the gold developed centers increases with respect to time of development, an interesting experiment would consist of plotting the average size of these gold specks against development time for a particular exposure. Extrapolation to zero

time might shed some light on the average size of the original latent image center. Meaningful experimentation of this nature would necessitate extremely carefully controlled conditions, and the measurements would be laborious. Nevertheless, it is an interesting possibility from the standpoint of supplying experimental evidence in regard to the size of the latent image.

Another aspect of this gold development is the rather high degree of symmetry with which the gold (and silver?) atoms deposit. Inspection of the illustrations shows that many of the gold developed centers appear to be somewhat octahedral (flattened) in their morphology. This is plausible because gold normally does crystallize with face-centered cubic symmetry.

General

In the preceding sections, *The Silver Gelatinate Combined Envelope* and *Arrested Organic Development*, some discussion was focused on the strongly scattering, often triangularly shaped, regions within the combined envelope. It may be recalled that these structures are observed irrespective of the type of fixation of the grain, but that enzymatic hydrolysis of the matrix gelatin is conducive to their formation. By way of general background, two other aspects in regard to these specific regions are noted at this point. First, these structures have not been observed in the combined envelopes for all photographic emulsions; the combined envelopes from emulsion types *A* and *B* do, however, exhibit these regions when prepared as described earlier. Second, if the grains are undeveloped, or developed by means of the arrested organic technique, these regions appear even though the grain is previously bathed in oxidizing agents such as ferricyanide or chromic acid. The importance of this latter point is that atomic silver, silver sulfide, or sulfide ion in association complexes are very probably removed at least from the grain surface.

Figures 5, 9, 10, 15, and 16 illustrate the structure of concern here. Figure 20 is also illustrated at this time; it demonstrates the importance of this triangularly shaped region during the intermediate stage of organic development. Note the filamentary growth of silver. This type of filamentary growth emanating from the triangularly shaped region is characteristic of a variety of arrested organic developments of a variety of exposures (tungsten and x-ray). Figure 20 is a very typical illustration of a fundamental step in the development of this type of grain.

It is interesting to speculate on the nature of these triangular regions from the standpoint of their serving as *sensitivity centers*.

The investigations by Lowe,[7] *et al.* are again referred to. They have postulated, with good evidence, the existence of primitive, nonoxidizable sensitivity centers. Loening[23] has postulated a silver-gelatin complex

FIG. 20. 25 600×. Emulsion type *A*. Tungsten exposure. Arrested organic development. Note the growth of filaments. This micrograph illustrates in a general way a variety of organic developments of a variety of exposures.

(independently of electron microscopy) on the grain surface. He has demonstrated the inefficiency of latent image formation in the absence of gelatin, and, in fact, indicates a reversal with prolonged exposure time. The gelatin presumably suppresses the natural fading of the latent image, and the silver-gelatin complex produces electron traps.

Planar *F*-center aggregates described by Mitchell[24] have been proposed as possible sensitivity centers. The triangularly shaped regions within the combined envelope suggest a correlation with the 111 plane of the crystal lattice. If one assumes a cube of silver bromide, the octahedral planes through the lattice are triangularly shaped; $d_{111} = 5.75$A. Although it is speculation only, the degree of "111-planarity" may be *greatest* at the corners, thereby enhancing the "triangular shape" associated with the structure in this plane. Mitchell's hypothesis that silver ions migrate into the *F*-center aggregates (voids) to compensate for the field compression is interesting in view of the high electron (microscopical illumination) scattering exhibited by these regions (Figs. 9 and 10). The relatively high electron scattering is most likely due to free silver (or silver ions complexed with gelatin).

It is not plausible that in the *original* grain a sufficient number of silver atoms are present at these sites to account for this electron scattering. However, during the course of the electron microscope specimen preparation, especially the enzymatic hydrolysis, these *F*-center

[23] E. E. Loening, "Chemical sensitization of a silver bromide sol," Bristol Report, reference 7, p. 126.

[24] J. W. Mitchell, "Lattice defects and latent image formation in silver halides," Bristol Report, p. 242.

aggregates might represent loci of high activity in the formation of silver atoms. The presumption in this connection is that "interstitial" silver ions are concentrated at these loci in the original grain. Consequently, no appreciable effect of oxidation treatments would be anticipated.

Little or no gelatin would be expected to exist within the grain, however, *F*-center aggregates at the exterior corners of the grain should be conducive to the formation of silver-gelatin complexes. Therefore, in undeveloped specimens the greater opacity of these regions could be due to high concentrations of coordinated silver ions.

There may be some attempt to associate these triangular regions with the tiny, flattened shadow casting octahedral crystals illustrated in Fig. 2. This is not the case; amongst several reasons it has been observed that these triangular regions appear in emulsions that do not contain the tiny grains.

An entirely different subject matter has to do with the role played by the combined envelopes in the "infection" of unexposed grains by exposed grains during normal photographic development. The degree to which grains are closely aggregated varies for different emulsions. For specific cases there is good evidence[10] that unexposed grains are completely developed if they are in close proximity to exposed (developable) grains. Figures 4–8 and 11 clearly illustrate that the combined envelopes from several grains are joined together. It suffices to mention that this continuum of silver gelatinate amongst the combined envelopes may serve as a medium for transporting silver halide from a normally undevelopable grain to the adjoining grain where the development process is in progress.

Attention is now directed to a more quantitative treatment of the photolysis of a silver halide grain during examination in the electron microscope. Figure 1 illustrates the complete print-out effect. The intensity of the illumination relevant to Fig. 1 is about 25×10^{-12} amperes per square micron or 16×10^{7} electrons (50 kev) per square micron per second. This is equivalent to 13 ergs/μ^2/sec. According to earlier[25] calculations in regard to x-ray exposures, only about 2×10^{-8} ergs per square micron of grain must be effectively absorbed to yield sufficient latent image so that a normally developed density of 1.5 above fog is produced. Similarly, Guenther and Tittel[26] have calculated a value of 46 ev to form one silver atom during print out exposures with x-rays. Again assuming 1×10^{10} silver ions per grain, approximately 20-fold more energy is incident to each grain each second than is theoretically required to photolyze it completely. The illumination beam in the electron microscope has its analog in the photoelectron formed after the absorption of x-ray quanta.

A more precise treatment of the electron microscope exposure must include the rate of energy dissipation within the grain. The range of a 50-kev electron in silver bromide can be taken directly from the data of Bethe[27] or Glocker.[28] The calculated range is about 9 microns in silver bromide. The illuminating electron thus completely penetrates the photographic grain, accompanied by a great deal of scattering. The theory of Bethe and Livingston[29] can be used to determine the rate of energy loss suffered by the electron.

From a theoretical curve an average value of $dE/dx \cong 0.06$ kev/0.1μ may be taken as the incremental energy loss suffered by the illuminating electron. For an assumed path length through the grain of 0.75μ, approximately 0.45 kev of energy is dissipated per electron. Using the earlier value of 16×10^{7} electrons incident to the grain per second, 7.2×10^{7} kev of energy is given up to the grain per second during normal illumination in the electron microscope.

The importance of the above result is better realized when cognizance of the ionization effects are taken. The value of 5.8 ev is now generally accepted[30] as the energy required to "ionize" a silver bromide molecule, according to the equation, $AgBr = Ag^{+} + Br^{0} + e^{-}$ (secondary or conduction electron). From the value of 7.2×10^{7} kev/grain/second, it follows that about 1.2×10^{10} ionization acts occur per grain per second. The "ionization" of the entire grain would require about 1 second on this basis.

The calculations to this point are in part based on the current density measured by the electron microscope photometer.[4] However, since the speed of the 50-kev electron (nonrelativistic) is about $1.3\times10^{14}\mu$/sec, the actual travel time through the grain is only 5.7×10^{-15} seconds. Finally, approximately 1.6×10^{24} ionization acts could theoretically occur based on the rate of energy loss and the transit time of the electron. The grain contains only 1×10^{10} molecules of silver bromide, hence the severity of the "over-exposure" is apparent.

These exposure conditions obviously do not apply to the grains in the emulsion of the photographic plate in the electron microscope. At a magnification of 10 000×, and for the illumination conditions just previously described, from 1 to 2 electrons per second are incident per square micron on the plate. Although this treatment is not meant to be quantitative, the number of ionization acts resulting from an exposure time of 1 second is of the order of 100 or less; the formation time for the conduction electrons would again be in the neighborhood of 5×10^{-15} seconds. Severe over-exposure is not the case here.

Thermal effects are of general interest in this electron microscopical approach. From known thermochemical data for silver bromide, it is easy to show that about 4×10^{-3} ergs must be absorbed by the average grain in order to melt (434°C). Consequently, an exposure of

[25] H. Hoerlin, J. Opt. Soc. Am. **39**, 891–897 (1949).
[26] P. Guenther, and H. Tittel, Z. Electrochem. **39**, 646 (1933).
[27] H. A. Bethe, Hand. d. Phys. **24**, 522 (1933).
[28] R. Glocker, Z. Naturforsch. **3A**, 147 (1948).
[29] H. A. Bethe, and M. S. Livingston, Revs. Modern Phys. **9**, 245 (1937).
[30] K. Alan Yamakawa, Phys. Rev. **82**, 522 (1951).

3.5×10^{-2} seconds to the illuminating beam would be required assuming that the absorbed energy of 7.2×10^{7} kev/grain/second is dissipated as thermal energy. Silver bromide is known to melt without decomposition. The result of the exposure in the electron microscope, illustrated in Fig. 1, is undoubtedly a photolytic or print out effect. The evolution of a gas (bromine) from the seething mass also suggests that melting in the usual sense does not occur.

SUMMARY

This paper describes several electron microscopical techniques which are useful for studying photographic emulsions from two major points of view. First, direct observations of importance to modern latent image theories are provided. Heretofore, these theories have necessarily been based on rather indirect evidence. Second, independent sensitometric data have been corroborated.

The replica techniques are limited to grain shape, size distribution, clumping tendency, etc. If a light microscopical analysis is inadequate because of the size range of the grains then this electron microscopical assumes greater significance. This is especially true where emulsion preparation is to be correlated with properties such as grain morphology. The replica technique has proved that in these emulsions photolytic silver, formed rapidly as well as slowly, does grow inwardly through the grain. This is new and contradicts the present hypothesis that such silver projects outwardly from the grain.

Certainly one of the most important contributions of this work is the demonstration of the existence of the silver gelatinate combined envelope. The information in the available literature strongly suggests that the significance of this structure has been overlooked, especially in regard to theory concerning latent image formation and grain development. Admittedly, further experimentation in this connection is in order. However, this paper has presented a clear picture of its existence and behavior based on direct electron microscopical observations and indirect potentiometric titrations. The effects of *p*H of the fixer, of the sequence of fixation and matrix gelatin degradation, of temperature, and of various methods for removing the matrix gelatin have all been demonstrated. A preliminary attempt is given to explain the structure of the combined envelope, especially the triangularly shaped, strongly scattering areas. The role played by these areas during latent image formation and the initial stages of development is clearly illustrated. Infectivity during emulsion development is now more readily understood because of the continuity of the combined envelopes between grains as illustrated in the various figures.

The manifestations of the arrested organic development procedure and the internal development after surface oxidation have been described. Clearly, this has been made possible because of the existence and utilization of the combined envelope. The distribution and depth of sensitivity centers in emulsions *A* and *B* have been illustrated so as to demonstrate the applicability of this technique. Such aspects as spectral sensitivity and relative surface and internal sensitivity, determined from sensitometric data, can be corroborated and studied in more detail as described herein. Other applications are left to the minds of the readers.

A note of caution is imperative. Carefully controlled specimen preparations are necessary. Furthermore, reliance on a few specimens and a few micrographs may be misleading because of the wide variations in the appearance of the specimen. Because of the extreme differences in grain sensitivity within a given emulsion, and because subtle differences are exaggerated by arrested organic development, for example, a precise statistical evaluation of the final specimen is impractical. Fortunately, it is a relatively convenient matter to prepare and examine fifty thousand grains (combined envelopes). Consequently, a good qualitative interpretation of the specimen is a practical matter. The illustrations included herein do portray the "average" specimen.

By a similar token the gold development technique is based on the utilization of the combined envelope. The apparent quantitative retention of the gold developed latent image centers, the slow and time-independent approach, and the high degree of reproducibility of results are desirable qualities that lend weight to this technique. This paper has presented the preparation details and speculations on the nature of the development. An attempt to provide a more precise explanation for the deposition of gold atoms in terms of thermodynamics and energy levels, as defined in recent years (through the advent of solid state physics) proved to be exceedingly difficult. The subsequent companion paper clearly defines the application of this gold development technique, the absence of a precise theory explaining the development notwithstanding.

Finally, based on the energy of the illuminating electron beam, a quantitative analysis of the rate of photolysis of a grain during direct examination is given.

ACKNOWLEDGMENTS

The authors are indebted to Earl Van Norman, Jr. and R. M. Ede of this laboratory for their meticulous care in preparing the numerous electron microscope specimens. Thanks are due to L. T. Hallett and the management of the laboratory for making possible a detailed study, partly described herein.

This project was initiated by the Ansco Division of General Aniline and Film Company, Binghamton, N. Y. The contributions made by H. Hoerlin and F. W. H. Mueller of Ansco are gratefully acknowledged. The former was particularly helpful because of his encouragement and guidance from the purely photographic point of view.

JOURNAL OF APPLIED PHYSICS VOLUME 24, NUMBER 12 DECEMBER, 1953

Electron Microscopical Studies of the Latent Image Obtained by Exposures to Alpha Particles, X-Rays, and Light*

H. HOERLIN, *Ansco, Division of General Aniline and Film Corporation, Binghamton, New York*

AND

F. A. HAMM, *General Aniline and Film Corporation, Central Research Laboratory, Easton, Pennsylvania*

(Received June 26, 1953)

The latent image of ordinary photographic emulsions has not been resolved. However, the slightly enlarged latent image as obtained by physical gold development can be demonstrated by means of the electron microscope. For the case of a fast negative emulsion it is shown that different types of exposures result in latent image centers of significantly different size distribution characteristics. High-intensity alpha-particle and x-ray exposures produce a very large number of finely dispersed centers; irradiation with light of optimum intensity and 1/100 sec duration forms a small number of centers; only very few specks result from exposures to light of very low intensity. The patterns observed are in line with expectations based on current photographic theory.

INTRODUCTION

PRESENT theories of the formation of the latent image and of the nature of the sensitivity centers rest upon a great deal of rather indirect evidence. Gurney and Mott[1] based their discussions of the photochemical process in silver halides on a series of classical experiments. Their analysis of the elegant work conducted by Hilsch and Pohl[2] on large silver halide crystals and by Eggert and Noddack[3] on photographic emulsions lead to the hypothesis that the latent image is formed by a primary photoconducting and a secondary electrolytic process. The formation of the latent image silver is believed to take place at discrete sensitivity centers, which provide trapping sites for the conduction electrons and subsequently attract the positively charged ions or lattice vacancies.

The undeveloped latent image formed by a normal photographic exposure has however never been demonstrated by optical or electron optical means. Apparently the number of silver atoms which must be produced in a modern emulsion in order to induce development is quite small; indeed Webb[4] and one of the authors[5] arrived independently and by different approaches at similar quantitative values, namely that under favorable circumstances the formation of about 10 silver atoms per grain suffices to render it developable. Aggregates of this kind cannot be resolved by present day techniques, nor has it been possible to detect the larger latent image resulting from exposures which correspond to the shoulder part of the characteristic curve.

Knowledge of the latent image size and of its geometrical distribution inside the grain and on the grain surface is however a matter of considerable practical and theoretical importance. One can assume that in a sensitive grain the structural imperfections of the silver halide microcrystals, which are produced and modified in the course of the precipitation and ripening processes, provide a variety of more or less effective electron traps. The depth of the traps in a grain is not constant and varies over a fairly wide range of values. The efficiency of their utilization in an exposure depends on the type, intensity, and duration of the irradiation and on the temperature of the silver halide.

For example, it is known that high intensity exposures of short duration are less efficient than conventional exposures of average intensity. This failure of the reciprocity law has been explained in terms of differences in trap utilization.[6] During the high intensity exposure a relatively dense electron cloud is produced throughout the grain and a large number of traps, even the shallowest ones in the interior of the grain, become operative. Consequently the latent image is greatly dispersed and only a few latent image centers have a chance to grow to the size which is needed to initiate development. Many exposed grains remain undeveloped.

In contrast, during exposures of optimum intensity (which, in well designed emulsions corresponds to exposure times of about 1/100 sec duration) a smaller number of traps become operative. In this case the conduction electrons are produced at a slower rate; trapping at deeper sites prevails and the available time permits the neutralization of the negatively charged trap by an interstitial silver ion or a bromide ion vacancy and its subsequent repeated use, thus enhancing the formation of larger, developable centers.

Finally, it is known that exposures to light of very low intensities, for example those used in astronomy, are also relatively inefficient. Here the quanta arrive at

* Presented in part at a meeting of the New York State Section of the American Physical Society, October 5, 1951, Rochester, New York.

[1] R. W. Gurney and N. F. Mott, Proc. Roy. Soc. (London) **A164**, 151 (1938).

[2] R. Hilsch and R. W. Pohl, Z. Physik **77**, 421 (1932).

[3] J. Eggert and W. Noddack, Z. Physik **20**, 299 (1923).

[4] J. H. Webb, J. Opt. Soc. Am. **38**, 312 (1948).

[5] H. Hoerlin, J. Opt. Soc. Am. **39**, 891 (1949).

[6] For discussions of the reciprocity characteristics of photographic emulsion see among others: J. H. Webb, J. Opt. Soc. Am. **26**, 367, (1936) and **40**, 3 (1950); P. C. Burton, and W. F. Berg, Phot. J. **86B**, 2 (1946) and **88B**, 84 (1948); E. Katz, J. Chem. Phys. **17**, 1132, (1949) and **18**, 499 (1950).

long intervals; only the deepest traps are operative and one assumes that the latent image is concentrated in a few centers only.

The distribution of the latent image is related to the effective speed of a photographic emulsion. It appeared therefore justified to make an effort to gain as much direct information on this subject as can be obtained under application of advanced techniques. With this in mind electron microscopical techniques described in the preceding paper[7] were applied. Physical gold development similar to that employed by James[8] was found to enlarge the latent image to a resolvable size. Satisfactory maintenance of the general image distribution pattern was achieved by careful separation of the combined gelatin envelope from the bulk gelatin. In brief, the application of the gold development technique outlined in the preceding companion paper is described herein.

During the initial stages of the project it was problematic whether one could succeed in detecting any differences in latent image distribution. It was therefore decided to confine the investigation to one photographic emulsion type only and to select as the main variable the extreme of available photographically active radiations. Exposures were made to alpha particles, x-rays, and to blue light of normal and very low intensities. The exposure times were selected to yield densities of slightly less than D_{max} for development in a commercial organic developer. This means that except for the alpha exposure almost every grain has received at least enough exposure to render it developable.

A double coated, fast negative bromoiodide emulsion (type *A* in preceding paper) of high contrast was selected for the experiment. The average trap depth of this emulsion was determined from the low-intensity reciprocity law failure shift as function of temperature, a method described by Webb;[9] the maximum trap depth was calculated according to Katz.[10] The values were found to be 0.7 ev and 1.5 ev, respectively.[11]

DISCUSSION

Alpha-Particle Exposures

Alpha particles from Polonium provided the exposure of highest intensity. The film was separated from the Polonium surface by a 1-mm air gap of normal pressure. The 5.3-Mev particles have a range of about 22μ in the emulsion employed; about 15 grains will be hit per particle and approximately 360 000 ev are transmitted to the individual grain. The silver halide to gelatin ratio by weight of the emulsion is close to 1.0; therefore half the total particle energy is dissipated in the gelatin.

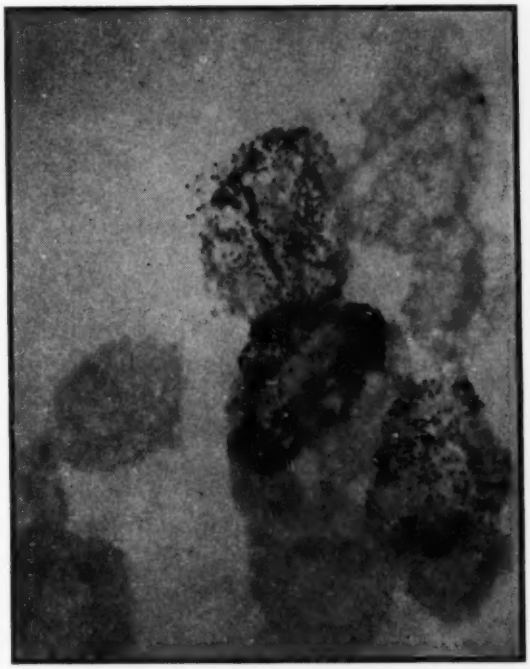

FIG. 1. 21 600×. Alpha particle exposed grains. (This and all subsequent electron micrographs represent the 48-hour gold development technique.)

Taking 2×10^9 cm/sec as the approximate velocity of the alpha particle, the exposure time for the individual grain is of the order of magnitude of 5×10^{-14} sec. During this extremely short period 60 000 electrons are thrown into the conduction band, since according to Yamakawa[12] 5.8 ev suffice to remove one electron from the filled band.

Although a considerable amount of recombination is presumed to take pleace, this dense electron cloud will almost certainly produce trap saturation, at least in the neighborhood of the path of the particle; that is, almost all traps in this area will receive one or very few electrons which are neutralized slowly by the sluggishly moving positive ionic charge carriers (interstitial silver ions). On the basis of latent image theory one must therefore expect that a very large number of widely dispersed and relatively small latent image centers are formed.

This expectation is fully confirmed. Figures 1 and 2 show the gold developed latent image as retained by the combined gelatin envelope. The grains exhibit several large patches which are dotted with numerous small specks; undoubtedly the degree of dispersion of the latent image is very high. These densely dotted areas are believed to correspond to the entrance and exit sites of the α particles; several grains show more than two such latent image patches which must be due to

[7] F. A. Hamm and J. J. Comer, J. Appl. Phys. 24, 1495 (1952).
[8] T. H. James, J. Colloid Sci. 3, 447 (1948).
[9] J. H. Webb, J. Opt. Soc. Am. 40, 3 (1950).
[10] See reference 6.
[11] Thanks are due E. T. Larson of the Ansco Research Laboratories for these determinations.
[12] K. Alan Yamakawa, Phys. Rev. 82, 522 (1951). This author used beta particles for the determination of the ionization energy in silver chloride; this value of 5.8 ev may therefore not be precisely accurate for these alpha exposures.

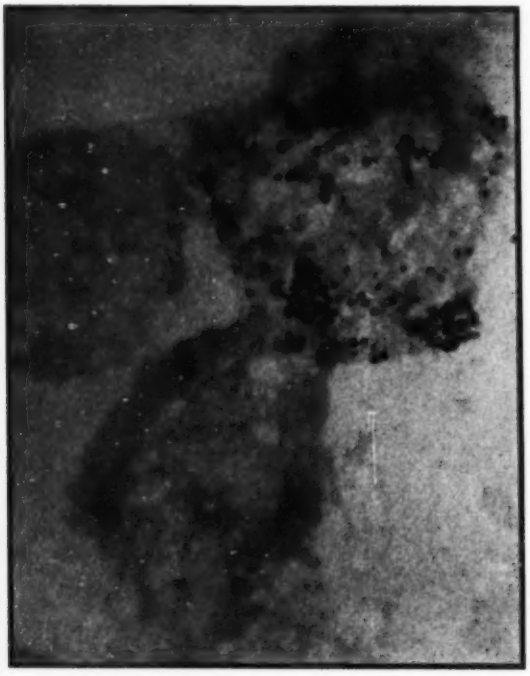

FIG. 2. 39 200×. Grain exposed to alpha particles. The densely dotted areas are believed to correspond to the entrance and exit sites of the particles.

multiple hits from the particles. It is also interesting to note that the diameter of these areas is approximately $\frac{1}{4}$ of the grain diameter; hence, the maximum range for the conduction electrons cannot be larger than about 0.2 micron.

The three micrographs shown are typical for more than 50,000 grains examined in the electron microscope. At least half the grains show no image whatsoever, some (Fig. 3) show a few large spots which are believed to be "fog." The fog of this emulsion when normally developed gives rise to a net density of about 0.10 which suggests that roughly 2 percent of the grains in an unexposed emulsion are developed. The large number of undeveloped grains is due to the fact that the double coated emulsion was exposed to alpha particles from one side only and that an emulsion mixture from both sides was used for the electron microscopical preparations. In fact based on a count of a thousand grains, 40 percent appeared to have been exposed by the α particles by virtue of their appearance after gold development. This agrees well with the penetrating power of the particle. By a similar token if the α-exposed emulsion side is removed before gold development virtually every grain shows the characteristics of an unexposed emulsion.

X-Ray Exposures

The samples were exposed to radiation from a GE Industrial x-ray unit operating at 65 kvp. The beam was slightly filtered to yield a wavelength band in the 0.18 to 0.40A range. When x-rays of this energy are absorbed in silver bromide, the grains are ionized primarily by the photoelectrons ejected from the K-shells of the silver and bromide ions. For example, a quantum of 65 kev will produce a 40-kev photoelectron, the remaining 25 kev being re-emitted as fluorescent x-radiation. The 40-kev electron travels through the emulsion for a distance of 4 grains, losing energy by ionization of the silver halide and of gelatin. Since heterogeneous radiation is employed, the energies of the photoelectrons vary, 10- to 20-kev electrons being in the majority. From range and energy loss data of electrons in silver halide[13] one can derive that the average gain receives approximately 10 kev per hit. Taking again Yamakawa's value of 5.8 ev as the energy required for a charged particle to produce an ion pair in silver bromide, one arrives at a minimum number of 1500 conduction electrons produced per grain during the passage of one photoelectron. The photoelectron travels at roughly 1×10^{10} cm/sec; hence the exposure time per grain is 10^{-14} sec. Thus, we are dealing with slightly shorter exposure times than in the case of alpha particles, and the total exposure per grain is smaller. Again the electron traps have to accommodate a large number of conduction electrons in a very short time and a great degree of dispersion has to be expected as postulated by Kornfield[14] and others.

Figures 4 and 5 show typical x-ray exposed grains. The individual centers are somewhat larger but less numerous than those produced by alpha particles. A

FIG. 3. 30 400×. Two envelopes show the finely dispersed latent image of alpha particles. Two other envelopes represent fog grains (fewer and larger specks).

[13] J. H. Webb, Phys. Rev. **74**, 511 (1948); see also reference 5.
[14] G. Kornfield, J. Opt. Soc. Am. **39**, 1020 (1949).

very extensive electron microscopical examination revealed that virtually every combined envelope contained developed centers. As one might expect, they exhibit on the whole a more irregular pattern than the alpha exposed grains, partially due to the fact that multiple hits are more frequent. In a few cases, approximately 5 percent of the total, typical "electron tracks" appear as shown in one grain of Fig. 4. Such tracks could conceivably represent the path of a photoelectron, making a grazing hit along a broad face of the grain. Actually this is not unreasonable to expect. Whereas the internally developed centers, if any, cannot retain their original position after fixation, it seems quite plausible that the developed surface specks are fairly tightly held in place by the adjacent gelatinate envelope. A greater lateral extension of the tracks, corresponding to the large dotted areas of the alpha particle entrance and exit sites, should not be expected because of the much smaller ionizing power of electrons.

Exposure to Light of Optimum Intensity

The film samples were exposed to an incandescent light source of 2800 K-color temperature, the intensity adjusted to yield D_{max} for an exposure time of 1/100 sec. This is the intensity of highest photographic efficiency for this particular emulsion, corresponding to the lowest point of the conventional reciprocity curve.

Exposures to alpha particles and 10-kev photoelectrons differ from exposures to light of optimum intensities in two ways. The first two are high-intensity exposures and furthermore in both cases the grains

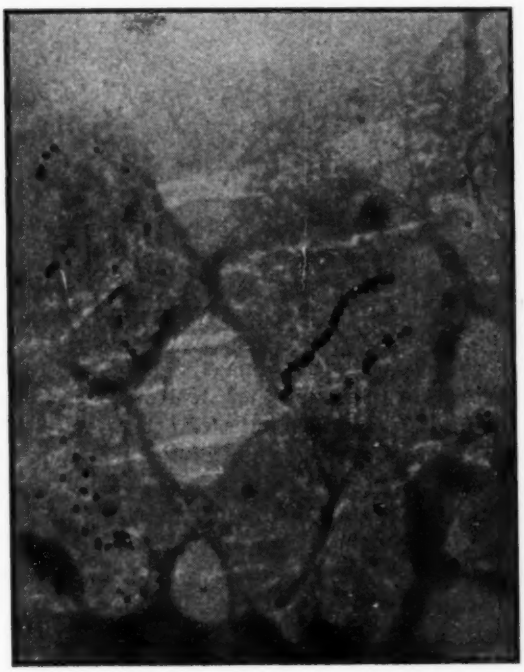

FIG. 4. 24 800×. Combined envelope of x-ray exposed grain. The "track" in one of the grains is believed to be due to a grazing hit by a photoelectron.

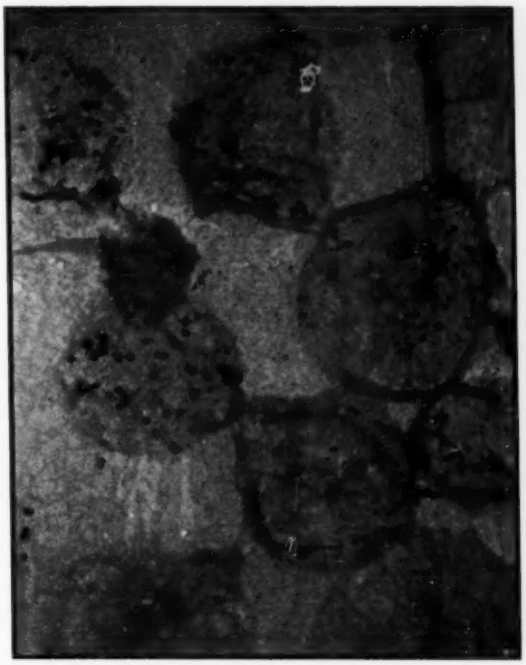

FIG. 5. 17 600×. Combined envelopes of x-ray exposed grains.

receive more energy than is needed to render them developable; in other words, the individual grains are overexposed, even under the conditions of such extremely short exposure times, the overexposure being greatest for the alpha particles. It is now interesting to observe the latent image distribution for the case of optimum exposure intensity with no or very little overexposure.

The corresponding electron micrographs are shown in Figs. 6 and 7. The gold developed latent images centers are considerably fewer in number but correspondingly larger than in the case of alpha particle and x-ray exposures. Virtually every developable grain shows from several to roughly 12 centers, which are two or three times larger than those for the 65-kvp x-ray exposures. The distribution over the grain appears to be more uniform, the pattern being determined primarily by the more random pattern of light absorption. In contrast to the charged particles which ionize the grain along a rather distinct path, the conduction electrons are produced singly, at a relatively slow rate, and their sites of origin are determined by the statistical nature of the light absorption. The number of traps of average depth at the surface of the grain is sufficient to take care of the majority of the conduction electrons. Again the electron microscopical picture of latent image distribution is fully in line with expectations.

Low-Intensity Light Exposure

It has been well established that low-intensity reciprocity law failure is due to the instability of the latent image during the initial stage of formation. A

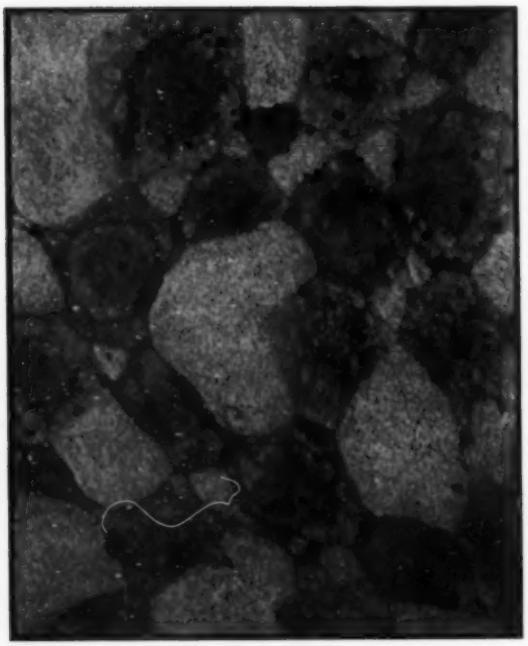

FIG. 6. 13 600×. Combined envelopes of grains exposed to tungsten light, 1/100-sec exposure time.

single silver atom which has been formed by the trapping of a conduction electron and the subsequent migration of an interstitial silver ion to the trapping site is believed to be unstable. Webb[9] assumes that such a nucleus disappears by thermal ejection of an electron followed by the diffusion of the silver ion. The speck

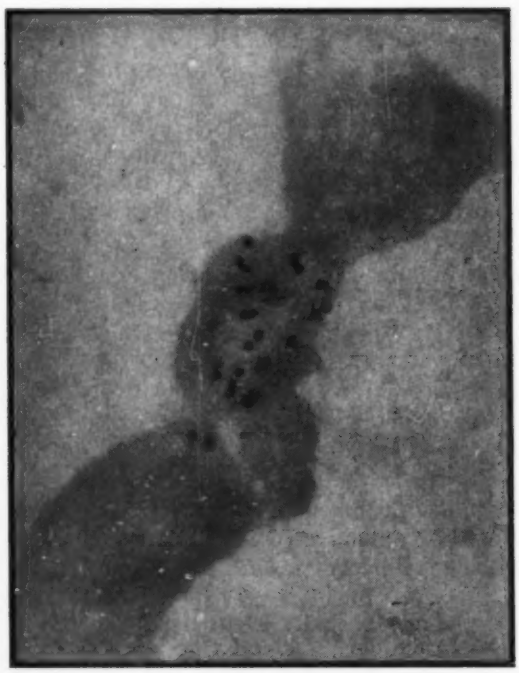

FIG. 7. 25 600×. Combind envelopes of grains exposed to tungsten light, 1/100-sec exposure time.

becomes, however, stable if within its lifetime a second silver atom is added thus forming the stable, but still undevelopable, sublatent image. The magnitude of the reciprocity law failure depends therefore on the average lifetime of the unstable sublatent image and the rate at which the light quanta are absorbed by the grain. It has been shown that the average grain of the emulsion under investigation requires the absorption of about 10 quanta to become developable[15] when exposed at 1/100 sec; hence the average time interval between the arrival of two quanta is approximately 1/1000 sec. This is short in comparison with the average lifetime of the unstable sublatent image; in this case very few of the silver atoms will have a chance to disintegrate before the formation of the second atom. Going to

FIG. 8. 32 800×. Combined envelopes of grains exposed to low intensity light. Exposure time 40 hours.

lower intensities and longer exposure times reciprocity law failure will become very noticeable when the average lifetime of the unstable subimage which is of the order of magnitude of 10 sec and the rate at which the quanta are absorbed are approaching each other. At very long exposure times the magnitude of the reciprocity law failure can be quite appreciable. In our particular emulsion the efficiency of the photographic process for a 40-hour exposure is only $\frac{1}{16}$ of its optimum. One must therefore assume that under the conditions of such long exposures only the deepest traps are operative; here the likelihood of thermal disintegration is at a minimum. Hence one must expect that the latent image is aggregating on very few centers only. This is evidently

[15] Note that the grains shown in the photomicrographs of Figs. 6 and 7 are possibly overexposed.

the case; the anticipated sparse population of large developed centers is illustrated in Figs. 8 and 9. These combined envelopes represent emulsions which had been exposed to tungsten light of very low intensity requiring an exposure of 40-hour duration to yield almost D_{max} when developed normally. Better than 90 percent of the grains show from 1 to 3 relatively large gold specks.

CONCLUSIONS

The exposures employed in the preceding experiment and the corresponding values of total energy absorbed, exposure time and number of conduction electrons produced per average grain, also rate of energy dissipation are summarized in Table I in a quantitative way.

TABLE I. Total energy absorbed, exposure time and number of conduction electrons produced per average grain for four different exposures.[a]

Exposing radiation	Total energy absorbed kev	Exposure time sec	Conduction electrons produced	Rate of energy dissipation kev/sec
Alpha Particle	360	5×10^{-14}	60 000	8×10^{15}
x-rays (electrons)	10	1×10^{-14}	1500	1×10^{15}
Light, optimum intensity	0.03	10^{-2}	10	3×10^{-4}
Light, low intensity	0.50	1.5×10^{5}	160	3×10^{-6}

[a] Data given are for the case of a single hit per charged particle per grain and in the case of light for the minimum exposure required to render the average grain developable.

Necessarily these data are of moderate precision only, nevertheless they demonstrate clearly the variety and the extremes of the conditions under which the silver halide grains have been investigated. The slightly enlarged latent image has been shown for exposure times and rates of energy dissipation extending over a range of almost 20 decades. The latent image distribution in individual grains was shown for the case of optimum exposure conditions and for the 1000-fold over-exposure obtained in bombardment with alpha particles. For the first time visible evidence has been provided for the correctness of important, basic features of present day latent image theory. The details demonstrated support strongly the validity of heretofore only indirectly derived conceptions.

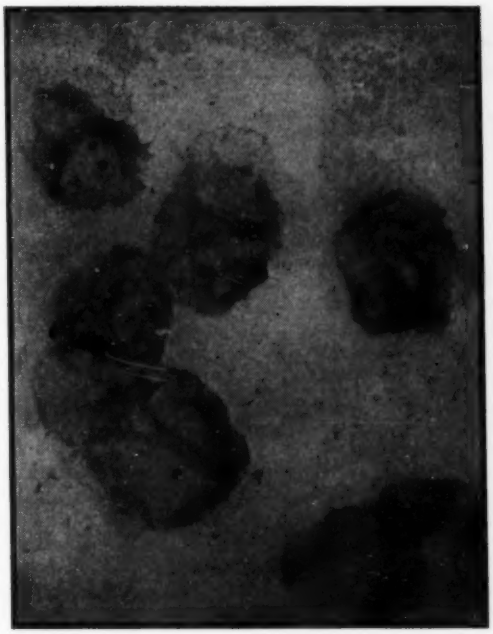

FIG. 9. 18 400×. Combined envelopes of grains exposed to low intensity light. Exposure time 40 hours.

ACKNOWLEDGMENT

The authors gratefully acknowledge the contributions made by J. J. Comer and Earl Van Norman, Jr. of the Central Research Laboratory. Their very careful preparation of a large number of specimens made possible this study.

Thanks are also due F. W. H. Mueller and E. T. Larson of the Ansco Laboratories for their many helpful discussions.

Letters to the Editor

A Modification of R-PAC for Interpretation of Patterson Maps in X-Ray Crystal Analysis*

RAY PEPINSKY
X-Ray and Crystal Analysis Laboratory, The Pennsylvania State College, State College, Pennsylvania
(Received June 1, 1953)

THE electronic analog computer R-PAC, which stores and plays back X-RAC signals, has been described previously.[1,2] The machine has two basic functions: the recording of X-RAC maps which are undistorted in both linear dimensions and signal amplitude, for various applications;[1,2] and direct computation with image-seeking techniques, and particularly those proposed by Buerger.[3]

Although the accurate recording of X-RAC maps and three-dimensional Patterson map interpretations require a machine of the type described previously, the image-seeking machine for two-dimensional Patterson functions can be of a simpler design. What is necessary for the latter application is a rapid method for storing and playing back positionally shifted, two-dimensional Patterson functions and for combining these shifted functions according to one or another of Buerger's techniques. Rapidity of computations is essential, since the selection of image-seeking lines or polygons is to a good extent a matter of trial and error, and the effects of a good number of choices of possible shifts, and consequences of various combinations of these, must be tested. Because of the wide range of frequencies of sinusoidal signals which are combined to form the synthesized function in X-RAC, it is not readily possible to phase-shift the complete X-RAC function without distorting it. The origin of the function can be shifted at will, of course, on an oscilloscope, by merely phasing the sweeps, but the present application requires the combination of complete functions, variously delayed with respect to one another.

The procedure utilized previously in this laboratory has been to prepare several photographic copies of a Patterson contour map, and to operate with geometrically shifted combinations of these in the manner described by Buerger.[3] Geometric distortions of the coordinate network of these maps, resulting from nonlinearities in recording from a cathode-ray tube presentation, generally require the redrawing of the maps on an accurate net. In addition to the advantage which would be gained if the influence of coordinate-net distortions could be eliminated, and, although the method which Buerger has developed for exploring the Patterson function with his minimum function is very rapid for a nonmachine method, it would be very useful if these explorations could be accomplished at much greater speed, without the necessity for hand-contouring of the resulting functions.

An excellent device for storing X-RAC patterns and playing them back at any desired phase with respect to the original signal has recently been developed by the Raytheon Manufacturing Company. This is the QK357 Recording-Storage Tube, described by Hergenrother and Luftman.[4] This cathode-ray tube has a high-resolution, storage-element target on which 400 light-to-dark variations can be resolved per diameter. The storage element can retain an input pattern for a week or more, and the recorded pattern can be played back, with fair amplitude fidelity, more than 30 000 times without appreciable signal deterioration. The pattern can be readily and rapidly erased and a new signal stored as desired. Speeds of writing, read-out, and erasure are entirely suited to the sweeps and other operational aspects of X-RAC.

Although the storage tubes can accommodate intensity-modulated signals, in the present application they are utilized for on-off signals only, no minimizing circuits are involved, and the amplitude-linearity requirements are all taken case of in X-RAC. The procedure follows that devised and utilized by Buerger in his computations with the minimum image-seeking function. (The minimizing circuits in the previous model of R-PAC could have been eliminated, as well, by adopting Buerger's technique. This fact should have been recognized earlier by the present writer.)

Buerger's minimum image-seeking method involves moving an image-seeking polygon over a Patterson map and setting down the *minimum value* attained at the polygon vertices at related points on a new map. In its simplest form the polygon reduces to a vector corresponding to the distance between two assumed atomic coordinates, which at earliest stages of the analysis should be atoms related by a rotation axis. (These rotational vectors serve to establish the cell origin.) As the map is scanned by the vector, the *minimum* of the values of the Patterson function at the ends of the vector is observed and set down on a new map at the vector mid-point. At later stages the image-seeking vector—or, more generally, the polygon—need not correspond to symmetry-related atomic peaks, and these peaks therefore may represent atoms of unequal scattering power. It is then necessary that the values at the extremes of the vector or at the polygon vertices be *weighted* in accordance with the weights of the atoms concerned.

The minimum value at the end points of the minimum-seeking vector or polygon can be computed electronically as outlined in the preceding R-PAC report.[2] However, Buerger has introduced a much simpler device, which operates directly on contour maps.[3] This produces an approximation to the exact minimum function, but one which is quite adequate at the stage of an analysis in which the image-seeking methods are applied. It has the very great advantage that the stored signals are only of on-off character.

In order to understand how Buerger's procedure is accomplished with the use of the storage-playback tubes, consider first a line image, corresponding to a rotation vector. The end points of the line are then equally weighted. Consider all regions of the Patterson map where the function is *zero or less*. The X-RAC signal for this function is fed to a coincident circuit, which provides a constant-amplitude output signal (a voltage plateau) whenever the X-RAC signal is zero (or negative, resulting from errors in Fourier coefficients or cutoff of the series). These constant-amplitude regions are recorded on storage tube A, the sweeps of which are *delayed* from those of X-RAC by an amount corresponding to an origin shift equivalent to the image-seeking vector. This signal is then played back, with the sweeps from tube A now phased to X-RAC; the playback signal is then mixed with the zero-level plateaus obtained directly from X-RAC. The mixed signal, *which is produced as a plateau of single height, whether or not the mixed plateaus overlap*, is then fed to a contouring circuit which fires whenever a leading or trailing edge of the combined pleateau signal is passed. The output of this is supplied to the X-RAC photographic oscilloscope P, or preferably to a second storage tube B, the sweeps of either being phased to those of X-RAC. The outlines of the combined zero regions are then photographically recorded from P or stored on B. Oscilloscopes P or B also carry the usual X-RAC coordinate lines, but *the origin of the coordinates is phased so that it lies half-way between the end points of the image-seeking line.*

The zero-level plateaus are then erased from tube A, and plateaus corresponding to Patterson signals *at contour level one and higher* are stored on this tube, with the sweeps delayed as in the foregoing step. Tube A sweeps are again phased identically with those of X-RAC, and signals from A are played back, mixed with the corresponding undisplaced one-level plateaus on X-RAC to produce a combined single-height plateau. This new signal is contoured as before. The contouring circuit records on oscilloscopes P or B the limits of all regions of one-level plateaus, whether these overlap or not. *Outside* these regions the value of the Patterson function at one or the other end of the scanning line image must be *less* than one contour level high. The contours on P are again photographed, or again stored on B.

This process is now repeated for values of the shifted Pattersons of height *two* contours or more, then of three contours, and so on for as many levels as is desired. In this way a contour map of the

entire minimum function is recorded from oscilloscope P, or stored on B and finally played back from B to P. The spacing between contours can be made as fine as is felt necessary. Actually, only the higher contours are of much significance.

Instead of contouring, the combined single-height plateau signals can be successively photographed on P, and a stepwise intensity-modulated pattern thereby obtained.

Use of the storage tube B eliminates a good deal of photographic recording time. The storage of each contour level of the minimum function can be accomplished in one or two X-RAC sweeps, with a stepping relay serving to switch from one contour level to another. The complete minimum function can be written on B in less than a minute. When contours are successively photographed from a standard cathode-ray tube, the speed of computation is limited by the time for successive photographic exposures, which at present amounts to five to ten seconds per exposure.

It should be noted that distortions of the coordinate net on the storage tube, caused by possible sweep nonlinearities at the storage element, do not affect the computations, since the nonlinearities are compensated automatically when the stored pattern is read out of the tube.

Buerger has discussed fully the strengthening of the image-seeking procedure by combining the effects of symmetry-related shifts or by replacing image-seeking vectors by polygons. The use of at least three storage tubes, in any one of a number of obvious possible procedures, would permit the computation of the effects of any number of shifts. When the values of the image-seeking points must be weighted unequally, the over-all amplitude of the X-RAC signal fed to the pleateau-producing circuit can be adjusted as necessary for this weighting.

The new scheme is not well suited to three-dimensional calculations, because, unless a storage system is available for a large number of Patterson sections, the coefficients for these must be re-inserted into X-RAC for each calculation. The previous R-PAC designs[2] are much more advantageous here.

The writer is extremely grateful to Dr. R. C. Hergenrother and the Raytheon Manufacturing Company for the loan of two QK357 tubes, to Dr. Johannes Baecklund for preliminary examinations of the utilization of the tubes in this application, and to Professor M. J. Buerger for discussions of the image-seeking procedures. Acknowledgment of the continued support of the Physics Branch of the U. S. Office of Naval Research is equally gratefully acknowledged.

* Development under Contract No. N6onr-26916, T. O. 16, with the U. S. Office of Naval Research.

[1] R. Pepinsky, in *Computing Methods and the Phase Problem in X-Ray Crystal Analysis* (X-Ray Crystal Analysis Laboratory, The Pennsylvania State College, State College, Pennsylvania 1952), pp. 273–274.
[2] R. Pepinsky and P. Jarmotz, J. Appl. Phys. **24**, 663 (1953).
[3] M. J. Buerger, *Acta Cryst.* **4**, 531 (1951).
[4] R. C. Hergenrother and A. S. Luftman, Electronics, 126 (March, 1953).

Resistivity of Thin Silver Films

URI OPPENHEIM AND JOSEPH H. JAFFE
The Weizmann Institute of Science, Rehovoth, Israel
(Received August 5, 1952)

IT is well known that the electrical resistivity of an evaporated silver film is a function of its thickness.[1–3] Although much work has been done on this subject, it is difficult to make direct comparisons between the findings of different laboratories, mainly because the methods employed for determining the thickness of the films have been as a rule inaccurate.

However, Scott and co-workers used an accurate interferometric method for thickness measurement,[4–6] and studied the properties of silver films which were prepared under carefully defined conditions. The relationship between the resistivity and thickness[3] given by them for films evaporated quickly (2 seconds) is shown in Fig. 1, curve A. We have repeated these measurements. The films were prepared under substantially the same conditions as those reported by Scott, and the thicknesses were measured by the same interferometric method. The curve of resistivity *versus* thickness found by us is shown in Fig. 1, curve B. It appears from Scott's curve that the resistivity starts to increase rapidly at a thickness of about 120A, whereas we have found that this so-called "critical thickness" is about 60A.

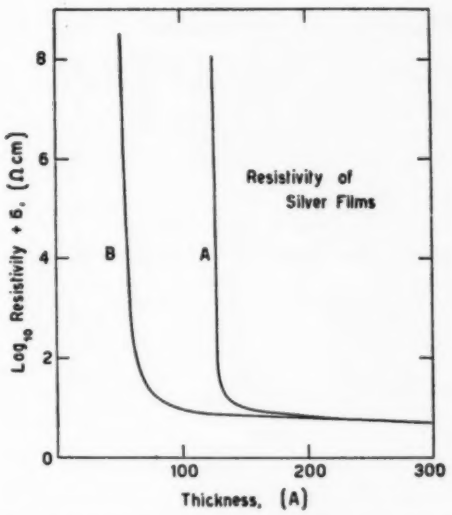

FIG. 1. The resistivity of evaporated silver films as a function of film thickness. Curve A: after Ells and Scott (reference 3). Curve B: present results.

We have been able to make a further indirect comparison. Oldham[7] has presented reflectivities of silver films in the near infrared region, and he too measured thickness interferometrically. By a comparison of his results with our own infrared reflectivity data which we happen to have assembled, we have deduced that the resistivity-thickness relationship of his films is similar to ours.

The values of the critical thickness found from these two determinations differ by a factor of two, and it seems hard to disregard the discrepancy. Whatever be the cause, its elucidation should contribute to a better understanding of the process of evaporation of silver in vacuum.

[1] J. C. Steinberg, Phys. Rev. **21**, 22 (1923).
[2] L. Hamburger and W. Reinders, Rec. trav. chim. **50**, 441 (1931).
[3] E. C. Ells and G. D. Scott, J. Appl. Phys. **23**, 31 (1952).
[4] O. Wiener, Ann. Physik **31**, 629 (1887).
[5] W. K. Donaldson and A. Khamsavi, Nature **159**, 228 (1947).
[6] Scott, McLauchlan, and Sennett, J. Appl. Phys. **21**, 843 (1950).
[7] M. S. Oldham, Ph.D. thesis, Iowa State College, Ames, Iowa (1949).

Experiments in Hydrodynamic Lubrication Using Water as a Lubricant

STANLEY ABRAMOVITZ
The Franklin Institute, Laboratories for Research and Development, Philadelphia, Pennsylvania
(Received July 18, 1953)

EXPERIMENTS have been made with a pivoted segmental thrust bearing (Kingsbury or Michell type) using water as a lubricant. These experiments have indicated an optimum shoe profile, convex in shape, that would not normally be required when using a conventional lubricant. Its influence in reducing starting friction prior to the formation of a hydrodynamic film is discussed.

According to a paper by Hardy and Doubleday[1] investigating kinetic friction properties of lubricants, the following is stated: "Water considered as a lubricant is of a remarkable character. It is neutral to clean surfaces of glass or steel in that it neither lowers nor raises the friction...." Although this statement has not been substantiated by extensive experimenta-

tion, it does indicate the possible absence of an effective boundary film.

Because of the low viscosity of water as compared to oil, extremely thin films are developed between the segmented shoe and runner surfaces. If it is assumed that at the start there is metal-to-metal contact with no effective boundary film, excessive wear and eventual seizure is likely to take place with most

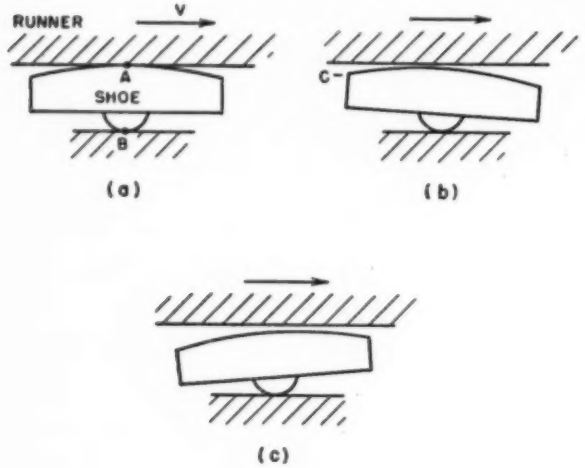

FIG. 1.

materials. It therefore follows that surface deformations and relatively large surface asperities become a critical factor in attaining a hydrodynamic film.

At the start of the test program, all material combinations tested, galled, and seized when the bearing was initially started. An attempt was then made to observe surface contact before galling occurred. An extremely hard runner material, tungsten carbide, was used against hard cobalt based alloy (Stellite) shoes. The runner was rotated by hand at a mean velocity of four feet per second with some clearance between the runner and shoe surfaces. While still rotating, the clearance was reduced and load was applied. Upon application of load, the bearing seized, but, because of the low torque imposed, the surfaces were not seriously affected. What did occur explained the reason why a hydrodynamic film could not be formed. The extremely hard runner face had burnished the surface of the segmented shoes at the four corners of each segment. This test was made in water at 200°F, and the shoes were installed with their surfaces flat to within two sodium light bands. The nature and location of the burnished areas indicated that the surface had distorted to a concave shape. The shoe surfaces were then made convex to 25 sodium light bands. The test described in the foregoing was tried, and a film was easily developed and maintained with little effort. A number of high-speed motor starts were made, after which the shoe surfaces were inspected. The burnished areas were now at the center of the segment and represented 15 percent of the total area of this segment.

Another experiment, illustrating the effect of shoe-surface convexity, was made with a tungsten carbide runner against shoes of an equally hard material. A series of tests was made starting with a flat surface and then increasing the curvature. After a number of power starts using a flat surface, the leading and trailing edge of the shoe segments showed dark discolored contact areas. As the curvature was increased and with the same number of power starts, the contact areas became lighter and more uniform towards the center of segment area. An optimum curvature was reached when no discolored area was visible after the prescribed number of starts.

A feasible explanation has been formulated for the starting friction connected with shoe surface curvature. It is as follows:

Figure 1(a) shows the runner and a shoe segment in the starting position. When the bearing starts, the force at point A tends to rotate the shoe about point B. As rotation continues, point C, Fig. 1(b), approaches the bearing surface. The angle of rotation is extremely small because of the large radius of curvature of the surface. The angular velocity about the instantaneous center B is extremely high. Thus, the high rate of approach traps fluid between the surfaces. This trapped film then facilitates the formation of a hydrodynamic wedge in which the shoe is tilted back to the stable position shown in Fig. 1(c). Theoretically, there would be no metal-to-metal friction between runner and shoe.

It can be seen that this explanation is most applicable when the true curvature is retained. This is indicated in the second experiment described, where the shoes were of a material with a high modulus of elasticity and hardness and therefore offered greater resistance to deformation and wear than the shoes used in the first experiment. Also, to reduce side leakage during operation, a cylindrical surface would be more effective than the spherical surface used in the experiments described.

In analyzing the operating characteristics for this type of surface configuration, a mathematical analysis of the pressure distribution disclosed the existence of a negative pressure towards the outlet edge of the pad. A more extensive analysis now in progress will produce the bearing operating factors as a function of the pad curvature.

[1] W. B. Hardy and I. Doubleday, Proc. Roy. Soc. (London) **A104**, 25 (1923).

Comment on "The Calibration of Photographic Emulsions for Electron Diffraction Investigations"

I. L. KARLE AND J. KARLE
Naval Research Laboratory, Washington 20, D. C.
(Received July 27, 1953)

IN a paper published under the above title,[1] Bartell and Brockway state, "It is assumed in the procedure described by Karle and Karle[2] that $F(D)$ (the ratio of the exposure to the optical density) is constant from densities of zero to about 0.25 for contrast lantern slides." This statement is incorrect. The constancy of $F(D)$ is an experimental observation in our Laboratory and not an assumption, as can be seen from reference to the description of our calibration method.[2] In particular, we quote from our paper,[2] "At low densities, it is *found* that $D_1/D_2=k$, a constant." D_1 and D_2 are the optical densities for two patterns of different exposures at equivalent radial points from the center of the pattern. Since the ratio of the exposures, E_1/E_2, is the same at all radial points, it follows that the ratio of the exposure to the optical density is a constant for low densities. This observation has been made between two and three hundred times in our Laboratory. Consequently, an actual experimental difference exists between the calibration results obtained by Bartell and Brockway[1] and the ones obtained by us. They report $F(D)=1+cD$ with $c\sim 0.3$, for optical densities up to 0.5, using Eastman contrast lantern slides.

In this connection, we should like to point out that our calibration results are in agreement with the detailed studies of the photographic action of fast electrons carried out by Becker and Kipphan,[3] Charlesby,[4] and Baker, Ramberg, and Hillier.[5] They find $F(D)$ to be constant for low optical densities (often up to $D=0.5$ and greater). For instance, Becker and Kipphan state,[3] "Allen Kurven (optical density *vs* coulombs/cm²) gemeinsam ist der anfanglich lineare. . . ." They covered a voltage range of 18 to 84 kv and used a variety of emulsions, including a low gelatin emulsion. Charlesby[4] used Ilford special rapid plates and Baker, Ramberg, and Hillier[5] used Eastman medium lantern slides. Our calibration results are also in agreement with the calibration results found for the electron diffraction experiments of Hastings

and Bauer.[6] They find that $F(D)$ is constant over the range 0.05–1.00 for Eastman spectroscopic VD plates and microfile film.

The deviation of $F(D)$ from constancy reported by Bartell and Brockway for low densities is of no great significance to molecular structure studies, the type of study to which the calibration procedure has been applied in our Laboratory. Since the deviation is important for the atomic structure investigation which has been reported by Bartell and Brockway,[7] an effort should be made to resolve the disagreements with the publications mentioned.

[1] L. S. Bartell and L. O. Brockway, J. Appl. Phys. **24**, 656 (1953).
[2] J. Karle and I. L. Karle, J. Chem. Phys. **18**, 957 (1950).
[3] A. Becker and E. Kipphan, Ann. Physik **10**, 15 (1931).
[4] A. Charlesby, Proc. Phys. Soc. (London) **52**, 657 (1940).
[5] Baker, Ramberg, and Hillier, J. Appl. Phys. **13**, 450 (1942).
[6] J. M. Hastings and S. H. Bauer, J. Chem. Phys. **18**, 17 (1950).
[7] L. S. Bartell and L. O. Brockway, Phys. Rev. **90**, 833 (1953).

Reply to Comment on "The Calibration of Photographic Emulsions for Electron Diffraction Investigations"

L. S. Bartell* and L. O. Brockway
Department of Chemistry, University of Michigan, Ann Arbor, Michigan
(Received September 17, 1953)

THERE is no disagreement between our views[1] and the conclusions presented in the publications[2–5] cited by Karle and Karle[6] regarding the initial proportionality of the variables D and E. This proportionality appears to be well supported by experimental evidence and, indeed, is probably more quantitatively established by the data of Karle and Karle and of ourselves than by the earlier articles.[2–4] Any difference of opinion, then, involves the point at which the deviation from proportionality is considered to become appreciable. It should be noted that the function, $F(D)=E/D$, introduced by us, emphasizes this deviation far more than does the conventional plot of D *vs* E, and that the deviation indicated by our experiments is very small in the region of D in dispute ($D<0.25$). Since the discrepancy amounts to only about 1 percent in the comparison of, say, the densities 0.15 and 0.25 in the $F_1(D)$ curve, an accuracy of a fraction of 1 percent at small D is required to resolve the question of whether this discrepancy, denied by Karle and Karle, is real.

Furthermore, contrary to the contention of Karle and Karle, there is no disagreement between our results and the results of Becker and Kipphan,[2] Charlesby,[3] and Baker, Ramberg, and Hillier,[4] in *any* region of the calibration curves. In the region with $D>0.3$, our results agree satisfactorily with those of the foregoing workers. In the disputed region an examination of the publications mentioned shows that the results fit either point of view equally well, the scattering of the experimental points being too great to distinguish between them. In reference to the work of Hastings and Bauer,[5] it should be pointed out that Bauer has published experimental curves for a number of emulsions including Eastman lantern slide plates[7] and these are in satisfactory agreement with our results. According to the data, not even the $F(D)$ curves for microfile film are completely constant to $D=1.0$.

Unfortunately, we have not had the opportunity to examine in any detail the data of Karle and Karle, but we are confident that any disagreement with our data is not large. The consistency of our results has strongly suggested that the form $F(D)=1+cD$ holds at small D but, in view of the smallness of the effect which is in a region that is difficult to measure with great accuracy and in view of our high regard for the work of Karle and Karle, we certainly do not consider our evidence for this limiting form as final. In fact, our article suggests conditions under which the expected limiting form would be in accord with the results of Karle and Karle. In any event, the aforementioned uncertainties do not invalidate the general calibration procedure described in the article.[1]

Finally, it is to be emphasized that, contrary to the claim of Karle and Karle, the disputed region had absolutely no bearing on the results of the atomic structure investigation[8] cited because, in this study, densities were kept well out of the uncertain range and sectors were chosen which minimized the remaining uncertainties in the emulsion. The effect discussed in the article on calibration[1] that is important in atomic structure studies (though really of any consequence only in the region of the K shell) is an unrelated effect which is undisputed to our knowledge.

* Present address: Department of Chemistry, Iowa State College, Ames, Iowa.
[1] L. S. Bartell and L. O. Brockway, J. Appl. Phys. **24**, 656 (1953).
[2] A. Becker and E. Kipphan, Ann. Physik (Lpz.) **10**, 15 (1931).
[3] A. Charlesby, Proc. Phys. Soc. (London) **52**, 657 (1940).
[4] Baker, Ramberg, and Hillier, J. Appl. Phys. **13**, 450 (1942).
[5] J. M. Hastings and S. H. Bauer, J. Chem. Phys. **18**, 17 (1950).
[6] I. L. Karle and J. Karle, J. Appl. Phys. **24**, 1522 (1953).
[7] Bauer, Keidel, and Harvey, Technical Report on project covered by contract N6 ori-213, Task Order I NR 052-040, Cornell University (1949).
[8] L. S. Bartell and L. O. Brockway, Phys. Rev. **90**, 833 (1953).

Note on the Stress Dependence of the Activation Energy of the Rupture Process

Edward W. LaRocca
U. S. Naval Ordnance Test Station, Inyokern, China Lake, California
(Received September 3, 1953)

IN the course of some investigations on the effects of hot combustion gases on stressed metals (to be described elsewhere), it was found that, in the case of a cold-worked nickel-chromium-iron alloy, relations between rupture time, temperature, and applied stress obey a rate process law, at temperatures between 900°C and 1150°C, in an atmosphere of burning propane.

However, use of the rate process equation, extrapolated to include other values of stress, is not in agreement with experimental data, because of changes in the activation energy with stress. As seen in Fig. 1, if one plots the logarithm of the reciprocal

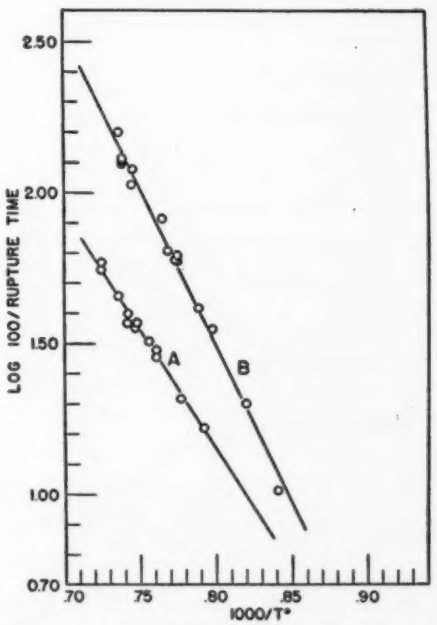

FIG. 1. Changes in slopes at different stress values for chromel wire.

of the rupture time in minutes against the reciprocal of the absolute temperature, a straight line is obtained, the slope of which is a measure of the activation energy. Line A in the diagram is a plot at a stress of 5380 psi, and B is that at 7500 psi. The

activation energy of the process at the lower stress is 36 kcal, and 48 kcal at the higher.

Further experiments are under way to determine whether the activation energy is truly stress dependent, since the difference in values is believed to be beyond the limits of the experimental error of the methods used.

Effect of Cross-Section Area and Compression upon the Relaxation in Permeability for Toroidal Samples of Ferrites

R. E. Alley, Jr., and F. J. Schnettler
Bell Telephone Laboratories, Murray Hill, New Jersey
(Received July 20, 1933)

We have investigated the effects of cross-section area and compression upon the relaxation frequency of a sample of NiZn ferrite and of a sample of MnZn ferrite. We found that change in cross-section area had no effect upon the relaxation frequency of the NiZn ferrite but caused the relaxation frequency of the MnZn ferrite to shift in a manner predicted by theory.[1] Compression reduced μ' for both materials. The relaxation frequency altered as expected for the MnZn but not for the NiZn ferrite.

A toroidal sample of each material was used. Originally, the samples were of the same nominal dimensions—750 mils o.d., 420 mils i.d., and 200 mils thick. Each sample was wound with 10 turns, and inductance and resistance measurements were made on a Maxwell bridge from 25 kc to 2 mc. The components of complex permeability ($\mu=\mu'-j\mu''$) were calculated from these data. Both materials showed relaxation frequencies below 1 mc.

The cross-section areas of the toroids were changed by grinding. Thicknesses were reduced and inner diameters increased, thus reducing the areas. The successive dimensions are tabulated in Figs. 1 and 2. After each dimension change, the toroids were rewound and measured. After measurements for the smallest cross-section areas, the samples were put under compression by encasing them in plastic[2] and measurements were made for this condition. Figures 1 and 2 show the results.

If the low-frequency relaxation results only from domain wall motion, a change in cross-section area would not be expected to affect the relaxation frequency. On the other hand, eddy current effects, either displacement, conduction, or both, will be influenced by cross-section area. Prache and Billottet[1] have shown that in this case the relaxation frequency would be inversely proportional to diameter for a circular cross section.

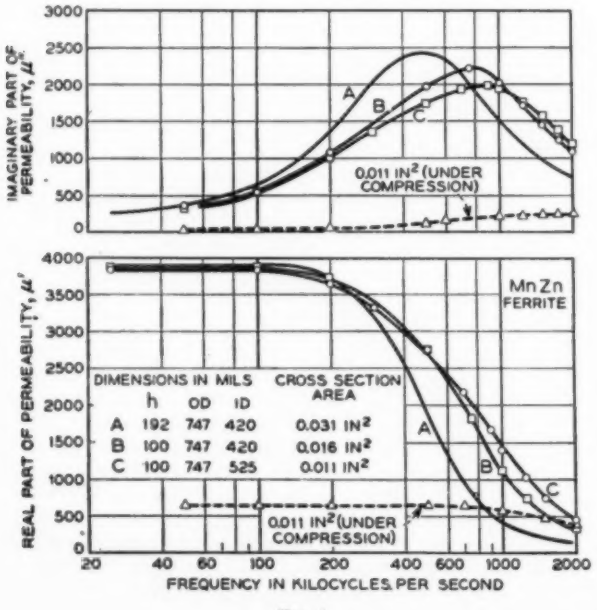

Fig. 1.

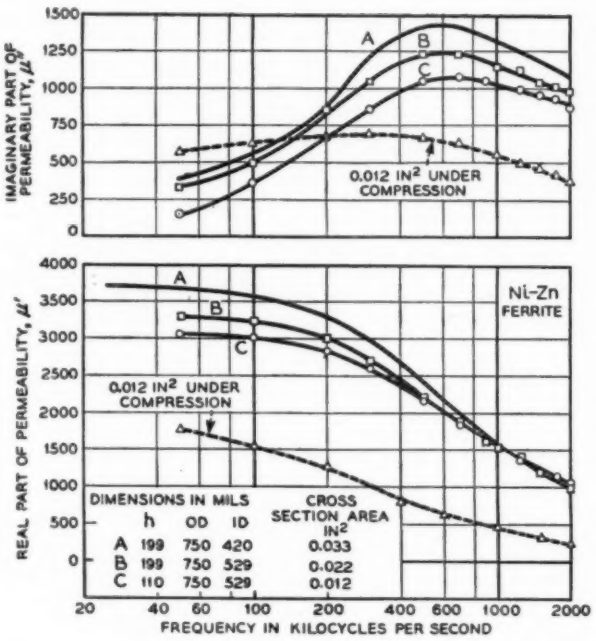

Fig. 2.

Figure 1 for MnZn ferrite shows definite shifts in both μ' and μ'' as cross-section area is changed. Table I compares the ratio of relaxation frequencies with the square roots of cross-section areas.

Table I.

Curves	(Area ratio)$^{\frac{1}{2}}$	Frequency ratio
A and *B*	1.4	1.5
A and *C*	1.7	1.7
B and *C*	1.2	1.2

The close agreement in Table I is as would be expected in the absence of domain wall relaxation. Essentially, it indicates that the true permeability of the material has not changed in this frequency range and, therefore, that the wall motion has not relaxed. Had the walls shown relaxation, there would be changes in the permeability with frequency, and the indicated correlation between relaxation frequency and dimensions would not be found. Thus the agreement between frequency ratio and square root of area ratio supports the conclusion that for this material the relaxation of permeability should be attributed to dimensional effects rather than to wall motion.

In contrast to the behavior of MnZn ferrite, the NiZn showed no change in relaxation frequency with dimensions. This behavior strongly supports the conclusion that in this material the relaxation should not be attributed to dimensional effects. As further evidence of this, the apparent dielectric constant of this sample was measured and found to be of the order of 1500, which leads to a predicted dimensional relaxation frequency of about 40 mc. Figure 2 shows a slight drop in low-frequency μ' with a decrease in cross-section area. This relatively small effect may be attributable to strains set up when the sample was ground to change its dimensions.

The two materials responded quite differently to compression. For the MnZn ferrite, μ' decreased to about $\frac{1}{2}$ the unstressed value,

and the relaxation frequency moved out just to the limit of the measuring equipment. Quantitatively, there was again good agreement between theory and experiment. The relaxation frequency increased from 850 kc to about 2000 kc, while the low frequency permeability decreased from 4000 to 650. Thus, the frequency ratio was 2.4, while the square root of the permeability ratio was 2.5. This behavior further supports the conclusion that the MnZn ferrite relaxation is a dimensional rather than a domain wall effect.

The NiZn ferrite behaved in a quite different fashion. μ' decreased to about $\frac{1}{2}$ the unstressed value, but the relaxation frequency decreased. At present, we are not prepared to offer any explanation of this unexpected behavior.

[1] P. M. Prache and H. Billottet, Cables and Transmissions **6A**, 317 (1952).
[2] H. J. Williams, *et al.*, Trans. Am. Inst. Elec. Engrs. (1953).

Internal Friction of Molybdenum during Tensile Deformation*

R. E. MARINGER
Battelle Memorial Institute, Columbus, Ohio
(Received July 18, 1953)

IN order to relate more closely internal friction and plastic deformation phenomena, internal friction tests have been run during tensile deformation. To do this, a specimen of 0.040-inch diameter molybdenum wire was mounted for a tensile test. An inertia bar and mirror were attached to the center of the specimen and set into oscillation. The decay of the oscillation was observed by means of an optical lever arm. The frequency employed was approximately 1.3 cycles per second.

Figure 1 shows a stress-strain curve and the corresponding stress-internal friction curve for a strain rate of 0.0008/min. At or slightly before plastic strain is observed in the stress-strain

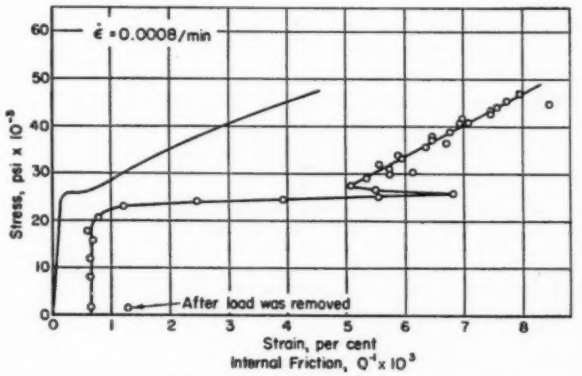

FIG. 1. Variation of internal friction with stress during tensile test.

curve, the internal friction rises sharply. Just after the discontinuous yield, the internal friction drops off suddenly. In the absence of a discontinuous yield, no drop in the internal friction is observed. When the load begins to increase, because of strain hardening, the internal friction increases approximately linearly with the stress. The slope of this linear portion is quite sensitive to strain rate, increasing with increasing strain rate. When the load is removed, the internal friction drops back to some value greater than the initial value.

It appears probable that this type of test may prove extremely useful in observing dislocation behavior during creep and tensile testing and may be of some fundamental value in extending the theory of dislocations.

* Supported by the U. S. Office of Naval Research.

Absorption of Microwaves in Gases

KRISHNAJI AND PREM SWARUP
Department of Physics, University of Allahabad, Allahabad, India
(Received July 20, 1953)

THE absorption of 3-cm electromagnetic waves has been studied in a number of gases in which the absorption has already been reported by three workers.[1-3] The technique of the measurement has been reported by the authors[4] earlier. In the present equipment a 3-meter absorption cell has been used so that the minimum measurable attenuation is 1×10^{-5} neper/cm.

The pressure variation of the absorption has been studied in all the gases, and it has been found that the pressure-absorption

TABLE I. Absorption coefficient[a] of gases at atmospheric pressure 745 mm of mercury and room temperature (35°C).

Gas	Wavelengths in cm										
	3.06	3.10	3.15	3.20	3.23	3.25	3.30	3.33	3.37	3.40	3.44
Ammonia	16.0	15.9	15.7	15.6	15.1	15.6	15.8	15.8	15.9	15.6	15.3
Ethyl chloride			7.5	8.3	8.0	7.6	7.8	7.5	8.2		
Acetaldehyde								15.9	16.0		

[a] Unit of absorption coefficient is 10^{-4} neper/cm.

curves in all the cases follow the general pattern of $\alpha(\nu)\alpha p^2$ indicating that the study is being made in a region far away from the resonant absorption region as reported earlier by Hershberger.[2]

Table I gives the absorption coefficient values in an unbounded medium in ammonia, ethyl chloride, and acetaldehyde, and Table II gives the absorption coefficient values in methyl iodide and acetone.

TABLE II. Absorption coefficient[a] of methyl iodide and acetone.

Gas	3.31-cm wavelength	Pressure
Methyl iodide	0.8 (also at 3.20 cm)	20 cm of Hg
Acetone	2.1	25 cm of Hg

[a] Unit of absorption coefficient is $.10^{-4}$ cm.

Our results in the case of ammonia are in close agreement with those of Hershberger and not with Millman and Raymond. The latters' value is 12.8 units at 3.189-cm wavelength. The results in the case of ethyl chloride agree with the values of both of them. In acetaldehyde, Millman's value of 15.6 at 3.23-cm wavelength is quite close to our value 15.9 at 3.33 cm. In the case of methyl iodide our value is 0.8 unit at 3.20-cm and 20-cm pressure compared to Millman's value of 1.4 at 3.227-cm wavelength and 17-cm pressure. In the case of acetone, agreement appears to be close, as our value is 2.1 units at 25-cm pressure, and Millman's value is 1.8 at 15-cm pressure.

[1] G. H. Millman and R. C. Raymond, J. Appl. Phys. **20**, 413 (1949).
[2] W. D. Hershberger, J. Appl. Phys. **17**, 495 (1946); and J. E. Walter and W. D. Hershberger, J. Appl. Phys. **17**, 814 (1946).
[3] R. Freymann, Physica **17**, 328 (1951).
[4] Krishnaji and Prem Swarup, J. Sci. Ind. Research (India) **B12**, 1 (1953).

Discussion on Paper entitled "Synthesis of Transfer Functions with Poles Restricted to the Negative Real Axis"

A. D. FIALKOW AND IRVING GERST
Polytechnic Institute of Brooklyn and Control Instrument Company, Brooklyn, New York
(Received May 7, 1953)

IN a recent paper[1] based upon a doctoral thesis,[2] Weinberg improved Guillemin's[3] procedure for the synthesis of certain *RC* (resistance capacitance) transfer functions so that fewer network elements are required. In the paper[1] he incorporated a method using "surplus factors" to transform the numerator of the transfer

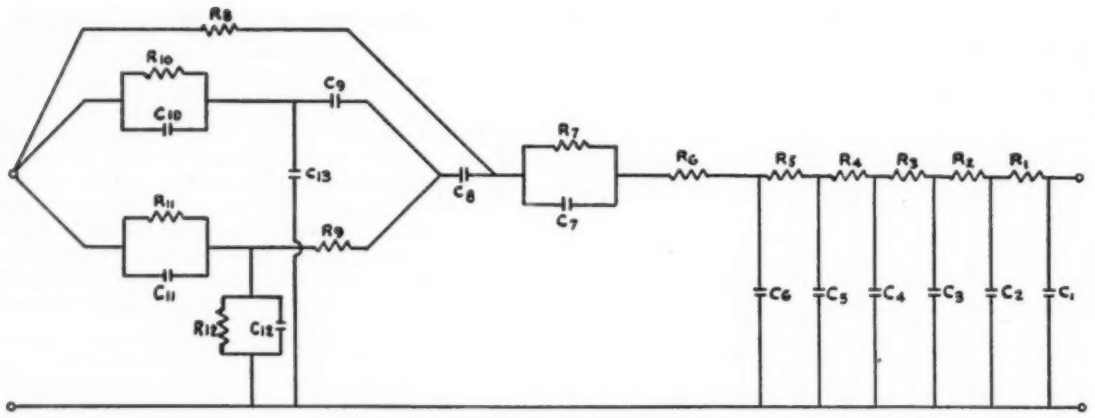

FIG. 1.

function into one having only positive coefficients, giving an indication of a proof. Apparently the author is unaware that we have used "surplus factors" in precisely this way in our synthesis[4-6] of *RC* transfer functions and that complete proofs of the mathematical basis for this application have already been given.[5,7]

It may also be of interest to note that merely by suitable specializations of our general synthesis procedure, we may effect element economies comparable to those of Weinberg. Thus, suppose that the transfer function is written as

$$A(p)=KN/D$$
$$=K(p^n+a_1p^{n-1}+\cdots+a_n)/(p^m+b_1p^{m-1}+\cdots+b_m).$$

Our synthesis involves an initial choice of a polynomial $F(p)$, such that D/F is an *RC* admittance and a decomposition of N and D, $N=N_1+N_2$; $D=D_1+D_2$, such that KN_1/D_1, KN_2/D_2 are each realizable transfer functions of lower degree than $A(p)$ and subsequent decomposition of the new numerators and denominators N_1, N_2, D_1, D_2, etc.

Economy of elements during network synthesis is accomplished by making a suitable choice of $F(p)$ and of the decompositions of numerator and denominator at each stage of the reduction process. With regard to the decomposition, two specializations are relevant here. (A) One useful method is to arrange the decomposition so as to obtain common factors in the numerator and denominator of the reduced transfer function. An extreme example of this technique would be one in which either $N_1=D_1$ or $N_2=D_2$. (B) Another simplification is always possible whenever the degree of the numerator is less than that of the denominator. It consists in choosing $N_1=0$, $N_2=N$. Similarly, if the numerator has a zero constant term, we may choose $N_1=N$, $N_2=0$. This special economy technique may require a decreased gain constant K, whereas our general synthesis procedure always realizes the transfer function with any preassigned K up to its maximum value.

These methods are applied to Weinberg's illustrative example to yield the following network of 25 elements. The maximum possible gain constant, $K=3.14\times10^4$, is realized. This compares to 26 elements and a gain of 1.48×10^4 given by Weinberg's network. Both networks are of similar structure. In our network, the values of the elements in ohms and farads are: $C_1=4.89\times10^{-10}$, $C_2=3.14\times10^{-8}$, $C_3=1.31\times10^{-6}$, $C_4=4.87\times10^{-5}$, $C_5=1.23\times10^{-3}$, $C_6=4.71\times10^{-2}$, $C_7=1.60\times10^{-1}$, $C_8=1.21\times10^{-1}$, $C_9=4.09$, $C_{10}=1.03\times10^2$, $C_{11}=1.03\times10^2$, $C_{12}=5.78\times10$, $C_{13}=1.19\times10^2$, $R_1=2.91\times10^4$, $R_2=4.41\times10^4$, $R_3=1.08\times10^5$, $R_4=3.16\times10^5$, $R_5=1.27\times10^6$, $R_6=4.67$, $R_7=1.14$, $R_8=5.20$, $R_9=1.01\times10^{-1}$, $R_{10}=1.74\times10^{-3}$, $R_{11}=6.13\times10^{-3}$, $R_{12}=4.25\times10^{-6}$.

We may identify various portions of the network with the element saving procedures which are used in their synthesis as follows (all details are omitted): The ladder network going from R_6 to the output results from the repeated application of (B) until a fourth-degree transfer function is obtained. The polynomial $F(p)$ has been chosen so that a common factor $(p+5.5)$ may be divided out of the transfer function, thereby reducing it to cubic, and the elements R_7, C_7 result from taking account of this common factor. At this point, (A) is applied to decompose the numerator and denominator of this cubic transfer function so that N_1 and D_1 have a common factor p and $N_2=D_2$. The element R_8 takes account of the last equation, while the remainder of the network realizes N_1/D_1. Further simplification of N_1 and D_1, resulting in fewer elements in the network may be possible but entails considerable computation.

[1] L. Weinberg, J. Appl. Phys. **24**, 207–216 (1953).
[2] L. Weinberg, Technical Report No. 201, Research Laboratory of Electronics, M.I.T. (1951).
[3] E. A. Guillemin J. Math. Phys. **28**, 22–42 (1949).
[4] A. Fialkow and I. Gerst, Bull. Am. Math. Soc. **57**, 182–183 (1951).
[5] A. Fialkow and I. Gerst, Quart. Appl. Math. **10**, 113–127 (1952).
[6] A. Fialkow, *Symposium on Modern Network Synthesis* (Polytechnic Institute of Brooklyn, 1952), pp. 50–65.
[7] G. Polya and G. Szegö, *Aufgaben und Lehrsätze aus der Analysis* (Dover Publications, New York, 1945), Vol. 2, p. 73, Ex. 190.

Further Discussion on "Synthesis of Transfer Functions with Poles Restricted to the Negative Real Axis"

LOUIS WEINBERG
Hughes Aircraft Company Research and Development Laboratories, Culver City, California
(Received September 28, 1953)

WE wish to thank Dr. Fialkow and Dr. Gerst for their comments on our paper. There are two main points raised in their letter. We will discuss them briefly.

First the question of surplus factors. In using the method we were attempting to show heuristically and with a minimum of mathematical proof that the basic Guillemin procedure[1] is completely general in its application, that is, it can realize the most general type of *RC* transfer function characteristic of the grounded to terminal-pair network. It is interesting to learn that Fialkow and Gerst also used surplus factors to eliminate negative coefficients and were perhaps led to this technique by the proofs given long ago by Meissner[2] and Poincaré.[3] When we formulated our technique and indicated a proof, we were not aware of their work. However, it is felt that the use of surplus factors for similar purposes is well established and almost common knowledge among many students of synthesis so that the proofs of mathematicians of the caliber of Meissner and Poincaré are not actually necessary to suggest the technique. Bode,[4] for example, employs surplus factors for the conversion of a nonminimum phase transfer impedance to a minimum phase one plus an all-pass network and also finds the technique useful in simplifying the basic structures necessary for the realization of a general

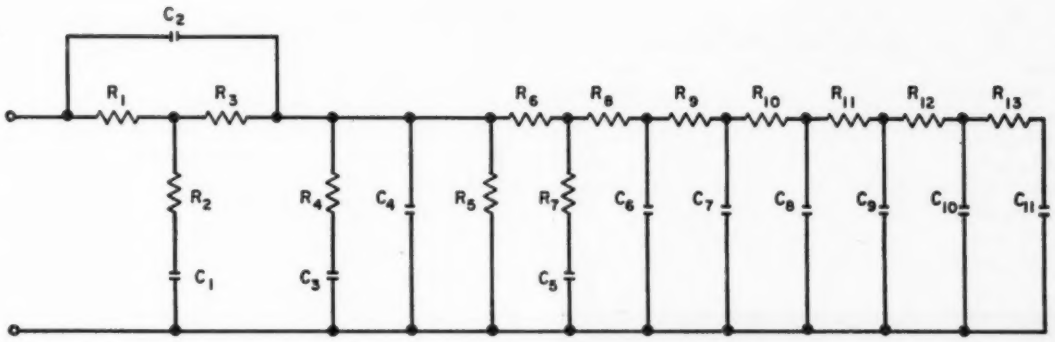

FIG. 1. Form of network realizing the given transfer function.

transfer function. Our use can be looked upon as merely a logical extension of Bode's.

In the foregoing we have used the phrase *general transfer function*. It should perhaps be pointed out that our use of the term differs from that of Fialkow and Gerst. We were attempting, as was Guillemin, to realize the general transfer function to within a constant multiplier. We were not concerned with maximizing this constant. Others have considered this problem, however, and Bower and Ordung[5] have demonstrated the maximum gain possible for a balanced *RC* network, followed by Fialkow and Gerst,[6-9] who extended the results to all grounded and ungrounded four-terminal *RC* networks.

The second major point raised by Fialkow and Gerst is the number of elements used in our illustrative example. We used 26 elements. They feel it significant to demonstrate that, at the cost of increased computation, they can achieve a network containing only 25 elements. They thus save 1 element. This saving would perhaps be significant if we had claimed that a network of 26 elements was an absolute minimum. But no such claim was made. They further state that "fewer elements in the network may be possible but (further simplification) entails considerable computation." Surely they are aware that there are procedures[10,11] in the literature which can with much less computation yield a network with a smaller number of elements, and that the required number may often be predicted almost at the start.

The illustrative example was intended to show a general technique for handling transfer functions with *more than one* pair of complex zeros. If we were interested in conserving even more elements in this *particular* example, since it contains only one pair of complex zeros, we would use a simpler network than paralleled ladders. Guillemin[12] teaches a procedure for realizing a transfer function with one pair of complex zeros and one finite pole as a bridged-tee network, and this could have been used for the illustrative example. Using our partitioning method, we now obtain in a straightforward manner and without much computation a network containing only 24 elements. For conveniences the form of network is shown in Fig. 1 without element values.

As a concluding remark, lest one obtain a wrong impression, it should be pointed out that no amount of additional computation can continue to decrease significantly the required number of elements, a network of only 20 elements, for example, being impossible.

[1] E. A. Guillemin, J. Math. Phys. **28**, 22–42 (1949).
[2] E. Meissner, Math. Ann. **70**, 223–235 (1911).
[3] H. Poincaré, Compt. rend. **97**, 1418–1419 (1883).
[4] H. W. Bode, *Network Analysis and Feedback Amplifier Design* (D. Van Nostrand Company, Inc., New York, 1945), pp. 236–237, 258–260.
[5] J. L. Bower and P. F. Ordung, Proc. Inst. Radio Engrs. **38**, 263–269 (1950).
[6] A. Fialkow and I. Gerst, Bull. Am. Math. Soc. **57**, 182–183 (1951).
[7] A. Fialkow and I. Gerst, Quart. Appl. Math. **10**, 113–127 (1952).
[8] A. Fialkow, Proceedings of the Symposium on Modern Network Synthesis, Polytechnic Institute of Brooklyn, 50–65, (1952).
[9] A. D. Fialkow and Irving Gerst, Proc. Inst. Radio Engrs. **41**, 392–395 (1953).
[10] Ordung, Hopkins, Krauss, and Sparrow, Proc. Inst. Radio Engrs., **40**, 1717–1723 (1952).
[11] B. J. Dasher, "Synthesis of *RC* transfer functions as unbalanced two terminal-pair networks," Technical Report No. 215, Research Lab. of Electronics, M.I.T. (November 20, 1951).
[12] E. A. Guillemin, "Notes for network synthesis course," Mass. Inst. Technol. (January–June, 1949, unpublished).

Electron Shadowgraphs and Afterglow Pictures of Gas Jets at Low Densities

A. E. GRÜN, E. SCHOPPER, AND B. SCHUMACHER
Hochspannungslaboratorium Hechingen and Technische Hochschule, Stuttgart, Germany
(Received May 14, 1953)

RECENTLY we have described an improved method of shooting corpuscular beams of high-current density and of low-particle energy from the vacuum into gases through a set of uncovered holes, which we called *dynamische Druckstufenstrecken*.[1,2]

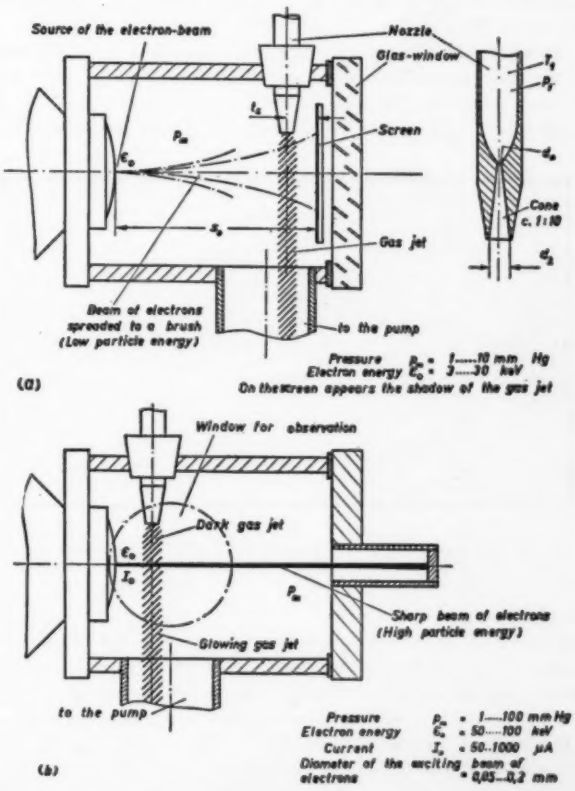

FIG. 1. Experimental arrangment for the observation of gas jets at low densities. (a) Electron shadowgraphs. (b) Afterglow pictures.

A parallel beam of electrons entering the gas in this way will become diffuse by scattering and absorption processes [see Fig. 1(a)] forming a more or less extended brush, according to the density of the gas and the energy of the electrons, respectively. A screen at a certain distance s_0 as shown in [Fig. 1(a)] is brightened over a large area.

Local variations of the density of the gas in the neighborhood of the screen, which are changing the scattering and absorption of the electrons, may be observed on it as shadows.

This supplies a convenient method of visualizing gas jets, which is useful especially in the region of low pressures on account

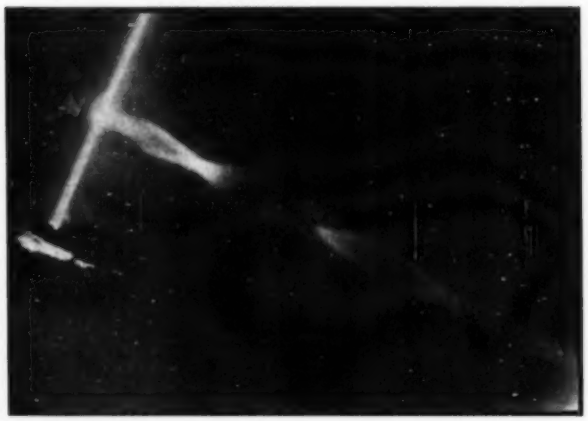

FIG. 2. Glowing gas beam of N_2-Ar excited by 50-kev electrons [Fig. 1(b)]. $p_1=3$ at $p_m=2$-mm Hg ($f=35$ mm, 1:3.5; exposure, 2 min).

of the failure of the well-known optical methods. It is applicable, as shown by one of us in a more detailed paper[3] in the region of 30 mm to 10^{-3} mm Hg.

Another possibility of making visible such jets of gas consists in the excitation of the gas in a small defined volume by a well-focused beam of electrons of high energy traversing the jet [Fig. 1(b)]. In a gas of a sufficiently long time of decay of the

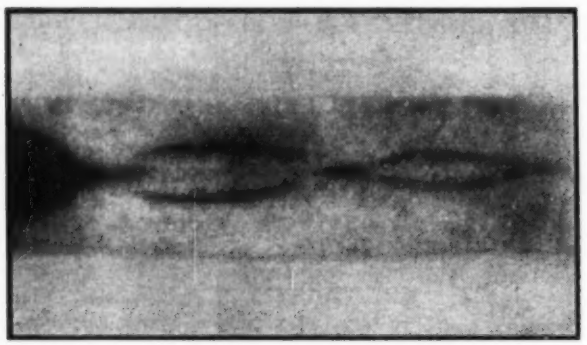

FIG. 3. Shadowgraphs of an N_2 gas beam emerging through a Laval nozzle. $p_1=4$ at $p_m=3.0$-mm Hg. $T_1=300°$K. $o=23$ kev. Nozzle: $d_0=0.3$ mm. $d_1=2.1$ mm. $l_2=11$ mm.

afterglow, the jet will be visible over a certain length of its path, regions of higher density appearing brighter. Figure 2 shows a luminescent jet emerging through a Laval nozzle similar to that of Fig. 3, consisting of a mixture of argon and nitrogen gas.

It is obvious that the latter method will also supply information on the mechanism of the afterglow itself.

[1] B. Schumacher, Optik **10**, 116, (1953).
[2] E. Schopper and B. Schumacher, Z. Naturforsch. **6**, 700 (1951).
[3] B. Schumacher, Ann. Physik (to be published).

Erratum: A Nonreciprocal Microwave Component

[J. Appl. Phys. **24**, 816 (1953)]

M. L. KALES, H. N. CHAIT, AND N. G. SAKIOTIS
Antenna Research Branch, Radio Division I, Naval Research Laboratory, Washington 25, D. C.

IN the equation for the propagation constant (on page 817) a factor $\mu_1\mu_2K_1$ has been omitted from the last term. The corrected equation should read

$$\tan K_2 l[\mu_2^2K_1^2-\mu_1^2\{K_2^2+(\beta\mu'/\mu)^2\}\tan K_1 d\tan K_1 d']$$
$$+\mu_1\mu_2K_1K_2[\tan K_1 d+\tan K_1 d']$$
$$-\mu_1\mu_2K_1\beta\mu'/\mu\tan K_2 l[\tan K_1 d-\tan K_1 d']=0.$$

Radiation from a Line Source Adjacent to a Conducting Half Plane*

JAMES R. WAIT
Radio Physics Laboratory, Defence Research Board, Ottawa, Canada
(Received June 8, 1953)

IN a recent interesting paper by R. F. Harrington,[1] the problem of a line source of electric current adjacent to a conducting half-plane was considered. The solution was obtained by a transform method, and the final expression for the field was given in the form of a contour integral. This integral was evaluated by numberical means for a special case.

It is the purpose of this note to show that an alternative method can be employed to solve this problem and obtain field expressions in terms of tabulated functions. The solution is outlined here.

The conducting half-plane is defined by $\phi=0$ with respect to a cylindrical coordinate system (ρ, ϕ, z). The line source of strength I amp varying as $\exp(i\omega t)$, is parallel to the edge of the plane (i.e., the z axis) and situated at ρ_0, ϕ_0. The resultant electric field E_z at (ρ, ϕ) is a solution of the wave equation so it must be of the form

$$Z_n(\beta\rho)e^{\pm in\phi},$$

where Z_n is a Bessel function of order n and where $\beta=2\pi/\lambda$ and λ is the wavelength. For the region $(\rho<\rho_0$, the solution, to remain finite, must contain only the Bessel function $J_n(\beta\rho)$ and for the region $\rho>\rho_0$ the Hankel function $H_n^2(\beta\rho)$ is appropriate to assure outgoing waves at infinity. The boundary conditions are that $E_z=0$ is zero at $\phi=0$ and $\phi=2\pi$, which requires that $n=m/2$ where m is an integer. The solutions are then given by

$$E_z=\sum_1^\infty A_m J_{m/2}(\beta\rho)H_{m/2}^2(\beta\rho_0)\sin\frac{n}{2}\phi \text{ for } \rho<\rho_0, \quad (1a)$$

and

$$E_z=\sum_1^\infty A_m J_{m/2}(\beta\rho_0)H_{m/2}^2(\beta\rho)\sin\frac{m}{2}\phi \text{ for } \rho>\rho_0. \quad (1b)$$

The coefficient A_m is now to be determined from the nature of the source. The magnetic field component H_ρ is given by

$$H_\rho=-\frac{1}{i\mu\omega\rho}\frac{\partial E_z}{\partial\phi},$$

and for $\rho=\rho_0$, and, if we let $\beta\rho_0\ll1$, it is seen that

$$H_\rho=-\frac{1}{i\mu\omega\rho_0}\sum_1^\infty A_m\frac{i}{\pi}\cos\frac{m}{2}\phi.$$

Now, the magnetic field H_ρ at $\rho=\rho_0$ is given by

$$H_\rho=\frac{I}{2\pi(\phi_0-\phi)\rho} \text{ as } \phi \text{ tends to } \phi_0.$$

If we equate these two expressions for H_ρ, it is easily seen from orthogonality considerations that

$$A_m=-\frac{\mu\omega I}{2}\sin\frac{m}{2}\phi_0.$$

If we substitute this expression into Eqs. (1a) and (1b), the final solution for the problem in completely specified in terms of Bessel functions of half integral order.[2]

The corresponding solution for the line source of magnetic current M is obtained in a smaller manner. The magnetic field is in the z direction and is given by

$$H_z^* = \frac{eM}{2\mu} \sum_{m=0}^{\infty} c_m J_{m/2}(\beta\rho) H_{m/2}^2(\beta\rho_0) \cos\frac{m}{2}\phi \cos\frac{m}{2}\phi_0 \text{ for } \rho<\rho_0 \quad (3a)$$

and

$$H_z^* = \frac{eM}{2\mu} \sum_{m=0}^{\infty} c_m J_{m/2}(\beta\rho_0) H_{m/2}^2(\beta\rho) \cos\frac{m}{2}\phi \cos\frac{m}{2}\phi_0 \text{ for } \rho>\rho_0, \quad (3b)$$

where $c_m=\frac{1}{2}$ for $m=0$ and $c_m=1$ for $m\neq 0$.

Of particular interest are the fields in the radiation zone such that $\beta\rho\gg 1$. The Hankel function can then be represented by the first term of its asymptotic series so that for the electric current source

$$E_z = -\frac{i\mu\omega I}{(2\pi\rho)^{\frac{1}{2}}} e^{-i(\beta\rho+\pi/4)} F(\phi), \quad (4a)$$

where

$$F(\phi) = \sum_{1}^{\infty} e^{im\pi/4} J_{m/2}(\beta\rho_0) \sin\frac{m\phi}{2} \sin\frac{m\phi_0}{2},$$

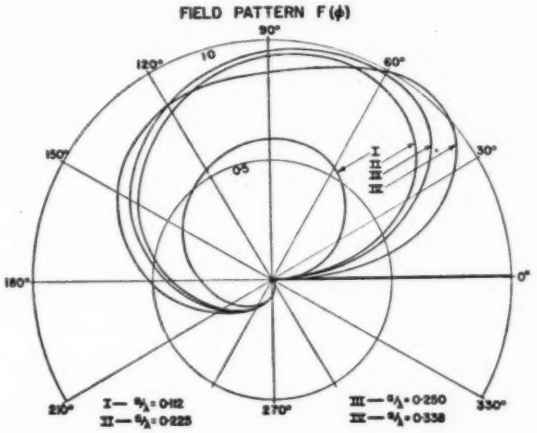

FIG. 1. The far field pattern of a line source of electric current adjacent to a conducting half plane.

and for the magnetic current source

$$H_z^* = \frac{eM}{2(2\pi\rho)^{\frac{1}{2}}} e^{-i(\beta\rho+\pi/4)} F^*(\phi), \quad (4b)$$

where

$$F^*(\phi) = \sum_{0}^{\infty} c_m e^{im\pi/4} J_{m/2}(\beta\rho_0) \cos\frac{m\phi}{2} \cos\frac{m\phi_0}{2}.$$

The magnitude of the functions $F(\phi)$ and $F^*(\phi)$ characterize the shape of the radiation patterns for the electric and magnetic current sources respectively which are adjacent to the conducting plane.

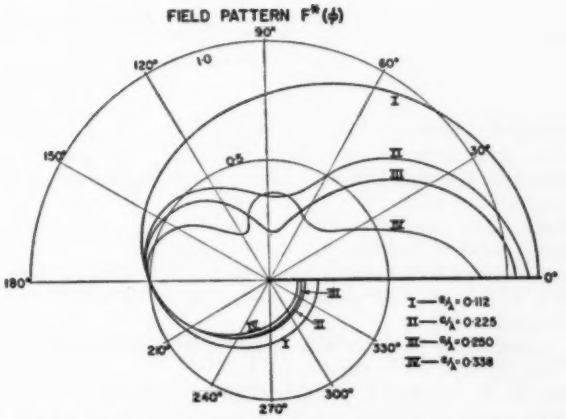

FIG. 2. The far field pattern of a line source of magnetic current adjacent to a conducting half-plane.

As an illustrative example these patterns are plotted in Figs. 1 and 2 for the case where the line source is a distance a from the half-plane and a distance a back from the edge (i.e., $\phi_0=45°$, $\rho_0=2^{\frac{1}{2}}a$). Several values of the ratio a/λ are chosen. The calculated pattern of the electric current source $F(\phi)$ for $a/\lambda=\frac{1}{4}$ agrees with Harrington's result.

As Harrington points out, the pattern $F(\phi)$ is also the far-zone pattern in the equatorial plane (i.e., $z=0$) of an electric dipole situated at $(\rho_0, \phi_0, 0)$ and parallel to the edge of the half-plane. Similarly, the pattern $F^*(\phi)$ is the corresponding pattern in the equatorial plane for a magnetic dipole at $(\rho_0, \phi_0, 0)$ whose axis is parallel to the edge of the half plane.

I would like to thank Mr. A. P. Dempster for his assistance in the numerical calculations.

* Work carried out under D.R.B. Project No. D-48-95-11-14.

[1] R. F. Harrington, J. Appl. Phys. **24**, 547 (1953).

[2] E. Jahnke and F. Emde, *Tables of Functions* (Dover Publications, New York, 1945), fourth edition, p. 154.

Errata: Epicentral Displacement Caused by Elastic Waves in an Infinite Slab

[J. Appl. Phys. **24**, 1240–1246 (1953)]

ALAN G. MENCHER
University of California, Los Angeles, California

I WOULD like to call attention to the following typographical errors in my paper.

In Eq. (12), $\langle\rho\langle\theta\rangle A\rangle$ should be replaced by $\langle\rho\langle A_\theta\rangle\rangle$. Following Eq. (30), $4x/9$ and $4/9$ should in each case be surrounded by parentheses.

Author Index to Volume 24

References with (L) are to Letters to the Editor

Abramovitz, Stanley. Experiments in hydrodynamic lubrication using water as a lubricant—1521(L)
Ackerman, Eugene. Pressure threshold for biologically active cavitation—1371
Affleck, J. H. (see Eisenstein, A.)—631
Akeley, Edward (see Swihart, James)—640
Alers, George A. Internal friction of quartz—324
Allen, William A. Free surface motion induced by shock waves in steel—1180
—— **and Earle B. Mayfield.** Time-resolved spectroscopy of ultraspeed pellet luminosity—131
Alley, R. E., Jr., and F. J. Schnettler. Effect of cross section area and compression upon the relaxation in permeability for toroidal samples of ferrites—1524(L)
Alpert, D. New developments in the production and measurement of ultra high vacuum—860
Amakasu, K. and T. Imai. Emission decay phenomena due to the contaminated anode—107(L)
—— **and T. Imai.** Errata: Emission decay phenomena due to the contaminated anode—817
Anders, F. J. (see Hoffman, R. W.)—231(L)
Archard, J. F. Contact and rubbing of flat surfaces—981
Armstrong, H. L. (see Simpson, J. H.)—25
—— Thermal effects in point contact rectifiers—1332(L)
Arnold, S. M. (see Koonce, S. Eloise)—365(L)
Arvin, Martin J. Thermoelectric effects in molybdenum disilicide—498(L)
Averbach, B. L. (see Rudman, P. S.)—365(L)

Bachman, C. H., G. L. Hall, and P. A. Silberg. Positive and negative ions in cathode-ray tubes—427
Baird, David C. and Willard S. Boyle. Method of determining electrical resistivities at low temperatures—958(L)
Baker, G. S., L. M. Slifkin, and J. W. Marx. Germanium under ultrasonic stress. I. Anelastic effects—1331(L)
——, **L. M. Slifkin, and J. W. Marx.** Germanium under ultrasonic stress. II. Dynamic yield point—1331(L)
Barnes, George (see Dyke, W. P.)—570
Bartell, L. S. and L. O. Brockway. Calibration of photographic emulsions for electron diffraction investigations—656
—— **and L. O. Brockway.** Reply to comment on "The calibration of photographic emulsions for electron diffraction investigations"—1523(L)
Bateman, J. B. (see Hartman, R. E.)—90
Beattie, H. J., Jr. Electron compounds of transition elements—1322
Bekefi, G. Diffraction of electromagnetic waves by an aperture in a large screen—1123
Belcher, H. V. (see Bestul, A. B.)—696
—— (see Bestul, A. B.)—1011
Belove, Charles. Tolerance coefficients for R-C networks—745
Belmont, E. (see Lehovec, K.)—1482
Bennett, Herbert S. Electromagnetic transmission characteristics of the two-dimensional lattice medium—785
Bergdolt, V. E. (see Giese, J. H.)—1389
Bergen, J. T. and W. Patterson, Jr. Anomalous viscous flow at very low rate of shear and small shearing stress—712
Berger, Erich R. Comments on "The Dirac delta function and the summation of Fourier series"—951(L)
Berman, Abraham S. Laminar flow in channels with porous walls—1232
Berry, Chester R. Effect of internal strains on linear expansion, x-ray lattice constant, and density of crystals—658(L)
Bestul, A. B. and H. V. Belcher. Degradation of polyisobutylenes on shearing in solution—1011
—— **and H. V. Belcher.** Temperature coefficients of non-Newtonian viscosity at fixed shearing stress and at fixed rate of shear—696
Bever, M. B., E. R. Marshall, and L. B. Ticknor. Energy stored in metal chips during orthogonal cutting—1176
Bever, Renate S. Diffusion of barium in an oxide-coated cathode—1008
Binford, F. T. (see Rupp, A. F.)—1069
Birdsall, Charles K. and John R. Whinnery. Waves in an electron stream with general admittance walls—314
Birkhoff, Garrett. Formation of vortex streets—98
Bishop, M. E. and S. H. Liebson. Growth of cadmium sulfide crystals—660(L); erratum—963
Blachman, Nelson M. Bounds for entropy—1340(L)
—— Output signal-to-noise ratio of a power-law device—783
Bohm, David (see Coleman, John H.)—497(L)
Borie, B. S., Jr. (see Jetter, L. K.)—532
Bowers, R. C., W. C. Clinton, and W. A. Zisman. Effect of halogenation on frictional properties of plastics—1066(L)
Bowman, F. E. (see Eggleston, R. R.)—229(L)
Boyle, Willard S. (see Baird, David C.)—958(L)
Bragg, J. K. (see Sharbaugh, A. H.)—814(L)
Brand, Frank A. (see Jacobs, Harold)—1340(L)
—— (see Jacobs, Harold)—1410(L)
Bridgman, P. W. Effect of pressure on the tensile properties of several metals and other materials—560
—— **and I. Šimon.** Effects of very high pressures on glass—405
Briggs, Lyman J. Limiting negative pressure of mercury in pyrex glass—488
Brillouin, L. Negentropy principle of information—1152
Brock, Paul. Nature of solutions of a Rayleigh-type forced vibration equation with a large coefficient of damping—1004
Brockway, L. O. (see Bartell, L. S.)—656
—— (see Bartell, L. S.)—1523(L)
Broder, J. (see Lehovec, K.)—513
Brown, Sanborn C. (see Gould, Lawrence)—1053
Bueche, F. Bulk viscosity of the system polystyrene—diethyl benzene—423
Burns, J. W. (see Smith, Charles S.)—15
Burwell, J. T. and E. Rabinowicz. Nature of the coefficient of friction—136

Campbell, R. (see Franklin, A. D.)—1040
Carhart, Richard R. Reflection of sound in the ocean from temperature changes—929
Carlin, Herbert J. and R. La Rosa. On the synthesis of reactance 4-poles—1336(L)
Carlson, J. F. and T. J. Hendrickson. Variational methods for problems in resistance—1462
Chait, H. N. (see Kales, M. L.)—816(L); erratum—1529
——, **N. G. Sakiotis, and R. E. Martin.** Reduction of the loss in ferrite materials in the microwave region—109(L)
Chaney, Jesse Gerald. Free space radiation impedance of rhombic antenna—536
—— Mutual impedance of rhombic antennas spaced in tandem—751
—— Simplification for mutual impedance of certain antennas—747
Chatterjee, J. S. Radiation field of a conical helix—550
Chertock, George. Flexural response of a submerged solid to a pulsating gas bubble—192
Chipman, D. L., B. E. Warren, and G. J. Dienes. X-ray measurements of radiation damage in black phosphorus—1251(L)
Clark, M. A. (see Montgomery, H. C.)—1337(L)
Clinton, W. C. (see Bowers, R. C.)—1066(L)

Coffin, Frances Dunkle and Sidney L. Simon. Electromotive force developed by creeping zinc crystal—1333(L)
—— **and Andrew L. Weiman.** Surface effect and the creep of zinc single crystals: I. Creep characteristics of clean and oxide-coated crystals—282
Cohn, Seymour B. Experimental verification of the metal-strip delay-lens theory—839
Cole, H. Approximate elastic spectrum of acoustic waves in AgCl from x-ray scattering—482
Coleman, John H. and David Bohm. Method for increasing the electrical resistivity of insulators under ionizing radiation—497(L)
Colli, Laura and Maria Teresa de Leonardis. Measurement of the drift velocity of electrons in the electrical field in argon-alcohol mixtures—255
Comer, J. J. (see Hamm, F. A.)—1495
Cosslett, V. E. and W. C. Nixon. X-ray shadow microscope—616
Cragg, L. H. (see Sharman, L. J.)—703
Crittenden, E. C. (see Hoffman, R. W.)—231(L)
Crowe, R. W. (see Sharbaugh, A. H.)—814(L)
Crowell, C. R. (see Redhead, P. A.)—331
Cullity, B. D. and Carl A. Julien. Effect of a Soller slit on the diffraction of x-rays by deformed crystals—541
Currie, Malcolm R. Utilization of degenerate modes in a spherical cavity—998
Curtis, C. W. (see Emrich, R. J.)—360

Davenport, W. B., Jr. Signal-to-noise ratios in band-pass limiters—720
Davis, Luther, Jr., and Lawrence G. Rubin. Some dielectric properties of barium-strontium titanate ceramics at 3000 megacycles—1194
de Hoop, A. T. Propagation constant in gentle circular bends in rectangular wave guides—matrix theory—1325
de Josselin de Jong, G. Consolidation around pore pressure meters—922
de Leonardis, Maria Teresa (see Colli, Laura)—255
Deal, W. E. (see Shreffler, R. G.)—44
Deschamps, Georges A. Determination of reflection coefficients and insertion loss of a wave-guide junction—1046
Dienes, G. J. Activation energy for viscous flow and short-range order—779
—— Effects of nuclear radiation on the mechanical properties of solids—666
—— (see Chipman, D. L.)—1251(L)
Dodd, Edward E. Statistics of liquid spray and dust electrification by the Hopper and Laby method—73
Dolan, W. W. (see Dyke, W. P.)—570
Donoghue, J. J. (see McClelland, J. D.)—963(L)
Doolittle, Arthur K. Comment on the temperature dependence of the viscosity of liquids—1067(L)
Drimmer, Bernard E. Average temperatures by parallel-connected thermocouples—225(L)
Ducoffe, Arnold L. Pressure response in supersonic wind tunnel pressure instrumentation—1343
Duncan, D. B. Response of linear time-dependent systems to random inputs—609
—— Response of undamped systems to noise—1252(L)
Duwez, Pol. Effect of the rate of cooling on the allotropic transformation temperatures of uranium—152
Dyke, W. P., J. K. Trolan, W. W. Dolan, and George Barnes. Field emitter: Fabrication, microscopy, and electric field calculations—570

Eckart, Carl. Generation of wind waves on a water surface—1485
Eggleston, R. R. and F. E. Bowman. Radiation damage of beta-brass—229(L)
Eisenstein, A., H. John, and J. H. Affleck. Double activators in oxide cathode base alloys—631
Ellinger, Joseph P. (see Fischer, Robert B.)—1051
Ellis, R. C., Jr., and S. P. Wolsky. New etches for germanium—1411(L)
Elrod, Harold (see Krieger, Irvin M.)—134
Emerson, R. C. First probability densities for receivers with square law detectors—1168
Emrich, Raymond J. (see Laponsky, Alfred B.)—1383
Emrich, R. J. and C. W. Curtis. Attenuation in the shock tube—360
Eshelby, J. D. Geometrical and apparent x-ray expansions of a crystal containing lattice defects—1249(L)
—— Screw dislocations in thin rods—176
Evans, Ronald T. (see Ludeke, Carl A.)—119

Felsen, L. B. and N. Marcuvitz. Slot coupling of rectangular and spherical wave guides—755
Ferry, John D. (see Fitzgerald, Edwin R.)—650
—— (see Grandine, Lester D., Jr.)—679
——, **Lester D. Grandine, Jr., and Edwin R. Fitzgerald.** Relaxation distribution function of polyisobutylene in the transition from rubber-like to glass-like behavior—911
Fett, Gilbert H. (see Kang, Chi Lung)—38
Fialkow, A. D. and Irving Gerst. Discussion on "Synthesis of transfer functions with poles restricted to the negative real axis"—1525(L)
Fine, Morris E. Elasticity and thermal expansion of germanium between −195 and 275°C—338
Finn, R. K. Determination of the drag on a cylinder at low Reynolds numbers—771
—— Determination of the drag on a cylinder at low Reynolds numbers—771; erratum—1050
Fischer, Robert B. and Joseph P. Ellinger. Replica technique in the study of chemical precipitation processes—1051
Fitzgerald, Edwin R. (see Ferry, John D.)—911
——, **Lester D. Grandine, Jr., and John D. Ferry.** Dynamic mechanical properties of polyisobutylene—650
Flammer, Carson. Vector wave function solution of the diffraction of electromagnetic waves by circular disks and apertures. I. Oblate spheroidal vector wave functions—1218
—— Vector wave function solution of the diffraction of electromagnetic waves by circular disks and apertures. II. The diffraction problems—1224
Flynn, P. A. (see Rudman, P. S.)—365(L)
Fowler, C. M. (see Kruse, H. W.)—1037
Franklin, A. D., R. Campbell, and J. Weinman. Measurement of particle size of fine ferromagnetic powders—1040
Fricke, Hugo. Electric permittivity of a dilute suspension of membrane-covered ellipsoids—644
Friedman, M. B. (see Ludloff, H. F.)—1247(L)
Fusfeld, Herbert I. Effect of cold work and anneal on resistivity of alpha brass—1062(L)

Geisler, A. H. (see Martin, D. L.)—498(L)
Gemant, Andrew. Tracer diffusion in the ground in radioactive leak location—93
Gerst, Irving (see Fialkow, A. D.)—1525(L)
Giese, J. H. and V. E. Bergdolt. Interferometric studies of supersonic flows about truncated cones—1389
Glaser, Frank W., David Moskowitz, and Benjamin Post. Investigation of boron carbide—731
Gold, Louis. Method of time-free solutions for radioactive decay and radionuclide production—88
Goodman, L. E. and J. G. Sutherland. Elastoplastic stress-optical effect in silver chloride single crystals—577
Gould, Lawrence and Sanborn C. Brown. Methods of measuring the properties of ionized gases at high frequencies. IV. A null method of measuring the discharge admittance—1053
Grandine, Lester D., Jr. (see Ferry, John D.)—911
—— (see Fitzgerald, Edwin R.)—650

—— **and John D. Ferry.** Dynamic mechanical properties of the system polystyrene-decalin—679
Green, M. (see Keck, P. H.)—1479
Green, T. D. (see Hartman, R. E.)—90
Grisdale, R. O. Formation of black carbon—1082
—— The properties of carbon contacts—1288
Grossweiner, Leonard I. A note on the analysis of first-order glow curves—1306
Groves, Willice E. Transmission of electromagnetic waves through pairs of parallel wire grids—845
Grün, A. E., E. Schopper, and B. Schumacher. Electron-shadowgraphs and afterglow pictures of gas jets at low densities—1527(L)
Gumowski, Igor. Summation of slowly converging series—1068(L); erratum—1330
Gutmann, F. and L. M. Simmons. Further note on the temperature dependence of the viscosity of liquids—1067(L)

Hadley, C. P. Thermionic emission from oxide-coated tungsten filaments—49
Hall, G. L. (see Bachman, C. H.)—427
Hall, Newman A. Nonequilibrium thermodynamics—819
Hamm, F. A. and J. J. Comer. Electron microscopy of photographic grains. Specimen preparation techniques and applications—1495
—— (see Hoerlin, H.)—1514
Hannay, N. B. (see MacNair, D.)—1335(L)
Harrington, Roger F. Current element near the edge of a conducting half-plane—547
—— Propagation along a slotted cylinder—1366
Harris, Lawrence A. Instabilities in the smooth-anode cylindrical magnetron—1335 (erratum)
Hart, Edward W. Magnetic analog for the interaction of dislocation loops—224(L)
Hartman, R. E., T. D. Green, J. B. Bateman, C. A. Senseney, and G. E. Hess. Preparation of uniformly dispersed specimens of particulate matter for electron microscopy—90
Hayashi, Chihiro. Forced oscillations with nonlinear restoring force—198
—— Stability investigation of the nonlinear periodic oscillations—344
—— Subharmonic oscillations in nonlinear systems—521
Hendrickson, T. J. (see Carlson, J. F.)—1462
Henkels, H. W. and J. Maczuk. Electrical properties of liquid selenium I—1056
Hertel, Paul, Jr., A. W. Straiton, and C. W. Tolbert. Dielectric constant measurements at 8.6-mm wavelength—956(L)
Hess, G. E. (see Hartman, R. E.)—90
Hewitt, W. H. (see Mason, W. P.)—166
Hickey, John S., Jr. Heat transfer at high-power densities—1312
Higgins, T. P. and A. W. Straiton. Characteristics of an elliptical electromagnetic resonant cavity operating in the TE_{111} mode—1297
Ho, Kuo-Chu and Robert J. Moon. Electrostatic potential plotting for use in electron optical systems—1186
Hoerlin, H. and F. A. Hamm. Electron microscopical studies of the latent image obtained by exposures to alpha particles, x-rays, and light—1514
Hoffman, R. W., F. J. Anders, and E. C. Crittenden. Evidence for the collapse of lattice vacancy aggregates to form dislocation rings—231(L)
Hogg, D. C. Electromagnetic field in the plane of a circular aperture due to incident spherical waves—110(L)
Holbrook, James G. Null characteristics of the rotating Adcock antenna system—530
Hollway, D. L. (see Murray, C. T.)—110(L)
Hopkins, I. L. On the Ferry reduction and the activation energy for viscous flow—1300
Horiuchi, Kazuo. Surface wave propagation over a coated conduction with small cylindrical curvature in direction of travel—961(L)
Houghton, William J. (see Thornton, J. Kendall)—1374
Howe, R. M. Probe studies of energy distributions and radial potential variations in a low pressure mercury arc—881
Hsiao, C. C. and J. A. Sauer. Effect of biaxial orientation on the ultimate strength and crazing of linear polymers—957(L)
Hufford, George A. Note on wave propagation through an inhomogeneous medium—268
Hutchison, T. S. X-ray line broadening from precipitation in Cu-Fe alloys—813(L)

Ibrahim, Ali K. Rigidity of elasto-viscous liquids—364(L)
Ichijō, Bunjirō. New method of measuring constant and loss angles of semiconductors—307
Ikegawa, Tatsuo (see Okada, Jun)—1249(L)
Imai, T. (see Amakasu, K.)—107(L)
—— (see Amakasu, K.)—817(L)
Isbell, Dwight E. (see Kelly, Joseph M.)—258
Ivey, Henry F. Approximate solutions of the space charge problem for some unusual electrode geometries—1466
—— Space charge limited currents between inclined plane electrodes. Approximate solutions—227(L)

Jackson, C. H. (see Roka, E. G.)—228(L)
Jacob, L. and J. R. Shah. Trajectories in the symmetrical electron lens—1261
Jacobs, Harold, Frank A. Brand, and Wesley Matthei. Forming silicon point contact transistors—1340(L)
——, **Wesley Matthei, and Frank A. Brand.** Enhanced alpha in formed silicon point contact—1410(L)
Jaffe, Joseph H. (see Oppenheim, Uri)—1521(L)
Jardetzky, W. S. Comment on the letter by R. D. Mindlin and T. Kane—499(L)
Jarmotz, Paul (see Pepinsky, Ray)—663(L)
Jetter, L. K. and B. S. Borie, Jr. Method for the quantitative determination of preferred orientation—532
John, H. (see Eisenstein, A.)—631
Julien, Carl A. (see Cullity, B. D.)—541

Kales, M. L. Modes in wave guides containing ferrites—604
——, **H. N. Chait, and N. G. Sakiotis.** Nonreciprocal microwave component—816(L); erratum—1529
Kalra, Surindra N. Force on a shorted ring in a UHF field in a coaxial cavity—1339(L)
Kamel, R. Measurement of the heat of activation for sodium ion diffusion in glass—1308
Kane, T. (see Mindlin, R. D.)—498(L)
Kang, Chi Lung and Gilbert H. Fett. Metrization of phase space and nonlinear servo systems—38
Kanter, I. (see Lee, E. H.)—1115
Kanzaki, Hiroshi. Pure gliding of metal crystals—811(L)
Karal, F. C. Motion of a sphere moving parallel to a plane boundary—147
Karle, J. (see Karle, I. L.)—1522(L)
Karle, I. L. and J. Karle. Comment on "The calibration of photographic emulsions for electron diffraction investigations"—1522(L)
Karush, W. and A. V. Martin. Thermal contraction of a split hollow cylinder—1427
Katz, H. Metal capillary cathodes—597
Kaufman, Irving. High energy bunched beam analyzer—1413(L)
Kaufman, Sol (see Wieder, H. H.)—156
Keck, P. H., M. Green, and M. L. Polk. Shapes of floating liquid zones between solid rods—1479
Keilson, Julian. More exact treatment of the equations describing dielectric relaxation and carrier motion in semiconductors—1198

—— On the diffusion of decaying particles in a radial electric field—1397
Keim, C. P. Enriching stable isotopes electromagnetically—1255
Kelly, Joseph M., Joseph O. Stenoien, and Dwight E. Isbell. Wave-guide measurements in the microwave region on metal powders suspended in paraffin wax—258
Kelly, J. M. and J. O. Stenoien. Effect of particle size on magnetic loss tangent of obstacle type artificial dielectrics—962(L)
Kerner, Edward H. Expansion of fissionable gas as a source of atomic power—815(L)
Kikuchi, Makoto and Tomio Onishi. Thermoelectric study of the electrical forming of germanium rectifiers—162
King, Ronold. Alternative method of solving Hallén's integral equation and its application to antennas near resonance—140
Kirchgessner, W. G. (see Smith, W. S.)—662(L)
Kirschbaum, H. S. Comments on Louis A. Pipes' Letter—661(L)
Klee, C. W. and H. E. Stauss. Sparking potentials between separating contacts—368(L)
Koehler, J. S. (see Weertman, J.)—624
Koenig, J. Frank. On the zeros of polynomials and the degree of stability of linear systems—476
Kohlenberg, Arthur. Exact interpolation of band-limited functions—1432
Koonce, S. Eloise and S. M. Arnold. Growth of metal whiskers—365(L)
Krieger, Irvin M. and Harold Elrod. Direct determination of the flow curves of non-Newtonian fluids. II. Shearing rate in the concentric cylinder viscometer—134
Krishnaji and Prem Swarup. Absorption of microwaves in gases—1525(L)
Kron, Gabriel. Set of principles to interconnect the solutions of physical systems—965
Kruse, H. W., G. P. Mellor, and C. M. Fowler. Beta-ray spectrometer line shapes with tilted sources—1037
Kuczynski, G. C. Some relations between the modulus of rigidity and the surface and sublimation energies—1250(L)
Kuh, Ernest Shiu-jen. Potential analog network synthesis for arbitrary loss functions—897
Kullback, S. Note on information theory—106(L)

Laponsky, Alfred B. and Raymond J. Emrich. Observation of shock formation and growth—1383
LaRocca, Edward W. Note on the stress dependence of the activation energy of the rupture process—1523(L)
La Rosa, R. (see Carlin, Herbert J.)—1336(L)
Leaderman, Herbert and Robert S. Marvin. Dynamic compliance, dynamic modulus, and equivalent Voigt and Maxwell models for polyisobutylene—812(L)
Lee, E. H. and I. Kanter. Wave propagation in finite rods of viscoelastic material—1115
Lehovec, K., J. Rosen, A. MacDonald, and J. Broder. Evaporation of germanium films from a carbon crucible—513
—— **and E. Belmont.** Preparation of *P-N* junctions by surface melting—1482
Levi, Roberto. New dispenser type thermionic cathode—233(L)
Lewin, L. Theory of wave-guide-fed slots radiating into parallel plate regions—232(L)
Liebson, S. H. (see Bishop, M. E.)—660(L); erratum—963
Lien, Roy Harold. Radiation from a horizontal dipole in a semi-infinite dissipative medium—1
Linder, E. G. (see Rappaport, P.)—1110
Lion, K. S. Method of increasing photographic sensitivity by electrical discharges—367(L)
Lo, Y. T. A note on the cylindrical antenna of noncircular cross section—1338(L)
Lowell, Herman H. Response of two-material laminated cylinder to simple harmonic environment temperature change—1473
Ludeke, Carl A. and William Pong. Extinction of predominantly subharmonic oscillations in nonlinear systems—96
—— **and Ronald T. Evans.** Coupling analog for nonlinear systems with more than one degree of freedom—119
—— **and Cohn L. Morrison.** Analog computer elements for solving nonlinear differential equations—243
Ludford, G., H. Polachek, and R. J. Seeger. On unsteady flow of compressible viscous fluids—490
Ludloff, H. F. and M. B. Friedman. Mach reflexion of shocks at arbitrary incidence—1247(L)
Lynch, R. T. (see MacNair, D.)—1335(L)
Lyons, W. James. Viscoelastic properties as functions of the distribution of activation energies—217

McCaig, M. Preferred direction in a magnetically hardened permanent magnet alloy—366(L)
McClelland, J. D. and J. J. Donoghue. Effect of neutron bombardment upon the magnetic susceptibility of several pure oxides—963(L)
McFadden, J. A. Summation of Fourier Series—364(L)
McKeehan, M. and B. E. Warren. X-ray study of cold work in thoriated tungsten—52
McMahon, M. E. (see Shulman, R. G.)—1267
McQuarrie, Malcolm. Time effects in the hysteresis loop of polycrystalline barium titanate—1334(L)
McSkimin, H. J. Measurement of elastic constants at low temperatures by means of ultrasonic waves—data for silicon and germanium single crystals, and for fused silica—988
MacDonald, A. (see Lehovec, K.)—513
MacNair, D., R. T. Lynch, and N. B. Hannay. Molded thermionic cathodes—1335(L)
Mackay, R. Stuart. Interesting nonlinear effects—311
—— Sinusoidal and relaxation oscillations sustained by nonlinear reactances—1163
Maczuk, J. (see Henkels, H. W.)—1056
Marcuvitz, N. (see Felsen, L. B.)—755
Maringer, R. E. Internal friction of molybdenum during tensile deformation—1525(L)
Marshall, E. R. (see Bever, M. B.)—1176
Martin, A. V. (see Karush, W.)—1427
Martin, D. L. and A. H. Geisler. Permanent magnet properties of cobalt-platinum alloys—498(L)
Martin, R. E. (see Chait, H. N.)—109(L)
Marvin, Robert S. (see Leaderman, Herbert)—812(L)
Marx, J. W. (see Baker, G. S.)—1331(L)
—— **and J. M. Sivertsen.** Temperature dependence of the elastic moduli and internal friction of silica and glass—81
Mason, W. P., W. H. Hewitt, and R. F. Wick. Hall effect of modulators and "gyrators" employing magnetic field independent orientations in germanium—166
Matthei, Wesley (see Jacobs, Harold)—1340(L)
—— (see Jacobs, Harold)—1410(L)
Mattson, R. H. and A. van der Ziel. Shot noise in germanium filaments—222(L)
Mayer, Ludwig. Electron optical image of an electron beam—105(L)
Mayfield, Earle B. (see Allen, William A.)—131
Mazenko, J. J. (see Schwertz, F. A.)—1015
Medicus, G. K. Ball of fire discharge with a pronounced current saturation—233(L)
Mellor, G. P. (see Kruse, H. W.)—1037
Mencher, Alan G. Epicentral displacement caused by elastic waves in an infinite slab—1240; erratum—1529
Meyer, H. I. Pore distribution in porous media—510
Meyer, R. (see Pakswer, S.)—501
Middleton, David. Statistical criteria for the detection of pulsed carriers in noise. I—371

—— Statistical criteria for the detection of pulsed carriers in noise. II—379
Mifsud, J. F. (see Nolle, A. W.)—5
Miller, K. S. and R. J. Schwarz. On the interference of pulse trains—1032
Miller, P. H., Jr., and B. R. Russell. Effect of distribution of lattice defects within crystals on linear expansion and x-ray lattice constant—1248(L)
Momma, Sennosuke. Deduction of the maximum torsional stress in a shaft with notches—959(L)
Monahan, James E. Effective length of an electrostatic analyzer—434
Montgomery, D. J. Effect of stiffness and nonuniformity on vibroscopic determination of filament cross-sectional area—1092
Montgomery, H. C. and M. A. Clark. Shot noise in junction transistors—1337(L)
Moon, Robert J. (see Ho, Kuo-Chu)—1186
Mooney, M. Test of the theory of secondary viscoelastic stress—675
Morrison, Cohn L. (see Ludeke, Carl A.)—243
Moskowitz, David (see Glaser, Frank W.)—731
Mott-Smith, H. M. Change of electron temperature in an electron beam—249
Motz, H., W. Thon, and R. N. Whitehurst. Experiments on radiation by fast electron beams—826
Munk, Max M. Gas flow past slender bodies—584
Murray, C. T. and D. L. Hollway. Equipotential plotting, using untreated writing paper—110(L)
Murray, Raymond L. and Lawrence T. Ratner. Electric fields with cyclotron dees—67

Nakayama, Tadayuki (see Yamaguchi, Shigeto)—658(L)
Naughton, John J. Solubility determination of some elemental gases in Pyrex at 1170°C—499(L)
Naumann, Virgil O. (see Wahlin, H. B.)—42
Nixon, W. C. (see Cosslett, V. E.)—616
Nolle, A. W. and J. F. Mifsud. Ultrasonic-wave study of swollen Buna-N rubber—5
Norton, Francis J. Diffusion of D_2 from D_2O through steel—499(L)

Okada, Jun and Tatsuo Ikegawa. Combustion rate of artificial graphites from 700°C to 2000°C in air—1249(L)
Ōkubo, H. Determination of surface stress by means of electroplating—1130
O'Meara, F. E. Reactor simulators—1200
Onishi, Tomio (see Kikuchi, Makoto)—162
Oppenheim, Uri and Joseph H. Jaffe. The resistivity of thin silver films—1521(L)

Pakswer, S. and R. Meyer. Arc drop and deionization time in inert gas thyratrons—501
Parker, E. N. Effect of turbulence on heat transfer in a pile with a liquid reactant—451
Parsons, K. A. Photoelastic studies of quenched cylinders and -spheres—469
Patterson, W., Jr. (see Bergen, J. T.)—712
Paxton, H. W. Initial yield in iron—104(L)
Pearson, John (see Rinehart, John S.)—462
Peebles, Glenn H. Attenuation of gamma rays. I. Transmission values for finite slabs of lead, iron, and the Compton scatterer—1272
—— Attenuation of gamma rays. II. Transmission values for various materials and geometries—1437
Pepinsky, Ray. A modification of R-PAC for interpretation of Patterson maps in x-ray crystal analysis—1520(L)
—— **and Paul Jarmotz.** R-PAC: Analog recorder-playback computer for crystal analysis—663(L)
Philipp, H. R. (see Sparks, I. L.)—453
Philippoff, Wladimir. Mechanical investigations of elastomers in a wide range of frequencies—685
Pierce, J. R. Spatially alternating magnetic fields for focusing low-voltage electron beams—1247(L)
—— **and L. R. Walker.** "Brillouin flow" with thermal velocities—1328
Pipes, Louis A. Correction to "A mathematical analysis of parallel-connected magnetic amplifiers with resistive loads"—661(L)
—— Matrix solution of equations of the Mathieu-Hill type—902
—— Operational analysis of traffic dynamics—274
Polachek, H. (see Ludford, G.)—490
Polk, M. L. (see Keck, P. H.)—1479
Pong, William (see Ludeke, Carl A.)—96
Post, Benjamin (see Glaser, Frank W.)—731
Preston, Glenn W. Equivalence of optimum transducers and sufficient and most efficient statistics—841
—— Theory of prediction of nonstationary stochastic processes—230(L)
Preuss, L. E. Study of the propagation mode for metallic vapors in shadow-casting by vacuum evaporation of Au^{198} and Cr^{51}—1401
Price, W. L. (see Tomlinson, T. B.)—1063(L)

Rabinowicz, E. (see Burwell, J. T.)—136
—— Looseness of wear fragments—367(L)
Rappaport, P. and E. G. Linder. Radioactive charging effects with a dielectric medium—1110
Ratner, Lawrence T. (see Murray, Raymond L.)—67
Redhead, P. A. and C. R. Crowell. Analysis of the linear RF mass spectrometer—331
Reich, Edgar and Peter Swerling. Detection of a sine wave in Gaussian noise—289
Rich, Stanley R. (see Roth, Wilfred)—940
Rinehart, John S. and John Pearson. Engravement of transient stress wave particle velocities—462
Roberts, T. E., Jr. Theory of the single-wire transmission line—57
Robinson, H. L. Diffraction patterns in circular apertures less than one wavelength in diameter—35
Roebuck, John R. Erratum: On the use of the Joule-Thomson effect to measure the work equivalent of heat thermodynamic theory—369
Rogers, F. T., Jr. Convection currents in porous media. V. Variational form of the theory—877
Rogosa, George L. and Guenter Schwarz. X-ray transmission studies of large imperfect crystals—954(L)
Roka, E. G., C. H. Jackson, and R. P. Ulrich. Evaporated point contact rectifiers—228(L)
Rosen, J. (see Lehovec, K.)—513
Roth, Wilfred and Stanley R. Rich. New method for continuous viscosity measurement. General theory of the ultraviscoson—940
Rouse, P. E., Jr., and K. Sittel. Viscoelastic properties of dilute polymer solutions—690
Rouze, S. R. and John H. L. Watson. Metallic grating replicas as internal standards for calibrating electron microscopes—1106
Row, Ronald V. Microwave diffraction measurements in a parallel plate region—1448
Rowland, Robert E. Analysis of fluorescent x-radiation by means of proportional counters—811(L)
Rubin, Lawrence G. (see Davis, Luther, Jr.)—1194
Rudman, P. S., P. A. Flynn, and B. L. Averbach. Measurements in clustering in solid Al-Zn alloys—365(L)
Rudnick, Philip. Detection of weak signals by correlation methods—128
Rumsey, V. H. Traveling wave slot antennas—1358
Rupp, A. F. and F. T. Binford. Production of radioisotopes—1069

Russell, B. R. (see Miller, P. H., Jr.)—1248(L)
Russell, R. B. On the Zr-Hf system—232(L)
Russo, Anthony L. (see Schwartz, Daniel S.)—1061(L)
Rutzler, John E. (see Skinner, Selby M.)—438

Sakiotis, N. G. (see Chait, H. N.)—109(L)
—— (see Kales, M. L.)—816(L); erratum—1529
Sauer, J. A. (see Hsiao, C. C.)—957(L)
Savage, Robert L. (see Skinner, Selby M.)—438
Schaffner, J. S. and J. J. Suran. Transient response of the grounded base transistor amplifier with small load impedance—1355
Schlicke, H. M. Quasi-degenerated modes in high-ϵ dielectric cavities—187
Schneider, P. J. Numerical method for porous heat sources—271
Schnettler, F. J. (see Alley, R. E., Jr.)—1524(L)
Schopper, E. (see Grün, A. E.)—1527(L)
Schultheiss, P. M. (see Tou, J.)—1210
Schumacher, B. (see Grün, A. E.)—1527(L)
Schwartz, Daniel S. and Anthony L. Russo. Schlieren photographs of sound fields—1061(L)
Schwarz, Guenter (see Rogosa, George L.)—954(L)
Schwarz, R. J. (see Miller, K. S.)—1032
Schwertz, F. A. and J. J. Mazenko. Nonlinear semiconductor resistors—1015
Scovil, Georgiana W. Hall effect in titanium—226(L)
Seeger, R. J. (see Ludford, G.)—490
Senseney, C. A. (see Hartman, R. E.)—90
Shah, J. R. (see Jacob, L.)—1261
Sharbaugh, A. H., J. K. Bragg, and R. W. Crowe. Use of the mercury cathode in the dielectric breakdown of liquids—814(L)
Sharman, L. J., R. H. Sones, and L. H. Cragg. Effects of rate of shear on inherent and intrinsic viscosities of polystyrene fractions—703
Sheingold, L. S. Susceptance of a circular obstacle to an incident dominant circular-electric wave—414
Sheldon, John and L. H. Thomas. Use of large scale computing in physics—235
Shulman, R. G. and D. M. Van Winkle. Pressure-welded p-n junctions in germanium—224(L)
—— **and M. E. McMahon.** Recovery currents in germanium P-N junction diodes—1267
Shortley, George. Use of Tschebyscheff-polynomial operators in the numerical solution of boundary-value problems—392
Shreffler, R. G. (see Walsh, J. M.)—349
—— **and W. E. Deal.** Free surface properties of explosive-driven metal plates—44
Siegman, A. E. (see Watkins, D. A.)—917
Silberg, P. A. (see Bachman, C. H.)—427
Simmons, L. M. (see Gutmann, F.)—1067(L)
Šimon, I. (see Bridgman, P. W.)—405
—— Forces acting on superconductors in magnetic fields—19
Simon, Sidney L. (see Coffin, Frances Dunkle)—1333(L)
Simpson, J. H. and H. L. Armstrong. Reverse characteristics of high inverse voltage point contact germanium rectifiers—25
Simpson, O. C. (see Thorn, R. J.)—297
—— (see Thorn, R. J.)—633
Sittel, K. (see Rouse, P. E., Jr.)—690
Sivertsen, J. M. (see Marx, J. W.)—81
Skinner, Selby M., Robert L. Savage, and John E. Rutzler. Electrical phenomena in adhesion. I. Electron atmospheres in dielectrics—438
Slifkin, L. M. (see Baker, G. S.)—1331(L)
Smith, Charles S. and J. W. Burns. Elastic constants of Cu—4 percent Si—15
Smith, W. S. and W. G. Kirchgessner. Method of preparing replicas for electron microscopic examinations—662(L)
Smythe, W. R. Charged disk in cylindrical box—773
—— Current flow in cylinders—70
Somers, Edward V. Propagation of acoustic waves in a liquid-filled cylindrical hole, surrounded by an elastic solid—515
Sones, R. H. (see Sharman, L. J.)—703
Sparks, I. L. and H. R. Philipp. Retarding potential method for measuring electrical conductivity of oxide-coated cathodes—453
Spiegel, M. R. Summation of series involving roots of transcendental equations and related applications—1103
Stauss, H. E. (see Klee, C. W.)—368(L)
Stenoien, Joseph O. (see Kelly, Joseph M.)—258
—— (see Kelly, Joseph M.)—962(L)
Stevenson, A. F. Solution of electromagnetic scattering problems as power series in the ratio (dimension of scatterer) wavelength—1134
—— Electromagnetic scattering by an ellipsoid in the third approximation—1143
Stewart, John L. Electron flow through small tubes with magnetic focusing—1236
Stone, W. M. On the statistical theory of detection of a randomly modulated carrier—935
Storch, Leo. Theorem on the impedance-transforming properties of reactive networks—833
Straiton, A. W. (see Hertel, Paul, Jr.)—956(L)
—— (see Higgins, T. P.)—1297
Strull, Gene. Production of a P-type Cds rectifier by high local heating of N-type crystals—1411(L)
Suran, J. J. (see Schaffner, J. S.)—1355
Sutherland, J. G. (see Goodman, L. E.)—577
Swarup, Prem (see Krishnaji)—1525(L)
Swerling, Peter (see Reich, Edgar)—289
Swihart, James and Edward Akeley. Axial motion of electrons in a linear accelerator with $\beta=1$—640

Takagi, Shunsuke. Theory of the formation of bubbles—1453
Taylor, G. I. Formation of a vortex ring by giving an impulse to a circular disk and then dissolving it away—104(L)
Taylor, William J. Fourier representation of Buerger's image-seeking minimum function—662(L)
Teichmann, T. and E. P. Wigner. Electromagnetic field expansions in loss-free cavities excited through holes—262
Theobald, J. K. Investigation of back diffusion of photoelectrons in various standard gases as it affects secondary electron emission coefficients—123
Thomas, Harry S. Motion of idealized vacuum tube filaments under shock—1341
Thomas, L. H. (see Sheldon, John)—235
Thomsen, John S. Graphical analysis of nonlinear circuits using impedance concepts—1379
Thon, W. (see Motz, H.)—826
Thorn, R. J. and O. C. Simpson. Temperature gradients in inductively heated cylinders—297
—— **and O. C. Simpson.** Spectral emissivities of graphite and carbon—633
Thornton, J. Kendall and William J. Houghton. An influence function for the beta activity of uranium (235) fission products—1374
Ticknor, L. B. (see Bever, M. B.)—1176
Tokuyasu, K. On damage to specimens by shadowing bombardment. I. Experiment—953(L)
—— II. Calculation—954(L)
—— Contour lines on the shadowed side in the electron microscope—956(L)
Tolbert, C. W. (see Hertel, Paul, Jr.)—956(L)
Tomlinson, T. B. Temperature dependence of low frequency fluctuations in thermionic emitters—611
—— **and W. L. Price.** Theory of the flicker effect—1063(L)

Tou, J. and P. M. Schultheiss. Static and sliding friction in feedback systems—1210
Tranter, C. J. Temperature rise in a heat-producing solid behind a surface defect—369(L)
Trolan, J. K. (see Dyke, W. P.)—570
Twersky, V. Reflection coefficients for certain surfaces—659(L)
Twomey, S. Identification of individual hygroscopic particles in the atmosphere by a phase-transition method—1099

Ulrich, R. P. (see Roka, E. G.)—228(L)
Urkowitz, Harry. Filters for detection of small radar signals in clutter—1024

van der Ziel, A. Simple method for measuring interface impedance—496(L)
—— (see Mattson, R. H.)—222(L)
—— Shot noise in semiconductors—222(L)
—— Noise in gas discharges—223(L)
—— Simpler explanation for the observed shot effect in germanium filaments—1063(L)
Van Winkle, D. M. (see Shulman, R. G.)—224(L)
von Trentini, Giswalt. Polystyrene and lucite rod antennas—960(L)

Wahlin, H. B. and Virgil O. Naumann. Transmission of hydrogen through palladium by electrolysis—42
Wainfan, N., W. C. Walker, and G. L. Weissler. Preliminary results on photoelectric yields of Pt and Ta and on photoionization in O_2 and N_2 in the vacuum ultraviolet—1318
Wait, James R. Potential of two current point sources in a homogeneous conducting prolate spheroid—496(L)
—— Potential of two current point sources in a homogeneous conducting prolate spheroid—496(L); erratum—1334
—— Radiation fields of a horizontal dipole in a semi-infinite dissipative medium—958(L)
—— Radiation from a line source adjacent to a conducting half plane—1528(L)
—— Radiation resistance of a small circular loop in the presence of a conducting ground—646
—— Transient magnetic dipole source in a dissipative medium—341
Walker, L. R. Starting currents in the backward-wave oscillator—854
—— (see Pierce, J. R.)—1328
Walker, W. C. (see Wainfan, N.)—1318
Wallmark, J. T. Space charge spread of reflected electron beams studied by a photographic method—590
Walsh, J. M., R. G. Shreffler, and F. J. Willig. Limiting conditions for jet formation in high velocity collisions—349
Warekois, E. P. (see Warren, B. E.)—951(L)
Warren, B. E. and E. P. Warekois. Measurements of stacking faults in cold-worked alpha brass—951(L)
—— (see McKeehan, M.)—52
—— (see Chipman, D. L.)—1251(L)
Watkins, D. A. and A. E. Siegman. Helix impedance measurements using an electron beam—917
Watson, John H. L. (see Rouze, S. R.)—1106
Wax, Nelson. Space charge requirements in some ideally focused electron-optical systems—727
Weertman, J. and J. S. Koehler. Internal friction and Young's modulus of cold-worked copper single crystals—624
Weiman, Andrew L. (see Coffin, Frances Dunkle)—282
Weinberg, Elliot H. Creep of zinc single crystals under direct shear—734
Weinberg, Louis. Darlington problem—776
—— Synthesis of transfer functions with poles restricted to the negative real axis—207
—— Synthesis of transfer functions with poles restricted to the negative real axis—1526(L)
—— Synthesis of unbalanced RLC networks—300
—— Test for zeros in the unit circle—1251(L)
Weinman, J. (see Franklin, A. D.)—1040
Weissler, G. L. (see Wainfan, N.)—1318
—— **and T. N. Wilson.** Work functions of gas-coated tungsten and silver surfaces—472
Whinnery, John R. (see Birdsall, Charles K.)—314
White, W. D. Nonlinear filters—1412(L)
Whitehurst, R. N. (see Motz, H.)—826
Wick, R. F. (see Mason, W. P.)—166
Wieder, H. H. and Sol Kaufman. Plastic electrets—156
Wiesner, J. B. (see Middleton, David)—1065(L)
Wigner, E. P. (see Teichmann, T.)—262
Wilkinson, M. K. Crystallographic variations of field emission from tungsten—1203
Willig, F. J. (see Walsh, J. M.)—349
Wilson, T. N. (see Weissler, G. L.)—472
Wolsky, S. P. (see Ellis, R. C., Jr.)—1411(L)

Yamaguchi, Shigeto and Tadayuki Nakayama. Titanium replica for electron microscopy—658(L)
—— Note on "Metallic shadowcasting using a nozzle system"—815(L)
—— A "double" camera for electron diffraction—1305

Zadeh, L. A. Comment on nonlinear filters—1412(L)
—— Optimum nonlinear filters—396
Zatzkis, Henry. Certain problem in heat conduction—895
Zieman, Clayton M. Dielectric constant of argon at 9700 Mc—110(L)
Zisman, W. A. (see Bowers, R. C.)—1066(L)

Subject Index to Volume 24

References with (L) are to Letters to the Editor

Absorption of microwaves in gases, Krishnaji and Prem Swarup—1525(L)
Acoustic waves in AgCl from x-ray scattering, Approximate elastic spectrum of, H. Cole—482
Acoustic waves in liquid-filled cylindrical hole, Propagation of, Edward V. Somers—515
Activation energy for viscous flow and short-range order, G. J. Dienes—779
Adcock antenna system, rotating, null characteristics of, James G. Holbrook—530
Allotropic transformation temperatures of uranium, Effect of rate of cooling on, Pol Duwez—152
Alloy, M. McCaig—366(L)
Alloys, T. S. Hutchison—813(L)
Alloys, Double activators in oxide cathode base, A. Eisenstein, H. John, and J. H. Affleck—631
Alloys, Measurements of clustering in solid Al-Zn, P. S. Rudman, P. A. Flynn, and B. L. Averbach—365(L)
Alpha, enhanced, in formed silicon point contact, Harold Jacobs, Wesley Matthei, and Frank A. Brand—1410(L)
Amplifiers, Charles K. Birdsall and John R. Whinnery—314
Analog computer elements for solving nonlinear differential equations, Carl A. Ludeke and Cohn L. Morrison—243
Analog, Coupling, for nonlinear systems with more than one degree of freedom, Carl A. Ludeke and Ronald T. Evans—119
Analog, Magnetic, for interaction of dislocation loops, Edward W. Hart—224(L)
Analog network synthesis for arbitrary loss functions, Ernest Shiu-jen Kuh—897
Analog recorder-playback computer for crystal analysis, Ray Pepinsky and Paul Jarmotz—663(L)
Analysis of first-order glow curves, Leonard I. Grossweiner—1306
Announcements—118, 369, 500, 649, 818, 964, 1142, 1254, 1299, 1409
Anomalous viscous flow at very low rate of shear and small shearing stress, J. T. Bergen and W. Patterson, Jr.—712
Antenna of noncircular cross section, cylindrical, Y. T. Lo—1338(L)
Antenna, rhombic, Jesse Gerald Chaney—536
Antennas, Ronold King—140
Antennas, Giswalt von Trentini—960(L)
Antennas, helical, J. S. Chatterjee—550
Antennas, rhombic, Jesse Gerald Chaney—751
Antennas, Simplification for mutual impedance of, Jesse Gerald Chaney—747
Approximate solutions of the space charge problem for some unusual electrode geometries, Henry F. Ivey—1466
Arc drop and deionization time in inert gas thyratrons, S. Pakswer and R. Meyer—501
Argon-alcohol mixtures, Laura Colli and Maria Teresa de Leonardis—255
Attenuation of gamma rays. II. Transmission values for various materials and geometries, Glenn H. Peebles—1437
Average temperatures by parallel-connected thermocouples, Barnard E. Drimmer—225(L)
Axial motion of electrons in linear accelerator with $\beta=1$, James Swihart and Edward Akeley—640

Ball of fire discharge with pronounced current saturation, G. K. Medicus—233(L)
Band-limited functions, Exact interpolation of, Arthur Kohlenberg—1432
Band-pass limiters, Signal-to-noise ratios in, W. B. Davenport, Jr.—720
Barium-strontium titanate ceramics at 3000 Mc, Dielectric properties of, Luther Davis, Jr., and Lawrence G. Rubin—1194
Beta-ray spectrometer line shapes with tilted sources, H. W. Kruse, G. P. Mellor, and C. M. Fowler—1037
Biaxial orientation on the ultimate strength and crazing of linear polymers, C. C. Hsiao and J. A. Sauer—957(L)
Black carbon, Formation of, R. O. Grisdale—1082
Black phosphorus, D. L. Chipman, B. E. Warren, and G. J. Dienes—1251(L)
Boron carbide, Investigation of, Frank W. Glaser, David Moskowitz, and Benjamin Post—731
"Brillouin flow" with thermal velocities, J. R. Pierce and L. R. Walker—1328
Buerger's image-seeking minimum function, William J. Taylor—662(L)
Bulk viscosity of the system polystyrene-diethyl benzene, F. Bueche—423
Buna-N rubber, Ultrasonic-wave study of, A. W. Nolle and J. F. Mifsud—5

Cadmium sulfide crystals, Growth of, M. E. Bishop and S. H. Liebson—660(L); erratum—963
Calibration of photographic emulsions for electron diffraction investigations, L. S. Bartell and L. O. Brockway—656
Calibration of photographic emulsions for electron diffraction investigations, L. S. Bartell and L. O. Brockway—1523(L)
—— I. L. Karle and J. Karle—1522(L)
Carbon contacts, Properties of, R. O. Grisdale—1288
Cathode-ray tubes, Positive and negative ions in, C. H. Bachman, G. L. Hall, and P. A. Silberg—427
Cathodes, H. Katz—597
Cavity resonators, Malcolm R. Currie—998
Charged disk in cylindrical box, W. R. Smythe—773
Cobalt-platinum alloys, Permanent magnet properties of, D. L. Martin and A. H. Geissler—498(L)
Cold work and anneal on resistivity of alpha brass, Herbert I. Fusfeld—1062(L)
Cold-worked alpha brass, B. E. Warren and E. P. Warekois——951(L)
Collapse of lattice vacancy aggregates to form dislocation rings, Evidence for, R. W. Hoffman, F. J. Anders, and E. C. Crittenden, Jr.—231(L)
Colloids, Hugo Fricke—644
Combustion rate of artificial graphites from 700°C to 2000°C in air, Jun Okada and Tatsuo Ikegawa—1249(L)
Compressible viscous fluids, On unsteady flow of, G. Ludford, H. Polachek, and R. J. Seeger—490
Compton scatterer, Glenn H. Peebles—1272
Computer elements for solving nonlinear differential equations, Carl A. Ludeke and Cohn L. Morrison—243
Computer for crystal analysis, Ray Pepinsky and Paul Jarmotz—663(L)
Computing in physics, John Sheldon and L. H. Thomas—235
Condensation nuclei, S. Twomey—1099
Conical helix, Radiation field of, J. S. Chatterjee—550
Consolidation around pore pressure meters, G. de Josselin de Jong—922
Contact and rubbing of flat surface, J. F. Archard—981
Continuous viscosity measurement, New method for. General theory of the ultra-viscoson, Wilfred Roth and Stanley R. Rich—940
Convection currents in porous media. V. Variational form of the theory, F. T. Rogers, Jr.—877
Creep of zinc single crystals under direct shear, Elliot H. Weinberg—734

Cross section area and compression upon the relaxation in permeability for toroidal samples of ferrites, R. E. Alley, Jr., and F. J. Schnettler—1524(L)
Crystallographic variations of field emission from tungsten, M. K. Wilkinson—1203
Cu—4 percent Si, Elastic constants of, Charles S. Smith and J. W. Burns—15
Current flow in cylinders, W. R. Smythe—70
CW magnetrons, Noise in, David Middleton, W. M. Gottschalk, and J. B. Wiesner—1065(L)

Darlington problem, Louis Weinberg—776
Degenerate modes in a spherical cavity, Utilization of, Malcolm R. Currie—998
Degradation of polyisobutylenes on shearing in solution, A. B. Bestul and H. V. Belcher—1011
Detection in noise, W. M. Stone—935
Detection of sine wave in Gaussian noise, Edgar Reich and Peter Swerling—289
Detection of weak signals by correlation methods, Philip Rudnick—128
Determination of drag on a cylinder at low Reynolds numbers, R. K. Finn—771; erratum—1050
—— R. K. Finn—771
Determination of reflection coefficients and insertion loss of a wave-guide junction, Georges A. Deschamps—1046
Dielectric breakdown of liquids, A. H. Sharbaugh, J. K. Bragg, and R. W. Crowe—814(L)
Dielectric constant measurements at 8.6-mm wavelength, Paul Hertel, Jr., A. W. Straiton, and C. W. Tolbert—956(L)
Dielectric constant of argon at 9700 Mc, Clayton M. Zieman—110(L)
Dielectric properties of barium-strontium titanate ceramics at 3000 Mc, Luther Davis, Jr., and Lawrence G. Rubin—1194
Dielectrics, J. M. Kelly and J. O. Stenoien—962(L)
Diffraction, Roger F. Harrington—547
Diffraction of electromagnetic waves, A. F. Stevenson—1134
Diffraction of electromagnetic waves by an aperture in a large screen, G. Bekefi—1123
Diffraction of electromagnetic waves by ellipsoid, A. F. Stevenson—1143
Diffraction of x-rays by deformed crystals, Effect of Soller slit on, B. D. Cullity and Carl A. Julien—541
Diffraction patterns in circular apertures less than one wavelength in diameter, H. L. Robinson—35
Diffusion, R. Kamel—1308
Diffusion of barium in an oxide-coated cathode, Renate S. Bever—1008
Diffusion of D_2 from D_2O through steel, Francis J. Norton—499(L)
Diffusion of decaying particles in a radial electric field, Julian Keilson—1397
Dipole, horizontal, James R. Wait—958(L)
Dirac delta function and the summation of Fourier series, Erich R. Berger—951
Direction finder, Adcock, James G. Holbrook—530
Dynamic compliance, dynamic modulus, and equivalent Voigt and Maxwell models for polyisobutylene, Herbert Leaderman and Robert S. Marvin—812(L)
Dynamic mechanical properties of polyisobutylene, Edwin R. Fitzgerald, Lester D. Grandine, Jr., and John D. Ferry—650
Dynamic mechanical properties of the system polystyrene-decalin, Lester D. Grandine, Jr., and John D. Ferry—679
Dynamics, traffic, Louis A. Pipes—274

Elastic constants of Cu—4 percent Si, Charles S. Smith and J. W. Burns—15
Elastic spectrum, Approximate, of acoustic waves in AgCl from x-ray scattering, H. Cole—482
Elastic waves at free surfaces, Comments on a note on critical reflections of, R. D. Mindlin and T. Kane—498(L)
—— W. S. Jardetzky—499(L)
Elasticity and thermal expansion of germanium between −195 and 275°C, Morris E. Fine—338
Elasto-plastic stress-optical effect in silver chloride single crystals, L. E. Goodman and J. G. Sutherland—577
Elasto-viscous liquids, On the rigidity of, Ali K. Ibrahim—364(L)
Electric circuits, Charles Belove—745
Electric field calculations, W. P. Dyke, J. K. Trolan, W. W. Dolan, and George Barnes—570
Electric fields within cyclotron dees, Raymond L. Murray and Lawrence T. Ratner—67
Electric permittivity of a dilute suspension of membrane-covered ellipsoids, Hugo Fricke—644
Electrical conductivity of oxide-coated cathodes, Retarding potential method for measuring, I. L. Sparks and H. R. Philipp—453
Electrical phenomena in adhesion. I. Electron atmospheres in dielectrics, Selby M. Skinner, Robert L. Savage, and John E. Rutzler, Jr.—438
Electrical properties of liquid selenium I, H. W. Henkels and J. Maczuk—1056
Electrical resistivities at low temperatures, Method of determining, David C. Baird and Willard S. Boyle—958(L)
Electrode geometries, Approximate solutions of the space charge problem for, Henry F. Ivey—1466
Electromagnetic field expansions in loss-free cavities excited through holes, T. Teichmann and E. P. Wigner—262
Electromagnetic field in plane of a circular aperture due to incident spherical waves, D. C. Hogg—110(L)
Electromagnetic scattering by an ellipsoid in the third approximation, A. F. Stevenson—1143
Electromagnetic scattering problems as power series in the ratio (dimension of scatterer) wavelength, A. F. Stevenson—1134
Electromagnetic theory, L. S. Sheingold—414
Electromagnetic transmission characteristics of the two-dimensional lattice medium, Herbert S. Bennett—785
Electromagnetic wave propagation, James R. Wait—646
Electromagnetic waves, Diffraction by an aperture in a large screen, G. Bekefi—1123
Electromagnetic waves, Transmission of through pairs of parallel wire grids, Willice E. Groves—845
Electromotive force developed by a creeping zinc crystal, Frances Dunkle Coffin and Sidney L. Simon—1333(L)
Electron beam technique for displaying short pulses, Paul D. Coleman and Murray D. Sirkis—952(L)
Electron beams studied by a photographic method, J. T. Wallmark—590
Electron compounds of transition elements, H. J. Beattie, Jr.—1322
Electron diffraction, L. S. Bartell and L. O. Brockway—656
Electron diffraction, "Double" camera for, Shigeto Yamaguchi—1305
Electron flow through small tubes with magnetic focusing, John L. Stewart—1236
Electron Microscope Society, Proceedings of the—1414
Electron Microscope Society of America, Program of the—111
Electron microscopic examinations, Method of preparing replicas for, W. S. Smith and W. G. Kirchgessner—662(L)
Electron microscopical studies, K. Tokuyasu—953, 954, 956(L)
Electron microscopical studies of the latent image obtained by exposures to alpha particles, x-rays, and light, H. Hoerlin and F. A. Hamm—1514
Electron microscopy, Robert B. Fischer and Joseph P. Ellinger—1051
Electron microscopy, Shigeto Yamaguchi and Tadayuki Nakayama—658(L)

Electron microscopy of photographic grains. Specimen preparation techniques and applications, F. A. Hamm and J. J. Comer—1495
Electron optical image of an electron beam, Ludwig Mayer—105(L)
Electron optical systems, Kuo-Chu Ho and Robert J. Moon—1186
Electron optics, L. Jacob and J. R. Shah—1261
Electron-shadowgraphs and afterglow pictures of gas jets at low densities, A. E. Grün, E. Schopper, and B. Schumacher—1527(L)
Electron stream with general admittance walls, Waves in, Charles K. Birdsall and John R. Whinnery—314
Electron temperature in an electron beam, Change of, H. M. Mott-Smith—249
Electrons in the electrical field in argon-alcohol mixtures, Measurement of the drift velocity of, Laura Colli and Maria Teresa de Leonardis—255
Electrostatic analyzer, Effective length of, James E. Monahan—434
Electrostatic potential plotting for use in electron optical systems, Kuo-Chu Ho and Robert J. Moon—1186
Ellipsoids, Hugo Fricke—644
Elliptical electromagnetic resonant cavity operating in the Te^{111} mode, T. P. Higgins and A. W. Straiton—1297
Emission decay phenomena due to the contaminated anode, K. Amakasu and T. Imai—107(L); erratum—817
Emulsions, photographic, L. S. Bartell and L. O. Brockway—656
Engravement of transient stress wave particle velocities, John S. Rinehart and John Pearson—462
Enriching stable isotopes electromagnetically, C. P. Keim—1255
Entropy, Bounds for, Nelson M. Blachman—1340
Epicentral displacement caused by elastic waves in an infinite slab, Alan G. Mencher—1240
Equations describing dielectric relaxation and carrier motion in semiconductors, Julian Keilson—1198
Equipotential plotting, using untreated writing paper, C. T. Murray and D. L. Hollway—110(L)
Errata—369, 661, 817, 963, 1050, 1334, 1335, 1529
Evaporated point contact rectifiers, E. G. Roka, C. H. Jackson, and R. P. Ulrich—228(L)
Experimental verification of the metal-strip delay-lens theory, Seymour B. Cohn—839
Explosions, John S. Rinehart and John Pearson—462
Explosive-driven metal plates, Free surface properties of, R. G. Shreffler and W. E. Deal—44
Extinction of predominantly subharmonic oscillations in nonlinear systems, Carl A. Ludeke and William Pong—96

Ferrite materials in the microwave region, Reduction of the loss in, H. N. Chait, N. G. Sakiotis, and R. E. Martin—109(L)
Ferrites, Modes in waveguides containing, M. L. Kales—604
Ferromagnetic powders, measurement of particle size, A. D. Franklin, R. Campbell, and J. Weinman—1040
Ferry reduction and the activation energy for viscous flow, I. L. Hopkins—1300
Field emitter: Fabrication, electron microscopy, and electric field calculations, W. P. Dyke, J. K. Trolan, W. W. Dolan, and George Barnes—570
Filament deformation, Harry S. Thomas—1341
Filters for detection of small radar signals in clutter, Harry Urkowitz—1024
First probability densities for receivers with square law detectors, R. C. Emerson—1168
Fissionable gas as a source of atomic power, Expansion of, Edward H. Kerner—815(L)
Flexural response of a submerged solid to a pulsating gas bubble, George Chertock—192
Flicker effect, Theory of, T. B. Tomlinson and W. L. Price—1063(L)
Floating liquid zones between solid rods, Shapes of, P. H. Keck, M. Green, and M. L. Polk—1479
Flow around objects, R. K. Finn—771
Fluorescent x-radiation by means of proportional counters, Analysis of, Robert E. Rowland—811(L)
Focusing low-voltage electron beams, Spatially alternating magnetic fields for, J. R. Pierce—1247(L)
Forces acting on superconductors in magnetic fields, I. Šimon—19
Formation of a vortex ring by giving an impulse to a circular disk and then dissolving it away, G. I. Taylor—104(L)
Formation of vortex streets, Garrett Birkhoff—98
Fourier representation of Buerger's image-seeking minimum function, William J. Taylor—662(L)
Fourier series, Summation of, J. A. McFadden—364(L)
Fragments, On the looseness of wear, E. Rabinowicz—367(L)
Free surface properties of explosive-driven metal plates, R. G. Shreffler and W. E. Deal—44
Friction, J. F. Archard—981
Friction, Nature of coefficient, J. T. Burwell and E. Rabinowicz—136
Friction of quartz, George A. Alers—324

Gamma rays, Attenuation of. I. Transmission values for finite slabs of lead, iron and the Compton scatterer, Glenn H. Peebles—1272
Gas-coated tungsten and silver surfaces, Work functions of, G. L. Weissler and T. N. Wilson—472
Gas discharges, Noise in, A. van der Ziel—223(L)
Gas flow past slender bodies, Max M. Munk—584
Gas solubility, John J. Naughton—499(L)
Gases, ionized. IV. A null method of measuring the discharge admittance, Lawrence Gould and Sanborn C. Brown—1053
Geometrical and apparent x-ray expansions of a crystal containing lattice defects, J. D. Eshelby—1249(L)
Germanium filaments, Shot noise in, R. H. Mattson and A. van der Ziel—222(L)
Germanium filaments, Simpler explanation for the observed shot effect in, A. van der Ziel—1063(L)
Germanium films from a carbon crucible, Evaporation of, K. Lehovec, J. Rosen, A. MacDonald, and J. Broder—513
Germanium, Hall effect modulators and "gyrators" employing magnetic field independent orientations, W. P. Mason, W. H. Hewitt, and R. F. Wick—166
Germanium, New etches for, R. C. Ellis, Jr. and S. P. Wolsky—1411(L)
Germanium *P-N* junction diodes, Recovery currents in, R. G. Schulman and M. E. McMahon—1267
Germanium, Pressure-welded *p-n* junctions in, R. G. Schulman and D. M. Van Winkle—224(L)
Germanium rectifiers, Thermoelectric study of electrical forming of, Makoto Kikuchi and Tomio Onishi—162
Germanium under ultrasonic stress. I. Anelastic effects, G. S. Baker, L. M. Slifkin, and J. W. Marx—1331(L)
Germanium under ultrasonic stress. II. Dynamic yield point, G. S. Baker, L. M. Slifkin, and J. W. Marx—1331(L)
Glass, Effects of very high pressures on, P. W. Bridgman and I. Šimon—405
Glass, Limiting negative pressure of mercury in, Lyman J. Briggs—488
Glass, Measurement of the heat activation for sodium ion diffusion in, R. Kamel—1308
Glass, Temperature dependence of the elastic moduli and internal friction of silica and, J. W. Marx and J. M. Sivertsen—81
Graphite and carbon, R. J. Thorn and O. C. Simpson—633

Graphites, artificial, Jun Okada and Tatsuo Ikegawa—1249(L)
Growth of metal whiskers, S. Eloise Koonce and S. M. Arnold—365(L)

Half-plane, conducting, Current element near the edge of, Roger F. Harrington—547
Hall effect in titanium, Georgiana W. Scovil—226(L)
Hall effect modulators and "gyrators" employing magnetic field independent orientations in Germanium, W. P. Mason, W. H. Hewitt, and R. F. Wick—166
Hallén's integral equation and its application to antennas near resonance, Alternative method of solving, Ronold King—140
Halogenation on frictional properties of plastics, Effect of, R. C. Bowers, W. C. Clinton, and W. A. Zisman—1066(L)
Heat conduction, Herman H. Lowell—1473
Heat conduction, Certain problem in, Henry Zatzkis—881
Heat-producing solid behind a surface defect, Temperature rise in, C. J. Tranter—369(L)
Heat transfer, P. J. Schneider—271
Heat transfer in a pile with a liquid reactant, Effect of turbulence on, E. N. Parker—451
Heat transfer of high-power densities, John S. Hickey, Jr.—1312
Helix impedance measurements using an electron beam, D. A. Watkins and A. E. Siegman—917
High energy bunched beam analyzer, Irving Kaufman—1413(L)
Hydrodynamic lubrication using water as a lubricant, Experiments in, Stanley Abramovitz—1521(L)
Hygroscopic particles in the atmosphere, Identification by a phase-transition method, S. Twomey—1099
Hysteresis loop of polycrystalline barium titanate, Malcolm McQuarrie—1334(L)

Impedance measurements using an electron beam, D. A. Watkins and A. E. Siegman—917
Impedance-transforming properties of reactive networks, Leo Storch—833
Induction heating, R. J. Thorn and O. C. Simpson—297
Influence function for the beta activity of uranium (235) fission products, J. Kendall Thornton and William J. Houghton—1374
Information theory, S. Kullbach—106(L)
Initial yield in iron, H. W. Paxton—104(L)
Instabilities in the smooth-anode cylindrical magnetron, Lawrence A. Harris—1335 (erratum)
Insulators under ionizing radiation, Method for increasing the electrical resistivity of, John H. Coleman and David Bohm—497(L)
Interference of pulse trains, K. S. Miller and R. J. Schwarz—1032
Interferometric studies of supersonic flows about truncated cones, J. H. Giese and V. E. Bergdolt—1389
Internal friction and Young's modulus of cold-worked copper single crystals, J. Weertman and J. S. Koehler—624
Internal strains on linear expansion, x-ray lattice constant, and density of crystals, Chester R. Berry—658(L)
Isotopes, C. P. Keim—1255

Jet formation in high velocity collisions, Limiting conditions for, J. M. Walsh, R. G. Shreffler, and F. J. Willig—349
Joule-Thomson effect to measure the work equivalent of heat thermodynamic theory, John R. Roebuck—369 (erratum)

Laminar flow in channels with porous walls, Abraham S. Berman—1232
Large scale computing in physics, Use of, John Sheldon and L. H. Thomas—235
Lattice defects, Geometrical and apparent x-ray expansions of a crystal containing, J. D. Eshelby—1249(L)
Lattice defects within crystals of linear expansion and x-ray lattice constant, Effect on distribution of, P. H. Miller, Jr., and B. R. Russell—1248(L)
Limiting negative pressure of mercury in pyrex glass, Lyman J. Briggs—488
Linear RF mass spectrometer, Analysis of, P. A. Redhead and C. R. Crowell—331
Liquid reactant pile, E. N. Parker—451

Mach reflexion of shocks at arbitrary incidence, H. F. Ludloff and M. B. Friedman—1247(L)
Magnet, Permanent, properties of cobalt-platinum alloys, D. L. Martin and A. H. Geissler—498(L)
Magnetic analog for interaction of dislocation loops, Edward W. Hart—224(L)
Magnetic loss tangent of obstacle type artificial dielectrics, J. M. Kelly and J. O. Stenoien—962(L)
Magnetically hardened permanent magnet alloy, Preferred direction in, M. McCaig—366(L)
Mathematical analysis of parallel-connected magnetic amplifiers with resistive loads, Correction to, Louis A. Pipes—661(L)
—— H. S. Kirschbaum—661(L)
Mathieu-Hill equations, Louis A. Pipes—902
Matrix solution of equations of the Mathieu-Hill type, Louis A. Pipes—902
Measurement of drift velocity of electrons in the electrical field in argon-alcohol mixtures, Laura Colli and Maria Teresa de Leonardis—255
Measurement of elastic constants at low temperatures by means of ultrasonic waves—data for silicon and germanium single crystals, and for fused silica, H. J. McSkimin—988
Measurement of particle size of fine ferromagnetic powders, A. D. Franklin, R. Campbell, and J. Weinman—1040
Measurements of clustering in solid Al-Zn alloys, P. S. Rudman, P. A. Flynn, and B. L. Averbach—365(L)
Measurements of stacking faults in cold-worked alpha brass, B. E. Warren and E. P. Warekois—951(L)
Measuring constant and loss angles of semiconductors, New method of, Bunjirō Ichijō—307
Measuring interface impedance, A. van der Ziel—496(L)
Measuring the properties of ionized gases at high frequencies. IV. A null method of measuring the discharge admittance, Lawrence Gould and Sanborn C. Brown—1053
Mechanical investigations of elastomers in a wide range of frequencies, Wladimir Philippoff—685
Membrane analogy, P. J. Schneider—271
Mercury arc, R. M. Howe—881
Mercury cathode in the dielectric breakdown of liquids, Use of, A. H. Sharbaugh, J. K. Bragg, and R. W. Crowe—814(L)
Metal capillary cathodes, H. Katz—597
Metal chips during orthogonal cutting, Energy stored in, M. B. Bever, E. R. Marshall, and L. B. Ticknor—1176
Metal crystals, Pure gliding of, Hiroshi Kanzaki—811(L)
Metal powders suspended in paraffin wax, Joseph M. Kelly, Joseph O. Stenoien, and Dwight E. Isbell—258
Metal-strip delay-lens theory, Experimental verification of, Symour B. Cohn—839
Metal whiskers, Growth of, S. Eloise Koonce and S. M. Arnold—365(L)
Metallic grating replicas as internal standards for calibrating electron microscopes, S. R. Rouze and John H. L. Watson—1106
Metallic shadow-casting using a nozzle system, Shigeto Yamaguchi—815(L)
Method for increasing the electrical resistivity of insulators under ionizing radiation, John H. Coleman and David Bohm—497(L)

Method of time-free solutions for radioactive decay and radionuclide production, Louis Gold—88
Metrization of phase space and nonlinear servo systems, Chi Lung Kang and Gilbert H. Fett—38
Microscope, V. E. Cosslett and W. C. Nixon—616
Microwave component, Nonreciprocal, M. L. Kales, H. N. Chait, and N. G. Sakiotis—816(L); erratum—1529
Microwave diffraction measurements in a parallel plate region, Ronald V. Row—1448
Microwave networks, Georges A. Deschamps—1046
Microwave oscillators, L. R. Walker—854
Modulus of rigidity and the surface and sublimation energies, Some relations between, G. C. Kuczynski—1250(L)
Molybdenum disilicide, Thermoelectric effects in, Martin J. Arvin—498(L)
Molybdenum during tensile deformation, Internal friction of, R. E. Maringer—1525(L)

Negentropy principle of information, L. Brillouin—1152
Neutron bombardment upon the magnetic susceptibility of several pure oxides, J. D. McClelland and J. J. Donoghue—963(L)
Noise, Nelson M. Blachman—783
Noise, Gaussian, Edgar Reich and Peter Swerling—289
Noise in CW magnetrons, David Middleton, W. M. Gottschalk, and J. B. Wiesner—1065(L)
Noise in junction transistors, H. C. Montgomery and M. A. Clark—1337(L)
Noise theory and applications, Edgar Reich and Peter Swerling—289
Nonequilibrium thermodynamics, Newman A. Hall—819
Nonlinear circuits using impedance concepts, Graphical analysis of, John S. Thomsen—1379
Nonlinear differential equations, Carl A. Ludeke and Cohn L. Morrison—243
Nonlinear effects, R. Stuart Mackay—311
Nonlinear filters, W. D. White—1412(L)
Nonlinear filters, L. A. Zadeh—1412(L)
Nonlinear mechanics, Paul Brock—1004
Nonlinear semiconductor resistors, F. A. Schwertz and J. J. Mazenko—1015
Nonlinear systems with more than one degree of freedom, Carl A. Ludeke and Ronald T. Evans—119
Non-Newtonian Fluids, Direct determination of flow curves. II. Shearing rate in concentric cylinder viscometer, Irvin M. Krieger and Harold Elrod—134
Nozzle system, Shigeto Yamaguchi—815(L)
Nuclear radiations on the mechanical properties of solids, G. J. Dienes—666
Numerical method for porous heat sources, P. J. Schneider—271
Numerical solution of boundary-value problems, Use of Tschebyscheff-polynomial operators in, George Shortley—392

Ocean temperature changes, Richard R. Carhart—929
Oil and gas reservoir calculations, H. I. Meyer—510
Operational analysis of traffic dynamics, Louis A. Pipes—274
Optimum nonlinear filters, L. A. Zadeh—396
Optimum transducers and sufficient and most efficient statistics, Equivalence of, Glenn W. Preston—841
Oscillations, forced, with nonlinear restoring force, Chihiro Hayashi—198
Oscillations, nonlinear periodic, Stability investigation of, Chihiro Hayashi—344
Oscillations, Subharmonic, in nonlinear systems, Chihiro Hayashi—521
Output signal-to-noise ratio of a power-law device, Nelson M. Blachman—783
Oxide cathodes, A. Eisenstein, H. John, and J. H. Affleck—631
Oxide coated cathodes, Renate S. Bever—1008
Oxides, J. D. McClelland and J. J. Donoghue—963(L)

Particulate matter for electron microscopy, Preparation of uniformly dispersed specimens of, R. E. Hartman, T. D. Green, J. B. Bateman, C. A. Senseney, and G. E. Hess—90
Photoelastic studies of quenched cylinders and spheres, K. A. Parsons—469
Photoelectric yields of Pt and Ta and on photoionization in O_2 and N_2 in the vacuum ultraviolet, N. Wainfan, W. C. Walker, and G. L. Weissler—1318
Photoelectrons in various standard gases as it affects secondary electron emission coefficients, J. K. Theobald—123
Photographic sensitivity by electrical discharges, Method of increasing, K. S. Lion—367(L)
Photoionization, N. Wainfan, W. C. Walker, and G. L. Weissler—1318
Plastic electrets, H. H. Wieder and Sol Kaufman—156
Plastics, Effect of halogenation on frictional properties, R. C. Bowers, W. C. Clinton, and W. A. Zisman—1066(L)
P-N junction preparation, Kurt Lehovec and Emanuel Belmont—1482
Pole figures, L. K. Jetter and B. S. Borie, Jr.—532
Polycrystalline barium titanate, Malcolm McQuarrie—1334(L)
Polyisobutylene, Herbert Leaderman and Robert S. Marvin—812(L)
Polyisobutylene in the transition from rubber-like to glass-like behavior, John D. Ferry, Lester D. Grandine, Jr., and Edwin R. Fitzgerald—911
Polyisobutylenes on shearing in solution, Degradation of, A. B. Bestul and H. V. Belcher—1011
Polymers, adhesion to metals, Selby M. Skinner, Robert L. Savage, and John E. Rutzler, Jr.—438
Polystyrene and Lucite rod antennas, Gisvalt von Trentini—960(L)
Polystyrene, plasticization of, F. Bueche—423
Pore distribution in porous media, H. I. Meyer—510
Pore pressure meters, G. de Josselin de Jong—922
Positive and negative ions in cathode-ray tubes, C. H. Bachman, G. L. Hall, and P. A. Silberg—427
Potential of two current point sources in a homogeneous conducting prolate spheroid, James R. Wait—496(L); erratum—1334
Preferred orientation, Method for the quantitative determination of, L. K. Jetter and B. S. Borie, Jr.—532
Preparation of *P-N* junctions by surface melting, Kurt Lehovec and Emanuel Belmont—1482
Preparation of uniformly dispersed specimens of particulate matter for electron microscopy, R. E. Hartman, T. D. Green, J. B. Bateman, C. A. Senseney, and G. E. Hess—90
Pressure response in supersonic wind tunnel pressure instrumentation, Arnold L. Ducoffe—1343
Pressure thresholds for biologically active cavitation, Eugene Ackerman—1371
Probe studies of energy distributions and radial potential variations in a low pressure mercury arc, R. M. Howe—881
Program of the Electron Microscope Society of America—111
Propagation along a slotted cylinder, Roger F. Harrington—1366
Propagation constant in gentle circular bends in rectangular wave guides—matrix theory, A. T. de Hoop—1325
Propagation mode for metallic vapors in shadow-casting by vacuum evaporation of Au^{198} and Cr^{51}, L. E. Preuss—1401
Propagation, Wave, through an inhomogeneous medium, George A. Hufford—268
P-Type Cds rectifier, Production of, by high local heating of *N*-Type crystals, Gene Strull—1411(L)
Pulse code modulation, K. S. Miller and R. J. Schwarz—1032

Quartz, Internal friction of, George A. Alers—324
Quasi-degenerated modes in high-ε dielectric cavities, H. M. Schlicke—187

Radar signals in clutter, Filters for detection of, Harry Urkowitz—1024
Radial electric field, Diffusion of decaying particles in, Julian Keilson—1397
Radiation by fast electron beams, Experiments on, H. Motz, W. Thon, and R. N. Whitehurst—826
Radiation damage in black phosphorus, D. L. Chipman, B. E. Warren, and G. J. Dienes—1251(L)
Radiation damage of beta-brass, R. R. Eggleston and F. E. Bowman—229(L)
Radiation field of a horizontal dipole in a semi-infinite dissipative medium, James R. Wait—958(L)
Radiation from a horizontal dipole in a semi-infinite dissipative medium, Roy Harold Lien—1
Radiation from a line source adjacent to a conducting half plane, James R. Wait—1528(L)
Radiation resistance of a small circular loop in the presence of a conducting ground, James R. Wait—646
Radioactive charging effects with a dielectric medium, P. Rappaport and E. G. Linder—1110
Radioactive decay and radionuclide production, Method of time-free solutions for, Louis Gold—88
Radioisotopes, Production of, A. F. Rupp and F. T. Binford—1069
Random inputs, Response of linear time-dependent systems to, D. B. Duncan—609
Rate of shear on inherent and intrinsic viscosities of polystyrene fractions, L. J. Sharman, R. H. Sones, and L. H. Cragg—703
Rayleigh-type forced vibration equation with a large coefficient of damping, Paul Brock—1004
Reactor simulators, F. E. O'Meara—1200
Reduction of the loss in ferrite materials in the microwave region, H. N. Chait, N. G. Sakiotis, and R. E. Martin—109(L)
Reflection coefficients for certain rough surfaces, V. Twersky—659(L)
Reflection of sound in the ocean from temperature changes, Richard R. Carhart—929
Relaxation distribution functions, John D. Ferry, Lester D. Grandine, Jr., and Edwin R. Fitzgerald—911
Replica technique in the study of chemical precipitation processes, Robert B. Fischer and Joseph P. Ellinger—1051
Resistivity of alpha brass, Effect of cold work and anneal on, Herbert I. Fusfeld—1062(L)
Resistivity of thin silver films, Uri Oppenheim and Joseph H. Jaffe—1521(L)
Response of linear time-dependent systems to random inputs, D. B. Duncan—609
Response of two-material laminated cylinder to simple harmonic environment temperature change, Herman H. Lowell—1473
Response of undamped systems to noise, D. B. Duncan—1252(L)
Retarding potential method for measuring electrical conductivity of oxide-coated cathodes, I. L. Sparks and H. R. Philipp—453
Reverse characteristics of high inverse voltage point contact germanium rectifiers, J. H. Simpson and H. L. Armstrong—25
Reversion method, Limitation of, W. J. Cunningham—952(L)
Rhombic antenna, Free space radiation impedance of, Jesse Gerald Chaney—536
Rhombic antennas spaced in tandem, Mutual impedance of, Jesse Gerald Chaney—751
Rigidity of elasto-viscous liquids—Ibrahim, Ali K.—364(L)
RLC networks, Louis Weinberg—300
R-PAC: Analog recorder-playback computer for crystal analysis, Ray Pepinsky and Paul Jarmotz—663(L)
R-PAC for interpretation of Patterson maps in x-ray crystal analysis, A modification of, Ray Pepinsky—1520(L)

Schlieren photographs of sound fields, Daniel S. Schwartz and Anthony L. Russo—1061(L)
Screw dislocations in thin rods, J. D. Eshelby—176
Semiconduction, Bunjirō Ichijō—307
Semiconductors, F. A. Schwertz and J. J. Mazenko—1015
Semiconductors, Equations describing dielectric relaxation and carrier motion in, Julian Keilson—1198
Semiconductors, Shot noise in, A. van der Ziel—222(L)
Series involving roots of transcendental equations and related applications, M. R. Spiegel—1103
Shadowed side in the electron microscope, Contour lines on, K. Tokuyasu—956(L)
Shadowing bombardment, On damage to specimens. I. Experiment, K. Tokuyasu—953(L)
Shadowing bombardment, On damage to specimens. II. Calculation, K. Tokuyasu—953(L)
Shock formation and growth, Observation of, Alfred B. Laponsky and Raymond J. Emrich—1383
Shock propagation in brass, Jacob Savitt—1335(L)
Shock tube, Attenuation in, R. J. Emrich and C. W. Curtis—360
Shock waves in steel, Free surface motion induced by, William A. Allen—1180
Shorted ring in a uhf field in a coaxial cavity, Force on, Surindra N. Kalra—1339(L)
Shot noise in germanium filaments, R. H. Mattson and A. van der Ziel—222(L)
Shot noise in junction transistors, H. C. Montgomery and M. A. Clark—1337(L)
Shot noise in semiconductors, A. van der Ziel—222(L)
Signal-to-noise ratios in band-pass limiters, W. B. Davenport, Jr.—720
Silver chloride crystals, L. E. Goodman and J. G. Sutherland—577
Single-wire transmission line, T. E. Roberts, Jr.—57
Sinusoidal and relaxation oscillations sustained by nonlinear reactances, R. Stuart Mackay—1163
Slot antennas, Roger F. Harrington—1366
Slot antennas, V. H. Rumsey—1358
Slot coupling of rectangular and spherical wave guides, L. B. Felsen and N. Marcuvitz—755
Slowly converging series, Summation of, Igor Gumowski—1068(L); erratum—1330
Society of Rheology Meeting, October, 1952—665
Soller slit, B. D. Cullity and Carl A. Julien—541
Solubility determination of some elemental gases in pyrex at 1170°C, John J. Naughton—499(L)
Solutions of physical systems, Set of principles to interconnect, Gabriel Kron—965
Space charge limited currents between inclined plane electrodes. Approximate solutions, Henry F. Ivey—227(L)
Space charge requirements in some ideally focused electron-optical systems, Nelson Wax—727
Space charge spread of reflected electron beams studied by a photographic method, J. T. Wallmark—590
Sparking potentials between separating contacts, C. W. Klee and H. E. Stauss—368(L)
Spectral emissivities of graphite and carbon, R. J. Thorn and O. C. Simpson—633
Spectrometer, P. A. Redhead and C. R. Crowell—331
Spectrometer, Beta-ray line shapes, H. W. Kruse, G. P. Mellor, and C. M. Fowler—1037
Spectroscopy of ultraspeed pellet luminosity, William A. Allen and Earle B. Mayfield—131
Sphere moving parallel to a plane boundary, Motion of, F. C. Karal—147

Spheroid, homogeneous conducting, James R. Wait—496(L)
Stability, J. Frank Koenig—476
Starting currents in the backward-wave oscillator, L. R. Walker—854
Static and sliding friction in feedback systems, J. Tou and P. M. Schultheiss—1210
Statistical criteria for the detection of pulsed carriers in noise. I, David Middleton—371
Statistical theory of detection of a randomly modulated carrier, W. M. Stone—935
Statistics of liquid spray and dust electrification by the Hopper and Laby method, Edward E. Dodd—73
Stochastic processes, L. A. Zadeh—396
Stochastic processes, nonstationary, Theory of prediction, Glenn W. Preston—230(L)
Stress dependence of the activation energy of the rupture process, Edward W. LaRocca—1523(L)
Stress, torsional, Sennosuke Momma—959(L)
Superconductors in magnetic fields, I. Šimon—19
Supersonic flows about truncated cones, Interferometric studies of, J. H. Giese and V. E. Bergdolt—1389
Supersonic wind tunnel pressure instrumentation, Pressure response in, Arnold L. Ducoffe—1343
Surface and sublimation energies, G. C. Kuczynski—1250(L)
Surface effects and the creep of zinc single crystals: I. Creep characteristics of clean and oxide-coated crystals, Frances Dunkle Coffin and Andrew L. Weiman—282
Surface stress by means of electroplating, Determination of, H. Ōkubo—1130
Surface wave propagation over a coated conductor with small cylindrical curvature in direction of travel, Kazuo Horiuchi —961(L)
Susceptance of a circular obstacle to an incident dominant circular-electric wave, L. S. Sheingold—414
Synthesis of reactance 4-poles, Herbert J. Carlin and R. La Rosa—1336(L)
Synthesis of transfer functions with poles restricted to the negative real axis, Louis Weinberg—1526(L)
—— A. D. Fialkow and I. Gerst—1525(L)
Synthesis of unbalanced RLC networks, Louis Weinberg—300

Temperature coefficients of non-Newtonian viscosity at fixed shearing stress and at fixed rate of shear, A. B. Bestul and H. V. Belcher—696
Temperature dependence of low frequency fluctuations in thermionic emitters, T. B. Tomlinson—611
Temperature dependence of the elastic moduli and internal friction of silica and glass, J. W. Marx and J. M. Sivertsen —81
Temperature dependence of the viscosity of liquids, Arthur K. Doolittle—1067(L)
—— F. Gutmann and L. M. Simmons—1067(L)
Temperature gradients in inductively heated cylinders, R. J. Thorn and O. C. Simpson—297
Tensile properties of several metals and other materials, Effect of pressure on, P. W. Bridgman—560
Tensor analysis of physical systems, Gabriel Kron—965
Theorem on the impedance-transforming properties of reactive networks, Leo Storch—833
Thermal contraction of a split hollow cylinder, W. Karush and A. V. Martin—1427
Thermal effects in point contact rectifiers, H. L. Armstrong—1332(L)
Thermal expansion of germanium, Morris E. Fine—338
Thermal stresses, K. A. Parsons—469
Thermal velocities, J. R. Pierce and L. R. Walker—1328
Thermionic cathode, New dispenser type, Roberto Levi—233(L)
Thermionic cathodes, molded, D. MacNair, R. T. Lynch, and N. B. Hannay—1335(L)
Thermionic emission, A. Eisenstein, H. John, and J. H. Affleck —631
Thermionic emission from oxide-coated tungsten filaments, C. P. Hadley—49
Thermionic emitters, T. B. Tomlinson—611
Thermocouples, Bernard E. Drimmer—225(L)
Thermodynamic, Newman A. Hall—819
Thermoelectric effects in molybdenum disilicide, Martin J. Arvin—498(L)
Thermoelectric study of electrical forming of Germanium rectifiers, Makoto Kikuchi and Tomio Onishi—162
Thermoelectricity, H. W. Henkels and J. Maczuk—1056
Thyratrons, deionization time, S. Pakswer and R. Meyer—501
Time-resolved spectroscopy of ultraspeed pellet luminosity, William A. Allen and Earle B. Mayfield—131
Titanium, Georgiana W. Scovil—226(L)
Titanium replica for electron microscopy, Shigeto Yamaguchi and Tadayuki Nakayama—658(L)
Tolerance coefficients for R-C networks, Charles Belove—745
Torsional stress in a shaft with notches, Sennosuke Momma—959(L)
Tracer diffusion in the ground in radioactive leak location, Andrew Gemant—93
Trajectories in the symmetrical electron lens, L. Jacob and J. R. Shah—1261
Transducers, Glenn W. Preston—841
Transfer functions with poles restricted to negative real axis, Synthesis of, Louis Weinberg—207
Transient magnetic dipole source in a dissipative medium, James R. Wait—341
Transient response of the grounded base transistor amplifier with small load impedance, J. S. Schaffner and J. J. Suran —1355
Transistor amplifier with small load impedance, J. S. Schaffner and J. J. Suran—1355
Transistors, Forming silicon point contact, Harold Jacobs, Frank A. Brand, and Wesley Matthei—1340(L)
Transistors, junction, H. C. Montgomery and M. A. Clark—1337(L)
Transition elements, H. J. Beattie, Jr.—1322
Transmission of hydrogen through palladium by electrolysis, H. B. Wahlin and Virgil O. Naumann—42
Traveling wave slot antennas, V. H. Rumsey—1358
Tschebyscheff-polynomial operators in the numerical solution of boundary-value problems, Use of, George Shortley—392
Tungsten and silver surfaces, G. L. Weissler and T. N. Wilson —472
Tungsten, Crystallographic variations of field emission from, M. K. Wilkinson—1203
Tungsten filaments, oxide-coated, Thermionic emission from, C. P. Hadley—49
Tungsten, thoriated, X-ray study of cold work in, M. McKeehan and B. E. Warren—52

Ultimate strength of polymers, C. C. Hsiao and J. A. Sauer —957(L)
Ultra high vacuum, New developments in the production and measurement of, D. Alpert—860
Ultrasonic viscometer, Wilfred Roth and Stanley R. Rich—940
Ultrasonic-wave study of swollen Buna-N rubber, A. W. Nolle and J. F. Mifsud—5
Uranium, Pol Duwez—152
Uranium (235) fission products, Influence function for the beta activity of, J. Kendall Thornton and William J. Houghton—1374

Vacuum tube filaments under shock, idealized, Motion of, Harry S. Thomas—1341
Variational methods for problems in resistance, J. F. Carlson and T. J. Hendrickson—1462

Vector wave function solution of the diffraction of electromagnetic waves by circular disks and apertures. I. Oblate spheroidal vector wave functions, Carson Flammer—1218
—— II. Diffraction problems, Carson Flammer—1224
Vibroscopic determination of filament cross-sectional area, Effect of stiffness and nonuniformity on, D. J. Montgomery—1092
Viscoelastic properties as functions of the distribution of activation energies, W. James Lyons—217
Viscoelastic properties of dilute polymer solutions, P. E. Rouse, Jr., and K. Sittel—690
Viscoelastic stress, secondary, Test of the theory, M. Mooney—675
Viscous flow, Activation energy for, G. J. Dienes–779
Viscous flow, Activation energy for, I. L. Hopkins—1300
Voltage sources, P. Rappaport and E. G. Linder—1110

Wave-guide-fed slots radiating into parallel plate regions, Theory of, L. Lewin—232(L)
Wave-guide measurements in the microwave region on metal powders suspended in paraffin wax, Joseph M. Kelly, Joseph O. Stenoien, and Dwight E. Isbell—258
Wave guides, L. B. Felsen and N. Marcuvitz—755
Wave guides containing ferrites, M. L. Kales—604
Wave propagation, Kazuo Horiuchi—961(L)
Wave propagation in finite rods of viscoelastic material, E. H. Lee and I. Kanter—1115
Wind tunnel instrumentation, Arnold L. Ducoffe—1343
Wind waves on a water surface, Generation of, Carl Eckart—1485
Work functions of gas-coated tungsten and silver surfaces, G. L. Weissler and T. N. Wilson—472

X-ray line broadening from precipitation in Cu-Fe alloys, T. S. Hutchison—813(L)
X-ray measurements of radiation damage in black phosphorus, D. L. Chipman, B. E. Warren and G. J. Dienes—1251(L)
X-ray shadow microscope, V. E. Cosslett and W. C. Nixon——616
X-ray study of cold work in thoriated tungsten, M. McKeehan and B. E. Warren—52
X-ray transmission studies of large imperfect crystals, George L. Rogosa and Guenter Schwarz—954(L)

Young's modulus, J. Weertman and J. S. Koehler—624

Zr-Hf system, R. B. Russell—232(L)
Zeros in the unit circle, Test for, Louis Weinberg—1251(L)
Zeros of polynomials and the degree of stability of linear systems, J. Frank Koenig—476
Zinc single crystals, Elliot H. Weinberg—734
Zinc single crystals, creep of, Frances Dunkle Coffin and Andrew L. Weiman—282

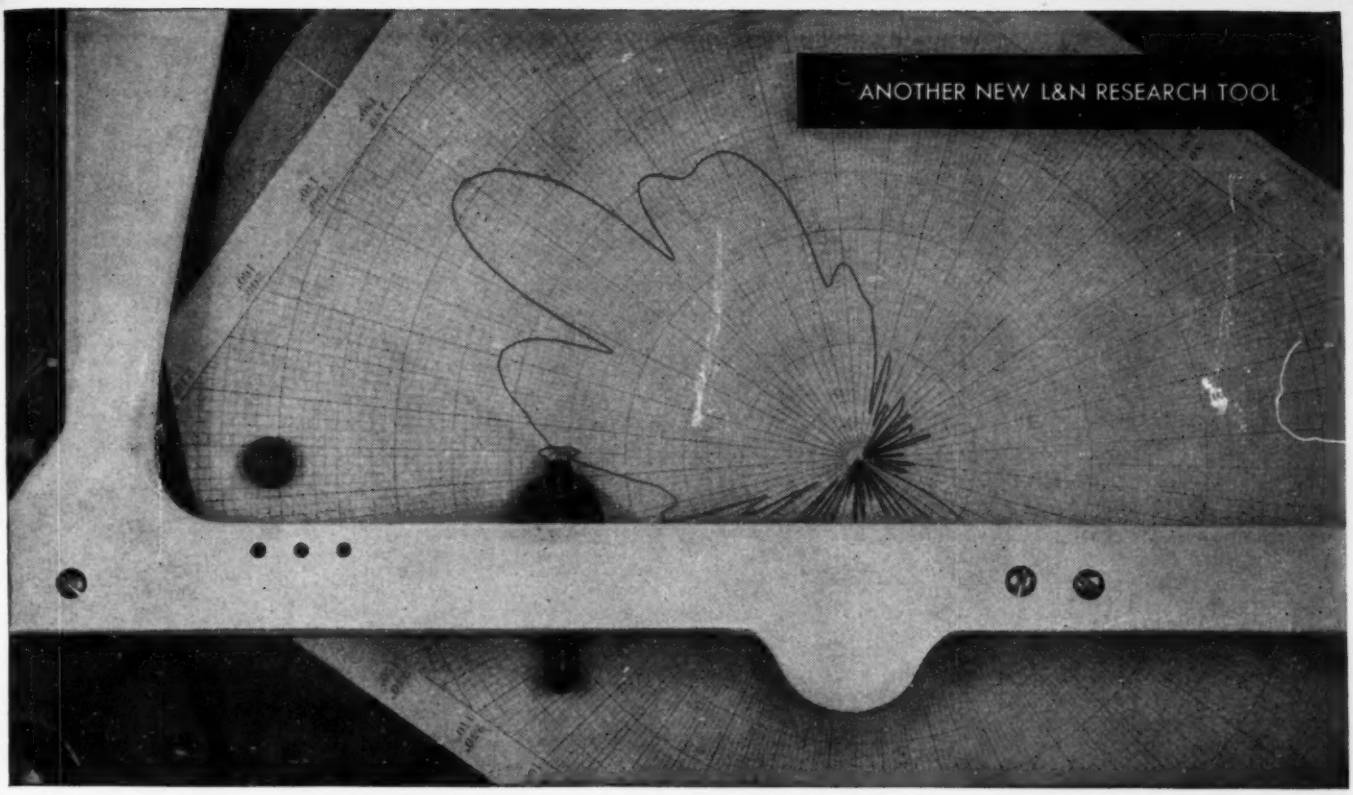

Plot Input vs. Angular Displacement . . .

automatically...

with this Speedomax® Polar Recorder

If you are measuring . . . or contemplate measuring . . . a signal or quantity as a function of angular displacement, it will pay you to investigate this new Speedomax Polar Recorder. Tedious point-by-point plotting is completely eliminated with the use of this instrument. You can use it to measure automatically antennae or sonar patterns, light distribution patterns, computer outputs, or any physical quantity that may be measured as a function of angular displacement.

Here's how it operates. Any change in the "r" signal causes the instrument recording pen to move, while any change in angular position causes the instrument chart to rotate.

The "r" function has a newly designed 5 inch pen-travel with zero at the chart center. A fast balancing speed—less than 2 seconds across a 5 inch radius—enables the instrument to record deviations of input signal rapidly. Quantities such as millivolts, power level, light intensity—and many others—can be used as the "r" function.

The "θ" variable or angular rotation of the chart paper is accomplished by means of a syncro-servo system consisting of a syncro-generator (external to the recorder), syncro control transformer, a-c amplifier and balancing motor. As the antenna, or other element, is rotated, its position is transmitted through this syncro-servo system to the balancing motor which rotates the chart in step with the antenna. Positional accuracy of the chart is better than three-fourths of a degree in relation to the syncro-generator. Maximum speed of chart rotation is 60 angular degrees per second.

Additional features include: chart table with illuminated center to help align the chart, an electrically energized pen lifter to facilitate setups, and 90 degree index lines on chart table with single index line on frame to align chart table.

For more facts on this versatile, time saving recorder, contact your nearest L&N Sales Office or write to Leeds & Northrup Co., 4978 Stenton Ave., Philadelphia 44, Pa.

LEEDS & NORTHRUP
instruments — *automatic controls • furnaces*

Jrl. Ad ND46(15)

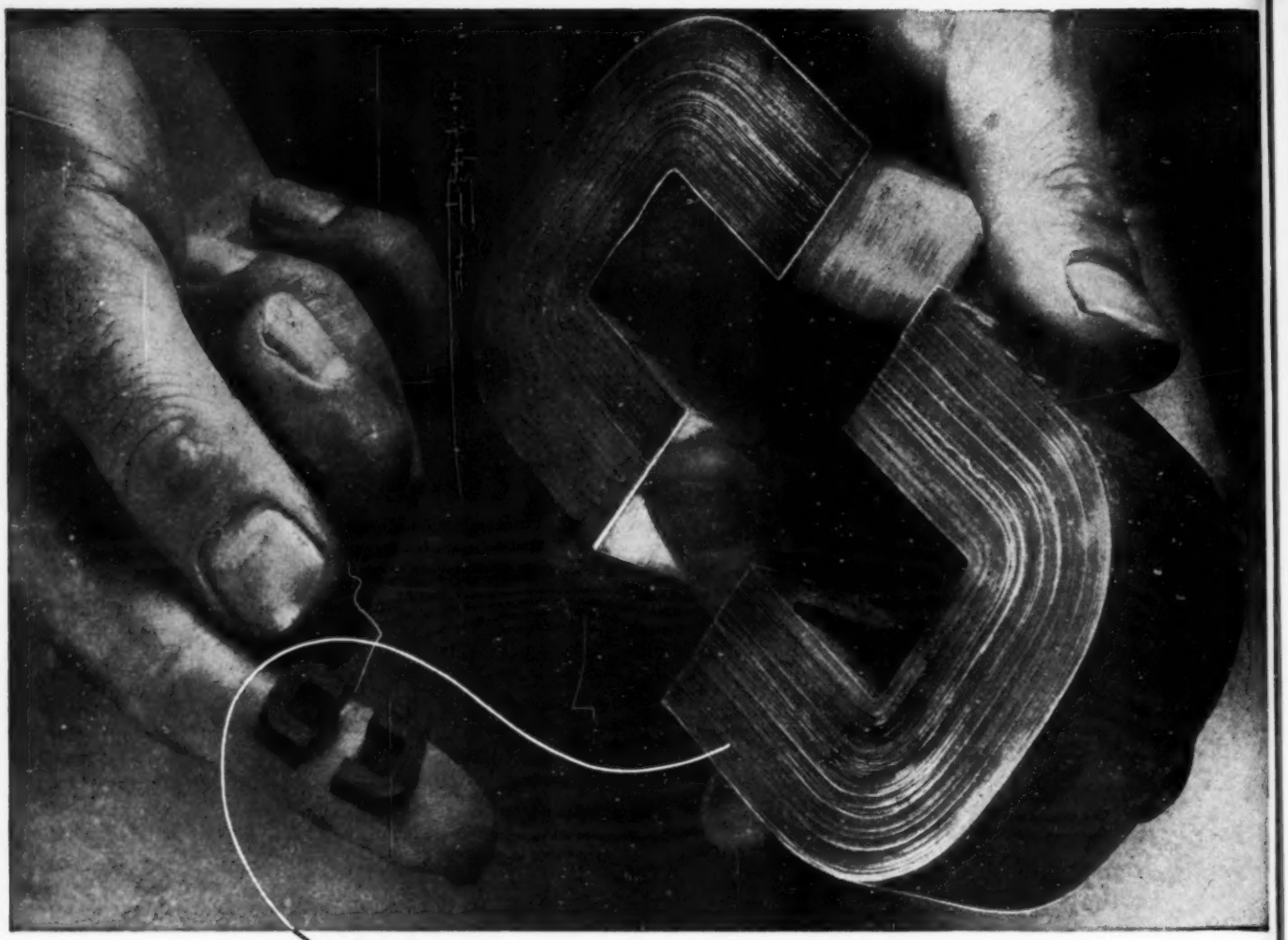

SILECTRON C-CORES...BIG or LITTLE

...any quantity and any size

Wound from precision rolled oriented silicon steel strip as thin as .00025"

For users operating on government schedules, Arnold is now producing C-Cores wound from ¼, ½, 1, 2, 4 and 12-mil Silectron strip. The ultra-thin oriented silicon steel strip is rolled to exacting tolerances in our own plant on precision cold-reducing equipment of the most modern type. Winding of cores, processing of butt joints, etc. are carefully controlled, assuring the lowest possible core losses, and freedom from short-circuiting of the laminations.

We can offer prompt delivery in production quantities—*and size is no object, from a fraction of an ounce to C-Cores of 200 pounds or more.* Rigid standard tests—and special electrical tests where required—give you assurance of the highest quality in all gauges. ● *Your inquiries are invited.*

THE ARNOLD ENGINEERING COMPANY

SUBSIDIARY OF ALLEGHENY LUDLUM STEEL CORPORATION

General Office & Plant: Marengo, Illinois

DISTRICT SALES OFFICES . . . New York: 350 Fifth Ave.

Los Angeles: 3450 Wilshire Blvd. Boston: 200 Berkeley St.

WBD 4363

How silent is the night?

Watching the serenity of Christmas skies, we are conscious of deep silence. Yet the stars are talking to us all the while—talking in radio waves that are full of meaning to scientists probing the depths of space.

The important discovery that some stars produce radio waves was made by a Bell Laboratories scientist while exploring atmospheric disturbances which might interfere with transoceanic telephone service. His discovery marked the birth of the fast-growing science of radio astronomy. It is telling us of mysterious lightless stars that broadcast radio waves, and it promises exciting revelations about vast regions of space concealed by clouds of cosmic dust.

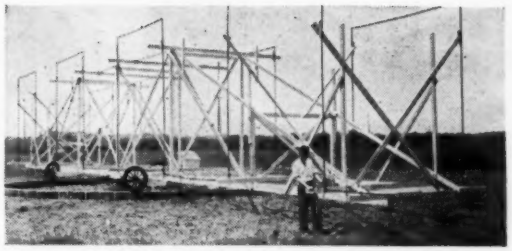

Directional radio antenna used by Karl G. Jansky, in the discovery of stellar radio signals at the Holmdel, New Jersey, branch of Bell Telephone Laboratories. In 1932 he detected waves of 14.6 meters coming from the direction of Sagittarius in the Milky Way.

It is another example of how Bell Telephone Laboratories scientists make broad and important discoveries as they seek ways to make your telephone serve you better.

BELL TELEPHONE LABORATORIES

EXPLORING AND INVENTING, DEVISING AND PERFECTING, FOR CONTINUED IMPROVEMENTS AND ECONOMIES IN TELEPHONE SERVICE

ENGINEERS
and PHYSICISTS

To those interested in advanced academic study while associated with research and development in industry, the following practical programs are offered:

1
HUGHES COOPERATIVE FELLOWSHIP PROGRAM

for Master of Science Degrees

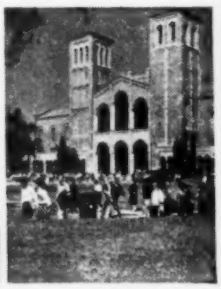

A group of participants in the Hughes Cooperative Fellowship Program (above left). Fellows study for Master of Science degrees at either University of Southern California (center) or University of California at Los Angeles (right).

This program is to assist outstanding individuals in studying for the Master of Science Degree while employed in industry and making contributions to important military work. It is open to students who will receive the B.S. degree in Electrical Engineering, Physics or Mechanical Engineering during the coming year and to members of the Armed Services being honorably separated and holding such B.S. degrees.

Candidates must meet entrance requirements for advanced study at the University of California at Los Angeles or the University of Southern California. Participants will work full time at the Laboratories during the summer, and 25 hours per week while pursuing a half-time schedule of graduate study at the university.

The salary will be commensurate with the individual's ability and experience. Tuition, admission fees and books for university attendance will be provided. Provision is made for an allowance to assist in paying traveling and moving expenses from outside the Southern California area.

2
THE HOWARD HUGHES FELLOWSHIPS

in Science and Engineering

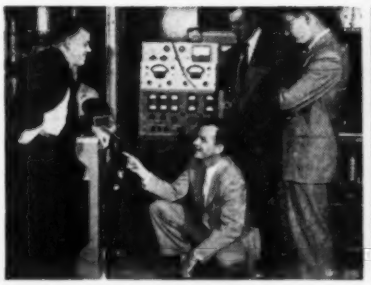

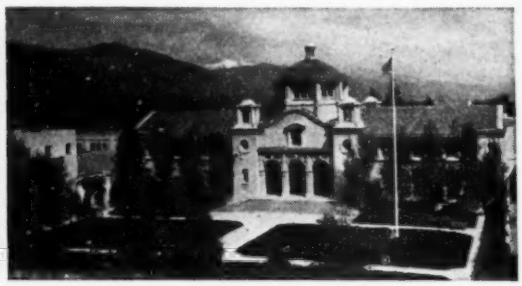

(From left to right) Hughes 1952 Fellows Truman O. Woodruff and Allen I. Ormsbee discuss tube processing station in Electron Tube Laboratory with 1953 Fellows Roy Gould and Baxter H. Armstrong. Their advanced study is at California Institute of Technology (above).

Eligible for these fellowships are those who have completed one year of graduate study in physics or engineering. Successful candidates must qualify for graduate standing at the California Institute of Technology for study toward the degree of Doctor of Philosophy in physics or engineering. In summers they will work full time in the Hughes Laboratories in association with scientists and engineers in their fields.

Fellows may pursue graduate research in the fields of physics, electronics engineering, electronic computing, aerodynamics, propulsion engineering, mechanical engineering, or information theory.

Each appointment is for twelve months and provides a cash award, a salary, and tuition and research expenses. A suitable adjustment is made when financial responsibilities of the Fellow might otherwise preclude participation in the program.

HOW TO APPLY: *For complete information concerning either of these Hughes Fellowship programs, write directly to us. Indicate the particular program in which you are interested. A detailed explanatory brochure and application forms will be mailed promptly.*

Address all correspondence to

HUGHES

RESEARCH AND DEVELOPMENT LABORATORIES
COMMITTEE FOR GRADUATE STUDY
Culver City, Los Angeles County, California

Vacuum Fusion Gas Analyzer

with complete installation and instruction

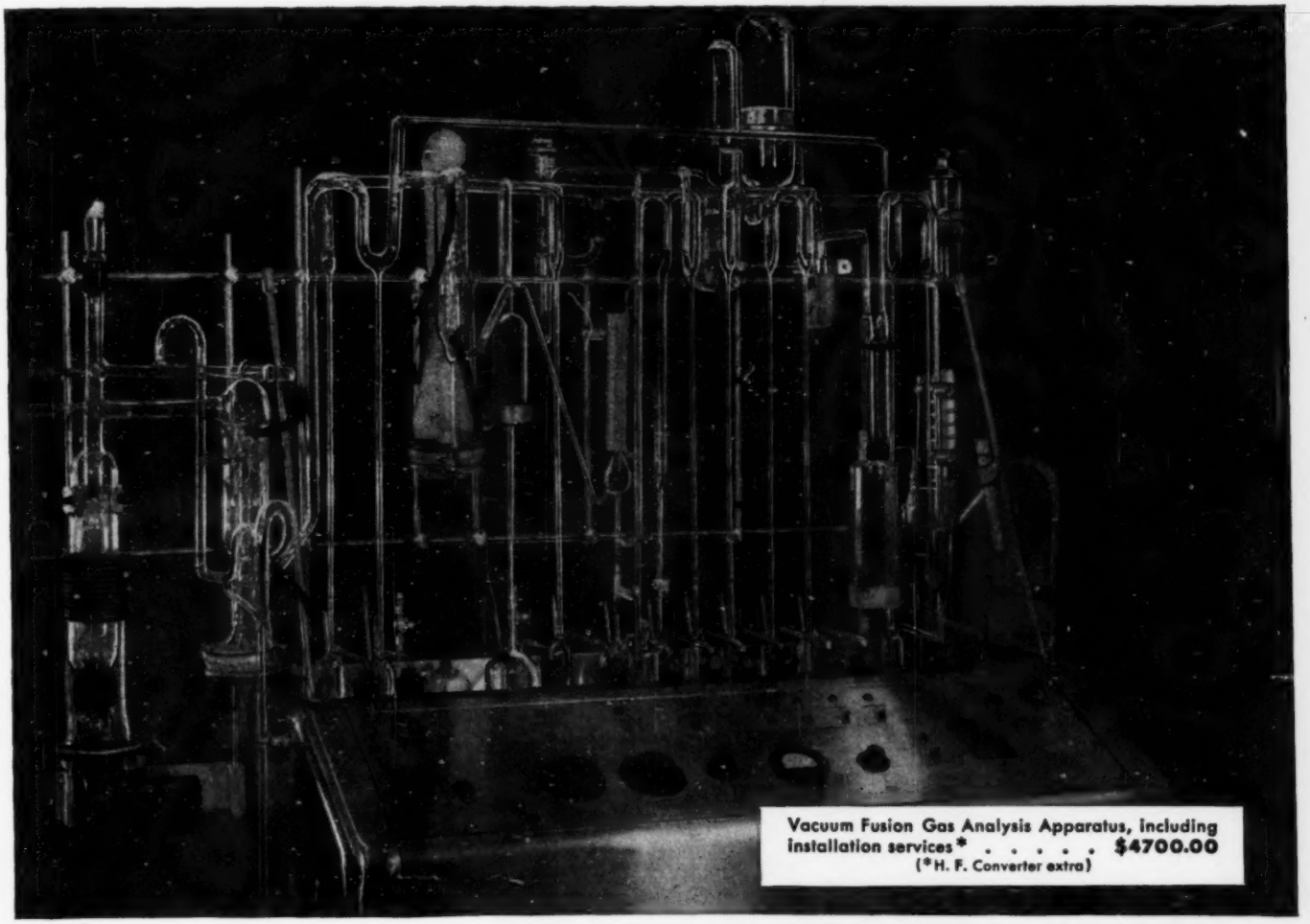

Vacuum Fusion Gas Analysis Apparatus, including installation services* $4700.00
(*H. F. Converter extra)

A packaged unit to determine the content of oxygen, nitrogen and hydrogen in metals

A wide variety of metals and alloys can be analyzed to determine the amount of oxygen, nitrogen and hydrogen contained either as combined or dissolved gas, in the range from one per cent to approximately 10^{-4} per cent by weight.

The oxygen and hydrogen content of titanium is reported within the same range of accuracy as for other metals.

The apparatus incorporates the best features and techniques reported in the literature or known to our laboratory and has been employed for some time in connection with our own metallurgical research activities.

Operating procedure is relatively simple and can be readily mastered. Installation, final testing and instruction of your operator is performed by one of our trained analysts.

Write for details of Type 09-1240 Vacuum Fusion Gas Analysis Apparatus.

ANALYTICAL SERVICE

Write for information about NRC Gas Analysis Service if your requirements do not justify the purchase of an instrument.

INDUSTRIAL RESEARCH
CHEMISTRY, METALLURGY
HIGH VACUUM ENGINEERING

NRC

PROCESS DEVELOPMENT
PHYSICS, DEHYDRATION
DISTILLATION, VACUUM COATING

National Research Corporation

EQUIPMENT DIVISION

SEVENTY MEMORIAL DRIVE, CAMBRIDGE 42, MASSACHUSETTS

graphic recording simplified by the new

XY plotter and recorder

Desk or rack mounted. Fits standard RCA or RMA rack mountings. Takes standard 11" x 16½" or 8½" x 11" graph paper. 4-Quadrant operation. Zero Offset and Scale Expansion adjustable on both axes. Unique ink pressure regulator assures trouble-free pen operation. Unit is self-contained with servo amplifiers, power supply and control circuits—mechanically rugged, attractively designed. Accurate to ±0.1% full scale, power consumption 150 watts. Write for catalog information.

For discrete point plotting or continuous-trace recordings on standard graph paper, Librascope produces a two coordinate portable recording instrument called the X-Y Plotter and Recorder. This unit is noteworthy for rapidity and accuracy of performance and is applicable to a great variety of data reduction operations.

Input choice includes:

- Punched Cards
- Decimal Keyboard (shown)
- Digital Computers
- Analog Signals (including polar coordinates)

Computers and Controls

LIBRASCOPE INCORPORATED

1607 FLOWER STREET • GLENDALE, CALIFORNIA

A SUBSIDIARY OF GENERAL PRECISION EQUIPMENT CORPORATION

If you desire the challenge of advanced design fields and qualify in education and experience, write to Dick Hastings, Personnel Director.

See this unit in operation at the Eastern Joint Computer Conference & Exhibition, Hotel Statler, Washington, D.C., December 8-9-10.

Complete HIGH-FREQUENCY ANALYSIS

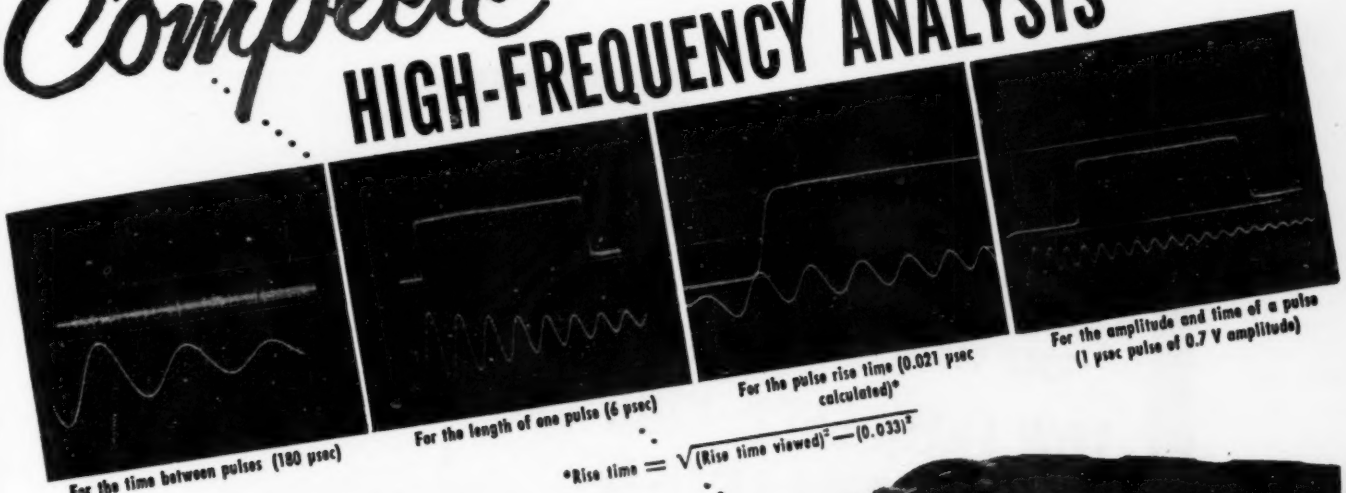

For the time between pulses (180 μsec)

For the length of one pulse (6 μsec)

For the pulse rise time (0.021 μsec calculated)*

For the amplitude and time of a pulse (1 μsec pulse of 0.7 V amplitude)

*Rise time $= \sqrt{(\text{Rise time viewed})^2 - (0.033)^2}$

with a DU MONT HIGH-VOLTAGE TYPE 303-AH

The new Du Mont Type 303-AH *is the high-voltage, high-frequency instrument for you — why?*

The 10,000 volts applied to the cathode-ray tube provides a bright, highly resolved presentation for viewing or recording short duration transients or high-frequency signals even at low repetition rates.

The metallization of the cathode-ray tube greatly increases brightness over normal screen brightness and prevents buildup of spurious screen charges, thus allowing faithful reproduction of short-duration transients having low repetition rates.

The BNC-type coaxial input permits convenient connection of pulse-type signals usually carried on coaxial lines.

The wideband vertical amplifier (3 db down) 10 MC has a pulse response of 0.033 μsec for faithful reproduction of short rise-times without overshoot.

The fast linear sweeps, 6"/μsec (0.065 μsec/cm) at 10 KV, take fullest advantage of the wideband amplifier for expanding and measuring short rise-times.

The 0.25 μsec signal delay line introduces no signal distortion and allows sufficient time for the sweep to start before the signal appears.

The provision for both amplitude and time calibration of 0.1, 1, 10 and 100 volts peak to peak and 0.1, 1, 10 and 100 μsec intervals insures accuracy and convenience of measurement.

The variable-intensity illuminated scale facilitates visual or photographic measurements.

Type 316-A probe available for low capacity input. Price $27.00.

- METALLIZED CATHODE-RAY TUBE
- SELF-CONTAINED
- HIGH VOLTAGE
- LIGHT WEIGHT
- FAST SWEEPS
- LOW COST

PRICE **$990**

WRITE FOR FULL DETAILS AND SPECIFICATIONS

DU MONT

ALLEN B. DU MONT LABORATORIES, INC. • INSTRUMENT DIVISION • 1500 MAIN AVE., CLIFTON, N.J.

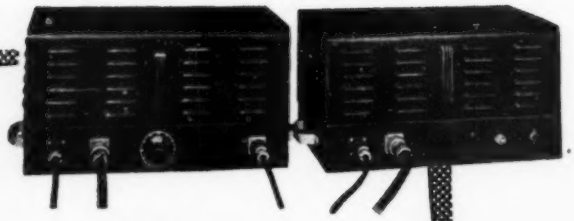

Announcing

THE NEW FARRAND LOW FREQUENCY–HIGH GAIN AMPLIFIER and REGULATED POWER SUPPLY

The Farrand Low Frequency High Gain Amplifier and associated Regulated Power Supply, although primarily developed for use with Farrand Hornig Type Thermocouples, can be utilized for other thermocouples, thermopiles and similar type detectors.

The amplifier operates on frequencies between 2 and 20 cycle signals. However, amplifiers are peaked for frequency response desired or most suitable for a particular application, therefore, any intermediate peak frequency response can be specified. With lower peak frequency amplifiers, e.g., 5 or 7½ cy., band width and gain are altered; gain increases and band width narrows, both, obviously desirable characteristics.

The gain provided is generally sufficient to produce full scale deflection on a balancing type recorder requiring 10 M.V. full scale signal when the amplifier input is 0.001 microvolt.

With full amplifier gain, it is then possible to observe the Johnson noise of typical thermocouples at an approximate output level of .1 volt across the 1500 ohm output load resistor.

The Power Supply to operate this Amplifier has sufficient regulation and freedom from noise which permits detection of the first stage tube noise and, thereby, enables observation of lowest thermocouple noise.

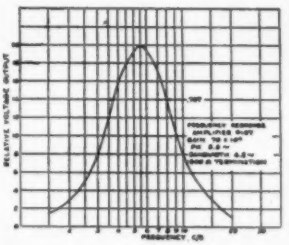

The frequency characteristic of the complete Amplifier when operating from a generator impedance equal to an average thermocouple.

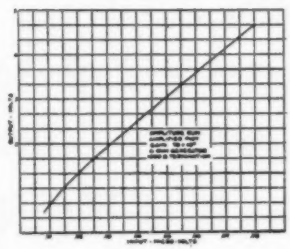

An amplitude curve as obtained from a generator of impedance representing the average thermocouple.

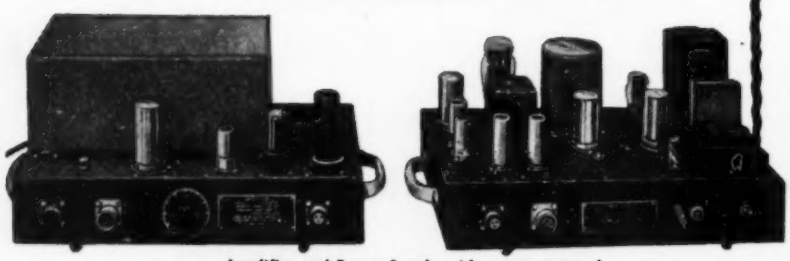

Amplifier and Power Supply with covers removed

For further information send for Farrand Bulletin No. 810

ENGINEERING
RESEARCH
DEVELOPMENT
DESIGN and
MANUFACTURE
of
PRECISION OPTICS,
ELECTRONIC AND
SCIENTIFIC
INSTRUMENTS

FARRAND OPTICAL CO. INC.

BRONX BOULEVARD & EAST 238th STREET, NEW YORK 70, N. Y.

Tracerlab®
Tracerlab has developed the most extensive line of nuclear instruments, radiochemicals and laboratory accessories available today. These products are described and illustrated in our general Catalog C, and in issues of our technical publication, Tracerlog, available on request. Regardless of your particular interest, if it concerns radioactivity, we can be of assistance to you.
130 High Street, Boston, Mass.
2295 San Pablo Ave., Berkeley, Calif.

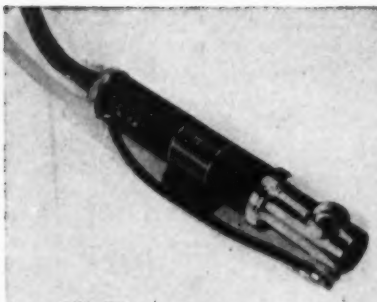

AEG-50

Power range 8 to 50 PKV. Beryllium window, grounded anode x-ray tube designed to provide high intensity, long wavelength x-radiation for diffraction analysis, microradiography, metal sheet thickness gauging, photo chemical applications and light materials radiography.

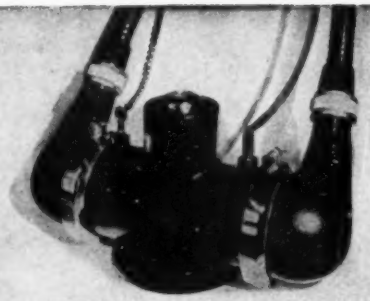

THERMAX

Power range from 50 to 150 PKV. A shockproof, industrial radiographic tube, lightweight and compact for simplicity of installation and ease of manipulation. Effective focal spot 2.3 mm. Approximate practical thickness limits: 4" of aluminum, 1" of steel or their equivalents.

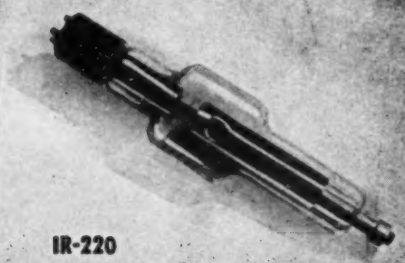

IR-220

Power range from 65 to 220 PKV. An oil-cooled x-ray insert tube designed for use in oil-insulated cable type shock-proof heads operating on rectified current. Thickness limits of 2" to 3" of steel or equivalents.

IR-260K

Power range 65 to 260 PKV. An oil-cooled x-ray insert tube for self-rectified operation in oil-insulated, self-contained heads. Special design features permit use on unrectified voltage while minimizing physical dimensions. Provides complete radiographic facilities for wide range of materials of varying thickness, from light alloy castings to 4½" of steel.

There's a MACHLETT X-ray Tube for Your Industrial Application

Machlett Laboratories, specialists in the design and production of electron tubes, offer industry a series of x-ray tubes extending over a wide power range and capable of handling almost every industrial radiographic application. These tubes have been so designed as to overcome the many problems inherent in industrial usage and provide the finest possible focus with adequate energy ratings, a wide operating range, minimum inherent filtration and a rugged overall construction.

Widespread use of industrial radiography has resulted in increased production of vitally needed minimum size, light weight, reliable castings. Also, it has aided measurably in the conservation of materials through non-destructive testing of many products at each stage in their manufacture.

For full technical data on all Machlett Industrial X-ray tubes, write to Machlett Laboratories, Inc., Springdale, Connecticut.

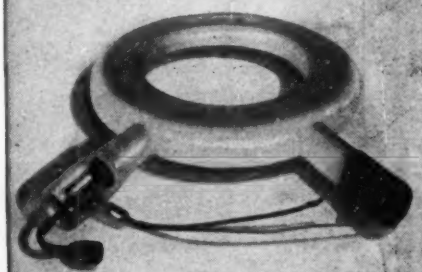

24 Million Volt Betatron Donut

Power range 10 to 24 MEV. High penetrating radiation permits assemblies (motors, castings and forgings) to be handled with speed and precision. Thickness limits of 3" to 25" of steel or equivalents.

MACHLETT X-RAY TUBES SINCE 1897 — TODAY THEIR LARGEST MAKER

FOR APPLICATION AND PRODUCT DEVELOPMENT NEWS IN
X-RAY INSTRUMENTATION AND ELECTRON MICROSCOPY

Send for your FREE COPY—
AVAILABLE BIMONTHLY

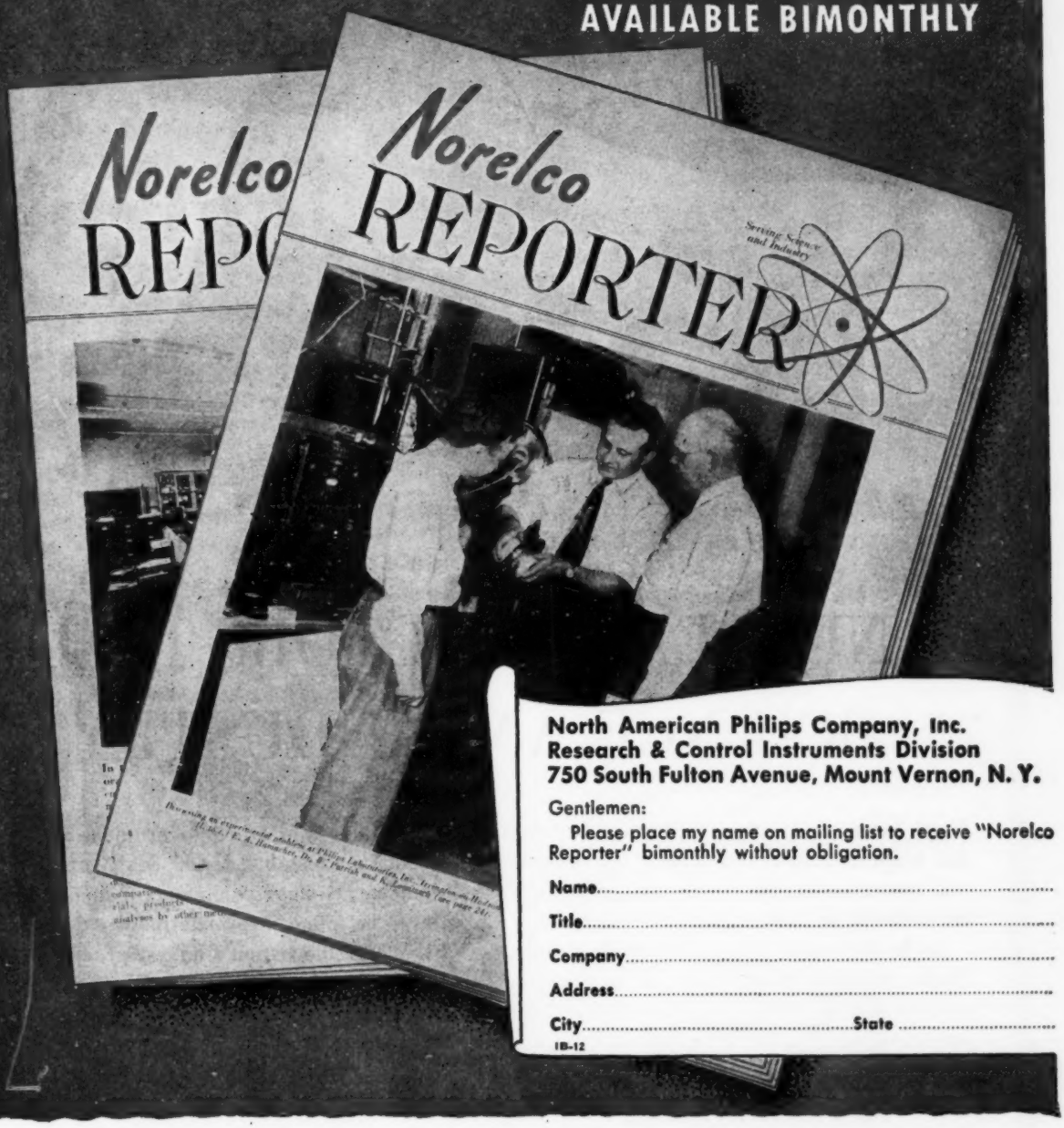

North American Philips Company, Inc.
Research & Control Instruments Division
750 South Fulton Avenue, Mount Vernon, N. Y.

Gentlemen:

Please place my name on mailing list to receive "Norelco Reporter" bimonthly without obligation.

Name.....

Title.....

Company.....

Address.....

City..... State .....

IB-12

A **Norelco** PRODUCT — NORTH AMERICAN PHILIPS COMPANY, INC.

Serving Science and Industry

Dept. IB-12 • 750 South Fulton Avenue, Mount Vernon, N. Y.
In Canada: Rogers Majestic Electronics Ltd., 11-19 Brentcliffe Road, Leaside, Toronto 17, Ontario

NORTH AMERICAN AVIATION
is ready to build

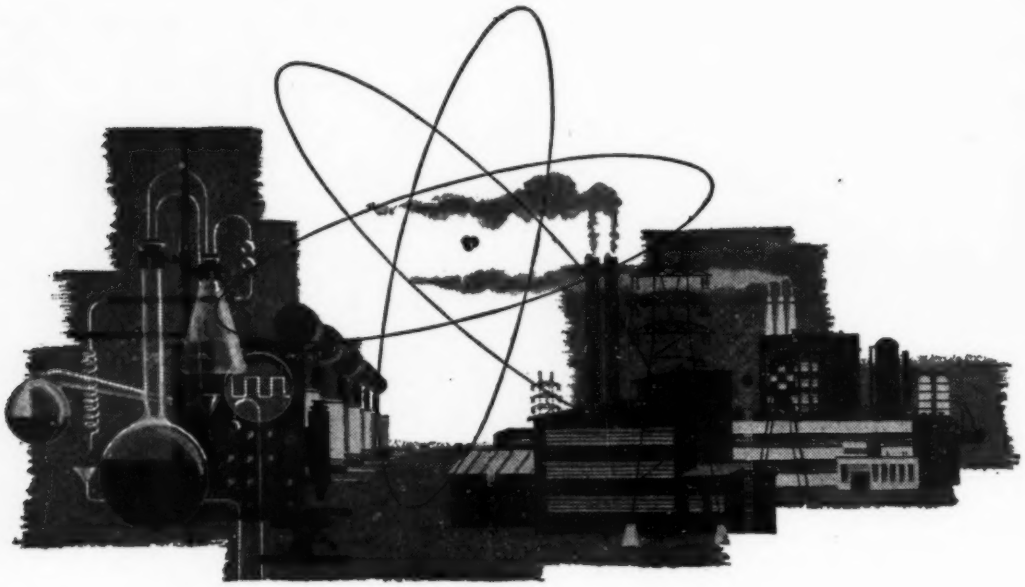

NUCLEAR REACTORS FOR SCIENCE AND INDUSTRY

North American Aviation is ready now to design and build nuclear reactors to fit the research and power production needs of any qualified educational, medical or industrial group.

As in the case of proposals now in process, North American will provide all engineering services necessary for reactor development and operation, offering the widest possible range of reactor application. North American is also prepared to supply accessory equipment . . . as well as a variety of services essential to the success of various atomic projects.

Through its work with the Atomic Energy Commission and other government agencies, North American has developed one of the most complete atomic research and production facilities to be found in private industry . . . staffed by one of the nation's largest groups of outstanding engineers and scientists.

North American invites your inquiry regarding reactor development or any other project in which atomic energy can be put to productive use. All reactor development is undertaken in accordance with the provisions of the Atomic Energy Act and subject to approval of the Atomic Energy Commission.

NORTH AMERICAN AVIATION, INC.

ATOMIC ENERGY RESEARCH DEPARTMENT • DOWNEY, CALIFORNIA

zero to 70,000 cycles per second

...recorded on one tape recorder, the Ampex Model 311

This versatile Ampex recorder is a combination of a wide-range direct recorder for high frequency phenomena and an fm-carrier recorder for highly transient or extremely low frequency phenomena requiring excellent amplitude accuracy. It provides a means for recording nearly every type of data encountered in laboratories and in industry.

The Ampex 311 uses two parallel channels on quarter-inch tape. The direct recording channel handles frequencies from 300 to 70,000 cycles per second. The fm-carrier channel has high transient accuracy in the range from 0 to 5,000 cps.

The Ampex 311 can record diverse types of data signals with a common time base. For instance, the fm channel might record high transient phenomena or low frequency signals while the direct channel records wide-band multiplexed signals or other high frequency information.

Even where serving only one need, the Ampex 311 is effectively a two-channel recorder, since the channel not being used to record data can be used for time signals. Thus, it can serve the same purposes in many cases as either a two-channel direct recorder or a two-channel fm-carrier recorder.

AMPEX Model 311
Combination Recorder
Two parallel channels cover a wide range of data situations:

The fm channel
- Frequency response, 0 to 5,000 cps. ± 1 db.
- Transient accuracy independent of minor tape flaws and irregularities.

The direct channel
- Frequency response, 300 to 70,000 cps. ± 3 db.
- Wide band multiplexed or fm-carrier data
- High frequency phenomena

For further information write to Dept. K-1370R-C

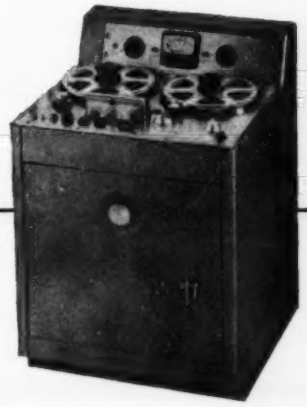

AMPEX
CORPORATION

AMPEX CORPORATION
934 Charter Street • Redwood City, California
Branch offices: New York, Chicago, Atlanta, San Francisco and College Park, Maryland (Washington, D. C. area)
Distributors: Radio Shack, Boston; Bing Crosby Enterprises, Los Angeles; Southwestern Engineering & Equipment, Dallas and Houston; Canadian General Electric Company, Canada

The Welch CATHETOMETER

Insures Precise Measurements and Observations

Vertical range 100 cm
Vernier reading to 0.05 mm
Telescope with rack and pinion
Working distance 45 cm to infinity
Tangent screw adjustment
Level sensitive to 50 seconds of arc
Vertical shaft of Stainless Steel

This cathetometer is intended for measurements and observations in both industrial and educational laboratories wherever an inexpensive instrument of good precision is needed. It is rigidly constructed and every essential adjustment can be made simply and positively.

The telescope is mounted horizontally on a carriage which may be moved up or down or around the 30-mm vertical rod. A tangent-screw adjustment permits precise leveling and a sensitive elevation adjustment is incorporated in the carriage. An auxilliary level in the base greatly accelerates the leveling process. Magnification is 12x at 45 cm.

No. 68A—Each $196.50

Write for descriptive circular.

W. M. WELCH SCIENTIFIC COMPANY
DIVISION OF W. M. WELCH MANUFACTURING COMPANY
ESTABLISHED 1880
1515 SEDGWICK STREET, DEPT. C-1 CHICAGO 10, ILLINOIS, U.S.A.

Kodak reports to laboratories on:

a new way to track down organic chemicals...a thin photorecording paper...the finest roll-film camera we make

Fine needles, fine haystack

Why is *o-Benzoic Sulfimide* (Eastman 38) like *2-Aminobenzothiazole* (Eastman 3940)?

One of our senior chemists, who knows the Eastman catalog about as well as he knows his children's names and ages, got to brooding recently that given one of these compounds, even *he* wouldn't have been able to name the other right off as one of its nearest relatives in our list. (Both consist of a C_3NS heterocycle fused to a carbocycle.) His unease about the difficulty in picking up such relationships among his own merchandise pricked him to spend a good many hours at home making up a deck of cards coded for each compound, that could be shuffled in various ways.

We now learn that another chemist, who works not for us but for Remington Rand, has done the job by punched cards. We ourselves

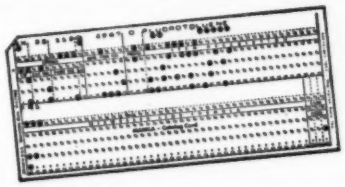

have encoded a fair amount of chemical data on punched cards, but this chemist has done it by the new Wiswesser notation for every Eastman Organic Chemical having a known structure. Thus electromechanical brains, such as are ensconced in many large organizations, can fill in their idle moments by discovering all sorts of important relationships among the more than 3500 organic compounds available from a single, completely dependable source—namely, us.

If you want to know more about what this man has done, or if you want to purchase our catalog in punched-card form, write Remington Rand Inc., 315 Fourth Avenue, New York 10, N. Y. In its conventional book form, the catalog remains free of charge. If you need a copy, write to Distillation Products Industries, Eastman Organic Chemicals Department, Rochester 3, N. Y. (Division of Eastman Kodak Company).

Linagraph 482

Our trade-mark "Linagraph" is applied to certain of our photographic papers and films which do their bit for progress by delivering crisp, black-line oscillograph traces on clean backgrounds. Time was when we beat the drum heavily for the versatility and virtually unlimited frequency response of photographic oscillography and the desirability of keeping consistent oscillographic records for future engineering reference. Then we came to realize that we were belaboring the obvious. The various oscillographs on the market are able to speak very creditably for themselves. We'll concentrate on continuing to squeeze improvements out of the photographic paper and film for them.

In pursuance of this policy, we now draw to your attention the new *Kodak Linagraph 482 Paper*, which has an extra thin, yet exceedingly durable paper base that makes it easier to get the best photocopies of your recordings and any pen or pencil notations they may have acquired. Furthermore, the crispness and blackness of the traces and the whiteness of the background are nowise dependent on cooling the processing solutions. Any temperature below 120 F will do.

The new paper is available in many widths and spoolings from most oscillograph manufacturers and from all Kodak Industrial Dealers. For information on how to make photocopies from it, write Eastman Kodak Company, Industrial Photographic Division, Rochester 4, N.Y.

The Chevron

The world's best known camera manufacturer has just announced its finest roll-film camera. While not surprising, this is nevertheless news.

The camera provides the size advantage of 2¼ x 2¼" negatives or color transparencies, yet is used at the eye-level position preferred by many. It has the world's fastest between-the-lens shutter, with rotating blades for smoother, more accurate exposure. There are ten speeds from 1/800 second to one second, plus "B." Flash synchronization is continuously adjustable for

top efficiency at all shutter speeds with both Class F and Class M flash bulbs and with electronic flash equipment like the Kodatron Speedlamp.

The lens is a 78mm *f*/3.5 Kodak Ektar Lens—a finer one we doubt you can buy. To provide the focusing accuracy such a lens merits, there is a split-field rangefinder operating from 3½ feet to infinity and based on such advanced design features as double V-bearings for moving its mirror, ball-bearing mounting for the focusing tube, and cams almost eight inches long machined to accuracy within .0005" throughout their length. The range-finding operation automatically applies the proper parallax correction to the adjacent viewfinder. An adapter is available to take No. 828 film for the larger 28 x 40 mm Kodachrome slides. Weight: 2½ pounds. Price: no fortune but a sensible $215 for a piece of equipment of strictly professional calibre. (Worth keeping in mind, for example, as a retirement gift for someone who respects noble instrumentation.)

Superlatives in print tire the eyes. If you want to see a well-built camera, go down to your Kodak dealer and ask him to show you the Kodak Chevron Camera. *Since quantities are still limited, there may be a little wait for delivery.*

Price quoted includes Federal Tax and is subject to change without notice.

This is one of a series of reports on the many products and services with which the Eastman Kodak Company and its divisions are ... *serving laboratories everywhere*

Kodak

M/Sgt. Hubert L. Lee
USA

Lt. Col. R. R. Myers
USMC

Major Carl L. Sitter
USMC

M/Sgt. Harold E. Wilson
USMCR

Pfc. H. A. Cafferata, Jr.
USMCR

T/Sgt. R. S. Kennemore
USMC

Sgt. J. C. Rodriguez
USA

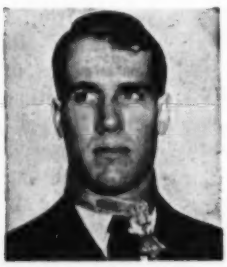

Lt. Thomas Hudner, Jr.
USN

Capt. Lewis L. Millett
USA

Capt. Raymond Harvey
USA

In all, 104 men have won the Medal of Honor in Korea. The men here stand as representatives of them—and of all the service men and women to whose devotion we in America owe our security this Christmas of 1953.

Peace...

their Christmas Wish for us!

THESE are some of the bravest men on earth.

Yet these young holders of the Medal of Honor were never fighters for the love of fighting. They are men of war with a dream of peace.

They want a world in which small wide eyes can gaze in rapture at a tinselled tree. Where a happy Christmas is a child's inalienable right—because fear and force have at last given way to peace and law and goodwill.

They have fought ably for peace, with courage "above and beyond the call of duty." Can we, at home, do something for it, too?

Yes. Beginning now, each of us who earns can put some part of his earnings into United States Defense Bonds. For by these Bonds we make our own families secure, first of all. Then, out of the security of our families, we build the strength of America—to *stay* at peace in a world where peace still is only for the strong.

★ ★ ★

You can invest in Defense Bonds *best* through the Payroll Savings Plan where you work or the Bond-A-Month Plan where you bank. Won't you begin—today?

The U.S. Government does not pay for this advertisement. It is donated by this publication in cooperation with the Advertising Council and the Magazine Publishers of America.

American Institute of Physics
PUBLICATION PROGRAM

For the American Physical Society

THE PHYSICAL REVIEW

Semi-monthly. Publishes original researches in experimental and theoretical physics.

Editor: S. A. Goudsmit, Brookhaven National Laboratory, Upton, L. I., N. Y.

Subscription price: Domestic $30.00; Foreign $32.00.
Yearly back number rate when complete year is available: $25.00 prior to 1949; $33.00 thereafter.
Single Copies: $3.00 prior to July 1929; $1.50 July 1929–December 1941; $3.00 January 1942–December 1946; $1.50 thereafter.
General index, 1893–1920: $4.00.
Note: Special rates quoted on large orders.

REVIEWS OF MODERN PHYSICS

Quarterly. Publishes discussions of developments and current problems of physics.

Editor: J. W. Buchta, University of Minnesota, Minneapolis 14, Minn.

Subscription price: Domestic, members of A.P.S., $3.00; non-members, $4.00.
Foreign: members of A.P.S., $3.40; non-members, $4.40.
Yearly back number rate when complete year is available: $8.00.
Single Copies: $2.25—Combined Issues: $4.50.

For the Optical Society of America

JOURNAL OF THE OPTICAL SOCIETY OF AMERICA

Monthly. Publishes original papers on optics in all its branches.

Editor: Wallace R. Brode, J.O.S.A., National Bureau of Standards, Washington 25, D. C.

Subscription price: Domestic $8.50; Foreign $10.00.
Yearly back number rate when complete year is available: $10.00.
Single Copies: $2.00, 1917–1921;
$1.00 thereafter.
Cumulative Index, 1917–1935: $2.00.

For the Acoustical Society of America

THE JOURNAL OF THE ACOUSTICAL SOCIETY OF AMERICA

Bi-monthly. Publishes original papers on acoustics.

Editor: Floyd A. Firestone, 57 East 55 St., New York 22, N. Y.

Subscription price: Domestic $12.00; Foreign $13.00.
Complete set: Vol. 1, October 1929–Volume 24, 1952—$279.00.
Yearly back number rate: $14.00.
Single Copies: $3.75 prior to Jan. 1947; $2.50 thereafter.
Cumulative index, Vols. 1–10, 1929–1939: $4.50.
Cumulative index, Vols. 11–20, 1939–1948: $5.00.

For the American Association of Physics Teachers

AMERICAN JOURNAL OF PHYSICS

Nine times yearly. Stresses educational, historical and philosophic aspects of physics.

Editor: Thomas H. Osgood, Department of Physics, Michigan State College, East Lansing, Michigan.

Subscription price: Domestic $6.00; Foreign $7.00.
Complete set: Vol. 1, 1933–Vol. 20, 1952—$140.00.
Yearly back number rate: $8.00.
Single Copies: $2.00, 1933–1936; $1.50 thereafter.

Under Institute Sponsorship

THE REVIEW OF SCIENTIFIC INSTRUMENTS

Monthly. Devoted to scientific instruments, apparatus and techniques.

Editor: Gaylord P. Harnwell, Randall Morgan Laboratory of Physics, University of Pennsylvania, Philadelphia, Pa.

Subscription price: Domestic, members of A.I.P. and Affiliated Societies, $6.00; non-members, $8.00.
Foreign, members of A.I.P. and Affiliated Societies, $7.00; non-members, $9.00.

Yearly back number rate when complete year is available: $10.00.

Single Copies: $1.00.

THE JOURNAL OF CHEMICAL PHYSICS

Monthly. Designed to bridge the gap between journals of physics and journals of chemistry.

Editor: Clyde A. Hutchison, Jr., Institute for Nuclear Studies, University of Chicago, Chicago 37, Illinois.

Subscription price: Domestic, members of A.I.P. and Affiliated Societies, $12.00; non-members, $15.00.
Foreign, members of A.I.P. and Affiliated Societies, $13.00; non-members, $16.00.

Yearly back number rate when complete year is available: $17.00.

Single Copies: $1.50.

JOURNAL OF APPLIED PHYSICS

Monthly. Designed particularly for those applying physics in industry and in other sciences.

Editor: Elmer Hutchisson, Case Institute of Technology, Cleveland 6, Ohio.

Subscription price: Domestic, members of A.I.P. and Affiliated Societies, $10.00; non-members, $12.00.
Foreign, members of A.I.P. and Affiliated Societies, $11.00; non-members, $13.00.

Yearly back number rate when complete year is available: $14.00.

Single Copies: $1.25.

PHYSICS TODAY

Monthly. A news and discussion journal on physics for physicists, but designed for readers in other fields as well.

Editorial Director: Gaylord P. Harnwell.

Managing Editor: Robert R. Davis, 57 East 55 Street, New York 22, N. Y.

Subscription price: To members of A.I.P.—no charge; Domestic, members of Affiliated Societies, $3.50; non-members, $4.00.
Foreign, members of Affiliated Societies, $4.50; non-members, $5.00.

Single Copies: $0.50 when available.

JOURNAL OF RHEOLOGY

Complete set: Vol. 1, October 1929–Vol. 3, 1932—$16.25.

Yearly back number rate: $5.50. Single Copies: $1.50.

Address orders to: Circulation Manager, American Institute of Physics

57 East 55 Street, New York 22, New York

AIR-SPACED ARTICULATED

CO-AX CABLES

offer a unique combination of

- ✔ FRACTIONAL CAPACITANCE
- ✔ HIGH IMPEDANCE
- ✔ MINIMUM ATTENUATION

ALONG WITH

- ✔ EXCEPTIONAL FLEXIBILITY
- ✔ LIGHT WEIGHT

38 STOCK TYPES

FOR ANY OF YOUR STANDARD OR SPECIAL APPLICATIONS

A few of the very low capacitance types are:

Type No.	*Capacit. μμ F/ft.*	*Impedance ohms*	*O.D.*
C.44	4.1	252	1.03″
C.4	4.6	229	1.03″
C.33	4.8	220	0.64″
C.3	5.4	197	0.64″
C.22	5.5	184	0.44″
C.2	6.3	171	0.44″
C.11	6.3	173	0.36″
C.1	7.3	150	0.36″

WE ARE SPECIALLY ORGANIZED TO HANDLE DIRECT ORDERS OR ENQUIRIES FROM OVERSEAS

SPOT DELIVERIES FOR U.S.

BILLED IN DOLLARS — SETTLEMENT BY YOUR CHECK

CABLE OR AIRMAIL TODAY

TRANSRADIO LTD.

CONTRACTORS TO H.M. GOVERNMENT

138A CROMWELL RD., LONDON, S.W.7, ENGLAND

CABLES: TRANSRAD LONDON

Capehart DIVISION OF IT&T

announces, with pride, new facilities which provide truly unexcelled opportunities for professional growth in Electronics.

Research, Development, and Production Engineers are needed to staff our growing operations in Radar and Pulse Systems, Antennas, Guided Missile Guidance Systems, Servomechanisms, Microwaves, Solid State Physics, Radio, Television, Vacuum Tubes, Computers, etc.

These positions are enhanced by an easy, relaxed, continuous welcome in one of America's most pleasant Communities.

RSVP

To

EMPLOYMENT DIRECTOR

CAPEHART-FARNSWORTH CO.

FT. WAYNE 1, INDIANA

0-30 KV at 2 MA

COMPACT and PORTABLE

BETA Series 201

high voltage power supplies, one of 120 standard designs, have a range of 0-30 KV at 2 MA, unregulated, with positive, negative or reversible polarity. The equipment is furnished with a direct-reading kilovoltmeter and load current meter.

Ruggedly built for reliable, trouble-free service, the BETA Series 201 are ideal for both research and industrial use. For detailed specifications on the Series 201 or for information on other BETA power supplies, write today.

Beta *Electric Corp.*
333 East 103rd Street, N.Y., N.Y.

PHILOSOPHICAL LIBRARY BOOKS

☐ **NUCLEAR PHYSICS**

By WERNER HEISENBERG

This new work, by one of the outstanding physicists of our time, begins with a short and fascinating history of the views about atoms in antiquity and also of the development of atomic theory.

With 18 halftone illustrations and 32 line illustrations. $4.75

☐ **MATTER-ENERGY MECHANICS**

By JACOB MANDELKER

This work represents a mechanics with the energy aspect of matter mc^2 as its basis. $3.75

☐ **ESSAYS IN SCIENCE**

By ALBERT EINSTEIN

The world of science as the distinguished physicist sees it. Abridged. $2.75

☐ **OUT OF MY LATER YEARS**

By ALBERT EINSTEIN

The book shows Einstein the philosopher, Einstein the scientist, and Einstein the man. $4.75

☐ **POCKET ENCYCLOPEDIA OF ATOMIC ENERGY**

By FRANK GAYNOR

More than 2,000 entries defining and explaining concepts and terms in nuclear physics and atomic energy makes this volume a vital handbook for all those concerned with atomic science.

Illustrations, charts, tables $7.50

☐ **HARWELL**

This book presents the first connected story to be published of the work and problems of the British Atomic Energy Research Establishment, Harwell, from its inception in 1946 until the end of 1951. $3.75

☐ **PHENOMENA, ATOMS AND MOLECULES**

By IRVING LANGMUIR

An approach to science that covers the human, sociological, and international aspects of modern science and atomic physics. $10.00

☐ **ATOMS, MEN AND GOD**

By PAUL E. SABINE

This book is the work of a Protestant layman, a research physicist, who shares with many thoughtful people of similar religious background the problem of reaching rational religious beliefs in this "age of the atom." $3.75

MAIL THIS COUPON TODAY

PHILOSOPHICAL LIBRARY, Publishers
15 East 40th St., Desk 612, New York 16, N. Y.

Send books checked. To expedite shipment I enclose remittance $.....

NAME.....

ADDRESS.....

Another Step in

Getting to the bottom of things

At John E. Fast and Co., the watchdogs of quality are on the job twenty-four hours a day, in every stage of capacitor production. Recording controls indicate the smallest variations in heat, humidity, pressure and vacuum at each process point. Every precaution is taken to assure that environmental conditions are held at precise levels specified by our engineers.

The air in our winding rooms, for example, is continuously filtered so that no foreign particles may settle upon the windings themselves and contribute to ultimate failures. Similarly, capacitors are assembled, after vacuum impregnation, in clean rooms, where relative humidity is controlled at all times. These safeguards against inclusion of extraneous matter or moisture have resulted in increasingly satisfactory life and allied performances in Fast capacitors.

Supplementing this automatic vigilance is a completely equipped quality-control organization which functions at every process-stage from incoming inspection to final testing. At points where statistical control is applicable, our inspectors utilize techniques which comply with or exceed specifications laid down by the Armed Services Procurement Branches.

At final testing stations each production lot is given 100% test and inspection. Our belief is that a single failure out of a thousand may satisfy any sampling requirement, but it may be extremely costly to the consumer. Our investment in precision testing devices and extensive laboratory equipments is great, but its worth is reflected in our national reputation as producers of quality components.

Comprehensive reports are maintained by inspection centers located at strategic production points. These reports are summarized weekly, and it is quite significant to note that both the President of the Company and the Vice-President and Chief Engineer meet each Saturday morning with supervisors, engineers and military representatives to discuss the various problems indicated by process averages, and yield analyses for each production department.

In these days when every hour taken from the production job is spared grudgingly, we still take these hours every week to analyze and combat any threat to quality performance. Increasingly rigid specifications for dimensional and operational characteristics have shown very clearly that control of quality can be achieved and maintained only by rigorous application of all the techniques and tools we are employing.

No greater assurance of excellence may be given than that which has established our reputation. Our fixed objective will always be to maintain that reputation.

AVAILABLE LITERATURE:
Tubular Capacitors in paper tubes 85° or 85°C rating: SEC. I, CATALOG 25
Polystyrene Capacitors in paper tubes or metallic containers: SEC. IV, CATALOG 25
Hermetically-Sealed Tubular Capacitors: SEC. VI, CATALOG 25
Subminiature Capacitors: Special Bulletin.
Jan C-25 Approved Capacitors: Refer to Jan C-25, "Specifications"

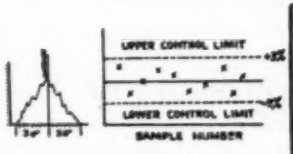

JOHN E. FAST & CO.

Capacitor Specialists For Over A Third of A Century

3175 North Pulaski Road, Chicago 41, Ill.

"WHEN YOU THINK OF CAPACITORS . . . THINK FAST"

Do You Need BINDING SERVICE?

Arrangements have been made for readers of American Institute of Physics publications to have their journals bound carefully and economically by Publishers Authorized Binding Service of Chicago, Illinois. To insure efficiency in handling, the bindery will send on request, prepared order forms, which offer substantial discounts to those using the forms.

Simply write to:

PAPE, Box 776, Highland Park, Illinois

Physical Review	*Holly Green*
Reviews of Modern Physics	*Vermilion*
Journal of the Optical Society	*Cocoa*
Journal of the Acoustical Society	*Vermilion*
American Journal of Physics	*Black*
Review of Scientific Instruments	*Slate*
Journal of Chemical Physics	*Med. Blue*
Journal of Applied Physics	*Scarlet*
Physics Today	*Indigo*

A vital message to the head of the family

Two ways you can protect your family against CANCER

. . . a check
. . . a check-up

Cancer strikes in one of every two families. Each year more than 60,000 American children under the age of eighteen lose a parent to cancer.

Yet many cancers can be cured, if discovered in time.

Every man should have a complete physical examination once a year. Women over thirty-five should have a complete physical examination twice a year.

Because of scientific advances, patients are being cured today who could not have been saved even five years ago.

The American Cancer Society asks your help in the fight against cancer. Your check today will help pay for costly research. Will help keep physicians informed of latest developments in detection and treatment. Will help pay for the training of doctors to specialize in cancer.

How soon we find cancer's cause and cure depends on how soon and how much help comes from people like you.

Invest your money today for your family's security tomorrow.

"Cancer" c/o Postmaster, (Your town)
Please send me free literature about cancer.
Enclosed is my contribution of $_____ to the cancer crusade.

Name_____

Address_____

City_____ State_____

Cancer strikes One in Five
STRIKE BACK...
Give to Conquer Cancer

CREEP TEST INSTRUMENTS • TELESCOPES • TOOLMAKER MICROSCOPES • COMPARATORS • OPTICAL INSTRUMENTS • SPECTROMETERS **Gaertner** REFRACTOMETERS • MICROMETER SLIDES • INTERFEROMETERS • SPECTROPHOTOMETERS • LABORATORY SUPPORTS CATHETOMETERS • CHRONOGRAPHS • OPTICAL BENCHES • SPHEROMETERS • SPECTROSCOPES • DIVIDING MACHINES PHOTOELASTICITY POLARISCOPES • MICROSCOPES • SPECTROGRAPHS • POLARIMETERS • MONOCHROMATORS

PRECISION SPECTROMETER

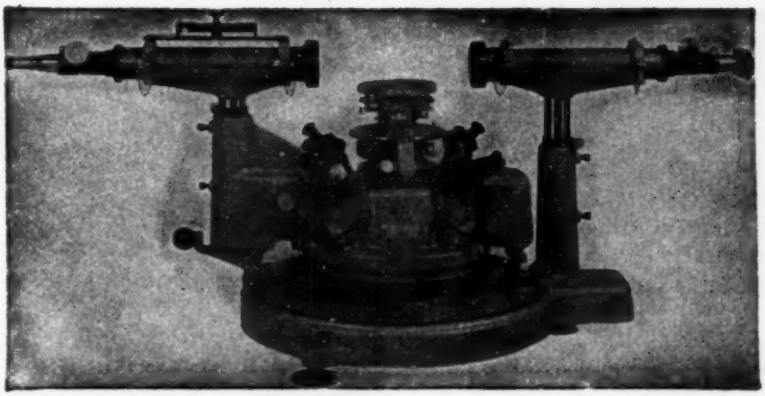

For highly accurate determinations of refactive indices and dispersion, measurement of prisms and wedge angles, and similar applications. Direct reading to 1 second. Polarizing and other attachments are available.

A completely new instrument incorporating many adjustments contributing to the attainment of high precision and operating convenience. Cat. No. L124.

Request Bulletin 157–52

THE GAERTNER SCIENTIFIC CORPORATION
1212 WRIGHTWOOD AVE. • CHICAGO 14 • U.S.A.

fused quartz for optics

Hanovia's three grades of optical quality fused quartz meet a wide range of requirements of the instrument designer. Manufactured under the highest standards of quality control, these quartz blanks assure perfect results in their appropriate applications.

ULTRASIL, the finest grade of fused quartz for prisms and lenses, is completely free of air bubbles and striae. It provides maximum ultraviolet transparency.

HOMOSIL is suitable for lenses transmitting wavelengths above 2300 angstrom units, and shows virtually no interference under crossed Nichols or polarizers.

OPTOSIL, a quality suitable for many optical applications, has far fewer and smaller air bubbles than commercial grades of clear, fused quartz.

Detailed technical data may be obtained on Hanovia fused quartz by writing to Dept. *JAP-1253.*

HANOVIA

CHEMICAL & MANUFACTURING CO.
Special Products Division
100 CHESTNUT STREET, NEWARK 5, N. J.

1835

CENTRAL RESEARCH LABORATORIES'
MICROWAVE DIELECTROMETER

Continues to be the instrument of choice for determining dielectric constant and loss in the microwave region

Features

- Measurements at 1000, 3000, and 8500 megacycles
- K from 1 to 100
- Tan δ from 0.0001 to 1.0
- 1 to 2 per cent accuracy for most measurements
- 1-inch diameter sample

The Microwave Dielectrometer consists of a slotted wave guide, precision traveling probe, klystron oscillators, probe-out-put amplifier, associated power supplies and equipment. The sample to be measured is inserted ahead of a short-circuiting plug, and the effect of this arrangement on the standing-wave pattern in the guide provides data for calculating the dielectric constant and loss of the material.

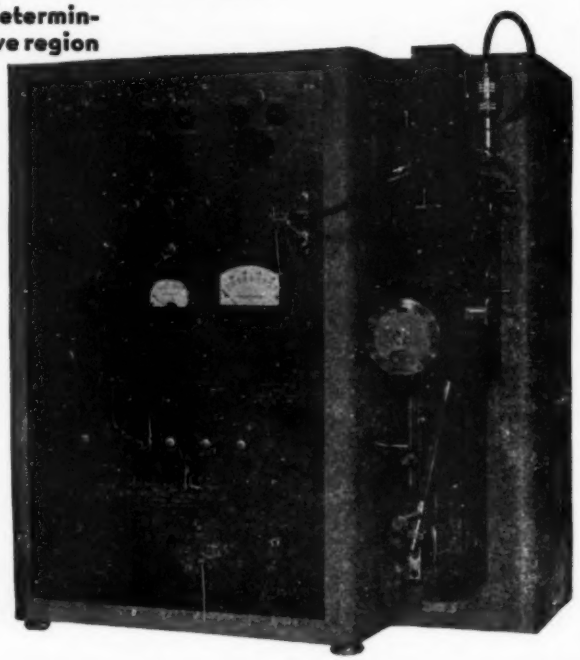

Write for Further Information

CENTRAL RESEARCH LABORATORIES, INC.
RED WING, MINNESOTA

Positions are now available for

PHYSICISTS AND ENGINEERS

of unusual ability

at

THE RAMO-WOOLDRIDGE CORPORATION

LOS ANGELES, CALIFORNIA

THIS NEW COMPANY, EXCEPTIONALLY WELL FINANCED, WILL CARRY ON RESEARCH AND DEVELOPMENT IN THE PHYSICAL SCIENCES AND WILL MANUFACTURE THE PRODUCTS DEVELOPED. EXTRAORDINARY ATTENTION HAS BEEN GIVEN TO THE ESTABLISHMENT OF A PERMANENTLY ATTRACTIVE ENVIRONMENT FOR THE CREATIVE PROFESSIONAL MAN.

Apply to our employment office at 6316 West 92nd Street, Los Angeles 45, California. Assurance is required that relocation of the applicant will not cause disruption of an urgent military project.

International Instrument Congress and Exposition

The American Institute of Physics, together with other scientific and professional groups, will be cooperating with the Instrument Society of America in the International Instrument Congress and Exposition to be held in the Philadelphia Museum and Convention Hall, September 13–25, 1954. As part of its participation, the Institute will arrange a program of invited scientific papers on subjects to be announced at a later date. The Institute is also sponsoring a group of exhibits at which leading manufacturers of scientific and laboratory equipment and products will display their latest models.

The following companies have thus far reserved space in our "Physics Section."

Baird Associates, Inc.
Brailsford & Co.
Brush Electronics Co.
Central Scientific Co.
Edmund Scientific Corp.
Electronic Instruments Div.
(Burroughs Company)
Gaertner Scientific
O. M. Giannini & Co.
Goodyear Aircraft Corp.
W. L. & E. Gurley
High Voltage Engineering Corp.
Hughes Aircraft Company
International Equipment Co.
Jarrell-Ash Co.
Kepco Laboratories
Lambda Electronics Corp.
Liston-Becker Instrument Co.
National Bureau of Standards
North American Aviation, Inc.
North American Philips Co.
Nuclear Development Assoc., Inc.
Nuclear Research Corp.
Rubicon Company
Specialized Instruments Corp.
Telecomputing Corp.
Tektronix, Inc.
Thomas, Arthur H. & Co.
Tracerlab, Inc.
Unicam Instrument
Vacuum Electronic Engineering Co.
Waterman Products Co., Inc.
W. M. Welch Manufacturing Co.

A limited number of booths are still available and interested companies are invited to address inquiries to the American Institute of Physics, attention T. Vorburger, 57 East 55 Street, New York 22, New York.

All members of the American Institute of Physics, including its five founder societies and nine affiliated societies are cordially invited to attend. Personal invitations and program information will be mailed them in due course.

SERVOTHERM

Infrared Radiation Instrumentation

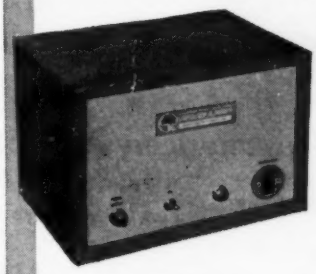

THERMISTOR POWER SUPPLY

Provides voltages required by bolometer bridge and preamplifier. Regulated and filtered permitting theoretical noise limits of amplification, while operating from 60 cycle line.

BOLOMETER and PREAMPLIFIER

Thermistor bolometers are fast, sensitive infrared and heat detectors. Especially rugged for industrial, scientific and military applications. Preamplifier provides noise-free initial amplification and mount.

For detailed specifications write Dept. JAP 12

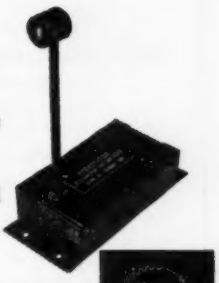

SERVO CORPORATION OF AMERICA
NEW HYDE PARK, NEW YORK

WANTED
PHYSICISTS
MS or PhD PREFERRED
Experienced in HEAT ENGINES and THERMODYNAMICS
HIGH PRESSURE experience also valuable
Or with knowledge of: . . . FLUID FLOW . . . HIGH SPEED PHOTOGRAPHY . . . HIGH TEMPERATURE MEASUREMENT

LET'S TALK FACTS ABOUT ROCKET POWER

Rocket power is no longer "the coming thing." It's here . . .

Nowhere is the fact more apparent than at Reaction Motors, pioneer and leading research and development organization whose engines have powered most of the record-breaking flights. A comparatively small company, RMI provides an ideal stimulating environment for young physicists with imaginative, inquisitive minds. Located in the Lakeland region of New Jersey, renowned vacation playground, it offers ideal year-round living conditions, with ample housing.

If You're Interested . . . If You Qualify . . .
Send Complete Resume and Salary Requirements to:
EMPLOYMENT MANAGER
REACTION MOTORS, INC.
Foremost Designers & Developers of Rocket Power
Rockaway, New Jersey
LESS THAN 1 HOUR FROM TIMES SQ.

PLACEMENT SERVICE REGISTER

OF THE

AMERICAN INSTITUTE OF PHYSICS

to be held in connection with the

American Physical Society Meeting

January 28, 29 & 30, 1954

Columbia University, New York, N. Y.

LOOKING FOR PHYSICISTS?

Universities, institutions, government laboratories, and companies wishing to post notices of positions may send descriptions of the openings on 8½ x 11 paper in multiple copies (*15 required*) to the Institute office, or post them on arrival at the meeting. If you plan to have a representative present, to interview applicants, please indicate his name at the bottom of the job description sheets.

SEEKING A NEW POSITION?

Applicants may obtain registration forms and further information from the Institute office. Preregistration is essential. Complete registration forms must be received at the Institute office by January 18, 1954 to insure their inclusion at this register.

INTERVIEWS.

It is to the advantage of the registrants to be present. Interviews will be arranged between employers' representatives and applicants attending the meeting.

PLEASE REPORT TO THE PLACEMENT OFFICE UPON ARRIVAL AT THE MEETING

AMERICAN INSTITUTE OF PHYSICS, 57 East 55th Street, New York 22, N.Y.

Nuclear Physics — Reprinted Again

BECAUSE of the demand for the thorough and comprehensive review of the developments in the field of nuclear physics, which appeared in the American Physical Society's quarterly publication, REVIEWS OF MODERN PHYSICS, the issues containing this article have again been reprinted.

Part A. **Stationary States of Nuclei** by H. A. BETHE AND R. F. BACHER.
148 journal pages. **April, 1936 issue.**

Part B. **Nuclear Dynamics, Theoretical** by H. A. BETHE.
176 journal pages. **April, 1937 issue.**

Part C. **Nuclear Dynamics, Experimental** by M. S. LIVINGSTON AND H. A. BETHE.
146 journal pages. **July, 1937 issue.**

COMPLETE SET of three issues.....**$6.75 a set**

SEPARATE COPIES of any of the issues.....**$2.25 a copy**

Send orders with remittance to

American Institute of Physics, 57 East 55 Street, New York 22, N. Y.

POSITION WANTED

Physicist-Engineer. British, age 44, married, 20 years academic and industrial experience in organizing and directing research and development laboratories: radiac and nucleonic instrumentation, information and data processing devices/digital and analogue/, radar, high-vacuum and solid state electronics—desires responsible position and commensurate salary with progressive firm or university, location immaterial but genial climate essential. Write Box 1253, 57 East 55 St., New York 22, N. Y.

TEACHING POSITION WANTED
(Starting September '54)

Physicist-PhD, with experience. Write Box 1053D, 57 East 55 St., New York 22, N. Y.

ENGINEER

PHYSICIST

Excellent opening for an ambitious top grade Research Physicist in the area of automatic control and industrial instrumentation.

Our position requires investigation into new and varied ways of detecting changes in physical process variables such as pressure, pH, flow, temperature and others.

A. Ph.D. degree or an M.S., with experience in instrumentation is preferred, but experience in related fields also considered.

Good laboratory conditions, many benefits with good salary and advancement. Work is interesting and challenging.

Send a brief resume, visit or call:
D. P. WHITELEY

Minneapolis-Honeywell, Brown Instruments Div.
WAYNE & WINDRIM AVES. PHILADELPHIA 44, PA.

POSITIONS OPEN

Research Analysts, Engineers, and Physicists for permanent positions in expanding mechanical research and development programs. All phases of engineering analysis, design and test in fluid mechanics, dynamics, vibrations, structures. For application and particulars write: Engineering Mechanics Department, Southwest Research Institute, P. O. Box 2296, San Antonio, Texas.

Lincoln Laboratory at M.I.T. has **Staff Research** positions available for exceptional Electrical Engineers with advanced training or experience in pulse circuitry and microwave applications. Please reply to Lincoln Laboratory, Personnel Department, P.O. Box 390, Cambridge 39, Mass.

POSITIONS OPEN

Massachusetts Institute of Technology's Digital Computer Laboratory of the Department of Electrical Engineering has staff openings for highly qualified engineers and scientists for work on the development of high-speed electronic digital equipment (including work on logical design, vacuum-tube circuitry, ferromagnetic and ferroelectric memory cells and computer elements, and magnetic drum usage).

There are also a few openings for work on use of high-speed digital computers to control large physical systems. This involves study of the control requirements of the whole system, reduction of these requirements to a simple pattern or sequence of control instructions, and translation of the pattern into computer code. Position requires appreciation of physical systems, ingenuity, and imagination. Prior experience with digital computers unnecessary, and training in computer principles will be provided; engineering experience in general is useful but not essential.

Persons transferring from other fields to acquire experience in digital computers for engineering and military uses are encouraged to apply and may come on leave of absence from their permanent organizations. Positions carry opportunity for advancement. Salary appropriate to candidate's experience and training. Address: Digital Computer Laboratory, MIT, 211 Massachusetts Avenue, Cambridge 39, Massachusetts.

APPLIED PHYSICIST

To fill an important position in a meteorological instrumentation project. Must have a good background in applied physics, electronics, and mechanical engineering. Should be familiar with temperature and humidity instrumentation, telemetering, coding systems, servomechanisms, and analog and digital computer techniques. A minimum of five years experience is required.

Excellent opportunities for professional growth are offered by this laboratory whose staff of engineers and scientists is active in the fields of radar, computers, servomechanisms, and nucleonics. Advanced study at local universities is encouraged and supplemented by special company-sponsored courses.

Applicants for this position will be invited to inspect our laboratory facilities and to meet the members of our technical staff.

Please send brief resume to:

Personnel Department
BENDIX AVIATION CORPORATION
Research Laboratories
4855 Fourth Avenue, Detroit 1, Michigan

INDEX TO ADVERTISERS

Name	*Page*
AMPEX CORPORATION	xiii
THE ARNOLD ENGINEERING COMPANY — Alnico Permanent Magnets.	ii
BELL TELEPHONE LABORATORIES	iii
BENDIX AVIATION CORPORATION	xxv
BETA ELECTRIC COMPANY — High Voltage DC power supplies, kilovoltmeters, electronic microammeters, portable projection oscilloscopes and regulated DC power supplies of all types.	xix
CAPEHART-FARNSWORTH CORP.	xviii
CENTRAL RESEARCH LABORATORIES, INC. — Chemistry, physics, electrical engineering. Consultation, research, development, production. High-speed Micro-oscillographs, Microwave Dielectrometers, Double Monochromators, X-Ray and Electron-Diffraction Cameras.	xxii
CENTRAL SCIENTIFIC COMPANY — Manufacturers of Cenco Physical Apparatus and Instruments to meet all requirements of University, College and High School Physics Laboratories. Specializing in high vacuum pumps and development of instruments and apparatus for various sciences.	Cover 4
ALLEN B. DUMONT LABORATORIES — Cathode Ray Tubes, Oscillographs and Accessory Apparatus.	vii
EASTMAN KODAK COMPANY — Plates for Photography, Photomicrography, Spectroscopy, Photometry, Astronomy; Wratten Light Filters; Cameras and Films.	xv
FARRAND OPTICAL COMPANY	viii
JOHN E. FAST & COMPANY	xx
THE GAERTNER SCIENTIFIC CORP. — Spectroscopes, Spectrometers, Spectrographs, Spectrophotometers, Helliostats, Measuring Microscopes, Comparators, Cathetometers, Reading Telescopes, Interferometers, Chronographs, Dividing Machines, etc.	xxi
GENERAL RADIO COMPANY — Manufacturers of electronic measuring instruments; vacuum-tube voltmeters, amplifiers and oscillators; wave analyzers, noise meters and analyzers, stroboscopes; laboratory standards of capacitance, inductance and frequency; impedance bridges, decade resistors and condensers, air condensers and variable inductors; rheostats. Variacs, transformers; other laboratory accessories.	Cover 3
HANOVIA CHEMICAL & MFG. CO.	xxi
HUGHES RESEARCH & DEVELOPMENT LABORATORIES	iv
LEEDS & NORTHRUP COMPANY — Manufacturers of Galvanometers, Resistors, Bridges, Condensers, Inductances, Potentiometers, Testing Sets; Temperature Measuring, Recording, and Controlling Apparatus; Instruments for Measuring and Controlling Conductivity of Electrolytes and Hydrogen Ion Concentrations.	i

INDEX—*Continued*

Name	*Page*
LIBRASCOPE, INCORPORATED	vi
MACHLETT LABORATORIES, INC.	x
MASSACHUSETTS INSTITUTE OF TECHNOLOGY	xxv
NATIONAL RESEARCH CORP. — Specialists in industrial applications of high vacuum in the fields of physics and chemistry; research design, consulting; low reflection glass surfaces, freeze drying, vacuum distillation, vacuum metallurgy and special products manufactured or processed under low pressure.	v
NORTH AMERICAN AVIATION, INC.	xii
NORTH AMERICAN PHILIPS COMPANY, INC. — Manufacturers of Searchray (X-Ray) Apparatus; X-Ray Diffraction Apparatus; Electronic Measuring Instruments; Direct Reading Frequency Meters; High Frequency Heating Equipment; Tungsten and Molybdenum in powder, rod, wire and sheet form; Fine Wire; Diamond Dies.	xi
PHILOSOPHICAL LIBRARY	xix
RAMO WOOLDRIDGE CORP.	xxii
REACTION MOTORS, INC.	xxiii
SERVO CORPORATION OF AMERICA	xxiii
TRACERLAB, INC. — Suppliers of instruments for measuring, detecting, health monitoring and surveying radioactive materials, and radioactive tracer analyses, isotope processing, synthesis, consulting and industrial research in radioactivity.	ix
TRANSRADIO, LTD.	xvii
W. M. WELCH SCIENTIFIC COMPANY — Manufacturers of high-vacuum pumps, both mechanical and diffusion; vacuum gauges; electrical measuring instruments; physics equipment; and other items for the physical and chemical laboratories.	xiv

SPECTROSCOPIST
PHYSICIST—ION OPTICS

Whether a native Californian or interested in locating here, you can't go wrong checking Beckman's few career positions now open. Our expansion of firm commercial business of building some of the world's finest scientific instruments can assure you of a secure future.

If the positions above fit your interest and abilities, communicate with our Technical Employment Manager.

BECKMAN INSTRUMENTS, INC.
1001 El Centro, South Pasadena 4, Calif.

"the G-R Microflash has been instrumental in the development of our Analog-to-Digital Converter"

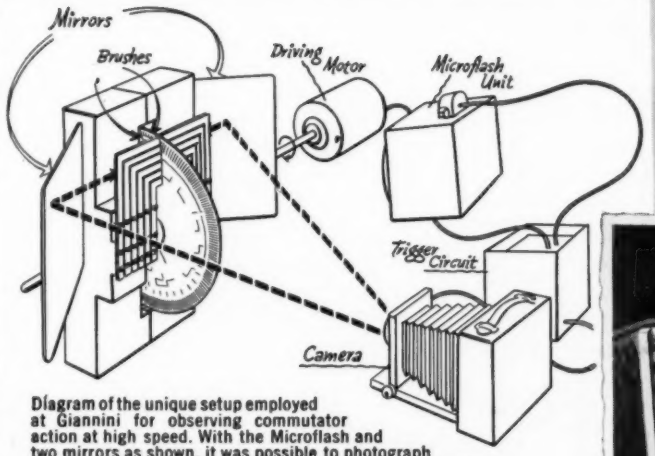

Diagram of the unique setup employed at Giannini for observing commutator action at high speed. With the Microflash and two mirrors as shown, it was possible to photograph both sides of the commutator at the same instant of time and with equal exposure.

When design engineers had to observe the brush contact points of a developmental analog to digital converter, while the commutator was actually rotating at high speed, they called for a G-R Type 1530-A Microflash. The high-intensity, short-duration flash provided by this equipment was instrumental in the development of the Giannini model 14310 Analog Position Encoder.

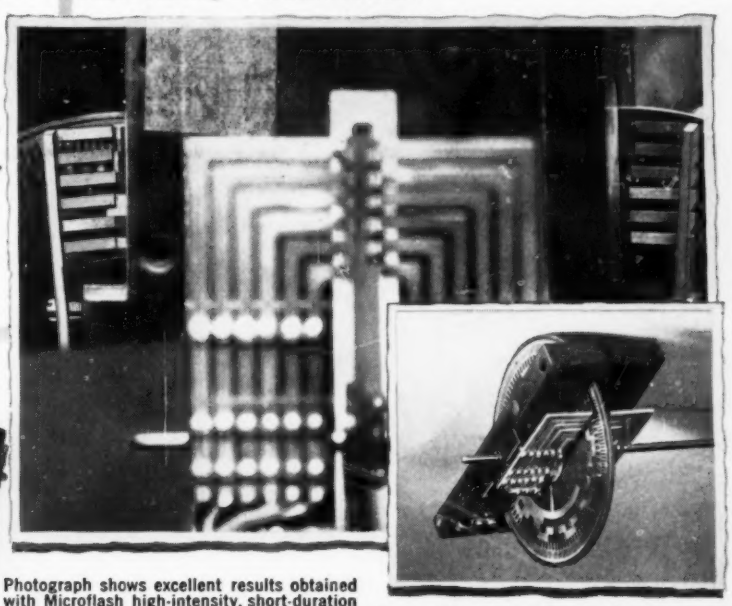

Photograph shows excellent results obtained with Microflash high-intensity, short-duration illumination. Back view of either side of commutator and front view are shown. Photos courtesy G. M. Giannini and Company, Inc.

Commutator of Angular Position Encoder is photo-engraved with twelve rows of conducting segments which contact twelve stationary brushes. This enables Encoder to measure angular rotation of 360 degrees with an accuracy of ±0.1%.

Type 1530-A Microflash $640

The Microflash has been successfully applied to the study of many phenomena in pure and applied science. It is widely used in studying the effects of abrasion, turbulence in liquids, and mechanical distortion at high rotational speeds.

Other applications include study of the disintegration of high-speed rotors, investigation of projectile flight and impact, and experimentation dealing with the propagation of fractures in various materials. In mechanical design, the Microflash is an indispensable tool for studying the action of springs, valves, cams, cranks, bearings and other parts moving at high speeds.

★ *G-R Type 1530-A Microflash provides an intense white light for single-flash photography of very rapidly moving objects — flash intensity is 20,000,000 beam candles — duration is only 2 millionths of a second*

★ *Power supply and trigger circuits are assembled in one metal case, lamp is in another — two sections lock together for complete protection of all controls and ease in transportation*

★ *Panel pushbutton initiates flash — alternative is to have flash tripped by noise or pressure wave associated with the action to be photographed; microphone and built-in amplifier are provided for such use*

★ *Additional jack is available for flashing from any simple external contactor — photoelectric cells, wire breaking under tension or impact, and many other easily-built devices will trip flash to suit the application*

★ *Conventional camera equipment is used*

★ *Accessories supplied include microphone with cable, tripod, spare pilot lamps and fuses, 2 spare flash lamps, and plug for connection to external-contactor trip jack*

★ *Dimensions are 24⅛ x 13¼ x 11¾ inches, overall — net weight is 72 pounds*

★ *Price:* **$640.00**

GENERAL RADIO Company

275 Massachusetts Avenue, Cambridge 39, Massachusetts, U. S. A.

90 West St. NEW YORK 6 920 S. Michigan Ave. CHICAGO 5 1000 N. Seward St. LOS ANGELES 38

Admittance Meters ☆ Coaxial Elements ☆ Decade Capacitors
Decade Inductors ☆ Decade Resistors ☆ Distortion Meters
Frequency Meters ☆ Frequency Standards ☆ Geiger Counters
Impedance Bridges ☆ Modulation Meters ☆ Oscillators
Variacs ☆ Light Meters ☆ Megohmmeters ☆ Motor Controls
Noise Meters ☆ Null Detectors ☆ Precision Capacitors
Pulse Generators ☆ Signal Generators ☆ Vibration Meters ☆ Stroboscopes ☆ Wave Filters
U-H-F Measuring Equipment ☆ V-T Voltmeters ☆ Wave Analyzers ☆ Polariscopes

Lifetime Accuracy

cenco MERCURIAL BAROMETERS

Above: Close-up of the conversion table in millimeters, millibars and inches.

Left: Cenco Mercurial Barometer with white lacquered metal mounting.

Accuracy . . . day in and day out . . . 'round the clock dependability . . . that's what you get in a Cenco Mercurial Barometer. Cenco features . . . patented improvements . . . precision manufacture . . . plus an effective method of filling under vacuum . . . combine to provide an instrument of unusual quality at a remarkably low price.

These instruments are built with the tube completely enclosed in hexagonal brass tubing to which the metric and English scales are attached. Patented construction of the mercury well permits fine adjustment and its transparent glass wall admits plenty of light for good visibility.

Cenco Mercurial Barometers are constructed as prescribed by the U. S. Weather Bureau and conform to correction charts established by the Bureau.

Order today for prompt delivery

No. 76890 Cenco Mercurial Barometer for altitudes 0 to 4000 ft. with scales ranging from 600 to 800 mm and 24.5 to 31.5 inches—verniers for reading to 0.1 mm or 0.005 inch. Each..... **$48.50**

No. 76891 Cenco Mercurial Barometer, same as No. 76890 but for altitudes from 1500 up to 10,000 feet. Scale ranges from 500 to 700 mm and 19.5 to 27.5 inches. Each..... **$56.50**

No. 76892 Barometer Mounting made of sheet metal for safe and convenient mounting of Cenco barometers. Finished in white lacquer to provide a light background for adjusting the zero index and vernier. With conversion table. Length, 37½ inches, width 3½ inches. Each... **$6.75**

cenco

. . . one dependable source of supply for everything you need in scientific instruments and laboratory supplies. Over 15,000 items . . . 14 branch offices and warehouses.

R.S.C.

CENTRAL SCIENTIFIC COMPANY
1700 IRVING PARK ROAD • CHICAGO 13, ILLINOIS
CHICAGO NEWARK BOSTON WASHINGTON DETROIT SAN FRANCISCO
SANTA CLARA LOS ANGELES TORONTO MONTREAL VANCOUVER OTTAWA

REFINERY SUPPLY COMPANY
624 EAST FOURTH STREET • TULSA 3, OKLAHOMA
2215 McKINNEY AVENUE • HOUSTON 3, TEXAS